Smart materials for microrobotics.
Motion Control and Power Harvesting

Programa de Doctorat: Enginyeria i Tecnologies Electròniques

Bienni: 2003-2005

Departament d'Electrònica

Facultat de Física

Universitat de Barcelona

Autor: Jordi Brufau Penella

Director: Manel Puig i Vidal

Agraïments:

Primer de tot vull agrair al Dr. Manel Puig i Vidal la oportunitat que m'ha donat per començar a treballar en el camp dels materials per a la micirorobòtica. Gràcies a ell he pogut realitzar aquesta tesi i formar-me com a investigador. Vull agrair també la paciència tinguda envers meu durant tots el anys que ha durat la execució del meu doctorat. També agrair al cap del departament Dr. Albert Cornet i a en Dr. Josep Samitier per permetrem treballar en el Departament d'Electrònica i en el SIC.

A un gran nombre de persones vinculades al departament agrair l'ajuda, tant professional com personal, que m'han donat durant tot aquest temps. En especial al Dr. Pere Miribel Català i al Dr. Ángel Diéguez Barrientos per la possibilitat que m'han ofert de treballar juntament amb els seus grups de recera. També al Dr. Javier Sieiro Córdoba per tot el que m'ha ensenyat i ajudat durant aquest temps.

A tota la gent amb qui he compartit passadís, laboratori i dinars, Mariano, Youcef, Josep, Romén, Gonzalo, Otero, Andreu, Oscar, Dani, etc. Un especial menció se la dedico a una de les persones mes entranyables i que mes m'ha ajudat en temes técnics i demés, Francisco Palacio.

A la meva família, la meva mare, el meu pare, els meus germans, cunyats, etc, per el suport que incondicionalment han mostrat durant tot aquest llarg camí. Un caluros agraïment per a la meva companya la Mireia que ha aguantat aquest últims mesos al meu costat. Als meus amics Juan, Diana, Marcelo, Laia, Alberto, Bàrbara i Coco.

I would like to give tanks to the people from the "Dipartimento di Ingegneria Elettrica, Elettronica e dei Sistemi, Università degli Studi di Catania" in Sicily (Italy)". Specially to Dr. Salvatore Graziani for accepting me in his lab and give me the opportunity to work with the IPMC, and to Pietro Giannone and Salvatore Stratzzeri for helping me in the research and for introducing me to the Sicily type of live.

Finally I want to give thanks to the people from the Aristotle University of Thessaloniky in Greece. To Dr Theodore Laopoulos and Kiriakos Tsiatmaikis for the great pleasure that has been working together.

Moltes gràcies a tots i totes!!!

Prologue

This thesis focuses on the use of smart materials in microrobotic applications. The development of materials with the capabilities to mechanically respond to electrical stimuli or, at the same time, to electrically respond to mechanical stimuli, has entailed the microrobotics rapid evolution.

Along this thesis the use of three smart materials families in the filed of microrobotics is studied. The materials used are the piezoelectric ceramics, the piezoelectric polymers and the ionic polymers metal composites IPMC. The similitude in the way they respond to external stimuli has motivated this study. The three materials respond with an induced mechanical strain under the application of an electric field and respond with an induced electrical charge variation when a mechanical pressure is applied. Although these materials respond similarly, their application in microrobotic systems entails different problems. In this thesis their use in different applications is studied and the problems enclosed with their use are treated.

First of all in this thesis the use of piezoelectric polymers and ionic polymers as materials for motion control of microrobots is studied. Their flexibility opens the door to new applications for microrobot systems as is the case of biomimetics. The first application regards the use of piezoelectric polymers in insect-like mm^3 microrobot. The microrobot is composed with three legs and one antenna or tool for object collision based on piezoelectric polymers. The object collision tool is used as a sensor for motion control to avoid collisions with other objects. The work presented consists on the development of theoretical models to predict the motion of the leg and the tool of the microrobot. The second application regards the development of a control system for controlling the motion of an ionic polymer IPMC underwater. It is difficult to obtain physical models that describe the motion of these materials, thus it is important to design control strategy to work with IPMCs. Furthermore in this thesis, the problem of manufacturing electrodes for IPMC is also treated.

In the second part of the thesis the use of piezoelectric ceramics to harvest power from mechanical vibrations is studied. Piezoelectric ceramics have higher energy densities compared with other methods for power harvesting from vibrations. In comparison with the piezoelectric polymers, the piezoelectric ceramics produce voltages and current levels more acceptable. From the study performed in this thesis the conditions for a maximum power generation are obtained and an optimum electronic circuit for energy storage and management is designed. At the end of the thesis the capabilities to harvest power using ionic polymers are studied.

TABLE OF CONTENTS

1. INTRODUCTION 1-1
1.1. Smart systems and materials 1-2
1.1.1. Classification 1-4
1.1.2. Piezoelectrics 1-9
1.1.2.1. Piezoelectric ceramics 1-11
1.1.2.2. Piezoelectric polymers 1-12
1.1.2.3. Modeling piezoelectrics 1-14
1.1.3. Ionic Polymer Metal Composites (IPMCs) 1-16
1.1.3.1. Modeling IPMC 1-19
1.2. MST and Microrobotics 1-22
1.2.1. Motion control 1-25
1.2.1.1. Micromanipulation and microassembling with microrobots 1-27
1.2.1.2. Insect-like microrobots 1-30
1.2.1.3. Fish-like microrobot 1-32
1.3. Power harvesting 1-34
1.3.1. Power from mechanical vibration 1-35
1.3.1.1. Magnetic induction converters 1-36
1.3.1.2. Electrostatic converters 1-37
1.3.1.3. Piezoelectric converters 1-37
1.3.1.4. Converters performances comparison 1-38
1.3.2. Alternative power sources 1-40
1.3.2.1. Solar energy 1-40
1.3.2.2. Heat converters 1-40
1.3.3. Autonomous power sources for microrobots 1-43
1.4. Thesis objectives 1-46
1.5. Overview 1-49
1.6. References 1-50

2. MOTION CONTROL IN MICROROBOTICS 2-1
2.1. Piezoelectric polymer based microrobotic actuator 2-3
2.1.1. The I-Swarm microrobot structure: 2-4
2.1.2. Actuator motion: 2-6
2.1.2.1. Design and manufacturing: 2-6
2.1.2.2. Physical model 2-7
2.1.2.3. Experimental test: 2-11
2.1.3. Contact sensing tool: 2-17
2.1.3.1. Design and manufacturing: 2-17
2.1.3.2. Physical model: 2-17
2.1.3.3. Experimental test 2-21
2.1.3.4. Control system 2-23
2.1.4. Conclusions: 2-24
2.2. Ionic polymer based microrobotic actuator. 2-27
2.2.1. The underwater microrobotic structure: 2-28
2.2.2. Actuator motion 2-31
2.2.2.1. Design and manufacturing: 2-31
2.2.2.2. Empirical model: 2-32
2.2.3. Motion control : 2-36
2.2.3.1. Simulation results: 2-40
2.2.3.2. Experimental validation 2-42
2.2.4. Manufacturing ionic polymers IPMC 2-48
2.2.4.1. Chemical deposition method. 2-48
2.2.4.2. Physical deposition by thermal evaporation 2-50
2.2.4.2.1. Sample preparation procedure: 2-51
2.2.4.2.2. Adhesion improvement: 2-52
2.2.4.2.3. Sodium counter-ion exchange 2-55
2.2.4.3. Experimental measurements: 2-55
2.2.5. Conclusions: 2-60

2.3. References:.....2-62

3. POWER HARVESTING FROM VIBRATIONS 3-1
3.1. General model for power harvesting from vibrations.....3-3
3.2. Piezoelectric power harvesting 3-10
3.2.1. Model for piezoelectric power harvesting from vibrations 3-15
3.2.1.1. Power generation with resistive load 3-21
3.2.1.2. Power generation with a complex load:.....3-22
3.2.1.3. Effectiveness function: 3-23
3.2.2. Micro power generation (MPG) device 3-24
3.2.2.1. Model identification:.....3-25
3.2.2.1.1. Mechanical measurements H(s).....3-26
3.2.2.1.2. Electrical measurements G(s) 3-27
3.2.2.1.3. Free deflection measurements R(s)/s:.....3-28
3.2.2.1.4. Parameter identification.....3-29
3.2.2.2. Model validation 3-31
3.2.2.2.1. Power generation with Resistive load.....3-31
3.2.2.2.2. Power generation with complex load.....3-35
3.2.3. Electronic circuitry for optimum energy management 3-37
3.2.3.1. AC/DC rectifier.....3-38
3.2.3.2. DC/DC buck boost converter:.....3-41
3.2.3.3. Power management.....3-46
3.2.4. Conclusions.....3-47
3.3. IPMC power harvesting 3-50
3.3.1. Model for ionic polymer power harvesting from vibrations.....3-51
3.3.2. Micro power generation (MPG) device 3-52
3.3.3. Model identification.....3-53
3.3.3.1. Electrical impedance.....3-54
3.3.3.2. Mechanical impedance 3-58
3.3.3.3. Free deflection 3-62

3.3.3.4. Model performances discussion 3-66
3.3.4. IPMC power generation performances 3-68
3.3.5. Conclusions 3-75
3.4. References: 3-77

4. FINAL CONCLUSIONS 4-1

A. APPENDIX A A-1
A.1. Euler-Bernoulli cantilever beam A-2
A.2. Piezoelectric bimorph cantilever smart beam A-8
A.2.1. Coefficient a11 ..... A-11
A.2.2. Coefficient a12 ..... A-12
A.2.3. Coefficient a21 ..... A-14
A.2.4. Coefficient a22 ..... A-14
A.3. Piezoelectric multilayer cantilever smart beam. A-16
A.4. Piezoelectric multilayer cantilever smart beam sensor/actuator: A-19
A.4.1. Short circuit conditions or charge sensing A-21
A.4.2. Open circuit conditions o Voltage sensing A-22
A.5. Piezoelectric multilayer cantilever smart beam with base excitation.... A-23

B. APPENDIX B B-1

LIST OF PUBLICATIONS …….

FIGURE LIST

1. Introduction

Figure 1-1 Poling process for a piezoelectric material. a) Polarization vectors oriented randomly, b) Polarization vectors aligned in applied electric field direction, c) Remanent polarization. 1-10
Figure 1-2a) Hysteresis curve for polarization. b) Relative increase/decrease in dimensions (strain S) in direction of polarization. Picture obtained from [APC INTER] 1-11
Figure 1-3 Crystal structure of a traditional piezoelectric ceramic a) At temperature above Curie point a cubic lattice with symmetric arrangement of positive and negative charge is formed. b) At temperature above Curie point a tetragonal lattice is formed possesing a electric dipole. 1-11
Figure 1-4 Schematic illustration showing random stacks of amorphous and crystal lamellae in piezoelectirc polymer. a) Represents the morphology after the film is melt cast, b) After orientation of the film by mechanically stretching to several times its original length, c) After depositing metal electrodes and poling through the film thickness. Picture obtained from Harrison2001. 1-13
Figure 1-5 PVDF structure. 1-14
Figure 1-6 P(VDF-TrFE) structure. 1-14
Figure 1-7 Reference axes. 1-15
Figure 1-8 IPMC structure. 1-17
Figure 1-9 A schematic diagram of the typical IPMC artificial muscle and its actuation principle. Picture obtained from Shahinpoor2001. 1-18
Figure 1-10 Two SEM micrographs (top) showing the cross-section (left) and close-up (right) of a typical IPMC. The bottom graph shows an x-ray line scan of Pt. As can be noticed, Pt is dense at the surface. Picture obtained from Shahinpoor2001. 1-18

Figure 1-11 A schematic diagram of the typical IPMC and its sensing principle. 1-19
Figure 1-12 SEM image of a silicon mirror assembly with a spider mite (http://mems.sandia.gov/) 1-22
Figure 1-13 Schemtic draw of a microrobot structure..... 1-24
Figure 1-14 Open loop motion control scheme. 1-26
Figure 1-15 Closed loop motion control scheme. 1-26
Figure 1-16 MINIMAN microrobot. 1-28
Figure 1-17 MICRON robot. 1-29
Figure 1-18 I-SWARM robot. 1-31
Figure 1-19a) Tadpole robot picture. At the left side there is the main body of the robot and at the rigth the polymer fin. b) Schematic draw for the tadpole robot structure. The body conatins the controller and the battery, while the tail is based on a IPMC actuator and the polymer fin. The total length of the robot is aprox 10cm. Figure obtained from Kim2005. 1-33
Figure 1-20 Picture for the MICRON setup with power floor. Picture obtained from the MICRON webpage. 1-43
Figure 1-21 Arena for the I-Swarm robots. Picture obtained from the ISWARM webpage. 1-44

2. Motion control in microrobotics

Figure 2-1 Five I-Swarm microrobots standing around an ordinary paper clip. Picture obtained from Snis2008_2. 2-4
Figure 2-2 The I-SWARM microrobot with sensors, communication, electronics, power source and locomotion capabilities is shown. 2-5
Figure 2-3 Direction motion possibilities of the microrobots 2-6
Figure 2-4 Schematic draw of the mulitlayer structure of the actuators, the image is not in scale. 2-7
Figure 2-5 Schematic draw with the intensive variables “F” force, “V_{in}” voltage and the extensive, “u” deflection and “i” current. 2-8

Figure 2-6 a) Picture of the PCB with the electrcical connector pins. b) Zoom of the legs with the conductive glue. 2-11
Figure 2-7 a) Top view of the experimental setup with the displacement sensor and the PCB. b) Later view of the experimental setup. 2-12
Figure 2-8 Experimental and simulated results for the microrobot leg response to a sinusoidal voltage sweep. 2-13
Figure 2-9 Experimental and simulated transfer function, at the top module, at the bottom phase. 2-14
Figure 2-10 Experimental response of the microrobot leg drived at its resonance frequency 7034Hz with a square signal 3.3V. 2-15
Figure 2-11 Picture of the locomotion and sensor platform of the ISWARM microrobot. Picture obtained from Snis_2008_2. 2-17
Figure 2-12 Schematic draw with the intensive variables "Va" actuation voltage and the extensive, "u" deflection and "Vs" sensor voltage. 2-18
Figure 2-13 Equivalent circuit for the microrobot tool. 2-21
Figure 2-14 a) Picture of the PCB with the electrcical connector pins. 2-22
Figure 2-15 Experimental and simulated results for the tool output voltage for a given 10V sinusoidal sweep input voltage. 2-23
Figure 2-16 Oscilloscope capture for the IC test. Channel 1 is input voltage and Channel 3 is output voltage. 2-24
Figure 2-17 Schematic draw of the microrobot structure. 2-28
Figure 2-18 The two displacement sensors analyzed; the CCD camera and the Laser displacement sensor. 2-29
Figure 2-19 Supplied 4*4cm^2 IPMC membrane from Discovery Technologies Inc. 2-31
Figure 2-20 Bubles formed in water due to hydrolysis when driving IPMC with 5V. a) straight beam, b) bend beam. 2-32
Figure 2-21 Step response for1cm*0.5cm IPMC strip. 2-34
Figure 2-22 Zoom showing the oscilations due to the natural frequency. 2-34

Figure 2-23 Fitted Step response: Blue line is experimental, Green line is fitted....2-35
Figure 2-24 MRAC basic blog scheme. 2-37
Figure 2-25 2nd order with relative degree of one MRAC control scheme. 2-37
Figure 2-26 Simulated step response. Up: (Green) output plant, (Blue) reference model output. Down: Error....2-41
Figure 2-27 Step response parameters adaptation simulated. TH0=θ0, TH1= θ1, TH2= θ2, THk = θk 2-41
Figure 2-28 Simulated 100mHz sinusoidal: Up: (Green) output plant, (Blue) reference model output. Down: Error....2-42
Figure 2-29 Parameters adaptation 100mHz simulated. TH0= θ0, TH1= θ1, TH2= θ2, THk = θk 2-42
Figure 2-30 Experimental setup for the MRAC implementation. 2-43
Figure 2-31 Experimental 100mHz Up :Green Output plant, Blue Ref model output. Down: Error....2-45
Figure 2-32 Parameters adaptation 100mHz experimental. TH0=θ0, TH1=θ1, TH2=θ2, THk =θk 2-45
Figure 2-33 Experimental 500mHz Up: Green Output plant, Blue Ref model output. Down: Error....2-46
Figure 2-34: Parameters adaptation 500mHz experimental. TH0=θ0, TH1=θ1, TH2=θ2, THk=θk....2-46
Figure 2-35 Experimental 1Hz Up: Green Output plant, Blue Ref model output. Down: Error 2-47
Figure 2-36 Parameters adaptation 1Hz experimental. TH0=θ0, TH1=θ1, TH2=θ2, THk=θk. 2-47
Figure 2-37 Two schematic diagrams showing different preparation processes: top left, a schematic diagram shows the initial compositing process; top right, its top view SEM micrograph; bottom left, a schematic diagram shows the surface electroding rocess, and bottom right, its top view SEM micrograph, where platinum has deposited predominately on top of the

initial Pt layer. Note that PIEM stands for perfluorinated ion exchange membrane. Pictures obtained from Shahinpoor2001 2-49
Figure 2-38 SEM micrograghs in cross-section of membrane electrode. 2, 4, 6 and 8 plating cycles respectively. Picture obtained from Onishi2000. 2-50
Figure 2-39 a) Schematic draw of the vaccum chamber of a Evaporator machine. b) Picture of the Univex 450 by Leybold. 2-51
Figure 2-40 a) Picture of two strip of IPMC with 15nm Ti and 400nm Au. The left side strip has never been wet. The right side strip has been immersed in watter. b) A microscope picture of the immersed sample surface with the NAVITAR x10. 2-52
Figure 2-41 a) Draw of the RIE machnie. A gas is insered in the chamber and an RF field produces plasma (pink), the plasma attach the sample. b) Picture of the Plasmalab 80 from Oxford Instruments used at Parc Científic de Barcelona. 2-53
Figure 2-42 a) SEM image of a Nafion surface. A small piece of dust is observed. b) SEM image of a Nafion treated with the RIE. 2-54
Figure 2-43 Picture of the samples, the golden are not treated with RIE and the mate is treated with RIE. 2-54
Figure 2-44 Hot plate with the smaples in a solution with NaCl salt. 2-55
Figure 2-45 Three samples studied: “A” is chemical deposited from Discovery Technology, “B” is the no-treated sample, “C” is the RIE treated sample. 2-56
Figure 2-46 Schematic draw of the setup for resonance frequency measurement. 2-57
Figure 2-47 Sinusoidal sweep response of the sample with physical deposition. 2-58
Figure 2-48 Sinusoidal sweep response of the sample with chemical deposition. 2-59
Figure 2-49 Frequency response of the Chemical and Physical desposited samples. 2-59

3. Power harvesting from vibrations

Figure 3-1 Spring mass damper with a sinusoidal force excitation applied at the mass. 3-3
Figure 3-2 Spring mass damper with displacement base excitation.....3-4
Figure 3-3 Representation of the power coefficient vs electrical and mechanical damping coefficient ratio. XI=ξ. 3-7
Figure 3-4 Shcematic draw of a cantilever piezoelectric based for vibration energy harvesting.....3-15
Figure 3-5 a)Lumped Equivalent Circuit for a piezoelectric cantilever composite beam. b) Equivalent Thevenin circuit. 3-18
Figure 3-6 Thevenin equivalent impedance Real and Reactive part for the piezoelectric based trasnducer Qp40w. 3-20
Figure 3-7 Power ratio function for the piezoelectric based trasnducer QP40w at the first mode. 3-23
Figure 3-8 a) Picture of the piezoelectric based QP40w from Mide Technology Corp. b) Schematic drawn of theQP40w cross section. 3-24
Figure 3-9 Two-port representation.....3-25
Figure 3-10 Picture of the experimental setup. 3-27
Figure 3-11 H(s) experimental transfer function....3-28
Figure 3-12 G(s) experimental transfer function....3-28
Figure 3-13 R(s)/s experimental transfer function 3-29
Figure 3-14 Experimental (black) and identified (grey) transfer functions.....3-30
Figure 3-15 1st mode transfer functions. a) Experimental Voltage, b) Simulated Voltage, c) Experimental Power, d) Simulated Power.....3-32
Figure 3-16 2nd mode transfer functions. a) Experimental Voltage, b) Simulated Voltage, c)Experimental Power, d) Simulated Power.....3-32
Figure 3-17 4th mode transfer functions. a) Experimental Voltage, b) Simulated Voltage, c) Experimental Power, d) Simulated Power.....3-33

Figure 3-18 a), c), e) are the power ratio funcion, and b), d), f) are the optimal inductanceload for a complete match for the first second and fourth mode respectively 3-35
Figure 3-19 4th mode power transfer fucnions with a 50mH load inductance. a) experimental, b) simulation. 3-36
Figure 3-20 a) Schematic of the standar AC connection. b) Schematic of the full bridge AC/DC rectifier 3-38
Figure 3-21 Waveforms measurements of the full bridge rectifier circuit with a load resistor 1.2kΩ. 3-39
Figure 3-22 Generated voltage vs resistors loads. V_{out}AC is the amplitued with the AC circuit, and V_{out}AC/DC is the voltage using the AC/DC circuit. 3-40
Figure 3-23 Power vs load resistor with the AC circuit and with the AC/DC circuit. 3-40
Figure 3-24 Schematic draw of the buck-boost DC/DC converter. 3-41
Figure 3-25 Picture of the buck-boost electrical circuit used for the measurements 3-42
Figure 3-26 Exp. measurements of the waveform signals of the buck-boost circuit with a 12kΩ load resistor. 3-43
Figure 3-27 Output power for load resistor using the buck-boost converter. 3-43
Figure 3-28 Buck-boost iInput and output voltage vs load resistors. 3-44
Figure 3-29 Output power for load resistor using the buck-boost configured with fs=9.6kHz, 25,2kHz and 54kHz to lead its input resistance as 2133Ω, 5.6kΩ and 12kΩ respectively. 3-45
Figure 3-30 Buck-boost converter input and output voltage vs load with fs=9.6kHz, 25,2kHz and 54kHz to lead its input resistance as 2133Ω, 5600 Ω and 12kΩ respectively 3-45
Figure 3-31 Power bursting shcematic drawn 3-46
Figure 3-32 Ionic polymer sample with Na+ as counter ion. 3-53
Figure 3-33 a) Piezoelectric ideal electrical impedance, b) ionic polymer electrical impedance. 3-55

Figure 3-34 Fitting curves for the absorbed current. Green is fitted and blue is measured. 3-57
Figure 3-35 Electrical admittance Bode plot. Green is fitted and blue is measured. 3-57
Figure 3-36 Equivalent permitivitty μ(s) frequency response. 3-58
Figure 3-37 Tip displacement response to an input impulse. 3-60
Figure 3-38 Power spectral density of the tip displacement. 3-60
Figure 3-39 Mechanical configuration for Young modulus measure 3-61
Figure 3-40 Simulated and measured tip force for an input base displacement. 3-62
Figure 3-41 Experimental and fitted tip deflection for a sinusoidal sweep applied voltage. 3-64
Figure 3-42 Experimental and simulated Bode plot for the transferfunction deflection/voltage. 3-65
Figure 3-43 Frequency response of the identified coupling coefficient. 3-65
Figure 3-44 Configuration for sening characterization. 3-67
Figure 3-45 Experimental and simulated bode plot for the sensor transfer function short circuit current for an applied tip displacement. 3-68
Figure 3-46 Experimental and simulated the short circuit curre vs base displacement transfer function (A/m). 3-71
Figure 3-47 Experimental and simulated open circuit voltage vs base displacement transfer function (V/m). 3-72

Appendix A

Figure A-1 Simple beam in transverse vibration and a free body diagram of a small element of the beam as it is deformed by a distributed force per unit length, denoted by f(x,t). A-3
Figure A-2 Representation of the four first mode shapes for a clamped-free beam. A-7
Figure A-3 a) Bimorph parallel configuration. b) Bimorph serial configuration. A-8
Figure A-4 Representation of the slope or spatial differentiation of the four first mode shapes in a clmape-free configiration. A-14

Figure A-5 Representation of the curvature of the beam or second spatial differentiation for the firts four mode shape in a clamped-free configuration. A-15
Figure A-6 Generic multilayer piezoelectric based cantilever. A-17
Figure A-7 Integration limits from the neutral axis A-17
Figure A-8 Generic multilayer actuator/sensor piezoelectric based cantilever. A-19
Figure A-9 Generic mulitlayer piezoelectric cantilever with base vibration for power harvesting. A-23

Appendix B

Figure B-1 Matlab-Simulink block diagram for the MRAC simulations. B-1

TABLE LIST

1. Introduction

Table 1-1 Comparison table: advantages and disadvantages among electronics and ionic polymers. Table obtained from Bar-Cohen2000_2. 1-8
Table 1-2 Comparison table for Smart materials performances. Table extracted from Herr2004 1-8
Table 1-3 Comparison table for piezoelectric ceramic PZT and piezoelectric polymer PVDF.....1-16
Table 1-4 Common virbation sources inside a laboratory. Table obtained from MELESGRIOT.....1-36
Table 1-5: Summary of maximum energy density of three types of converters. Table obtained from Roundy2003.....1-38
Table 1-6 Comparison of energy scavenging and energy storage methods. Note that leakage effects are taken into consideration for batteries.Table obtained from Roundy2003.....1-42

2. Motion control in microrobotics

Table 2-1 Material and geometrical parameters for the legs of the microrobots 2-12
Table 2-2: Fitted values for the transfer fiunction model.....2-35
Table 2-3 Measured surface resistance for the three samples. 2-56
Table 2-4 Measured values for the resonance frequency for the three samples.....2-57
Table 2-5 Measured values for the Capacitance for the three samples 2-57

3. Power harvesting from vibrations

Table 3-1 Quick pack QP40w piezoelectric transducer specifications 3-24
Table 3-2 QP40w identified model parameters for the 1st 2nd and 4th vibration modes.....3-30
Table 3-3 Maxmimum power generation and optimal load for a impedance modulus adaptation for the three modes. Experimental vs Simulated values 3-33
Table 3-4 Identified parameters of the equivalent permittivity.....3-57
Table 3-5 Identified parameters of the coupling coefficient function. 3-66

Nomenclature

A = cross sectional area
A_{in} = input base acceleration
β = air damping coefficient
B = internal damping coefficient
B_{in} = input base velocity
c = damping coefficient
c_{elec} = electrical induced damping
c_{mec} = mechanical induced damping
c_n = modal damping coefficient
C_A = actuator capacitor
C_n = equivalent modal capacitor
C_p = piezoelectric capacitor
C_S = sensor capacitor
d_{ij} = piezoelectric coefficient
D = duty cycle
D_i = electric displacement vector
η = effectiveness
ε_o = vacuum permittivity
ε_r = relative permittivity
ε_{ij} = dielectric permittivity
E_i = electric field
E_{elec} = electrical energy
E_{dens} =energy density
f = applied force per unit length
F = input applied
F_{blk} = blocked force
F_{on} = induced force
γ = input frequency
g = adaptation gain
G_n = modal gain factor
h = height
i = electrical current
I = cross section area inertial moment
J = current density
k = spring constant
k_{ij} = electromechanical piezoelectric coupling coefficient
K_n = modal spring constant
λ_n = normalized natural frequency
L = length
L_c = clamped length
L_F = free length
m = mass
m_n = modal mass
M = bending moment

M_v = induced bending moment
μ = relative permittivity
N_n = transformer modal gain
ω = frequency
ω_n = natural frequency
p = water pressure
P = polarization vector
P_{av} = average electrical power
P_{mod} = average electrical power with modulus impedance adaptation
P_{compl} = average electrical power with complex impedance adaptation
Q = electrical charge
Q_F = solvent flux
ρ = mass density
r = radius of curvature
r_n = modal temporal equation
R = resistance
R_{dc} = leakage resistance
R_e = electrode resistance
R_{TH} = Thevenin equivalent resistance
s_{ij} = compliance matrix
S_i = mechanical strain
θ = adaptation parameter
Θ_n = modal electromechanical coupling term
T = period
T_{disch} = discharging time
Ti = mechanical stress
u = deflection
u_n = modal deflection
U_n = modal deflection
v = deflection velocity
V = voltage
V_{SH} = shear force
w = width
W_n = mode shape
ξ = damping ratio
ξ_{elec} = damping electrical ratio
ξ_{mec} = damping mechanical ratio
X_{TH} = Thevenin equivalent reactance
y_b = base vibration displacement
Y = young modulus
Y_C = static young modulus
Z = relative displacement
Z_{TH} = Thevenin equivalent impedance

1. INTRODUCTION

Microrobotic systems have sustained a rapid evolution as new intelligent materials with advances features and capabilities have appeared. The new technological trends involve the design of autonomous, efficient and sustainable systems with full functionalities integration. These trends have entailed the research on advanced materials that exhibit electromechanical responses. Some of the expectations for these new intelligent or "Smart" materials are: microsystems technology compatibility, active response to electrical and mechanical stimuli and high degree of reliability and biocompatibility.

The primary goal of the research presented in this thesis is to enhance the understanding of the performances and capabilities of some "smart materials" in microrobotic systems. The thesis focuses in the use of three different smart material families in microrobotics motion control and power harvesting. In this introduction the reader is initiated in the field of smart materials with particular focus in three families which are specifically used in microrobot applications: the piezoelectric ceramics, the piezoelectric polymers and the ionic polymers. Subsequently, the introduction continues giving a general view of the microrobotic systems. Here, the advantages and disadvantages of using the above mentioned materials in microrobot motion control, are discussed within the description of various microrobotic projects classified in three families according to the application. Afterwards, the introduction goes on to a discussion of the power solutions for microrobots. This discussion is centered in those solutions that convert dust energy from the environment (the microrobot´s surroundings) into useful electrical power. A special emphasis is done in the use of the smart materials in the conversion of mechanical vibrations into electrical energy. The introduction closes with the presentation of this thesis' objectives and the way they are accomplished.

1.1. Smart systems and materials

There is a constant grown interest in the design of artificial systems that could mimic functionalities accomplished in biological systems through the emulation of their capabilities and integrated design [Bar-Cohen2003]. The pass through evolution has provided these systems with very interesting functionalities. Biological systems have the exceptional quality of being able to interact with the environment and take decisions based on the information they get from it. The human body is a perfect example of an advanced biological system that reacts to the world by sensing and responding. When our hand touches a hot object, it sends a signal to the brain, this signal is processed in the brain and a decision is made. The brain then sends a signal to the muscles and the hand is removed from the hot object. From a technological point of view, the design of analogous mechanisms that can interact "smartly" with their environment could have a tremendous impact in many fields. Those systems are named "Smart systems or structures".

It's quite difficult to find an accepted definition for Smart systems by the scientific community, a possible one is: "structures that continuously and actively monitor and optimize themselves and their performance through emulating biological systems with their adaptive capabilities and integrated designs." [Schwartz2002]. Nowadays, the drive to innovation is stronger than ever. Consequently, expectations and needs for engineering applications have increased tremendously. Some of these requirements and expectations are summarized as [Akhras2000]:

- High degree of reliability, efficiency and sustainability. Not only of the structure but also of the whole system.
- High security of the infrastructures particularly when subjected to extreme and unconventional conditions.
- Full integration of all the functions of the system.
- Continuous health and integrity monitoring.
- Damage detection and self-recovery.
- Intelligent operational management system.

In order to accomplish with the technology requirements the prospects for the Smart systems are [Akhras2000]:

- New sensing materials and devices.
- New actuation materials and devices.
- New control devices and techniques.
- Self-detection, self-diagnostic, self-corrective and self-controlled functions of smart materials/systems.

The key point in the evolution of the Smart systems is the appearance of a new class of materials able to sense and respond at the same time, the so called "Smart Materials". Actually by definition smart materials are those materials that can sense and respond to the environment around them in a predictable and useful manner [parliament2008]. The use of materials that react to the environment producing some kind of response is not new. In fact, in 1824, Brewster [Brewster1824] had observed the phenomenon of pyroelectricity in various crystals, among which Rochelle salt, but perhaps the first systematic studies where those of brothers Pierre and Jacques Curie in 1880 who discovered piezoelectricity [Curie1880]. Following the work from Pierre and Jacques Curie in 1916, the first engineering application using piezoelectric ceramics was developed by Langevine. It consists of an underwater ultrasonic source [Hill1973]. The use of polymers as smart materials also dates from 1880. In that year, Roentgen conducted a first experiment where a plastic rubber band was observed to change its mechanical properties in response to electric field application. A further milestone was recorded at 1925 with the discovery of the piezoelectric polymer called electred [Eguchi1925]. Since those days, many different types of smart materials with different performances have been discovered and designed. In the last decade, new polymers have emerged that respond to electrical stimulation with a significant shape or size change. This kind of polymers is called Electro Active Polymers (EAP). The attractive characteristics of polymers such as light weigh, fracture tolerance, flexibility and sometimes biocompatibility, have opened the door to a large number of new applications unattainable in the past. Nowadays Smart materials and Smart systems are different from existing materials and structures because they have the means to sense their surrounding environment, process the sensory information, and through commands the actuators act in a beneficial and controlled way to respond to the changing environment.

New applications arouses in a wide variety of fields. In civil engineering: for structural health monitoring or vibration suppressions [El-Diraby2002]. In marine engineering: for new propulsion methods [Pitt2002] or in adaptive sails whose weave adapts to wind speed [Spillman1996]. In aeronautical applications: with adaptive wings [DARPA]. In space application with new inflatable structures [Bar-

Cohen2000]. In biomedicine with active catheters [Haga1998], prosthetics [Herr2003] and haptic interfaces for assisted surgery [MEMICA]. In robotics and androids [Hanson2001], as well as in microrobotics [Seyfried2004] and much more applications.

During the last decade the scientific community has watched, amazed, at the fast evolution in smart materials research. This evolution has entailed an increase in research publications of this field. In response to this evolution in the research of smart materials, now conferences and publication of journals specifically on this field are taking place. Perhaps, one of the most important conferences in the field is the EADAP (ElectroActive Polymer Actuators and Devices) that takes place every year in San Diego. This conference is supported by the SPIE society. Also, two relevant journals are completely dedicated to this field: the Smart Materials and Structures from IOP publishing and the Journal of Intelligent Material Systems and Structures from SAGE publishing.

Today, many researchers, Institutes, companies and universities are carrying out research on smart materials. However, some of the more relevant research groups in this field are found in the United States of America others, are located in Europe, Japan, China and South Korea. From the American part is important to note the participation of the Virginia Polytechnic Institute and its CIMSS (Center of Intelligent Material Systems and Structures), the Artificial Muscles Research Institute (AMRI) from Maine and the Nondestructive Evaluation and Advance Actuators (NDEAA) Laboratory from NASA. From the European part, the Swiss federal laboratory for materials EMPA, Micromuscle AB from Sweden, the University of Bristol in UK and the Universities of Pisa and Catania in Italy. From Japan, we have the University of Osaka and Kobe and the EAMEX Corporation. From South Korea, there is the Inha University. These Institutions, together with a huge number of other groups, universities and researchers from around the world, are the ones responsible for the evolution of these materials. In the following lines, a classification with a brief explanation of the different smart material families is shown.

1.1.1. Classification

Nowadays there are a large number of different types of smart materials. However, it is possible to classify them by families. At this point, the materials are first divided in two major groups: the non-polymeric materials and the polymeric materials. In the polymeric materials, or EAPs, a subdivision in two groups is done. The first group is formed by those polymers electrically activated named “Electronic EAPs”. The other group is formed by those polymers that involve mobility or diffusion of ions, they are named “Ionic EAPs”. In the following lines, some of the most important smart materials from each family are briefly presented.

a) Non-polymeric smart materials:

Piezoelectric ceramics: Piezoelectrics are materials that exhibit an electrical polarization with an applied mechanical stress (direct effect), or a dimensional change with an applied electric field (converse effect). Piezoelectrics is a mature technology with numerous applications in microrobotics [Brufau2005], adaptive optics [PI], microphones [KNOWLES], etc. The piezoelectric effect is extensively discussed in section 1.1.2.

Shape memory alloys (SMA): SMAs are actuators that, upon proper thermal and mechanical treatment, have the ability to remember up to two shapes which they had previously occupied. Thus applying heat the alloy change from one state to the other. Some of the current SMA applications include use in biomedicine as catheters [Haga1998], spacecraft [NASA], aircraft [DARPA], automobiles [Colli2006], robotics [Liu2004], etc.

Electrorheological/Magnetorhelogical fluids: Electro-rheological (ER) and magneto-rheological (MR) materials are fluids, which can experience a dramatic change in their viscosity. These fluids can change from a thick fluid (similar to motor oil) to nearly a solid substance within the span of a millisecond when exposed to a magnetic or electric field; the effect can be completely reversed just as quickly when the field is removed. MR fluids experience a viscosity change when exposed to a magnetic field, while ER fluids experience similar changes in an electric field. The composition of each type of smart fluid varies widely. Some applications are in car shocks [Yao2002], haptic gloves [MEMICA], damping washing machine vibration [Chrzan2001], etc.

Elesctrostrictives: These materials have the same properties as the piezoelectrics, but the mechanical change is proportional to the square of the electric field. This characteristic will always produce displacements in the same direction. Some applications are micropositioning [PI] and adaptive optics [Hom2000].

Magnetostrictors: These materials (used in actuators) exhibit a change in shape (strain or elongation) when an external magnetic field is applied. The reverse effect is called piezomagnetism (used in sensors), where a magnetic field is produced/altered upon application of a mechanical strain. Magnetostrictive sensors and actuators are used for MEMS mirror deflectors [NASA], vibration and noise control [Fukuda2003], motors [Kim2002] and position and mechanical torque sensors [Odachi2001].

b) Polymeric smart materials (EAP)

Electronic EAPs:

Dielectric EAPs: Polymers with low elastic stiffness and high dielectric constant can be used to induce large actuation strain by subjecting them to an electrostatic field. This dielectric EAP, also known as electro-statically stricted polymer (ESSP) actuators, can be represented by a parallel plate capacitor The induced strain is due to electrostatic forces which are proportional to the square of the electric field multiplied by the dielectric constant and is inversely proportional to the elastic modulus. Some applications are in artificial muscles [Kwak2005] and robotics [Bar-Cohen2000].

Ferroelectric polymers: A ferroelectric polymer is a polymer possessing spontaneous polarization that can be reoriented applying an electric field. There are different types of ferroelectric polymers some of them are piezoelectric polymers, electrets polymers or electrostrictive polymers. These materials are used in different applications as in microrobotics as motion actuators [Brufau2006], as force sensors [Dario1984], etc. Two piezoelectric polymer types, the PVDF and the P(VDF-TrFE) are described in more detail at section 1.1.2.2..

Electrostrictive graft elastomers: The electrostrictive graft elastomer consists of flexible backbone chains, each with side chains, called grafts. Neighboring backbone grafts physically cross-link and form crystal units. The flexible backbone chain and the crystal graft unit consist of polarized monomers, which contain atoms with electric partial charges, generating dipole moments. When the elastomer is placed into an electric field, external rotating moments are applied to the dipole moment. This stimulates electrostrictive strain in the graft elastomer. Some applications are focused on position actuators [Su2000].

Liquid Crystal Elastomers (LCE): LCE are composite materials that consist of monodomain nematic liquid crystal elastomers and conductive polymers that are distributed within their network structure. The actuation mechanism of these materials involves phase transition between nematic and isotropic phases over a period of less than a second through temperature increase via Joule heating. The reverse process is slower, taking about 10 sec, and it requires cooling to cause expansion of the elastomer to its original length. Applications are in artificial muscles [Spillman2007], and mechanically tunable optical elements [Camacho-Lopez2004].

Ionic EAPs

Ionic Polymer Gels (IPG): Polymer gels can be synthesized to produce strong actuators, having the potential of matching the force and energy density of biological muscles. These materials (e.g., polyacrylonitrile) are generally activated by chemical reactions, changing from an acid to an alkaline environment causes the gel to become dense or swollen, respectively. When activated, these gels bend as the cathode side becomes more alkalinic and the anode side more acidic. However, the response of this multilayered gel structure is relatively slow because of the need to diffuse ions through the gel. Applications are in artificial muscles [Bar-Cohen2003], robotics [De Rossi1992] and androids [Hanson2001].

Conductive Polymer (CP): Conductive polymers typically function via the reversible counter-ion insertion and expulsion that occurs during redox cycling. Oxidation and reduction occur at the electrodes inducing a considerable volume change mainly due to the exchange of ions with an electrolyte. A sandwich of two conductive polymer electrodes (e.g., polypyrrole or polyaniline, or PAN doped in HCl) with an electrolyte between them forms an EAP actuator. When a voltage is applied between the electrodes, oxidation occurs at the anode and reduction at the cathode. Ions (H+) migrate between the electrolyte and the electrodes to balance the electric charge. Addition of the ions causes swelling of the polymer and conversely their removal results in shrinkage and as a result the sandwich bends. Some of it´s applications are in medical equipment [DREMED], artificial muscles [EAMEX] and valves for drug delivery [Abidian2006].

Ionic Polymer Metal Composite (IPMC): IPMC is an ionic EAP that bends in response to an electric activation as a result of mobility of hydrated cations inside its polymer network. IPMC material consists of a polymeric ionomer membrane covered with a metal to form the electrodes. The ionomer is designed and synthesized to selectively allow diffusion of mobile cations as well as a solvent (typically water) through nanoscale pores and channels of the polymeric matrix, while the anions are covalently bonded to the fixed polymer matrix. The actuation mechanism consists of applying an electric field between electrodes. This field produces a solvent flux of hydrated cations and free water through the cathode. This solvent flux creates an electro-osmotic differential pressure resulting in a bending motion towards the anode side of the IPMC. The use of IPMC is being extended to several different applications which are: linear actuators [Yamakita2005] and three-dimensional actuators [Kim2002], micro-grippers [Lumia2008], exoskeleton human joints [Shahinpoor2005], wing flaps [Lee2006], biomedical applications [Bonomo2008], etc. This material is discussed extensively in section 1.1.3.

Table 1-1 briefly shows a comparison of the main differences between electronic and ionic EAP [Bar-Cohen2000_2]. The electronic EAPs present faster responses than the ionic EAPs. This is due to the fact that the last ones involve motion of ions that process with certain inertia. Furthermore, the electronic ones are able to produce

higher forces and stand in DC. By the other hand the ionic EAPs are very interesting in biomimetic applications because ions are involved in their transduction effect. Actually in human muscles the release of ions Ca+ is responsible for turning on and off the conformational changes associated with muscle striction.

EAP type	**Advantages**	**Disadvantage**
Electronic EAP	- Can operate in room conditions for a long time. - Rapid response (ms levels). - Can hold strain under DC activation. - Induces relatively large actuation forces.	- Requires high voltages (~150 MV/m) - Requires compromise between strain and stress
Ionic EAP	- Requires low voltage - Provides mostly bending actuation (longitudinal mechanisms can be constructed) - Exhibit Large bending displacements.	- Except for CP, ionic EAPs do not hold strain under DC voltage - Slow response (fraction of a second) - Bending EAPs induce a relatively low actuation force - Except for CP, it is difficult to produce a consistent material (particularly IPMC) - In aqueous systems the material sustains hydrolysis at >1.23-V

Table 1-1 Comparison table: advantages and disadvantages among electronics and ionic polymers. Table obtained from Bar-Cohen2000_2.

To conclude with the smart materials classification, it is interesting to present a comparison table on the different families. Table 1-2 reports Shape Memory Alloys (SMA) as the material producing the highest mechanical stress thus the highest force. However, these materials are thermally activated so a very slow response is expected. Following the SMA, piezoelectrics, magnetostrictors and electrostrictors are materials producing high forces while consuming considerable amounts of power. On the other hand, the EAP produces low forces but high strains, thus relatively large displacements can be expected. Moreover, these materials have a low activation voltage.

Properties	**PZT**	**EAP**	**SMA**	**Electrostrictive**	**Magnetostrictive**
Actuation strain	0.1-0.3%	>10%	<8%	0.1%	0.58-0.81%
Stress (Mpa)	30-40	0.1-3	700	50	50
Reaction speed	µs	µs	s	µs	ms
Drive Voltage	50-800V	2-7V	10-150V	100V	10V
Consumed power	watts	mwatts	watts	watts	watts
Energy density ($J\ m^{-3}$)	10^2	10^3	10^7	10^3	10^3

Table 1-2 Comparison table for Smart materials performances. Table extracted from Herr2004

This thesis focuses on the study and application of three classes of smart materials, the piezoelectric ceramics (PZT), the piezoelectric polymers (PVDF) and the ionic polymers metal composites (IPMC). These materials have the same intrinsic features: first they respond with an induced mechanical strain when subjected to an external electric field, second they suffer charge redistribution when forced with a mechanical strain. These features make these materials adequate to use in microrobotics as bending actuators, sensors and even as micropower generators. Piezoelectric ceramics are used in those microrobotic systems where high forces and very precise motion is needed. Piezoelectric polymers allow the design of more flexible microrobots and an easier integration of force and displacement sensors. Ionic polymers metal composites open the door to new microrobot applications, such as those where very large strokes are needed and where underwater motion is required.

1.1.2. Piezoelectrics

The piezoelectric effect is a property that exists in many materials. The term "piezoelectric" comes from the Greek word "πιεζω" meaning stretch which is adjoin with the term "electric" from electricity. The rough translation is, therefore, pressure - electric effect. In a piezoelectric material, the application of a force or stress results in the development of a charge in the material. This is known as the direct piezoelectric effect. Conversely, the application of a charge to the same material will result in a change in mechanical dimensions or strain. This is known as the indirect piezoelectric effect.

Piezoelectricity was discovered at the Sorbonne in 1880 by Pierre and Jacques Curie [Curie1880]. The first step toward an engineering application was taken place around 1916, also in France by Paul Langevin [Hill1973], who constructed an underwater ultrasonic source consisting of a piezoelectric quartz element sandwiched between steel plates; this device was to serve for submarine detection. While piezoelectricity did not become practical for this purpose until many years later, experimentation started during World War I [Graff1981].

Piezoelectric materials belong to the same class of materials as dielectrics and ferroelectrics. Therefore, in order to talk about the piezoelectric effect, it is important to start with dielectrics. A dielectric material is one that when subjected to an external electric field, its internal charges suffer a small displacement. When a dielectric material is submitted to an external electric field, the separation of charges forms a dipolar moment. There are two types of dielectrics. The first ones, are the dielectrics with non-polar molecules, in which the dipolar moment for each molecule is null. This is because the center of positive and negative charges coincides. The other ones are the dielectrics with polar molecules which, due to the internal charge distribution, each presents a dipolar moment.

Ferroelectric materials are those polar dielectric materials that, when submitted to an external electric field, the direction of polarization of their single crystals monodomains changes. All piezoelectric materials are ferroelectrics but not all ferroelectrics are piezoelectrics. The piezoelectrics are those ferroelectric materials that present a mechanical deformation when polarization vectors reorients. While piezoelectric effect is observed in some natural crystal structures as in quarts, tourmaline, Rouchelle salt, etc., this effect is not potent enough. Therefore, development and manufacturing of high level piezoelectric ceramics has been necessary to obtain materials with increased piezoelectric effect.

Normally, when a piezoelectric material is synthesized, it does not have a net polarization. To transform the material to piezoelectric it has to be treated in some way, this is the poling process that serve to align the internal dipoles.

The poling process begins with the material having all the polarization vectors of the monodomains oriented randomly Figure 1-1a. Applying a sufficiently high electric field at a temperature slightly below the Curie point, the dipoles align in the direction of the field Figure 1-1b. During this alignment the material strains due to the reorientation of the monodomains in the direction of the electric field. When the electric field and temperature are released, most of the dipoles are locked in a configuration near alignment. This is an anisotropic dielectric state Figure 1-1c.

Analogous to corresponding characteristics of ferromagnetic materials, a poled ferroelectric material exhibits hysteresis. Figure 1-2a shows a typical hysteresis curve created by applying an electric field to a piezoelectric ceramic element. The curve represents the history of the polarization vector under electric field application. Figure 1-2b plots the relative change in the dimension of the ceramic element along the direction of polarization, corresponding to the change in the electric field.

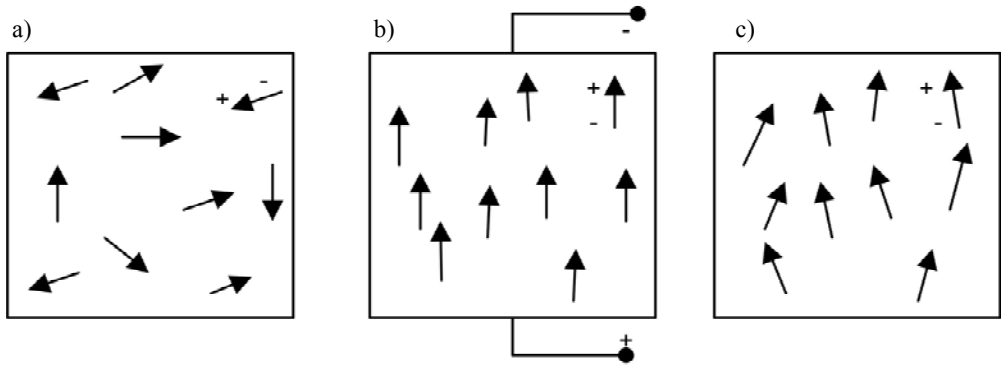

Figure 1-1 Poling process for a piezoelectric material. a) Polarization vectors oriented randomly, b) Polarization vectors aligned in applied electric field direction, c) Remanent polarization.

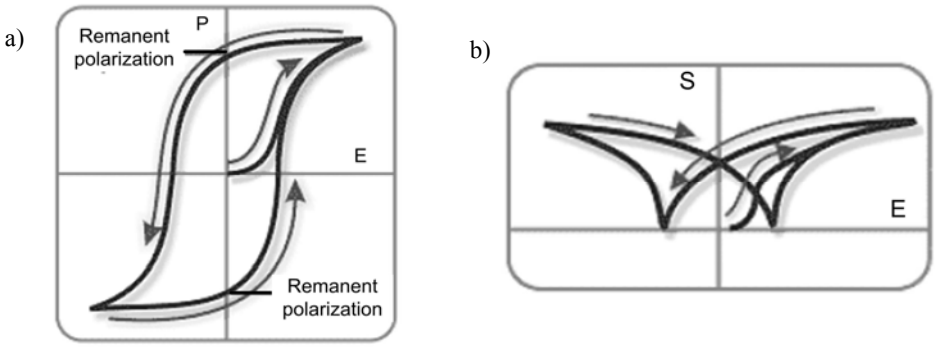

Figure 1-2a) Hysteresis curve for polarization. b) Relative increase/decrease in dimensions (strain S) in direction of polarization. Picture obtained from [APC INTER]

1.1.2.1. Piezoelectric ceramics

Piezoelectric ceramics belong to the class of the Perovskites crystal structures. They form a crystalographic structure, rombohedral and tetragonal as shown in the Figure 1-3. The representative chemical formula for perovskite compounds is ABO_3, where A is an ionic divalent atom (A^{2+}), B is a tetravalent metal (B^{4+}) and O the oxygen (O^{2-}). In its composition it is normal to identify niobate, titanate o zirconate. The first piezoelectric ceramic was synthesized in the early 40's and it was the BaTiO3. Nowadays the most frequently used is the so called Lead Zirconate Titanate or (PZT) with the formula $Pb(Zr_xTi_{1-x})O3$. This material has large piezoelectric properties and was first discovered by Jaffe et al. in 1958 [Jaffe1958].

To prepare a piezoelectric ceramic, fine powders of the metal oxide component are mixed in specific proportions and then heated to form a uniform powder. The powder is mixed with an organic binder and is formed into structural elements having the desired shape (discs, rods, plates, etc.). The elements are fired according to a specific time and temperature program, during which the powder particles sinter and the material attains a dense crystalline structure. The elements are cooled, then

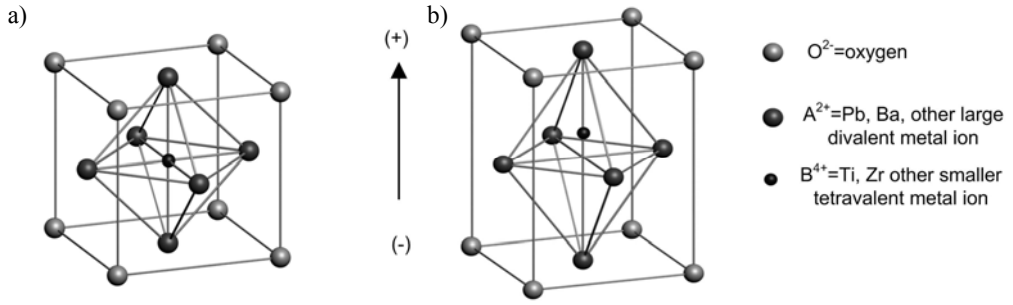

Figure 1-3 Crystal structure of a traditional piezoelectric ceramic a) At temperature above Curie point a cubic lattice with symmetric arrangement of positive and negative charge is formed. b) At temperature above Curie point a tetragonal lattice is formed possesing a electric dipole.

shaped or trimmed to specifications, and electrodes are applied to the appropriate surfaces. A fired ceramic is a semi-organized mass of fine crystallites. Above a critical temperature, the Curie point, each perovskite crystal in the fired ceramic element exhibits a simple cubic symmetry with no dipole moment. Figure 1-3a) shows a schematic of a cubic lattice. At temperatures below the Curie point, however, each crystal has tetragonal or rhombohedral symmetry and a dipole moment. Figure 1-3b) shows the tetragonal lattice. The dipole moments are oriented differently among different ceramic grains. Regions of like-oriented dipoles are called domains and each domain carries a net dipole moment. However the domains are randomly oriented and the element has no net polarization. To finally give a net polarization to the elements, it is yield to a poling process.

1.1.2.2. Piezoelectric polymers

The word "polymer" come from the Greek words "πολυ" that is "many", and "μέρος" that is "part". A polymer is a very big organic molecule composed of repeating structural units connected by covalent chemical bonds. Polymers compared to ceramics, are much lightweight and poses more flexibility, are readily manufactured into large areas and can be cut and formed into complex shapes. These features make piezoelectric polymers capable of performing some applications that piezoelectric ceramics can not perform.

There are four critical aspects for a polymer to be piezoelectric regarding morphology [Harrison2000]. These are: a) the presence of permanent molecular dipoles, b) the ability to orient or align the molecular dipoles, c) the ability to sustain the dipole alignment once it is achieved, d) the ability of the material to undergo large strains when mechanically stressed.

In order to render a semicrystalline polymer into a piezoelectric polymer, the semicrystalline polymer must have a polar crystalline phase. The semicrystalline polymer morphology consists on crystalline regions within amorphous regions. Figure 1-4a) depicts an illustrative draw of the polymer morphology after polymerization. Most semicrystalline polymers have several polymeric phases. To induce a polar crystalline phase, a material preparation procedure is needed. It consist on mechanically stretching the polymer up to several times its original length, this aligns its amorphous strands in the film plane. Figure 1-4b) depicts the alignment after mechanically stretching. Then the application of a high electric field facilitates the uniform rotation of the crystallites. Figure 1-4c) depicts the final morphology.

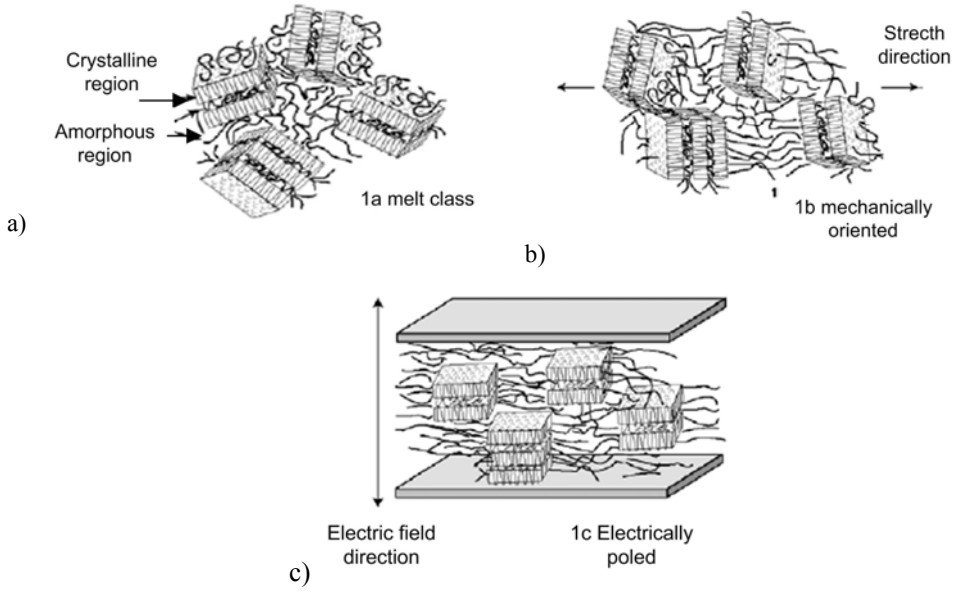

Figure 1-4 Schematic illustration showing random stacks of amorphous and crystal lamellae in piezoelectirc polymer. a) Represents the morphology after the film is melt cast, b) After orientation of the film by mechanically stretching to several times its original length, c) After depositing metal electrodes and poling through the film thickness. Picture obtained from Harrison2001.

As in the case of ceramics, piezoelectric polymers belong to the ferroelectrics class, they have a spontaneous polarization and the polarization can be reversed. Thus piezoelectric polymers present non-linear effects as hysteresis.

One of the pioneers in the field of piezoelectric polymers was Kawai [Kawai1969]. He observed in 1969 a strong piezoelectric effect in a polyvinilydene fluoride (PVDF). Since then, a strong research activity in PVDF piezoelectric polymers and its copolymers trifluorethylene (TrFE) and tetrafluorethylene (TFE) has been taking place. In the following paragraphs, a brief explanation of these two piezoelectric polymer families is offered.

Polyvinylidene fluoride (PVDF)

The polyvinylidene fluoride is a semicrystalline polymer with the repeating unit $–CH_2-CF_2-$, see Figure 1-5. This unit is inherently polar. The spatially symmetrical disposition of the hydrogen and fluorine atoms along the polymer chain gives rise to unique polarity effects that influence the electromechanical response, solubility, dielectric properties, crystal morphology and yield to an unusually high dielectric constant

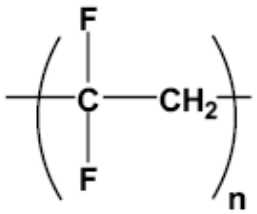

Figure 1-5 PVDF structure.

PVDF is typically 50% crystalline and has at least four crystal phases of which at least three are polar. The most stable non-polar phase results upon casting PVDF from melt. The phase is transformed into polar phase by stretching the material at elevated temperatures. After poling, the polar phase presents a good stability at room temperature.

Poly(vinylidene fluoride-trifluorethylene) P(VDF-TrFE)

This copolymer is formed from the polymerization of vinylidenefluoride (VDF) and trifluorethylene (TrFE) Figure 1-6

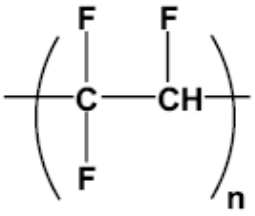

Figure 1-6 P(VDF-TrFE) structure.

The advantage of this copolymer is that it forms a polar phase after polymerization which eliminates the need for mechanically stretching. The addition of the fluoride atom into the chain increases the crystallinity up to 90%, yielding a higher remanent polarization and lower coercive fields. The TrFE monomer has a smaller dipole moment so the total piezoelectric constant of the copolymer is reduced compared to the PVDF. Although this decreases its piezoelectric features, one of the advantages of using the P(VDF-TrFE) is its ability to process easier and faster than other materials, making this a favorable characteristic for its use in several applications.

1.1.2.3. Modeling piezoelectrics

Nowadays there are a huge number of applications that uses piezoelectric materials. For over a century, researchers have been investigating and using piezoelectric materials as actuators and sensors. During this time, a wide variety of models have been proposed, which will not be detailed in this section, and all the research devoted to this field has let to the development of a “Standard on Piezoelectrics”. This standard is the most widely recognized description of the

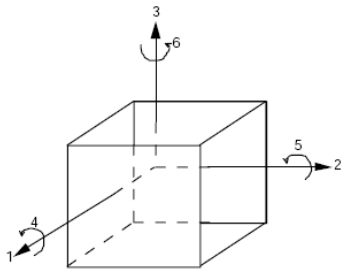

Figure 1-7 Reference axes.

piezoelectric behavior and was published by the Standards Committee of the IEEE Ultrasonics, Ferroelectrics, and Frequency Control Society [STANDAR] in 1966 and then revised in 1987. This document presents a consensus of a broad of expertise on the subject and is periodically revised. The standard states precise and fundamental relations that describe piezoelectrics, which outlines the basis of the model of piezoelectric behavior. The standard proposes a collection of methods for measuring the material's piezoelectric parameters. These basic relations are derived from thermodynamic principles and the fundamental physical properties of crystals. Before introducing the equations, a brief explanation on the tensorial notation is given as an introduction. Because piezoelectric materials are anisotropic dielectrics it is required to describe the effect of the different input vectors in all directions. The notation to define the directions is depicted in Figure 1-7

The indices 4, 5 and 6 refer to rotation. Once introduced, the constitutive equations are represented with the subscripts that define the directions.

$$[S_i] = [s_{ij}] \cdot [T_j] + [d_{ik}] \cdot [E_k] \qquad \textit{Eq 1-1}$$

$$[D_i] = [\varepsilon_{lm}] \cdot [E_m] + [d_{\ln}] \cdot [T_n] \qquad \textit{Eq 1-2}$$

Piezoelectricity is a cross coupling between the mechanical variables "S" (strain), "T" (stress), and the dielectric variables "E" (electric field) and "D" (electric displacement). In dielectrics, the displacement vector "D" is related to the electric field with the dielectric permittivity parameter "ε_{im}". Piezoelectrics are anisotropic dielectric materials, thus the permittivity is a matrix. The coupling appears because on piezoelectric materials a mechanical deformation reorients its internal dipoles, this dipole motion is traduced in a change in its charge density. This coupling is modeled as a linear term relating "D" and "T" by the piezoelectric constant matrix "d_{in}". In the mechanical equation, the strain is related to the stress with the compliance matrix "s_{ij}" that is inversely equal to the Young modulus matrix "Y_{ij}". Then the piezoelectric effect is described as a linear term relating the strain "S" and electric field "E" by means of the piezoelectric constant matrix "d_{ik}". The electric field orientates the electric dipoles forcing the material to elongate or contract.

	Emax (V/µm)	d_{31} (pm/V)	$\varepsilon/\varepsilon_0$	k_{31} (CV/nm)	Yield strength (N/m^2)	Young modulus (N/m^2)	Energy density (mJ/cm^3)
PZT	10	320	3800	0.4	2e7	5e10	600
PVDF	190	20	13	0.1	5.2e7	0.3e10	4700

Table 1-3 Comparison table for piezoelectric ceramic PZT and piezoelectric polymer PVDF

Furthermore the piezoelectric standard has some drawbacks. Piezoelectric materials are ferroelectrics, thus they posses some nonlinear effect. This effect is not considered in the equations. Moreover, the relation does not consider any mechanical or electrical loss, neither hysteresis.

The Standard on piezoelectric was proposed for piezoelectric ceramics. However, the equations representing the piezoelectric effect are used for both, the ceramics and the polymer materials. Differences arouse in the values of the material's parameters.

Table 1-3 presents a comparison of the material parameters for piezoelectric ceramics PZT and piezoelectric polymers PVDF. Piezoelectric polymers have, approximately 10 times lower piezoelectric coefficient (d_{31}) than piezoelectric ceramics. However they can withstand higher electric fields "E_{max}" thus they are able to produce the same level of strain. Moreover the polymer yield strength is higher. Considering the Young modulus, piezoelectric ceramics are harder materials which make them better candidates to be used as actuators to generate high forces. In contrast, the softness of piezoelectric polymers together with the fact that their relative permittivity is 100 times smallest makes polymers as good choice to be used as force sensors. Both materials have relatively large energy densities; therefore it could be possible to use them as energy generators.

1.1.3. Ionic Polymer Metal Composites (IPMCs)

Ionic polymeric materials suitably made into a functionally-graded composite with a conductor such as metal that acts as a distributed electrode, can exhibit large dynamic deformation when placed in a time-varying electric field. Conversely, dynamic deformation of the material can produce dynamic electric fields across their electrodes.

IPMC were originally developed as fuel cells membranes. It is not until the early 90's where their actuating and sensing properties discovered [Mauritz2004]. The actuating properties were first reported by Adolf et al. [Adolf1993] and Oguro, et al. [Oguro1993]. Oguro et al. coined the word ICPF (ionic conductive polymer film) and Shahinpoor et al. [Shahinpoor1998], coined the word IPMC (ionic polymer metal composites) in 1998.

These ionic transducers are manufactured from a base polymer coated with a metal to act as surface electrode. The polymer membrane is an ionomer membrane that selectively passes ions of a single charge. The most common used membrane is Nafion ™ from the company DuPont ™ [DUPONT]. This polymer is the result of incorporating perfluorovinyl ether groups terminated with sulfonate groups into a tetrafluorethylene backbone (Teflon). Figure 1-8 shows the IPMC molecular structure.

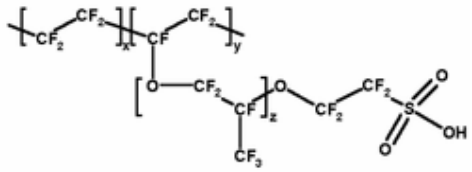

Figure 1-8 IPMC structure.

Such fluorcarbone polymers have a linear backbone with no crosslinking and a relatively few fixed acidic groups SO_3H attached. The large polymer backbone determines their mechanical strength. Short side-chain provides acidic groups that interact with water and the passage of appropriate ions. When solvent by water, hydrophobic zones around the fluorcarbone backbones and hydrophilic zones around the fixed ionic groups SO_3- coexist. Therefore, the ionic groups attract water and can move water under an electric voltage through nanoscale pores and channels where ions along with water migrate within the polymer matrix [Shahinpoor2001].

The transduction effect in an IPMC is the consequence of solvent transport (water) and charge transport (ions). Figure 1-9 depicts a schematic drawing of the transduction effect. The drawing shows how at the initial step, this is when the membrane hydrates, the acid side groups dissolve. A proton (+H) is given away, which remains wrapped in water molecules. The rest SO3- remains fixed to the chain and also enclosed in water. After that, an electric filed is applied between both sides of the membrane, hence the free cations (+H) move towards the cathode electrode dragging the water molecules with them. This electrophoresis-like ion-water movement is the responsible for creating effective strains for actuation. The accumulation of water molecules in the cathode creates a pressure gradient respect the anode that forces a bending towards the anode.

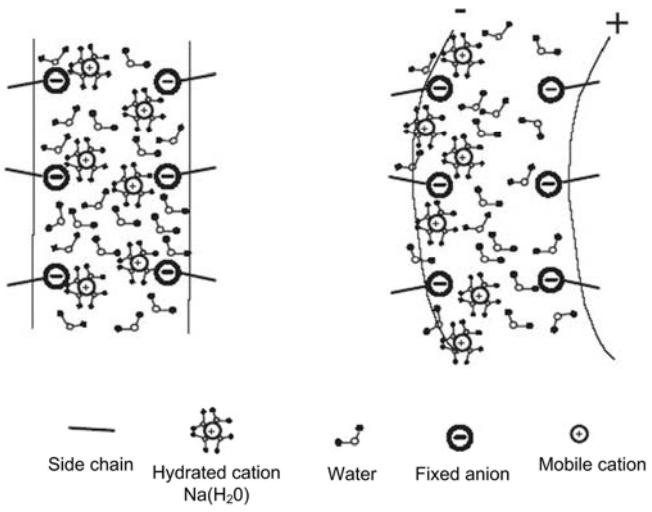

Figure 1-9 A schematic diagram of the typical IPMC artificial muscle and its actuation principle. Picture obtained from Shahinpoor2001.

The electrodes are developed to form a composite material in the membrane surface. One of the most accepted technique to develop the electrodes was proposed by Oguro [Oguro2001]. It is based on soaking the membrane in a platinum salt solution to allow platinum-containing ions to diffuse through via the ion exchange process. Then a proper reducing agent is introduced to platinize the materials by molecular plating. As can be seen in Figure 1-10, the metallic platinum particles are not homogeneously formed across the membrane but concentrate predominantly near the interface boundaries. Shahinpoor et al. [Shahinpoor2001] have experimentally observed that the platinum particulate layer is buried microns deep (typically 1–20 μm) within the IPMC surface and is highly dispersed.

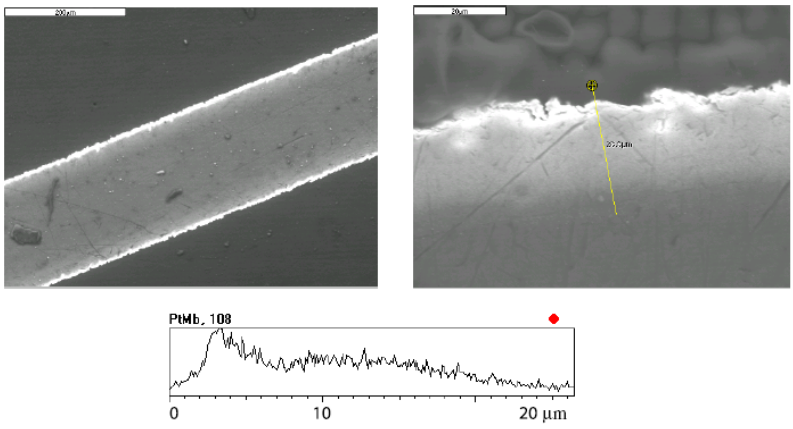

Figure 1-10 Two SEM micrographs (top) showing the cross-section (left) and close-up (right) of a typical IPMC. The bottom graph shows an x-ray line scan of Pt. As can be noticed, Pt is dense at the surface. Picture obtained from Shahinpoor2001.

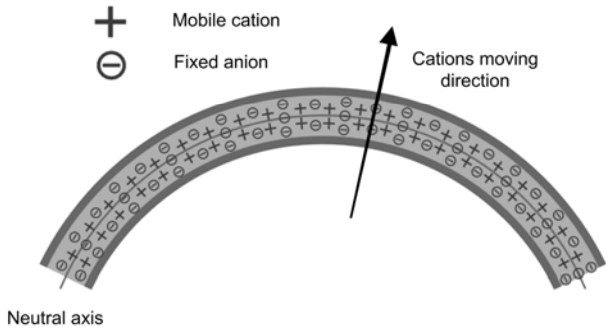

Figure 1-11 A schematic diagram of the typical IPMC and its sensing principle.

IPMC presents also sensing capabilities. By mechanically bending the material, it is possible to change the distribution of the charges with respect to the membrane neutral axis (see Figure 1-11). The applied stress will contract one side of the membrane while spreading the other, the hydrated ions will move consequently towards the region characterized by a lower charge density. A deficit of negative charges and an excess of positive ones, will therefore results in the expand side. In the contracted side the opposite will occur. This phenomenon produces a voltage drop collected at the metal electrodes.

1.1.3.1. Modeling IPMC

Since IPMC were proposed first as actuators and then as sensors, many efforts on developing accurate models to predict its performances have been made. Unfortunately, still today, there is not a clear understanding of the effects responsible for the electro-chemo-mechanical transduction. The researches focused on modeling can be classified in three groups. The first is formed by researchers that try to find "physical models". Physical models come from selecting and modeling the set of underlying mechanisms responsible for the actuation and sensor effects. The second group is formed by those devoted to designing "black box" models where the physics are only a minor consideration and the model parameters are based solely on system identification. The last group is formed by researchers that seek for "gray box" models. This last type of modeling consists of a mixture of a few well established physical laws combined with some empirical identification. While black box models are only useful from an engineering point of view, the gray box models can give some insight into which physical models can be used.

One of the first physical models was proposed by De Gennes et al. [De Gennes2000]. They developed a static model based on irreversible thermodynamics. Their model started with the standard Onsager relation [Onsager1931], where two forms of transport were considered: charge transport (with a current density "J" normal to the membrane) and solvent transport (with a flux "Q_F"). The conjugate forces are the electric field "E" and the mechanical force $\nabla p = \partial p/\partial z$, where "p" is

the (scalar) water pressure in the network. "L_{12}" and "L_{21}" are the cross coupling coefficients.

$$J = \sigma E - L_{12}\nabla p \qquad \textit{Eq 1-3}$$

$$Q_F = L_{21}E - K\nabla p \qquad \textit{Eq 1-4}$$

After, Tadokoro et al. [Tadokoro2000] proposed a physical model where ionic motion was considered. The application of an electric field causes the hydrated cations to move towards the cathode dragging the water molecules with them. The resulting change in water concentration produces an anode contraction and a cathode elongation on the cathode, inducing a bending of the membrane. It also adds another effect in a lower time scale, the osmotic pressure that causes the water to diffuse so equalize its concentration across the thickness. This slow diffusion results in a relaxation of the first induced bend. Moreover another effect was considered: the electrostatic forces that appear between adjacent fixed ionic groups. This is a result of the charge imbalance caused by the ion migration, which induces a small amount of curvature towards the cathode that is in the opposite direction of the initial curvature.

While Tadokoro model was validated with experimental measurements, another different model was proposed and also validated by Nemat-Nasser et al. [Nemat-Nasser2000]. In their paper they consider a cluster model. While the application of an electric field forces the hydrated cation to move towards the cathode, a locally imbalanced net charge density results. This unbalanced net charge and the associated electrostatic forces produce stresses that act in the polymer backbone, resulting in an electrically induced curvature. Based on their experimental results, they concluded that the electrically induced curvature is mainly based on electrostatic forces.

The discrepancies on the different physical models are attributed to the fact that the chemical and physical mechanisms responsible of the electro-chemo-mechanical transduction have not been conclusively identified. Also the material parameters that appear in many of the proposed equations are not well known and do not lend themselves to be directly measured. These statements are strongly supported by the fact that the detailed physical models proposed by Tadakoro and Nemat-Nasser do not agree on the role of actuation mechanisms, yet they both compare well to experiments.

From an engineering point of view, sometimes more simplistic models are enough. The black box model is a simple model based on the fitting experimental data. The first black box model was proposed by Kanno et al [Kanno1994]. By acquiring the response to a voltage step input, they fitted a function with four different time constants. While black box models are easier to obtain, their scope is limited as they can not accommodate any change in actuator dimensions. Following

this work, Mallavarapu et al. [Mallavarapu2001] proposed an extended black-box model to consider higher order effects.

The other class of models applied to IPMCs is the gray box models. These models are an alternative to the complicated physical models and the simplistic black box models. These models incorporate well understood and easily modeled physical laws, as well as empirically determined parameters to represent processes that are complex and still not entirely known and understood. One of the first works on gray box modeling was proposed by Kanno et al. [Kanno1996], where a three stage model was proposed. Each stage was connected in series and represent, the electrical stage, the stress-generation stage and the mechanical stage respectively. In the electrical stage, the IPMC was divided in small segments of 1mm connected in series, each segment poses serial resistor and a parallel capacitor with a loss resistor. The input of the electrical stage was considered as the input voltage while the output was considered the current. This current was then considered as the input to the stress generation stage. The stress-generation was modeled as a second order equation. Then the generated stress was used as the input of the mechanical stage that is considered as a dynamic finite element with proportional damping. The model did not consider the bidirectionality of the transduction; this means that they consider that the mechanical part does not affect the input. Newburry et al proposed a novel gray-box model. [Newbury2003], [Newbury2003_2] considering a bidirectional two port linearly coupled scalable model. Newbury starts his model by considering the piezoelectric equations and identifies frequency dependence in the permittivity, piezoelectric coefficient and the young modulus. The experimental results validated the model´s bidirectionality. Other interesting gray-box model was proposed by Bonomo et al. [Bonomo2007]. They used a two stage cascade model. First of all,, the dependence of the IPMC's absorbed current on the voltage applied across its thickness is taken into account; a nonlinear circuit model is proposed to describe this relationship. Then the transduction of the absorbed current into the IPMC mechanical reaction is modeled. The same research group proposed an interesting gray-box model that allows working with the IPMC underwater. For this, the classical Euler–Bernoulli cantilever beam theory and the concept of hydrodynamic functions are used. [Brunetto2008]

Once the different smart materials families have been introduced, a brief introduction to the use of smart materials in microrobotics is presented. In the next few pages, an overview of a microrobot system is presented focusing on the use of the smart materials for motion control, and its use for vibration power harvesting. Several microrobotic projects developed by the Department of Electronics show the usefulness of smart materials in microrobotic motion control and power harvesting.

1.2. MST and Microrobotics

The recent evolution in microrobotic systems have been colligated to the evolution in the technology of microsystems. Micro-Systems Technology (MST), also known as Micro-Electro-Mechanical Systems (MEMS) in USA, is the technology that permits structuring at a very small scale. With this technology it is possible to integrate actuators, sensors and control systems monolithically in the same structure.

MST technology started from the modification of integrated circuit IC fabrication techniques and materials to create very small mechanical devices. It is generally accepted that the first MEMS device was a gold resonating MOS gate structure that appeared in the 1967. The device was based on an electrostatic controlled small resonating cantilever beam [Nathanson1967]. Nowadays the MST technology has evolved and there are many fabrication techniques that permit the development of highly advanced systems. Figure 1-12 is an impressive image. The picture shows a MEMS structure developed at the "Sandia national laboratory" at USA [SANDIA] designed for silicon mirror assembly where a spider mite is slip in. The picture gives an idea of the dimensions of this structure.

MEMS are implemented using a number of different materials and manufacturing techniques; the choice of which will depend on the device being created. Most common used materials are silicon, polymers and metals.

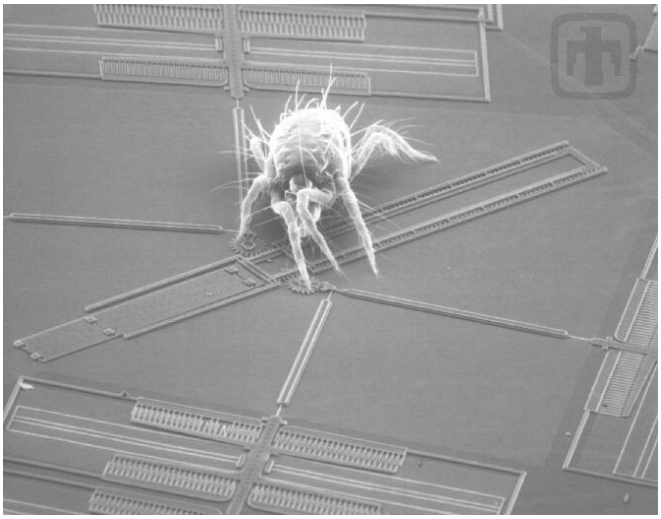

Figure 1-12 SEM image of a silicon mirror assembly with a spider mite (http://mems.sandia.gov/)

Silicon: This material is traditionally the most employed in MST and is a matured technology. When mechanically excited, this material presents almost no energy dissipation. In addition, silicon is very reliable as it suffers very little fatigue. A very interesting feature of silicon MEMS is that it can integrate some sort of electronics. The Integrated Circuits are done in Silicon wafer and using compatible MST. Some of the techniques used to produce Silicon MEMS are: deposition of materials, patterning through photolithography and etching.

Polymer: More recently, polymers are being used in MEMS. Polymer materials have the advantages of being cheaper, more flexible and sometimes biocompatible. Techniques used for developing MEMS with polymers are: injection molding, embossing and others.

Metals: In some cases, it is of interest to produce MEMS based on metals. The techniques for developing metallic MEMS are: electroplating, evaporation, LIGA and sputtering processes.

Research efforts are being done in developing MST techniques to microstructure other types of materials. The possibility to design small systems with embedded smart materials opens the door to new field of applications for MST. One of these fields that takes advantage of this evolution is robotics and microrobotics. To understand what a microrobot is, it is important to first understand what a robot is. The concept of “robot” is quite extended. Several definitions for “robotics” can be found. In the following lines, some of them are stated.

The North American Robotic Industry Association (RIA) gives a definition of a robot as: “An industrial robot is a multifunctional programmable manipulator designed to move pieces, tools and special devices through a wide variety of movements programmed for the execution of different tasks”.

Another definition comes from the International Organization of Standardization ISO (ISO 8373) that states: “An industrial robot is an automatically controlled, reprogrammable, multipurpose manipulator programmable in three or more axes”.

At the present, these two definitions solely apply for industrial robots; they can not be used to define other kind of robots as insect-like robots, human robots and several others. In an effort to obtain a general definition refer to Karel Čapek who used for the first time the word “robot” in his 1920’s theatrical piece the R.U.R. (Rossum's Universal Robots, in Czech "Rossumovi univerzální roboti"). The word robot comes from the word “robota” meaning "self labor", and, figuratively, "drudgery" or "hard work" in Czech. In fact, robots have always been conceived to work as “servants” for the human.

In the same way it is difficult to find a generally accepted definition for “microrobot”. Furthermore, a possible one is to define a microrobot as a robot that

interacts with the environment in a micrometric scale. It is a wrong concept to think in microrobots only as miniature objects that move slowly. While some microrobots have dimensions in the range of cm^3 and mm^3, others are in the range of dm^3. The size depends on the application of the microrobot such as maintenance and inspection in industry, micro surgery in medicine, micro operation in biology, biomimetics, etc.

The research on microrobotics started at the 90's decade at Japan supported by the Ministry of International Trade and Industry (MITI). During that decade different laboratories started to build microrobots for different purposes. It is possible to make different types of classification for microrobotics however there are three important criteria to consider when classifying: mobility (yes/not), autonomy (onboard energy/not onboard energy) and control (cables/without cables)

An interesting group of microrobots are the autonomous microrobots. A definition of an autonomous microrobot was proposed by Fukuda et al. which states: "Autonomous micro robots are defined as the micro robot which consists of the actuator, sensors and processor, and which build the closed-loop control system in itself "[Fukuda1995]. The algorithm of autonomous micro robot needs the function of controlling the devices inside itself, and deciding the motion of itself according to the surrounding. Autonomous robots are considered as Smart systems.

Autonomous microrobotic systems are developed to work in a wide variety of applications. Each application has its own specifications and requirements thus different microrobots are designed. However, it is possible to define four different main elements that make up all autonomous microrobots [Breguet2006]: energy, communication, onboard electronics and sensors and actuators modules. Figure 1-13 depicts a schematic draw of a microrobotic structure where the four elements form part of the MEMS backbone of the robot.

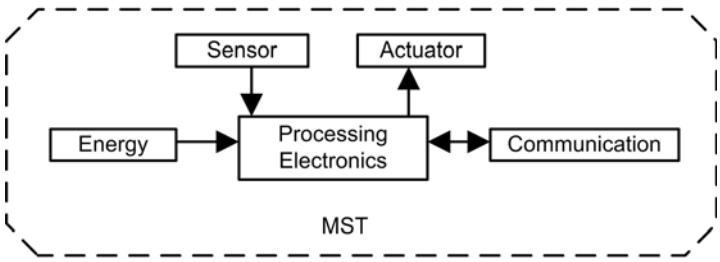

Figure 1-13 Schemtic draw of a microrobot structure.

• **Energy module:** The energy is probably one of the most challenging problems when designing autonomous microrobots. The amount of power that the microrobots can relay on restricts the design and performances of the system. It is very useful to determine the appropriate energy module before starting the specific

design of the other parts of the microrobot. Some of the most common ways to supply energy to the microrobot are: wires, battery, wireless energy transmission or energy harvesting.

- **Communication module:** Normally the microrobots are designed to perform specific tasks. It is compulsory to equip them with a communication module. Due to the small size of the robots, and therefore of the antenna (a few millimeters), radio frequency in the GHz range is not applicable. A common solution is the use of InfraRed communication.

- **Onboard electronics module:** The onboard electronics is the heart of the robot. It is the responsible of the control of the robot and is the part of the robot that gives the intelligence to the system. Nowadays, it is possible to integrate in a very small area (typically 4 mm^2) a complete micro-processor with its peripheries.

- **Sensors and actuators module:** The sensors and actuators must be designed considering the restrictions on powering, the applications requirements and the materials technological facilities. They are the responsible for the interaction with the environment.

The actuators are the elements of the microrobot that transform the electrical energy into mechanical energy. In mobile microrobots the actuators are responsible for motion and are characterized by two energy transformations. The electrical to mechanical transformation and the mechanical to mechanical that will generally amplify the actuator strain. The first transformation has been generally obtained using piezoelectric and electrostatic converters. However the evolution in smart materials has opened the door to new interesting possibilities. The second energy transformation, the mechanical to mechanical is generally obtained with specific motion principles. Some common used principles are the stick-slip principle, the inchworm principle or the walking mechanism [Breguet2006]. The selection of a specific motion principle for a microrobot is not an easy task and depends on the application and the material technology available.

1.2.1. Motion control

In mobile autonomous microrobots the motion control is applied at different levels. Sometimes it is applied to control the motion trajectory for translation or rotation of the microrobot. Other times it is applied to control the motion of different elements in a multirobot application. It is also applied for controlling the motion of certain microrobot tools with respect a sample. Other times is applied locally for controlling the motion of the different actuators of the microrobot. Although the motion control is applied at different levels with different elements it is possible to distinct two general control methods.

The first one is the open loop control system. Figure 1-14 depicts a schematic draw of the control scheme. The working principle starts with a command input passed to a controller with the desired task to perform. The controller distributes the energy to the system in accordance with the command input. The system is the responsible to translate the electrical energy into motion energy.

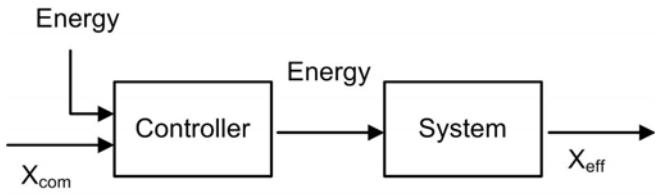

Figure 1-14: Open loop motion control scheme.

The second is a closed loop control. Figure 1-15 depicts a schematic draw of the control scheme. In this case the sensor measures the effective position of the system and transforms it into a processable signal. The controller processes the difference signal between reference and effective signal and transforms this difference signal into an energy equivalent signal. This energy is transformed within the system into motion energy. The possibility to use sensors makes closed loop control systems feasible for high precision applications.

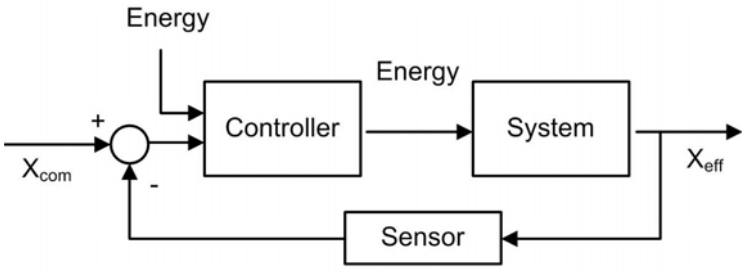

Figure 1-15: Closed loop motion control scheme.

The selection of a control type and its specific implementation depends on the application of the microrobot system and the active materials used for actuation. In the next lines different examples of control approaches classified in three applications where smart materials are used are presented.

1.2.1.1. Micromanipulation and microassembling with microrobots

Nowadays there are a lot of applications where the manipulation and motion of objects with resolution in the μm or nm range is required. Microassembly in MST production, cell manipulations in biomedical research, eye and plastic surgery are just a few good example. Although the manipulations vary from application to application, almost the same operations are done in every case, such as grip, transport, position, release, adjust and fix in place. As well as in the processing steps like cutting, soldering, gluing, removal of impurities, manipulate and assemble small Microsystems [Rembold1997]. A microrobotic system prepared to work with micromanipulation and microassembling must posses the following requirements:

- Robust and weight to avoid vibration problems.
- Posses a very precise drive for robot motion.
- An easy integration of different tools with enough degree of freedom.
- Very precise control of the tools.

These requirements suggest the use of piezoelectric ceramics as actuators for the microrobot. Piezoelectric ceramics are able to produce a large force, which is needed to move a robot. These materials are controllable and quite stable. Moreover, several high resolution micro fabrication techniques for thick and thin film printing of piezoelectric layers exist [Morita2003]. The high resolution specification suggests using closed loop motion control.

The author of this thesis belongs to the research group “Instrumentation and Communication Systems (SIC)” from the Department of Electronics of the Univerisitat de Barcelona. This group has participated in several European investigation projects related to microrobotics since 1998. Onboard electronics for powering, motion, and sensor and actuator interface have been their main activity. As examples of micromanipulation and microassempling microrobots two of these projects are presented.

MINIMAN (Miniaturised robot for micro manipulation) (ESPRIT Contract number 33915) **(1998-2002):**

The goal of the MINIMAN project was to develop smart microrobot with 5 degrees of freedom and a size of a few cubic cm, capable of moving and manipulating with the use of tube-shaped and multilayered piezoactuators. Some of the capabilities of the robot were the handling and assembly of micromechanical parts under a light microscope and in the vacuum chamber of a scanning electron microscope.

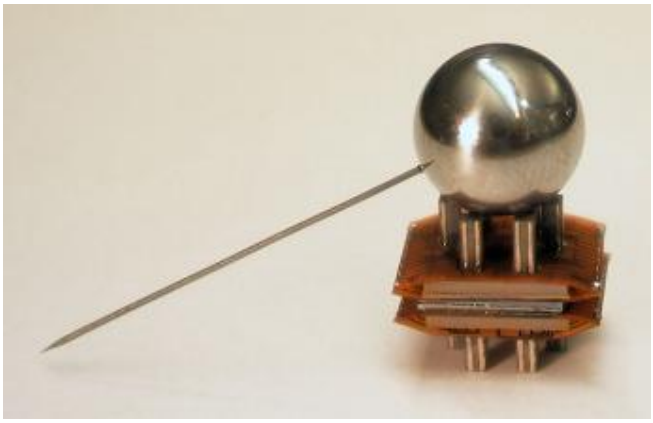

Figure 1-16 MINIMAN microrobot.

The microrobot structure consists of two monolithic piezoelectric drive units with six piezoelectric ceramic elements on each one, placed together back to back, with power electronic on-board [Miribel2002], Figure 1-16. The lower drive unit is the micropositioning platform and is the responsible for the robot motion. The upper drive unit controls the tool and is the responsible of the manipulation [Simu2002]. The energy is supplied with wires and the electrical signals too.

Each actuator element consists of four segmented piezoelectric ceramic multilayer stack actuator that produces a 3 axial motion. Controlling the voltage signals applied to each of the 6 actuator elements, a motion mechanism is achieved. The drive responsible of the robot motion is driven with the "inertia principle" [Simu2002] while the drive responsible of the tool motion, with the "quasistatic principle" [Simu2006]. Quasistatic principle produces a higher accuracy in motion and can be used at lower frequencies.

The motion control of the microrobot is performed in closed loop. A first loop is used to control the position and motion of the microrobot. It is based on a CCD camera used as a sensor to detect the position of the microrobot. The desired motion is sent to a controller that corrects the voltage signals sent to the piezoelectric elements by comparing the real position with the reference input. A second closed loop is used for the manipulation. In this case a light microscope is used to detect the position of the microrobot tool and the sample. [MINIMAN]

MICRON (Miniatured cooperative robots advancing towars the nano-range) (IST-2001-33567) **(2002-2006):**

The goal of the European Union IST project MiCRoN, was to achieve the development of a multi-robot manipulation system capable of handling µm-sized objects. The system is based on a small cluster of about a few cubic-centimeter-sized mobile autonomous robots. These wireless agents, each equipped with onboard electronics, cooperate within a desktop environment to execute a range of tasks associated with the assembly and processing of units from the micro to the nano-range.

Figure 1-17 shows a picture of a Micron robot. Each robot is equipped with a 3 DOF locomotion platform, a rotational tool actuator, a power pack, a positioning system, a communication module and onboard integrated electronics for control and communication [Brufau2005]. Later on, different robots were mounted depending on the task to be performed, such as syringe [Tagliareni2005], a gripper [Eisinberg2006] and an AFM microscope [Brufau2005_2].

The motion platform is a steel frame, in which a flexible structure is cut out for motion amplification, and four piezoelectric ceramic bars are assembled [Driessen2003]. The rotational tool is a monolithic actuator that consists of three multilayered piezoelectric bimorph actuators. [Snis2005]. The motion platform is driven with the stick slip principle, and the rotational tool with the quasistatic principle. The stick slip is also a dynamic principle that permits faster motions than the quasistatic but produces bounces.

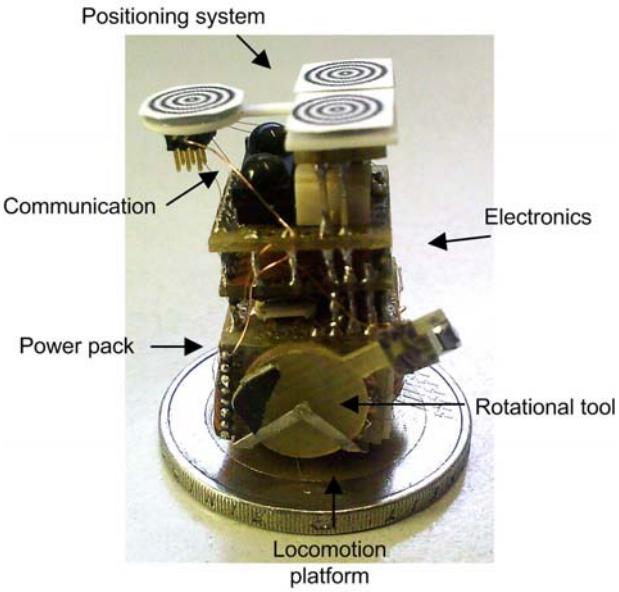

Figure 1-17 MICRON robot.

A CCD camera is used to detect the position of the different microrobots. The motion control is performed using two closed loops. A first close loop is used at the beginning to calibrate each robot. The calibration is devoted to obtain a dynamic motion model for each robot. This model is then used to make an inverse open loop actuation. Once the microrobots are calibrated, a second control loop is implemented to control the motion of the robots. This control is a closed loop control that uses the same camera as sensor [MICRON].

1.2.1.2. Insect-like microrobots

Biomimetic microrobots are of great interest. By looking at the nature it is possible to find very efficient mechanisms for motion and sensing. A special interest is emphasized in studying insects. Insects are point out for two main reasons; the first is because of their body structure, since motion and morphology are relatively simple but extremely efficient. The second reason is for their collective execution. Taking into consideration the natural world's evolution, it is evident that insects have been a very successful species, mainly due because of their ability to organize into large co-operative communities and swarms. In several insects the mechanical structure for locomotion is based on shells and muscles in contrast to bones and muscles in larger animals.

As a result, an insect-like microrobot must have the following features:

- Must be reduced in dimensions and light weight.
- The structure must be of a flexible material with embedded actuators as it emulates the shell.
- It must have some embedded sensor.
- It must possess some kind of communication unit.
- A small intelligence.
- Small power consumption.

These requirements suggest that the active materials must be polymeric materials. Piezoelectric polymers are presented as good candidates since they are easily processed, biocompatible, they can work as sensors and as actuators and are flexible and lightweight. Normally in insect-like microrobot projects the accuracy of motion is not an input constrain. It is more relevant to develop biomimetic elements with power and intelligence autonomy and with integrate embedded sensors and actuators. As an insect like example, another project developed by the SIC group and other European partners is presented.

ISWARM (Intelligent Small World Autonomous Robots for Micro-Manipulation) (FP6-2002-IST-507006) **(2003-2007)**

I-SWARM project aims to take a leap forward in robotics research by combining experts in microrobotics, in distributed and adaptive systems as well as in self-organizing biological swarm systems. The project aims at technological advances to facilitate the mass-production of microrobots, which can then be employed as a "real" swarm consisting of up to 1,000 robot clients. These clients will all be equipped with limited, pre-rational on-board intelligence. Figure 1-18 shows a picture of an I-Swarm small robot.

Each microrobot consists of a double side flexible printed circuit board (FPC) acting like the backbone or shell of the robot, and connecting the different modules, a three legged locomotion module with an integrated tactile sensor, a capacitor for energy storage, an specific electronics (ASIC), an IR communication module and a solar cell.

In the lower part of the FPC, four appendixes projects. These appendixes are etched in the same FPC where a multilayer P(VDF-TrFE) structure has been grown. Three of the four appendixes act as the legs for the robot, while the other acts as a tactile sensor. The legs permit motion of the robot (forward, back and rotational motion). Due to low power consumption requirements, legs must be driven with low voltage. The motion principle used is the “resonance motion”, square voltage signals are applied at the mechanical resonance of the leg. This kind of motion is more uncontrollable and reduces the accuracy of the robot.

In this project the motion control for each microrobot is enveloped in a general distributed control of the behavior of the whole swarm. The robot itself drives its mobile platform, the three legs, in open loop. However each robot has integrated a sensor tool for detecting object collision. If a collision happens the motion is modified.

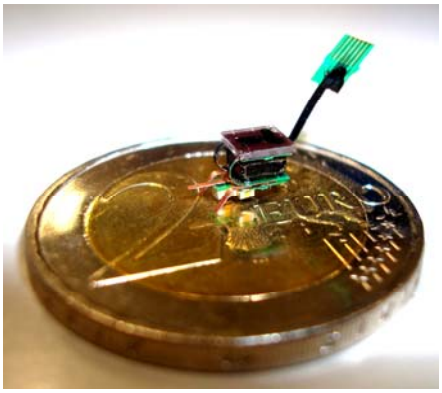

Figure 1-18 I-SWARM robot.

1.2.1.3. Fish-like microrobot

Moving forward with the study of biommimetic robots, fish-like microrobots is now considered. For a long time the aeronautic designers have focus their research in the development of efficient propulsion systems, however, almost always deciding for the use of screw motors. Conversely, in water fish reach some performances that machines still can not achieve. Some fish are able to swim very fast with low muscular power (Gray's paradox); others can change quickly their path and accelerate very fast. These performances are enviable: high efficiency, great maneuverability, high acceleration, noiseless motions, etc. [Laurent 2001]

Therefore a fish-like microrobot must have the following features:

- Free dimensions but light weight.
- Anatomic structure similar to a fish.
- Flexible body with actuators to produce a fish like motion.
- Produce an optimal thrust.
- Furthermore, it is possible to apply for requirement of a wireless energy.

From all these requirements it seems that the best choice of material to be used as the actuator is the Ionic polymer Metal Composites (IPMCs). These polymers are light and flexible, its deformations are important even for small voltages, its energy consumption is low and its shape makes it easy to use with fins. Moreover, it works perfectly in water. The drawback of this actuator is its very complex behavior.

Normally the input constrains for a fish like robots are the development of motion principles similar to those observed in real fishes. In this section the work developed by Kim et al. is presented as an example. [Kim2005].

IPMC TADPOLE ROBOT: In this work the authors focused on the development of a wireless tadpole robot capable of high thrust, based on biomimetic undulatory motion using cast IPMC actuators. They investigated the undulatory motion of the tadpole in Nature and employed an IPMC actuator as a propulsion tail fin for imitating the undulatory tadpole robot in water.

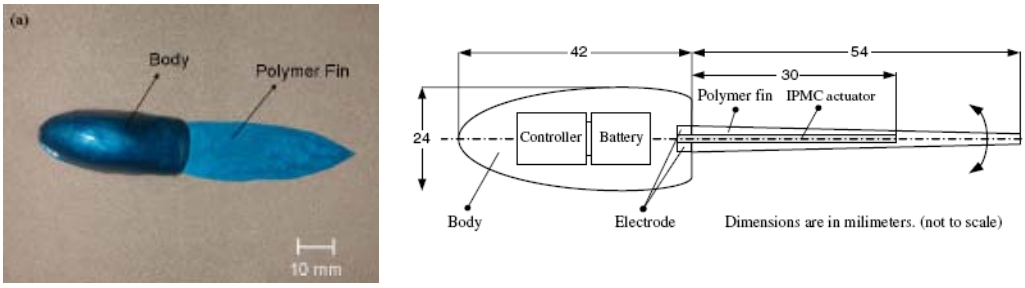

Figure 1-19a) Tadpole robot picture. At the left side there is the main body of the robot and at the rigth the polymer fin. b) Schematic draw for the tadpole robot structure. The body conatins the controller and the battery, while the tail is based on a IPMC actuator and the polymer fin. The total length of the robot is aprox 10cm. Figure obtained from Kim2005.

Figure 1-19 shows a picture and a schematic draw of the tadpole microrobot. The microrobot consists of the body that has been mold equal to that of a real tadpole, one polymer fin tail driven by a cast IPMC actuator, and the controller module. The controller module is located inside the body and includes a wireless power source, electrodes, and a frequency modulator.

The fish-like motion of the tadpole robot is managed by applying a voltage signal to the cast IPMC. The propulsion systems produce a thrust to overcome the drag force. The total thrust depends on the frequency of excitation as well as the shape of the curvature of the fin's tail. Controlling the frequency and the duty cycle of the applied signal makes it possible to control de velocity and the direction of motion.

After introducing the use of smart materials in microrobotics and detecting the advantages and disadvantages for each, an introduction to the power harvesting is presented. Smart materials are mainly used as sensor or actuators in microrobot systems, however new research activities indicate that these materials could be used for generating energy. With the objective of developing more embedded and smarter systems each time, in the following section, the ability of smart materials to generate electrical energy is introduced. This section starts with a general view of energy harvesting and then focuses in the mechanical vibration to electrical energy conversion.

1.3. Power harvesting

The first energy cell, the battery, was invented by Alessandro Volta in 1799 [Trassati1999]. His invention predated the first mechanical to electrical energy converter device discovered by Michael Faraday [Faraday1849]. At the beginning, batteries were the only way to generate electrical energy. It was until the end of the 19th century when electricity arrived to the cities by wires that battery use was relegated to mobile platforms.

Battery technology has undergone a tremendous progress since it was first discovered. This progress enabled the explosion of a huge number of new applications such as all mobile devices. However, new trends in technology in addition with some intrinsic limitations of batteries have motivated the research for new energy generation solutions.

New trends point to the development of Smart systems. These systems, presented at the beginning of the introduction, are conceived to actively "monitor and optimize themselves". The requirements and expectations for these systems are: efficiency, sustainability, intelligence, autonomy, a high degree of integration, etc. These expectations rule out the use of batteries for energy sources. Batteries have a limited life span, which in contrast to the concept of "Smart", produce pollutant residues. New energy solutions must have a very long life span and must be sustainable. A very interesting publication of the "Economist Group" about future trends was presented in 2003 by the Microsoft chairman and chief software architect Bill Gates [Gates2003]. The publication was named "The Disappearing Computer". In that publication, he envisioned a future world where ubiquitous embedded systems will interact with people whether they know it or not. Those envisioned systems will have to run without batteries and use power harvesting systems to transform environmental energy into usable electrical energy.

"As people find more ways to incorporate these inexpensive, flexible and infinitely customizable devices into their lives, the computers themselves will gradually "disappear" into the fabric of our lives. We are still a long way from a world full of disembodied intelligent machines, but the computing experience of the coming decade will be so seamless and intuitive that--increasingly--we will barely notice it. At the same time, computing will become widespread enough that we will take it for granted--just as most people in the developed world today trust the telephone service."

"The pervasiveness and near--invisibility of computing will be helped along by new technologies such as cheap, flexible displays, fingernail-sized MEMs (microelectromechanical systems) chips capable of storing terabytes of data, or inductively powered computers that rely on heat and motion from their environment to run without batteries."

Thus, the solution for this energy problem seems to be the designing new systems. Systems capable of continuously transforming energy from the environment into electrical energy useful for supplying electronic devices. This procedure is known as “power harvesting”.

There are different ways to harvest power; however this thesis focuses in the use of piezoelectrics and ionic polymers. These materials when subjected to mechanical stress generate electric charges; consequently, it is possible to use them to convert mechanical energy, i.e. from mechanical vibrations, into electrical energy.

1.3.1. Power from mechanical vibration

Our environment is constantly affected by vibrations surrounding us. These vibrations have different nature and come from different origins. Today, while some mechanical vibrations are almost imperceptible for us, i.e. vibrations of a transformer, others, have devastating effects as it is the case for some earthquakes. The advantage of using mechanical vibrations to generate electrical power before using other techniques has to do with its availability in many and diverse environments. Some of these environments are away from light or electromagnetic fields or in constant temperature environments, etc.

The characteristics of the mechanical vibrations depend on the environment in which they are transmitted and in which they where originated. Normally a very low frequency vibration is originated from the mechanical motion of a big mass. Seismic waves produced by earthquakes have generally very low frequency vibrations in the range of 0.3Hz-8Hz [FABREEKA]. The amplitude of these vibrations depends on factors as the power of the earthquake, the distance from the epicenter, etc… Other low frequency vibrations can be found for example in the coast due to the collision of sea waves with rocks. On the other hand, inside buildings, higher frequency mechanical vibrations appear. Table 1-4 lists some of the most common vibrations sources inside a laboratory. It is typical to have vibrations in the range from 4Hz-100Hz [MELESGRIOT]. Some of the more important contributions are due to structural motion of the building. However other sources as air compressors, foot traffic, transformers or elevators are also present in a laboratory. Higher frequency vibrations from 1kHz to up, may affect some machinery. Rotating machinery vibrations are commonly caused by bearing components, gear teeth, reciprocating elements, turbine blades and the like, and have a discrete spectrum based on the fundamental frequency of rotation.

The vibration sources commented before, are not necessary steady state. However, a simple occasional impulse is enough to generate electricity. This electricity can be stored somehow. After the repetition of several impulses the amount of stored energy could be enough to support the power requirements of a device. These intermittent vibrations sources are viable sources of energy. However, steady state vibration sources exist and these are the most promising for powering

Source	Frequency (Hz)	Amplitude (in.)
Air Compressors	4–20	10^{-2}
Handling Equipment	5–40	10^{-3}
Pumps	5–25	10^{-3}
Building Services	7–40	10^{-4}
Foot Traffic	0.55–6	10^{-5}
Acoustics	100–10,000	10^{-2} to 10^{-4}
Air Currents	Labs can vary depending on class	Not applicable
Punch Presses	Up to 20	10^{-2} to 10^{-5}
Transformers	50–400	10^{-4} to 10^{-5}
Elevators	Up to 40	10^{-3} to 10^{-5}
Building Motion	46/height in meters, horizontal	10^{-1}
Building Pressure Waves	1–5	10^{-5}
Railroads	5–20	±0.15g
Highway Traffic	5–100	±0.001g

Table 1-4 Common virbation sources inside a laboratory. Table obtained from MELESGRIOT.

electronics. Rotating machinery is an example of steady state source. These machines present the most natural application of energy harvesting from mechanical vibration. It is desirable to instrument these machines with sensors to monitor their performance and predict failures so that preventive maintenance can be performed. These applications also have a long lifetime requirement that may be met more easily by harvesting energy than by using batteries.

Researchers have long designed systems to harvest energy from mechanical vibrations. Usually, by exploiting the oscillations of a proof mass. These kinds of converters are also known as “Inertial Converters”. There are different ways to convert this energy into electrical energy. In fact, there are three kinds of physical principles that can be used. These are: magnetic induction converters, electrostatic converters and piezoelectric converters.

1.3.1.1. Magnetic induction converters

The magnetic induction transducer is based on Faraday’s law. It is based on the motion of an electric conductor through a magnetic field. Typically the conductor is wound in a coil to make an inductor. The relative motion between the coil and magnetic field causes a current to flow in the coil. As the relevant magnitude here is the magnetic flux through a circuit, the size of the coil is inversely related to the obtained f.e.m. and therefore, to the generated energy. This means that big transducers with large area coils will perform better than smaller transducers. [Mateu2005]. However MST technology has permitted the development of smaller devices.

Some of the most relevant works regarding the design of electromagnetic power generators are commented. The first one is a publication from MIT Amirtharajah & Chandrakasan, [Amirtharajah1998] which presented a generator using discrete components that generates power in the order of 400 μW using human walking as a vibrational power source. Williams et al. [Williams2001] from the University of Shiefield, presented a $1mm^3$ size electromagnetic micro-generator, able to generate 0.3 μW from a 4 MHz excitation input. Li et al.[Li2000] from the University of Hong Kong has fabricated an electromagnetic MEMS VDRG with a volume of 1 cm^3. The micro-generator generates 10 μW powered at 2 V DC with 64 Hz input frequency and 1000 μm input vibration amplitude. More recently, researchers from our department, at the University of Barcelona, have presented an electromagnetic inertial microgenerator, compatible with Si technology, based on a fixed micromachined coil and a movable magnet. An optimized design has the ability to generate power up to hundreds of μW, with voltage levels compatible with standard DC rectification circuits. [Serre2007]

1.3.1.2. Electrostatic converters

Electrostatic generation consists of two conductors separated by a dielectric (i.e. a capacitor), which move one respect to the other. As the conductors move, the energy stored in the capacitor changes, thus providing the mechanism for mechanical to electrical energy conversion. Electrostatic converters allow two methods for working, one constrains the voltage in the variable capacitor, and therefore its charge oscillates from its maximum to its minimum value. The other constrains the charge in the variable capacitor thus the voltage oscillates from a maximum and a minimum.

Meninger et al. [Meniger2001] from the MIT pointed out the benefits of working with the charge constrains and designed a device that is capable of 3.8 μW/cm3 according to simulations. Roundy et al. [Roundy2002] designed an electrostatic vibration-to-electricity converter using MEMS fabrication technology. Simulation of the optimized design demonstrated that 116 $\mu W/cm^3$ is possible to harvest from input vibrations of $2.25m/s^2$ at 120 Hz. Later Chiu et al. [Chiu2007] presented a converter with 3.3 V supply voltage and 1 cm2 chip area constraints, the output power is $200\mu W/cm^2$ for the optimal load of 8 MΩ. The device was fabricated in a silicon-on-insulator wafer.

1.3.1.3. Piezoelectric converters

Piezoelectric generators are based in the active properties of these materials. Due to the piezoelectric effect, when the material is mechanically stressed, its internal electrical dipoles are reoriented and an induced electrical field is therefore generated. If a simple resistive load is attached to the piezoelectric material, an electrical current is generated through it. Therefore electrical power is generated from mechanical vibrations. The geometrical and the mechanical configuration play a significant role in the amount of energy harvested. Most common converters work in the 31 mode of operation.

Piezoelectric converters were first studied by Umeda et al. [Umeda1996]. They proposed to use the power generated when a free-falling steel ball impacted a plate with a piezoelectric ceramic wafer attached to its underside. Following Umeda a large amount of works have been published. Kymissis [Kymissis1998] proposed a completely autonomous circuit able to harvest the energy from human walking with a piezoelectric shoe insert to supply an RF transmitter. Roundy et al. [Roundy2004] developed a 1cm3 converter based on a commercial piezoelectric cantilever with a tip mass attached that is able to generate 375 $\mu W/cm^3$ from driving vibrations of $2.5m/s^2$ at 120 Hz. Finally, a custom designed radio transceiver that consumes 12mW when transmitting has been powered at a duty cycle of 1.6%.

1.3.1.4. Converters performances comparison

When designing systems for power harvesting from vibrations, there are a lot of variables that have to be taken in mind before choosing a solution. Some of the more important ones are volume restrictions, the specifications of the vibration source and environment, the available electronic and mechatronic technology, etc… Although all these aspects will influence in the solution, it is interesting to make a quantitative comparison in terms of energy density inherent to each type of converter.

Table 1-5 presented by Roundy et al. [Roundy2003], shows the expressions for the three energy converters density functions. Moreover a computation of the theoretical and practical maximum values is shown. The piezoelectric energy density equation is obtained considering the energy density in a dielectric material and the electric field induced by a mechanical stress "T". The energy density equation for an electrostatic converter is directly computed as the energy density in a dielectric material, the energy density in the electromagnetic is directly computed as the energy of a magnetic field. The quantitative comparison is based on evaluation of the maximum energy densities that these materials can sustain. In the case of the piezoelectric converter, the maximum energy density is achieved when the material sustains the maximum stress before breaking, this is named the "yield strength". The values for the calculation for the maximum are done considering the more expensive single crystal PZN-PT. However the Practical maximum value from the table is computed with the values of the most common PZT-5H. The electrostatic energy density is computed considering an electric field of 100MV/m for the Theoretical maximum energy and 30MV/m for the Practical. Maximum energy,, the dielectric permittivity assumed is the permittivity of void. In the case of the electromagnetic

Type	Governing Equation	Practical Maximum	Theoretical Maximum
Piezoelectric	$E_{dens} = T_y^2 k^2 / 2Y$	17.7 mJ/cm^3	335 mJ/cm^3
Electrostatic	$E_{dens} = \varepsilon E / 2$	4 mJ/cm^3	44 mJ/cm^3
Electromagnetic	$E_{dens} = B^2 / 2\mu_o$	4 mJ/cm^3	400 mJ/cm^3

Table 1-5: Summary of maximum energy density of three types of converters. Table obtained from Roundy2003.

converter, a maximum magnetic field of 0.1T for Practical and 1T for Theoretical are assumed. Table 1-5 shows that piezoelectric converters have higher practical energy densities than the other two options. Nevertheless, it is important to have in mind other qualitative and performance comparisons for these converters.

- Electromagnetic converters produce very low voltages. This is a serious problem because the signal generated from the converter is an AC signal so it needs to be rectified. In order to increase this signal a very big transformer has to be used so the dimensions of the whole system increase. These converters have other problems intrinsically associated to them. The role of the magnetic fields in the transduction process can produce interferences with its associated electronic circuitry. These converters have the advantage of being easily micromechanized.

- Electrostatic converters have the disadvantage of needing an external power source to charge the capacitor beforehand; moreover they need a mechanical stop in order to avoid the contact between the two plates. This mechanical stop will increase the damping of the system. In contrast, these converters produce higher voltages than the electromagnetic ones, and can be directly rectified. A very interesting advantage of these converters is their easy integration in micromechanic systems that allow the design of compact and specifically designed systems.

- Piezoelectric converters have the highest energy density. The voltage and current levels are in an acceptable range and are easily modified to fulfill the input specifications. These converters do not need any magnetic field or mechanical stop. However PZT film is not a normal material for general silicon processing, often requiring many more mask steps. Therefore, the potential for integration with microelectronics is less than that for electrostatic converters [Roundy2003]. The difficulties in microstructuring the piezoelectric materials have limited the design of more complex mechanical structures that could increase the harvesting of power. However, it is much easier to implement simple converters than with other methods. A piezoelectric converter can easily be designed with a commercial piezoelectric cantilever and a mass attached at its tip for matching the vibration frequency. Such a simple device is able to generate enough power to drive a transceiver inside a building [Roundy2000].On the other hand, electrostatic and electromagnetic converters require complicated structuring designs.

1.3.2. Alternative power sources

Conversion of energy through mechanical vibrations is not the only way to harvest energy from the environment; in this section other forms of environmental dust energy are presented.

1.3.2.1. Solar energy

Solar energy is widely used as a power source in many applications. In fact, solar radiation varies around the world due to weather conditions, longitude and latitude, etc… However, it is possible to give an averaged value for a direct bright sun of about 100mW/cm^2. It is also possible to use the emitted light inside a building; in this case an average value of about 100μW/cm^2 is expected. [Paradiso2005]

The conversion principle for changing light into electrical energy is based in the photovoltaic effect. This effect is the result from the interaction between light and matter, the absorption of the photon energy by the photovoltaic cell generates electrical current. Silicon solar cells are a mature technology for a large scale. Photovoltaic systems are found from the Megawatt to the miliwatt range, producing electricity for a wide range of applications with efficiencies from 12% to 25%. There are thousand of companies that supply silicon solar cells and expend millions of dollars to improve its efficiencies while reducing costs. However, new materials with tremendous challenging potential applications are being used to form photovoltaic cells. Nanosolar [NANOSOLAR], Konarka [KONARKA], and other companies are developing energy-producing material with solar cells embedded in thin sheets of plastic, which promises to drastically reduce solar power's cost. This "power plastic" can be laminated onto any surface, from rooftops to laptops to automobiles [Krikke2005].

1.3.2.2. Heat converters

The use of heat gradients to generate energy was one of the first ways to accomplish energy conversion that we known. The classical "vapor machines" used the expansion of a gas, that when heated, moved a "piston" by pressure and generated a mechanical motion. However this kind of systems could not be considered as an energy harvesting system, since it would need to combust some kind of substance or material. On the other hand, in the environment, there are different constant sources of wasted heat that can be used to generate electrical power. The human body is always at the same temperature even the environmental temperature changes, this heat gradient can be used to generate electrical current. In fact, there are several applications that waste heat when working, some motor engines, ovens, laptops, etc.

There are different methods or principles to convert a heat gradient into electrical energy. In the following paragraphs, an overview of two of these principles is given.

Thermoelectric generators These kinds of generators have been of great interest in the recent years. They are based on a junction of two dissimilar materials "n" and "p" semiconductors. These are connected by a metal conductor at the hot and at the cold side of the gradient. A temperature gradient across the thermoelectric material , drives electron charge carriers from the hot to the cold junction and produce a voltage. Thermoelectric generators are a good choice since they can be microfabricated with classical microfabriaction techniques. In 1997 Stordeur et al. designed a first micropower thermoelectric generator able to produce 20μW with ΔT=20K [Stordeur1997]. Nowadays, some companies are selling products based on thermoelectric generators. For example, Seiko placed for sale a thermal wristwatch that uses 10 thermoelectric modules to generate sufficient microwatts to run its mechanical clock [SEIKO]. Also, Applied Digital Solution presented the Thermo Life, that is a thermoelectric generator measuring 0.5cm^2 and 1.6mm thick, that can supply energy to a biosensor when in contacts with the skin. It is able to supply, with a 5ºC gradient temperature, 5μA at 3V [AppliedSolutions].

Pyroelectric generators: This effect is manifested in polar materials when these are subjected to temperature changes. The effect is similar to the piezoelectric effect, but instead of electric charges appearing when the material is deformed, superficial charges appear, in a certain direction, when the material changes its temperature. The main difference between both principles is that pyroelectricity must be used in time varying temperature systems while thermoelectricity is used in DC systems. However, it is possible to use mechanical switches to use pyroelectric generators with constant temperature systems. While the use of pyroelectric generators is less extended, research efforts to improve the performances are being done [Sebald2008], [Sebald2008_2].

Next, a comparison on the different energy harvesting technologies is presented. The comparison has been extracted from the analysis made by Shad Roundy in his dissertation submitted at the Virginia Polytechnique Inststute [Roundy2003]. Table 1-6 shows the energy densities for a set of different environmental scavenged power sources and for some energy reservoirs. The table is composed by three columns. The first one shows the energy density during the first year. The second column shows the energy density for the first year and up to the tenth year of life. This information is given to show the decrees in the performances of the energy reservoirs after several uses. The third column shows the source of information.

While this table of comparison is by no means exhaustive, it does provide a broad cross section of potential methods to scavenge energy and energy storage systems. Except for the nuclear uranium based sources, it is clearly seen that the energy reservoir undergoes to a considerable reduction of its energy density (one

order of magnitude) after the first year of use. This degradation in performances reduces the number of applications where this energy sources could be used. In contrast, the scavenging sources theoretically present the same performances after one year of life; therefore, it is possible to think in applications where the systems are completely autonomous for a long time. Comparing the different scavenging sources, it is clear that the most energetic is the solar solution in a sunny day. This is a much extended solution due to the ubiquitous of solar light. Mechanical vibrations are presented as the next more energetic solution. Because mechanical vibrations surrounds us everyday in our daily life and some theoretical and experimental implementations demonstrate generations of about 200μW/cm^2, big efforts are being done to accomplish designs for harvesting this energy. The last raw of the scavenged solutions shows the shoe insert solution. Some researchers have pointed out the possibility to use the energy damped in the sole of a shoe to drive some kind of wearable device. It is possible to harvest about 300 μW/cm^2 in normal walking conditions. The table shows other sources however the amount of energy these sources provide is very small.

		Power Density (μW/cm^3) 1 Year lifetime	Power Density (μW/cm^3) 10 Year lifetime	Source of information
Scavenged Power Sources	Solar (Outdoors)	15,000 - direct sun 150 - cloudy day	15,000 - direct sun 150 - cloudy day	Commonly Available
	Solar (Indoors)	6 - office desk	6 - office desk	Author's Experiment
	Vibrations	200	200	Roundy *et al* 2002
	Acoustic Noise	0.003 @ 75 Db 0.96 @ 100 Db	0.003 @ 75 Db 0.96 @ 100 Db	Theory
	Daily Temp. Variation	10	10	Theory
	Temperature Gradient	15 @ 10 °C gradient	15 @ 10 °C gradient	Stordeur and Stark 1997
	Shoe Inserts	330	330	Starner 1996 Shenck & Paradiso 2001
Energy reservoirs	Batteries (non-recharg. Lithium)	45	3.5	Commonly Available
	Batteries (rechargeable Lithium)	7	0	Commonly Available
	Hydrocarbon fuel (micro heat engine)	333	33	Mehra et. al. 2000
	Fuel Cells (methanol)	280	28	Commonly Available
	Nuclear Isotopes (uranium)	6x10^6	6x10^5	Commonly Available

Table 1-6 Comparison of energy scavenging and energy storage methods. Note that leakage effects are taken into consideration for batteries.Table obtained from Roundy2003.

1.3.3. Autonomous power sources for microrobots

The selection of an adequate power source for a specific microrobotic system is always a difficult task. Actually, many possible power scavenging schemes should be considered when looking for a viable source of energy to be used for powering a microrobot. First thing to consider is the application or environment where the microrobot would work at. This will restrict the number of possible scavenging schemes. Ultimately, the power source or sources must be small enough to fit onboard the robot, supply enough energy for locomotion and last long enough to perform the microrobot's task.

For instance, consider the European project MICRON concerning a cluster of mobile autonomous microrbots. In this project, a set of some microrobots were conceived to execute a collective task for manipulation. The powering solution adopted was an inductive power source i. e., a strong alternating magnetic field is applied that induces a current through a receiving coil (Robot Coil) incorporated into each robot. The applied magnetic field is generated by an array of coils embedded in the workplace's base plate (Power Floor) [Gao2005]. This method was selected because it allows a wireless powering. The MICRON applications allow working in a workbench with a Power Floor, and the dimension restrictions of the robot still lets one use the Robot Coil. The total power supplied to the robots is 400mW, enough for the robots powering. Figure 1-20 shows a picture of the whole system. The grated floor corresponds to the power floor.

When the dimension of the robot decreases drastically, this is the case of the I-SWARM microrobots; an inductive powering is not longer good enough. While the possibility to develop microcoils and integrate them in the robots exists, the problems arouses from the fact that to produce enough voltage in the micro coil, a very strong external magnetic field must be present, which is not only difficult to achieve, but the

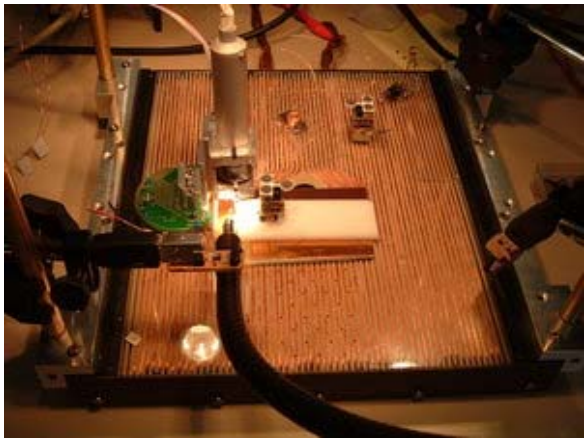

Figure 1-20 Picture for the MICRON setup with power floor. Picture obtained from the MICRON webpage.

Figure 1-21 Arena for the I-Swarm robots. Picture obtained from the ISWARM webpage.

thermal and magnetic interference could also be serious. The solution adopted in the ISWARM robots uses α-SI solar cells. The solar cells are located at the top part of the microrobot in a 3x3mm^2 plate. The whole system works in a controlled arena, where the light from a beamer is sent to transmit the energy. The solar cell modules are able generates up to 1mW, which is enough for the microrobots. Figure 1-21 shows two pictures of the final arena setup.

Inductive and solar energy transmissions are probably the most used techniques for powering autonomous mobile microrobots. One interesting feature of these techniques is that there is no physical contact between the energy source and the scavenger. The transmission is through magnetic fields or light respectively. As a result, the environment where the robot works is mechanically unaffected by the transmission. On the other hand, other possible technologies for energy scavenging as using piezoelectric materials for transform mechanical vibrations to electrical energy are much more hostile with the environment. Harvesting mechanical vibrations is not such a good choice to be used in those micropositioning applications where the vibration source could affect the final positioning.

Piezoelectric power harvesting from vibrations could be used in other type of systems where a microrobot is devoted to monitor and control some performances of a vibrating source. Other interesting applications could be in distributed microrobots where the elements of the robot are spatially separated. A piezoelectric power generation module could be located in vibrating sources while the other modules are located in mechanically isolated positions. However, one of the most promising applications for the piezoelectric power harvesting is in wireless sensor networks that consist of large numbers of spatially distributed sensors that have wireless connection with each other and possess its own autonomous power module. These networks are devoted to cooperatively monitor physical or environmental parameters

in a certain environment. These kinds of networks are being extensively studied by many researchers. One of the most active groups is located at the University of Berkley and is named the PicoRadio group leaded by Jan Rabaey [PICORADIO]. This group is dedicated to advancing the field of Wireless Sensor Networks in all areas: RF circuit design, networking, positioning, low voltage digital design, antenna design, and low power analog design. In [Rabaey2000] Rabaey et al. set the basics of the whole architecture of these networks. The nodes of the network are restricted to a total size of one cubic centimeter, weigh less than 100 grams, and cost substantially less than one dollar. The nodes must use ultra-low power to eliminate frequent battery replacement and a maximum power-dissipation level below 100 microwatts is expected. This low level power dissipation can be easily achieved with piezoelectric energy harvesting from vibration.

1.4. Thesis objectives

The fundamental goal of this research is to enhance the scientific and engineering communities understanding of the performances and capabilities of some "smart materials" in microrobotics systems. Among the whole smart materials family, in this thesis we focus on those electroactive induced strain materials as piezoelectric ceramics and polymers, and ionic polymers. In particular we focus on the study of the performances and capabilities of piezoelectric polymers and ionic polymers to form part in a microrobotic motion control system. Moreover we study the ability of piezoelectric ceramics and ionic polymers to harvest vibration energy from the ambient.

The main objective is accomplished through the resolution of "specific objectives". During this thesis we have participate in different research projects and we have initiate collaborations with other research groups. This has been a very good opportunity to apply the best "Smart Material" for specific application and analyze in depth its performances. These specific objectives are described in the following lines:

- The first objective is to study the capabilities of a piezoelectric polymer low voltage actuated microstructures for microrobot motion. Piezoelectric polymers are widely used in microrobotic applications as sensors however its use as actuators is very limited. Their low piezoelectric coefficient implies high driving voltages which limits its use in microrobotics. The possibility to microstructure the material and develop thin layer multilayer structures opens the door to the use of piezoelectric polymers for advance Smart systems with specific capabilities.

The work developed with piezoelectric polymers is performed with the support on a European project called I-Swarm (FP6-2003-IST-507006). The aim of this project is the realization of a "real" microrobot swarm. Each robot is formed by a polymeric backbone containing three piezoelectric polymer legs P(VDF-TrFE) and a piezoelectric polymer vibrating contact tool. The project take advantage of the novel possibility to manufacture very thin P(VDF-TrFE) layers to develop low voltage driven small legs for the robot based on multilayer structures deposited on the backbone of the microrobot. Moreover, the thin layer deposition technique allow to design a vibrating contact tool in the same way the legs are done, but leaving one layer free for sensing. This technology has been developed by the Uppsala University, the technological partner of the I-Swarm consortium.

The objective is accomplished through the theoretical analysis of the performances of the piezoelectric polymer based microrororobot legs and tool. A linear theoretical model is developed in order to predict the dynamic performances of the legs in terms of material and geometrical parameters. The model is validated along an experimental characterization in a real robot leg. The performances of the

piezoelectric based vibrating contact tool are also theoretically analyzed and the material and geometrical parameters optimizing its performances are identified. The model developed serves as a design tool for the programming of the microrobot integrated circuit electronics for object detection.

• The next objective regards the use of the "novel" materials IPMCs as underwater microrobotic motion actuators. In this case, the objective is to implement an appropriate control strategy for motion. Nowadays IPMC are in an early stage of development. It is still not possible to obtain IPMC samples with performances guaranteed. All samples that can be obtained are in a research step and they undergo to variable performances. Thus it is necessary to develop advanced control strategies to assure a certain dynamic response.

This objective has been carried out within the integrated action HG2007-08 with the Electronics laboratory at the Aristotle University of Thessaloniky in Greece. The aim of the project is to design a micropositioner bending actuator to work in underwater conditions. The project takes advantage of the physics involved in the IPMC transduction to design the microactuator as a cantilever formed with this material.

The control strategy adopted is based on an adaptive control scheme that adapts its control law to cope with the fact that the internal parameters of the actuator drift with time. The control system implemented is a second order Model Reference Adaptive Control. The strategy permits to assure the same dynamics performances of the ionic polymer motion for low frequency motion.

• Another objective is to implement a new manufacturing process for electrode deposition on IPMCs. The expansion of ionic polymers to work as actuators and sensors in microrobotic systems is being limited by different aspects. One regards the low accuracy in the prediction of their dynamics response that is solved using control strategies, and the other regard the possibility to microstructure and pattern the polymer. The objective is to propose an electrode deposition process compatible with MEMS technology. The main used technique for electrode deposition is based on a chemical deposition. Using this method the deposited metal penetrates in the membrane and diffuses inside it. This diffusion limits somehow the minimum spacing between metal layers for patterning electrodes.

This objective has been carried out with the collaboration of the Nanotechnology platform of the "Parc Cientific de Barcelona" at the University of Barcelona. The proposed technique is based on the physical vapor deposition technique of the metal electrodes on a pretreated Nafion surface. The surface is first etched with a reactive ion beam to improve mechanical adhesion and at the same time permit the electromechanical transduction. Although the transduction effect is reduced compared with the chemical technique, the technique is compatible with most MEMS and NEMS manufacturing processes.

• The next objective regards the study of the harvesting capabilities of piezoelectric ceramics and ionic polymers to convert energy from mechanical vibration sources, moreover the design of optimal electrical circuits to store/manage the electrical energy.

This objective has been carried out within the CICYT Spanish project TEC2005-08066-C02. To accomplish with the objective, the part regarding the IPMC was carried out in Italy with the collaboration of the "Dipartimento di Ingegneria Elettrica, Elettronica e dei Sistemi, Università degli Studi di Catania" in Sicily (Italy). The part regarding the piezoelectric ceramics has count with the collaboration of the "SMART SELF-POWERED BIO ELECTRONIC SYSTEMS" research line of the Instrumentation and Communication Systems research group (SIC) at the Department of Electronics in the University of Barcelona.

The study performed develops a linear theoretical model to predict the harvested power using a piezoelectric based cantilever beam vibrating from its base. The model takes into account the complex nature of the electrical impedance of the piezoelectric beam to define the optimum electrical load conditions for the maximum energy generation. The developed model is compared with other models in literature that neglect the complex nature of the beam. The theory developed is applied to a real composite piezoelectric beam and a discreet electronic circuit to fulfill the requirements of impedance adaptation is developed. While the proposed circuit needs external power sources to generate its control signal, the concept of impedance match is demonstrated.

To analyze the possibility to use ionic polymers there is the need for developing physical models that permits the identification of the parameters that plays a significant role in the power generation. However the difficulties associated in the development of physical models suggest applying for another approach. Therefore the modeling technique adopted is the gray box approach. In this case the model obtained for the piezoelectric transducer is adopted but the material parameters are experimentally identified. Although the identified parameters have other meaning in ionic polymers than in piezoelectric ceramics, it is possible to extract some conclusion of which are the real parameters affecting the performances.

The execution of this objective entails a better comprehend on which are the capabilities, the problems and solutions, the advantages and disadvantages on the use of these three smart materials families in microrobotic systems for motion control and power harvesting. Along this thesis different engineering approaches are performed to accomplish the objectives: different modeling techniques as physical models, gray box models and empirical models are developed, experimental characterization and system identification techniques, manufacturing and white room procedures for MEMS systems, advanced instrumentation techniques and electronic circuit design and more.

1.5. Overview

In this thesis the work developed to accomplish with the objectives is presented. The whole work is presented in two chapters, one regarding the motion control and the other regarding the power harvesting. In this point the organization of these chapters is described:

Chapter 2 regards the use of smart materials in motion control for microrobotics. This chapter is divided in two sections. The first part, Section 2.1., presents the study of the capabilities of a piezoelectric polymer low voltage actuated microstructures for microrobot motion. The study is started with the description of the insect-like microrobot structure. Then a brief explanation of the manufacturing process and the structure of the actuator and tool is presented. After, the theoretical analytical model is developed along with a proposal of a lumped electrical model equivalent circuit. for the microrobot's tool in terms of geometrical and material parameters. The section finishes with an experimental validation of the dynamic response of the actuator and tool of a real microrobot.

The second part of chapter, Section 2.2., regards the use of ionic polymers as underwater microrobotic motion actuators. The section starts with the description of the microrobotic structure. Then an empirical model is developed to describe the dynamic motion response of an ionic polymer strip working underwater. The next point presents the development of an advanced Model Reference Adaptive Control for control of the polymer underwater motion. The control is first simulated and then experimentally implemented. Following the motion control, the manufacturing technique for electrode deposition on ionic polymers is discussed in Section 2.2.4. First of all the classical chemical deposition technique is described. Then a physical vapor deposition technique with a reactive ion etching surface pretreatment is proposed. Both techniques are experimentally compared in terms of dynamic motion performances.

Chapter 3 regards the use of smart materials for power harvesting from vibrations. The chapter starts with the presentation of a general model for power harvesting extensively accepted at bibliography. Then a more detailed analytical model considering a cantilever based piezoelectric transducer is presented. The model is then validated with a commercial piezoelectric based transducer. Then an electronic circuit prototype for optimum energy management is implemented. The last part of the chapter, Section 3.3., presents a study of the harvesting capabilities of ionic polymers. A gray-box model is identified and then used to predict the power generated. The thesis finishes with the presentation of the conclusion obtained from the study.

1.6. References

[Abidian2006] M. R. Abidian, D. H. Kim, and D. C. Martin, "Conducting-polymer nanotubes for controlled drug release," *Advanced Materials,* vol. 18, pp. 405-+, 2006.

[Adolf1933] D. Adolf, M. Shahinpoor, D. Segalman and W. Witkowski 1993 Electrically controlled polymeric gel actuators, (world's first patent on synthetic artificial muscles) US Patent Specification 5250167 (Issued 5 October)

[Akhras2000] G. Akhras "Smart Materials and Smart Systems for the Future", Canadian Military Journal, Vol.1, No. 3, 2000, pp. 25-31

[Applied solutions] http\\www.:appliedsolutions.com

[Amirtharajah1998] R. Amirtharajah and A. P. Chandrakasan, "Self-powered signal processing using vibration-based power generation," *Ieee Journal of Solid-State Circuits,* vol. 33, pp. 687-695, 1998.

[APC INTER]. 2002. Piezoelectric Ceramics: Principles and Applications, APC International, LTD., Mackeyville, PA.

[Bar-Cohen2000] Y. Bar-Cohen, "Electroactive polymers as artificial muscles capabilities - Potentials and challenges," *Robotics 2000, Proceedings,* pp. 188-196, 2000.

[Bar-Cohen2000_2] Y. Bar-Cohen and S. Leary, "Electroactive polymers as artificial muscles changing robotics paradigms," *ACTUATOR 2000. 7th International Conference on New Actuators and International Exhibition on Smart Actuators and Drive Systems. Conference Proceedings|ACTUATOR 2000. 7th International Conference on New Actuators and International Exhibition on Smart Actuators and Drive Systems. Conference Proceedings,* pp. 201-4|688, 2000.

[Bar-Cohen2003] Y. Bar-Cohen and C. Breazeal, "Biologically inspired intelligent robotics," *Smart Structures and Materials 2003: Electroactive Polymer Actuators and Devices (Eapad),* vol. 5051, pp. 14-20, 2003.

[Bonomo2005] C. Bonomo, L. Fortuna, P. Giannone, S. Graziani, and S. Strazzeri, "A method to characterize IPMC membrane sensor," *Proceedings of the IEEE Instrumentation and Measurement Technology Conference (IEEE Cat. No.05CH37627C)|Proceedings of the IEEE Instrumentation and Measurement Technology Conference (IEEE Cat. No.05CH37627C),* pp. 5 pp.|CD-ROM, 2005.

[Bonomo2007] C. Bonomo, L. Fortuna, P. Giannone, S. Graziani, and S. Strazzeri, "A nonlinear model for ionic polymer metal composites as actuators," *Smart Materials & Structures,* vol. 16, pp. 1-12, 2007.

[Bonomo2008] C. Bonorno, P. Brunetto, L. Fortuna, P. Giannone, S. Graziani, and S. Strazzeri, "A tactile sensor for biomedical applications based on IPMCs," *Ieee Sensors Journal,* vol. 8, pp. 1486-1493, 2008.

[Breguet 2006] J.-M. Breguet, S. Johansson, W. Driesen, U. Simu A review on actuation principles for few cubic millimeter sized mobile micro-robots ACTUATOR 2006, 10th international Conference on New Actuators, 14-16 June 2006, Bremen, Germany

[Brewster1824] D. Brewster, Edinburgh. J. Sci., 1, 208-215, Observations on the pyroelectricity of minerals 1824

[Brufau2005] J. Brufau, A. Puig-Vidal, J. Lopez-Sanchez, J. Samitier, W. Driesen, J. M. Breguet, N. Snis, U. Simu, S. Johansson, T. Velten, J. Gao, J. Seyfried, R. Estana, H. Woern, and Ieee, "MICRON: Small autonomous robot for cell manipulation applications," *2005 Ieee International Conference on Robotics and Automation (Icra), Vols 1-4,* pp. 844-849, 2005.

[Brufau2005_2] J. Brufau-Penella, A. Saiz-Vela, J. Otero, J. López-Sánchez, P. Miribel-Català, M.Puig-Vidal, J. Samitier "Autonomous Atomic Force Microscopy System Based on Self-Sensing AFM Probes", DCIS XX Conference on Design of Circuits and Integrated Systems Lisboa, Portugal November, 23-25, 2005 ISBN 972-99387-2-5

[Brufau2006] J. Brufau-Penella, J. Sanchez-Martin, and M. Puig-Vidal, "Pizeoelectric polymer

model validation applied to mm size microrobot I-Swarm (Intelligent Swarm) - art. no. 61660Q," *Smart Structures and Materials 2006: Modeling, Signal Processing, and Control,* vol. 6166, pp. Q1660-Q1660, 2006.

[Brunetto2008] P. Brunetto, L. Fortuna, S. Graziani, and S. Strazzeri, "A model of ionic polymer-metal composite actuators in underwater operations," *Smart Materials & Structures,* vol. 17, 2008.

[Camacho-Lopez2004] M. Camacho-Lopez, H. Finkelmann, P. Palffy-Muhoray, and M. Shelley, "Fast liquid-crystal elastomer swims into the dark," *Nature Materials,* vol. 3, pp. 307-310, 2004.

[Chiu2007] Y. Chiu, C. T. Kuo, and Y. S. Chu, "MEMS design and fabrication of an electrostatic vibration-to-electricity energy converter," *Microsystem Technologies-Micro-and Nanosystems-Information Storage and Processing Systems,* vol. 13, pp. 1663-1669, 2007.

[Chrzan2001] M. J. Chrzan and J. D. Carlson, "MR fluid sponge devices and their use in vibration control of washing machines," *Smart Structures and Materials 2001: Damping and Isolation,* vol. 4331, pp. 370-378, 2001.

[Colli2006] M. Colli, A. Bellini, C. Concari, A. Toscani, and G. Franceschini, "Current-controlled shape memory alloy actuators for automotive tumble flap," *IECON 2006. 32nd Annual Conference on IEEE Industrial Electronics (IEEE Cat. No. 06CH37763)|IECON 2006. 32nd Annual Conference on IEEE Industrial Electronics (IEEE Cat. No. 06CH37763),* pp. 3987-90|CD-ROM, 2006.

[Curie1880] P. Curie Développement, par pression, de l'électricité polaire dans les cristaux hémièdres à faces inclinées Note de P. et J. Curie. C.R. T.91 (1880) 294-295.

[Dario1984] P. Dario, D. De Rossi, C. Giannotti, F. Vivaldi, and P. C. Pinotti, "Ferroelectric polymer tactile sensors for prostheses," *Ferroelectrics|Ferroelectrics,* vol. 60, pp. 199-214, 1984.

[DARPA] http://www.darpa.mil/

[de Genees2000] P. G. de Gennes, K. Okumura, M. Shahinpoor, and K. J. Kim, "Mechanoelectric effects in ionic gels," *Europhysics Letters,* vol. 50, pp. 513-518, 2000.

[de Rossi1992] D. De Rossi, M. Suzuki, Y. Osada, and P. Morasso, "Pseudomuscular gel actuators for advanced robotics," *Journal of Intelligent Material Systems and Structures|Journal of Intelligent Material Systems and Structures,* vol. 3, pp. 75-95, 1992.

[DREMED] http://www.dremed.com/

[Driesen2003] W. Driesen, A. Bergander, T. Varidel, and J. M. Breguet, "Energy consumption of piezoelectric actuators for inertial drives," *MHS2003. Proceedings of 2003 International Symposium on Micromechatronics and Human Science (IEEE Cat. No.03TH8717)|MHS2003. Proceedings of 2003 International Symposium on Micromechatronics and Human Science (IEEE Cat. No.03TH8717),* pp. 51-8|ix+360, 2003.

[DUPONT] http://www.dupont.com

[EAMEX] http://www.eamex.co.jp/index_e.html

[Eguchi1925] M. Eguchi, "On the permanent electret," *Philosophical Magazine,* vol. 49, pp. 178-192, 1925.

[Eisinberg2006] A. Eisinberg, K. Houston, I. Izzo, A. Menciassi, P. Dario, R. Gustafsson, U. Simu, and S. Johansson, "Design and fabrication of PZT-actuated tools for micromanipulation," *Journal of Micromechatronics|Journal of Micromechatronics,* vol. 3, pp. 329-57, 2006.

[El-Diraby2002] T. E. El-Diraby, and K. F. Kashif, (2002). "Modes of application of smart structures and systems in construction", 1st Int'l Conf. on Construction in the 21st Century, Florida International Univ., Miami, FL, April 24-26

[Fabreeka] http://www.fabreeka.com/tech/facility_planning.pdf

[Faradya1849] M. Faraday, Experimental Researches in Electricity I (London: Taylor) Chapt. 238 p. 68 1849

[Fukada2003] E. Fukada, M. Date, and K. Sekigawa, "Vibration control by magnetostrictive actuator coupled with negative inductance circuits," *Japanese Journal of Applied Physics Part 1-Regular Papers Short Notes & Review Papers,* vol. 42, pp. 7124-7128, 2003.

[Fukuda1995] T. Fukuda, H. Ishihara, and F. Arai, "Microrobotics, current of art and future," *Proceedings 1995 INRIA/IEEE Symposium on Emerging Technologies and Factory Automation. ETFA'95 (Cat. No.95TH8056)|Proceedings 1995 INRIA/IEEE Symposium on Emerging Technologies and Factory Automation. ETFA'95 (Cat. No.95TH8056),* pp. 29-39 vol.3|3 vol. (xi+709+603+580), 1995.

[Gao2005] J. Gao, "Inductive power transmission for untethered micro-robots," *IECON 2005. Thirty-First Annual Conference of the IEEE Industrial Electronics Society (IEEE Cat. No.05CH37699)|IECON 2005. Thirty-First Annual Conference of the IEEE Industrial Electronics Society (IEEE Cat. No.05CH37699),* pp. 6 pp.|CD-ROM, 2005.

[Gates2003] http://www.microsoft.com/presspass/ofnote/11-02worldin2003.mspx

[Graff1981] K. F. Graff, "A History of Ultrasonics," Chapter 1 of "Physical Acoustics," Vol. 15, Mason and Thurston, editors, Academic Press, 1981.

[Haga1998] Y. Haga, Y. Tanahashi, and M. Esashi, "Small diameter active catheter using shape memory alloy," *Micro Electro Mechanical Systems - Ieee Eleventh Annual International Workshop Proceedings,* pp. 419-424, 1998.

[Hanson2001] D. Hanson, G. Pioggia, Y. Bar Cohen, and D. de Rossi, "Androids: application of EAP as artificial muscles to entertainment industry," *Smart Structures and Materials 2001: Electroactive Polymer Actuators and Devices,* vol. 4329, pp. 375-379, 2001.

[Harrison2000] J. S. Harrison ; Z. Ounaies, Piezoelectric Polymers, NASA Center: Langley Research Center Publication Year: 2001 Added to NTRS: 2006-01-17 Document ID: 20020044745; Report Number: ICASE- 001-43, NAS 1.26:211422, NASA/CR-2001-211422

[Herr2003] H. Herr , A.Wilkenfeld User-Adaptive Control of a Magnetorheological Prosthetic Knee, Industrial Robot: An International Journal 2003; 30: 42-55.

[Herr2004] H. Herr and R. Kornbluh, "New horizons for orthotic and prosthetic technology: artificial muscle for ambulation," *Smart Structures and Materials 2004: Electroactive Polymer Actuators and Devices (Eapad),* vol. 5385, pp. 1-9, 2004.

[Hill1973] CR. Hill Medical ultrasonics: an historical review. Br J Radiol 1973;46:899–905 1973

[Hom2000] C. L. Hom, P. D. Dean, and S. R. Winzer, "Modeling electrostrictive deformable mirrors in adaptive optics systems," *Smart Structures and Material 2000: Smart Structures and Integrated Systems,* vol. 3985, pp. 394-405, 2000.

[ISWARM] http://wwwipr.ira.uka.de/i-swarm/MainPage/Robots/R_Images1.htm

[Jaffe1958] H. Jaffe. Piezoelectric Ceramics Presented at the Sixtieth Annual Meeting, The American Ceramic Society, Pittsburgh, Pa., April 28, 1958 (Electronics Division. No. 2).

[Kanno1994] R. Kanno, A. Kurata, M. Hattori, S. Tadokoro and T. Takamori 1994 Characteristics and modelling of ICPF actuator Japan-USA Symp. on Flexible Automation 2 691–8

[Kanno1996] R. Kanno, S. Tadokoro, T. Takamori, and M. Hattori, "Linear approximate dynamic model of ICPF (ionic conducting polymer gel film) actuator," *1996 Ieee International Conference on Robotics and Automation, Proceedings, Vols 1-4,* pp. 219-225, 1996.

[Kawai1969] H. Kawai, "The Piezoelectricity of Poly(vinylidene Fluoride)," Jpn. J. Appl. Phys. , Vol. 8, (1969) pp. 975-976

[Kim2002] K. J. Kim and M. Shahinpoor, "A novel method of manufacturing three-dimensional ionic polymer-metal composites (IPMCs) biomimetic sensors, actuators and artificial muscles," *Polymer,* vol. 43, pp. 797-802, 2002.

[Kim2002_2] W. J. Kim, J. H. Goldie, M. J. Gerver, J. E. Kiley, and J. R. Swenbeck, "Extended-range linear magnetostrictive motor with double-sided three-phase stators," *Ieee Transactions on Industry Applications,* vol. 38, pp. 651-659, 2002.

[Kim2005] B. Kim, D. H. Kim, J. H. Jung, and J. O. Park, "A biomimetic undulatory tadpole robot using ionic polymer-metal composite actuators," *Smart Materials & Structures,* vol. 14, pp. 1579-1585, 2005.

[KNOWLES] http://www.knowles.com/

[KONARKA] http://www.konarka.com

[Krikke2005] J.Krikke. Sunrise for energy harvesting products Published by the IEEE CS and IEEE ComSoc ■ 1536-1268/05/$20.00 © 2005 IEEE

[Kwak2005] J. W. Kwak, H. J. Chi, K. M. Jung, J. C. Koo, J. W. Jeon, Y. Lee, J. D. Nam, Y. Ryew, and H. R. Choi, "A face robot actuated with artificial muscle based on dielectric elastomer," *Journal of Mechanical Science and Technology,* vol. 19, pp. 578-588, 2005.

[Kymissis1998] J. Kymissis, C. Kendall, J. Paradiso, and N. Gershenfeld, "Parasitic power harvesting in shoes," *Digest of Papers. Second International Symposium on Wearable Computers (Cat. No.98EX215)|Digest of Papers. Second International Symposium on Wearable Computers (Cat. No.98EX215),* pp. 132-9|xiv+174, 1998.

[Laurent2001] G. Laurent and E. Piat, "Efficiency of swimming microrobots using ionic polymer metal composite actuators," *2001 Ieee International Conference on Robotics and Automation, Vols I-Iv, Proceedings,* pp. 3914-3919, 2001.

[Lee2006] S. G. Lee, H. C. Park, S. D. Pandita, and Y. Yoo, "Performance improvement of IPMC (ionic polymer metal composites) for a flapping actuator," *International Journal of Control Automation and Systems,* vol. 4, pp. 748-755, 2006.

[Li2000] W. J. Li, T. C. H. Ho, G. M. H. Chan, P. H. W. Leong, and H. Y. Wong, "Infrared signal transmission by a laser-micromachined vibration-induced power generator," *Proceedings of the 43rd Ieee Midwest Symposium on Circuits and Systems, Vols I-Iii,* pp. 236-239, 2000.

[Liu2004] C. Y. Liu and W. H. Liao, "A snake robot using shape memory alloys," *IEEE ROBIO 2004: Proceedings of the IEEE International Conference on Robotics and Biomimetics,* pp. 601-605, 2004.

[Lumia2008] R. Lumia; M. Shahinpoor, IPMC microgripper research and development Journal of Physics: Conference Series, Volume 127, Issue 1, pp. 012002 (2008).

[Mallavarapu2001] K. Mallavarapu and D. J. Leo, "Feedback control of the bending response of ionic polymer actuators," *Journal of Intelligent Material Systems and Structures,* vol. 12, pp. 143-155, 2001.

[Mateu2005] L. Mateu and F. Moll, "Review of energy harvesting techniques and applications for microelectronics," *VLSI Circuits and Systems II, Pts 1 and 2,* vol. 5837, pp. 359-373, 2005.

[Mauritz2004] K. A. Mauritz and R. B. Moore, "State of understanding of Nafion," *Chemical Reviews,* vol. 104, pp. 4535-4585, 2004.

[MELLESGRIOT] http://www.mellesgriot.com/pdf/CatalogX/X_31_3-7.pdf

[MEMICA] http://ndeaa.jpl.nasa.gov/nasa-nde/memica/memica.htm

[Meninger2001] S. Meninger, J. O. Mur-Miranda, R. Amirtharajah, A. P. Chandrakasan, and J. H. Lang, "Vibration-to-electric energy conversion," *Ieee Transactions on Very Large Scale Integration (Vlsi) Systems,* vol. 9, pp. 64-76, 2001.

[MICRON] http://vision.eng.shu.ac.uk/mmvlwiki/index.php/Micron

[MINIMAN] http://vision.eng.shu.ac.uk/mmvlwiki/index.php/Miniman

[Miribel2002] P. Miribel-Catala, E. Montane, J. Lopez-Sanchez, M. Puig-Vidal, S. A. Bota, J. Samitier, U. Simu, and S. Johansson, "Smart power integrated circuit for a piezoelectric miniature robot," *Analog Integrated Circuits and Signal Processing,* vol. 33, pp. 191-200, 2002.

[Morita2003] T. Morita, "Miniature piezoelectric motors," *Sensors and Actuators a-Physical,* vol. 103, pp. 291-300, 2003.

[NANOSOLAR] http://www.nanosolar.com
[NASA] http://www.nasa.gov/
[Nathanson1967] H.C. Nathanson, et al., "The Resonant Gate Transistor", IEEE Trans. Electron Devices, March 1967, vol. 14, no. 3, pp 117-133.
[Nemat-Nasser2000] S. Nemat-Nasser and J. Y. Li, "Electromechanical response of ionic polymer metal composites," *Smart Structures and Materials 2000: Electroactive Polymer Actuators and Divices (Eapad),* vol. 3987, pp. 82-91, 2000.
[Newbury2003] K. M. Newbury and D. J. Leo, "Linear electromechanical model of ionic polymer transducers - Part I: Model development," *Journal of Intelligent Material Systems and Structures,* vol. 14, pp. 333-342, 2003.
[Newbury2003_2] K. M. Newbury and D. J. Leo, "Linear electromechanical model of ionic polymer transducers - Part II: Experimental validation," *Journal of Intelligent Material Systems and Structures,* vol. 14, pp. 343-357, 2003.
[Odachi1999] Y. Odachi, Y. Kashiwagi, T. Harasawa, and Y. Kouketsu, "Magnetostrictive torque sensor|has male and female connectors provided in stator detent for stator rotation regulation," Toyoda Automatic Loom Works; Toyoda Jidoshokki Seisakusho Kk, 1999.
[Oguro1993] K. Oguro, K. Asaka and H. Takenaka 1993 Actuator element US Patent Specification 5268082 (Issued December)
[Oguro2001] K. Oguro Prep. Proc. Ion-Exchange Polymer Metal Composites (IPMC) Membranes Web at http://ndeaa.jpl.nasa.gov/ nasande/lommas/eap/IPMC PrepProcedure.htm 2001
[Onsager1931] L. Onsager, "Reciprocal relations in irreversible processes. I," *Physical Review,* vol. 37, pp. 405-426, 1931.
[Paradiso2005] J. A. Paradiso and T. Starner, "Energy scavenging for mobile and wireless electronics," *Ieee Pervasive Computing,* vol. 4, pp. 18-27, 2005.
[Parliament2008] www.parliament.uk/parliamentary_offices/post/pubs2008.cfm
[PI] http://www.physikinstrumente.com/
[PICORADIO] http://bwrc.eecs.berkeley.edu/Research/Pico_Radio/
[Pitt2002] D. M. Pitt, J. P. Dunne, and E. V. White, "SAMPSON smart inlet design overview and wind tunnel test - Part I - Design overview," *Smart Structures and Materials 2002: Industrial and Commercial Applications of Smart Structures Technologies,* vol. 4698, pp. 13-23, 2002.
[Rabaey2000] J. M. Rabaey, M. J. Ammer, J. L. da Silva, D. Patel, and S. Roundy, "PicoRadio supports ad hoc ultra-low power wireless networking," *Computer,* vol. 33, pp. 42-+, 2000.
[Rembold1997] U. Rembold and S. Fatikow, "Autonomous microrobots," *Journal of Intelligent & Robotic Systems,* vol. 19, pp. 375-391, 1997.
[Roundy2002] S. Roundy, P. K. Wright, and K.S.J. Pister Micro-Electrostatic Vibration-to-Electricity Converters Proceedings of IMECE'02 2002 ASME International Mechanical Engineering Congress & Exposition New Orleans, Louisiana 17-22, 2002
[Roundy2003] S. Roundy Energy scavenging for wireless sensor nodes with a focus on vibration to electricity conversion Berkeley, CA, 2003.
[Roundy2004] S. Roundy and P. K. Wright, "A piezoelectric vibration based generator for wireless electronics," *Smart Materials & Structures,* vol. 13, pp. 1131-1142, 2004.
[SANDIA] http://mems.sandia.gov/)
[Schwartz 2002] Encyclopedia of Smart Materials, Volumes 1-2 Edited by: Schwartz, Mel © 2002 John Wiley & Sons ISBN: 978-0-471-17780-7
[Sebald2008] G. Sebald, E. Lefeuvre, and D. Guyornar, "Pyroelectric energy conversion: Optimization principles," *Ieee Transactions on Ultrasonics Ferroelectrics and Frequency Control,* vol. 55, pp. 538-551, 2008.
[Sebald2008_2] G. Sebald, S. Pruvost, and D. Guyomar, "Energy harvesting based on Ericsson pyroelectric cycles in a relaxor ferroelectric ceramic," *Smart Materials &*

Structures, vol. 17, 2008.

[SEIKO] http://www.seikowatches.com

[Serre2007] C. Serre, A. Perez-Rodriguez, N. Fondevilla, J. R. Morante, J. Montserrat, and J. Esteve, "Vibrational energy scavenging with Si technology electromagnetic inertial microgenerators," *Microsystem Technologies-Micro-and Nanosystems-Information Storage and Processing Systems,* vol. 13, pp. 1655-1661, 2007.

[Seyfried2004] J. Seyfried, M. Szymanski, N. Bender, R. Estana, M. Thiel, and H. Worn, "The I-SWARM project: intelligent small world autonomous robots for micro-manipulation," *Swarm Robotics. SAB 2004 International Workshop. Revised Selected Papers (Lecture Notes in Computer Science Vol.3342)|Swarm Robotics. SAB 2004 International Workshop. Revised Selected Papers (Lecture Notes in Computer Science Vol.3342),* pp. 70-83|vii+174, 2005.

[Shahinpoor1998] M. Shahinpoor, Y. Bar-Cohen, J. O. Simpson, and J. Smith, "Ionic polymer-metal composites (IPMCs) as biomimetic sensors, actuators and artificial muscles - a review," *Smart Materials & Structures,* vol. 7, pp. R15-R30, 1998.

[Shahinpoor2001] M. Shahinpoor and K. J. Kim, "Ionic polymer-metal composites: I. Fundamentals," *Smart Materials & Structures,* vol. 10, pp. 819-833, 2001.

[Shahinpoor2005] M. Shahinpoor and K. J. Kim, "Ionic polymer-metal composites: IV. Industrial and medical applications," *Smart Materials & Structures,* vol. 14, pp. 197-214, 2005.

[Simu2002] U. Simu and S. Johansson, "Fabrication of monolithic piezoelectric drive units for a miniature robot," *Journal of Micromechanics and Microengineering,* vol. 12, pp. 582-589, 2002.

[Simu2006] U. Simu and S. Johansson, "Analysis of quasi-static and dynamic motion mechanisms for piezoelectric miniature robots," *Sensors and Actuators a-Physical,* vol. 132, pp. 632-642, 2006.

[Snis2005] N. Snis, U. Simu, and S. Johansson, "A piezoelectric disc-shaped motor using a quasi-static walking mechanism," *Journal of Micromechanics and Microengineering,* vol. 15, pp. 2230-2234, 2005.

[Spillman1996] W. B. Spillman, J. S. Sirkis, and P. T. Gardiner, "Smart materials and structures: What are they?," *Smart Materials & Structures,* vol. 5, pp. 247-254, 1996.

[Spillmann2007] C. A. Spillmann, J. Naciri, B. D. Martin, W. Farahat, H. Herr, and B. R. Ratna, "Stacking nematic elastomers for artificial muscle applications," *Sensors and Actuators a-Physical,* vol. 133, pp. 500-505, 2007.

[STANDAR] ANSI/IEEE Std 176-1987 IEEE Standard on Piezoelectricity

[Stordeur1997] M. Stordeur, I. Stark (1997), "Low power thermoelectric generator – self-sufficient energy supply for micro systems", Proc. ICT'97 16th Int. Conf. Thermoelectrics, pp.575-7.

[Su2000] J. Su, J. S. Harrison, T. L. S. Clair, Y. Bar-Cohen, and S. Leary, "Electrostrictive graft elastomers and applications," *Electroactive Polymers (EAP). Symposium (Materials Research Society Symposium Proceedings Vol.600)|Electroactive Polymers (EAP). Symposium (Materials Research Society Symposium Proceedings Vol.600),* pp. 131-6|xiii+336, 2000.

[Tadokoro2000] S. Tadokoro, S. Yamagami, T. Takamori, and K. Oguro, "Modeling of Nafion-Pt composite actuators (ICPF) by ionic motion," *Smart Structures and Materials 2000: Electroactive Polymer Actuators and Divices (Eapad),* vol. 3987, pp. 92-102, 2000.

[Tagliareni2005] F. Tagliareni, M. Nierlich, O. Steinmetz, T. Velten, J. Brufau, J. Lopez-Sanchez, M. Puig-Vidal, and J. Samitier, "Manipulating biological cells with a micro-robot cluster," *2005 IEEE/RSJ International Conference on Intelligent Robots and Systems|2005 IEEE/RSJ International Conference on Intelligent Robots and Systems,* pp. 1414-19|CD-ROM, 2005.

[Trassatti1999] S. Trasatti; 1799-1999 : Alessandro volta's 'electric pile'. two hundred years, but it doesn't seem like it Journal of electroanalytical chemistry ISSN 1572-6657 Source / Source 1999, vol. 460, no1-2, pp. 1-4 [4 page(s) (article)]

[Umeda1996] M. Umeda, K. Nakamura, and S. Ueha, "Analysis of the transformation of mechanical impact energy to electric energy using piezoelectric vibrator," *Japanese Journal of Applied Physics Part 1-Regular Papers Short Notes & Review Papers,* vol. 35, pp. 3267-3273, 1996.

[Williams2001] C. B. Williams, C. Shearwood, M. A. Harradine, P. H. Mellor, T. S. Birch, and R. B. Yates, "Development of an electromagnetic micro-generator," *Iee Proceedings-Circuits Devices and Systems,* vol. 148, pp. 337-342, 2001.

[Yamakita2005] M. Yamakita, N. Kamamichi, T. Kozuki, K. Asaka, and Z. W. Luo, "Control of biped walking robot with IPMC linear actuator," *2005 IEEE/ASME International Conference on Advanced Intelligent Mechatronics, Vols 1 and 2,* pp. 48-53, 2005.

[Yao2002] G. Z. Yao, F. F. Yap, G. Chen, W. H. Li, and S. H. Yeo, "MR damper and its application for semi-active control of vehicle suspension system," *Mechatronics,* vol. 12, pp. 963-973, 2002.

2. MOTION CONTROL IN MICROROBOTICS

The recent evolution in microrobotic systems has been colligated to the evolution in the technology of microsystems and to the advances in the research of new active materials. The requirements and expectations of new "Smart systems" in developing more efficient and sustainable systems with full integration of functions, have forced the evolution of new motion control based in new smart materials.

Most of the microrobotic systems involving motion developed in this last decade were based in the use of piezoelectric ceramics for motion actuation. That was a consequence of the possibility to manufacture microsytems technology for developing piezoceramic systems. Piezoelectric ceramics are hard materials that can produce high forces when driven with relatively small electric fields. Moreover these materials produce movements with extremely high resolution depending on the driving signals. In addition, they present a very fast response and a high reliability. All these material performances had permitted the development of high precision microrobots and advanced tools for micromanipulation and micropositioning.

Nowadays new emerging prospects in the design of microrobotic systems have entailed the appearance of new materials to accomplish with these new expectations. Some of these prospects are microrobots that mimic biological systems, microrobots that work inside the body as endoscopic tools, microrobot that work underwater, etc. Therefore requirements for the new materials as flexibility, water compatibility, low power consumption, low voltage activation and biocompatibility are expected. The early state of development of such microrobotic systems implies the need of determining and studying the performances, capabilities and limitations of the different materials. Moreover it is important to define manufacturing process compatible with microsystems technologies.

In this chapter the use of two polymeric smart materials in flexible microrobotics for motion control is studied. The materials under study are the piezoelectric polymers and the ionic polymers. The chapter is divided into two parts:

- The first part of the chapter regards the motion control of the piezoelectric polymer microrobot from the I-SWARM project. The locomotion platform of this microrobot was designed by the Uppsala University project partner. It is formed with a novel microstructuring technique that allows the development of P(VDF-TrFE) multilayer structures. This thin layer deposition technique permits to drive the

structure with low voltage. The work realized in this chapter is devoted to analyze the performances of the microrobot motion actuators and its contact sensor tool. The analysis consists on the development of a physical model to help us to understand its behavior and the experimental characterization of their electromechanical response. Furthermore, for the contact sensor an equivalent circuit model, compatible with IC design software, is designed.

- The second part of the chapter regards the motion control for an IPMC strip working underwater. In this case a close loop control is needed to assure a certain dynamics of the actuator response. IPMC materials are submitted to slow time scale fluctuations of its dynamic response. The proposed control is based on an adaptive control strategy to overcome these slow fluctuations and assure a certain dynamics. At the end of the chapter a novel manufacturing technique for electrode deposition is proposed. While most common techniques used for developing electrodes are based on the diffusion of metal particles inside the IPMC membrane, this new technique allows a more precise control of the pattern of the electrodes. The technique is compatible with standard MST technologies.

2.1. Piezoelectric polymer based microrobotic actuator

The work presented in this section is performed in the framework of the European project I-Swarm (FP6-2003-IST-507006). The aim of this project is the realization of a "real" microrobot swarm. One thousand of micro-manufactured autonomous robots mm^3 size will be designed for the collective execution of different tasks in the small world. A swarm of microrobots could be able to perform tasks that are not possible with only one single microrobot or either with a small quantity of them. One objective of the project is the observation of a self-organized response of the microrobot swarm similar to those appearing in nature by individual communities, i.e. ants, bees, etc.

Regarding the microrobots actuation, a bioinspired approach is pursued. In insects, the mechanical structure for locomotion is based on shells and muscles in contrast to e.g. bones and muscles in larger animals. A shell structure where bending hinges are used as joints is e.g. one way to "mimic" the biological world with artificial structures. Agile limbs and antennas can be made when a suitable "muscle" or "smart material" is integrated with the shell structure. The structure or backbone of the robot is polymeric, and it consists on a Flexible Printed Circuit Board (FPCB). The FPCB gives flexibility, electrical connects, three-dimensionality and high-quality material properties. The FPCB processing technology allows for well-defined structures (the shells in the insect robot) and well-controlled grooves for the bending hinges. As "smart material" for sensing and actuation a piezoelectric polymer is used because its flexibility and its low energy consumption. Actually the polymer used is a the Poly(vinylidene fluoride-trifluorethylene) P(VDF-TrFE). One of the main challenges in the manufacturing of the microrobots has been the possibility to construct thin multilayer piezopolymer structures that allow a low voltage driving since these materials needs high electric fields to operate.

The mechanical structures have been implemented using a novel dry etching technique developed by the ISWARM project partner: Angstrom Laboratory at the Upssala University (Sweden). It is based on three limbs or legs and one antenna. The legs consist on piezopolymer multilayer actuators driven at their resonance frequencies with low voltage signals. Controlling how these signals are applied to the robot it is possible to produce motions upwards, downwards and rotations. The antenna or contact sensor is also based on a piezopolymer multilayer structure but in this case two piezoelectric layer of the ten layers and are used as sensor layers. Piezoelectric polymers are smart materials that can work as actuator or as sensors. Thus this antenna take advantage of this performance, while it is actuated, the motion produced is measured in the sensing layer. If the antenna or tool touches an object, the amplitude and frequency of tool resonance changes, thus the sensing signal changes and the collision is perceived by the robot. Actually the brain or heart of the microrobot is based in a specific Integrated Circuit mounted in the FPCB. This IC is

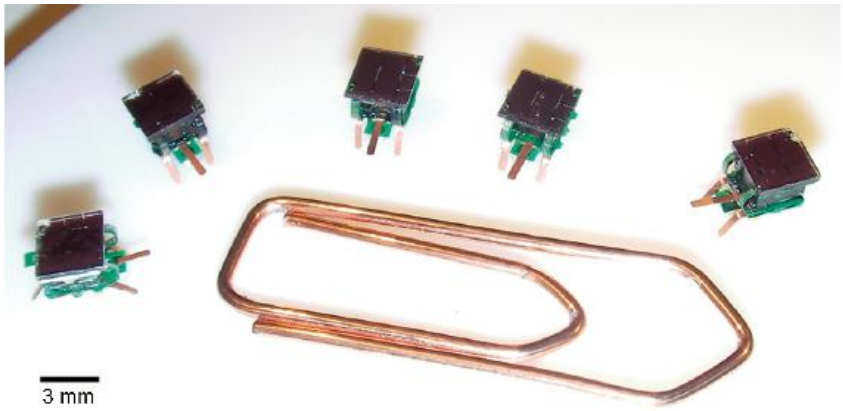

Figure 2-1 Five I-Swarm microrobots standing around an ordinary paper clip. Picture obtained from Snis2008_2.

also the responsible to control the motion and sensing microrobot capabilities. Figure 2-1 shows five I-Swarm microrobots standing besides and ordinary clip.

This section of the chapter focuses on developing models and on experimental characterization of the legs and tool performances. The models developed are physical models based on well established physical relations that allow the prediction of their performances in terms of material and geometrical parameters. Moreover, an equivalent circuit model is proposed for the microrobot tool. This equivalent circuit is used together with IC simulation software to design a control algorithm for the measurement and detection of microrobot contact/colision.

2.1.1. The I-Swarm microrobot structure

Polymer Microsystems technology is a good solution to build the I-Swarm microrobots due to its low cost for mass production. The integration of dry Electro Active Polymer (EAP) onto Flexible Printed Circuit (FPC) defines a competitive polymer building technology for the I-Swarm robots. The proposed microrobot structure is based on FPCB which give flexibility, electrical connections to the different modules and, at the same time, is used as the backbone of the robot. A picture of the finally assembled I-Swarm microrobot is depicted at Figure 2-2

The microrobot swarm is located on a benchmark platform where a light emitting beamer will be used to transfer energy and program the robots. Each robot is based on five different modules:

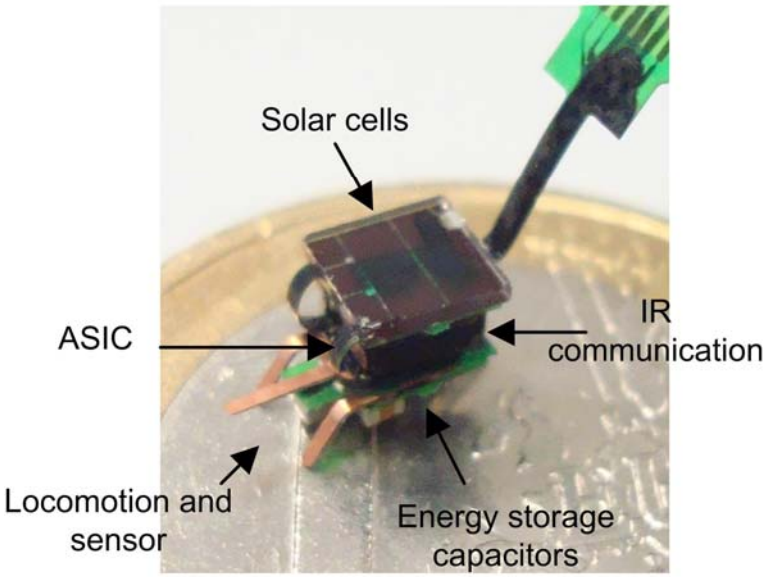

Figure 2-2 The I-SWARM microrobot with sensors, communication, electronics, power source and locomotion capabilities is shown.

Solar cells are located at the top of the microrobot. Their purpose is to scavenge energy coming from a beamer and to serve as a local positioning system [Boletis2006]. In the case of energy scavenging, the beamer is an energy source for the robots and the solar cells are the energy scavengers. The light power is therefore converted into electrical power. For the local positioning system the beamer transmits information by modulating the light intensity which is sensed by the photodiodes (independent solar cell segments).

Energy storage capacitors are mounted on the robots to store the electric energy acquired from the solar cells. The energy storage has two main functions: to deliver stable and continuous power when the power from solar cells fluctuates; and to provide short high-power pulses for communication and locomotion modules.

An IR-communication module based on Infra-Red Light Emitting Diodes (IR-LEDs), Photodiodes (PDs) and a top mirror is mounted. The objective is to communicate with other swarm agents within some mm range. The top mirror has the function to reflect emitted light from the LEDs in a direction parallel to the floor of the arena, on which other microrobots are located, and to deflect the incoming light down to the PDs. The IR-module allows communication and passive perception (for collision avoidance). [Alonso2007]

An ASIC integrated circuit assembled in the robot is able to manage movement, communications and sensing at the lowest level. All the features of the

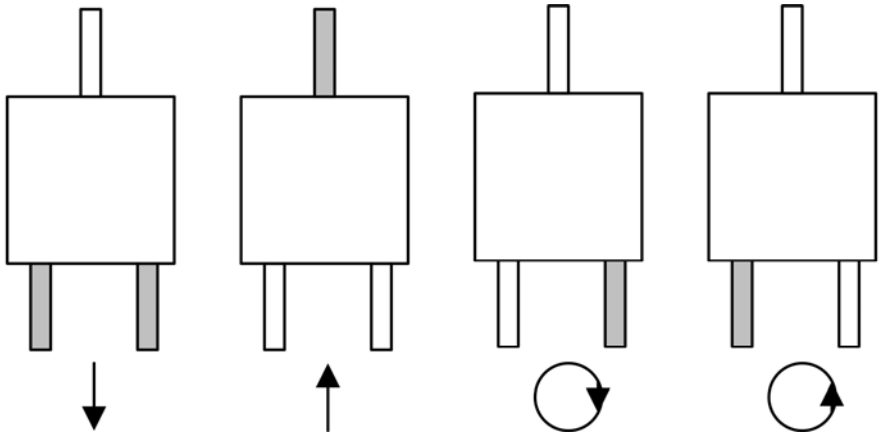

Figure 2-3 Direction motion possibilities of the microrobots

robot are controlled by software. The IC provides the interface to program the robot and the hardware platform to run the software. [Casanova2007]

The locomotion module is based on three legs folded in 55º angle and a horizontal tactile sensor in form of vibrating cantilever. The legs and tool are built on the same flexible printed circuit and consist on a multilayer piezoelectric polymer structure. They are actuated with the signals coming from the ASIC. The robot motion is based on the resonance driving principles [Uchino1996]. The leg is forced to bend by applying a voltage signal at its resonance. During part of the bending the leg is in contact with the floor, thus the mass of the robot move. During the rest of the motion, the leg move back free while the robot mass is hold by the other legs. The final kinematics of the robot is controlled exciting one or two of the three legs supporting the robot. These allow, up, down and rotation movements Figure 2-3. For a detailed description of the kinematics refer to [Snis2008_2].

2.1.2. Actuator motion

In this point the electromechanical behavior of the legs or actuators of the microrobot are analyzed. First of all a brief explanation of the manufacturing technique is presented, following a physical model is proposed. The physical model helps to determine how the different material and geometrical parameters affects the response of the limbs. Next an experimental characterization is realized and the ISWARM actuator model is validated.

2.1.2.1. Design and manufacturing

The Iswarm locomotion unit was completely developed by the Uppsala University, Department of Engineering Sciences at Sweden. The locomotion unit is based on three legs formed with active polymers. The piezoelectric polymer P(VDF-TrFE) was chosen as the active material because of its compelling properties like: good chemical and thermal stability, it can be easily processed and miniaturized, it is

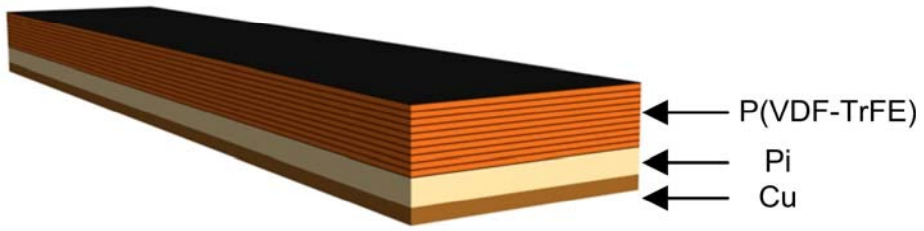

Figure 2-4 Schematic draw of the mulitlayer structure of the actuators, the image is not in scale.

lightweight, cheap, and can be spin coated. Because of the maximum voltage project restriction (3.3V in driving signals), a multilayer structure was chosen. Figure 2-4 shows a schematic draw of the actuators structure. The structure is a monomorph based on a multilayer structure mounted on a non-active substrate. This substrate is formed by a first Cupper Cu layer and a Polymide Pi layer. The multilayer consists on ten active layers sandwiched between electrode layers. The electrodes are connected in parallel to force high active electric fields between layers.

The fabrication process starts with a Flexible Printed Circuit Board (FPCB) made of a Polymide substrate and a Cupper mask. This FPC serves as the backbone of the robot and at the same time as the substrate of the monomorph structure. To define the microrobot base structures, the FPCB is patterned with photolithography process. Then a PVDF layer is spin coated and cured at the oven to form the 2μm active layers. After, an Al electrode layer is physical evaporated through a shadow mask to form 0.1μm electrode. The process is repeated to finally form the ten layers for the multilayer structure. The next step is to attack the structure with an Inductive Conductive Plasma ICP machine to remove the precise polymer layers and permit the parallel connection of the different layers. Conductive glue is used to interconnect the different electrodes. The final step is to polarize the active material by applying a high electric field at a high temperature. To find a more detailed description on the design and manufacturing process reefer to [Snis2008] and [Edqvist2008].

2.1.2.2. Physical model

In this point an analytical physical model is presented. The model is devoted to describe the actuating response of the I-Swarm microrobot leg. The mechanical structure modeled is shown at Figure 2-5. This structure consists on "m" layers, attached together, with the same length "l" and the same width "w". Each of these layers has its own height "h_i" ("i" denotes the number of layer), Young module matrix "Y_{xxi}", density "ρ_i", dielectric permittivity matrix "ε_{xxi}" and piezoelectric coefficient matrix "d_{xxi}". We define this vectors and matrix for an easy understanding of the mathematics, for those non-piezoelectric layers "d_{xxi}" and "ε_{xxi}" should be

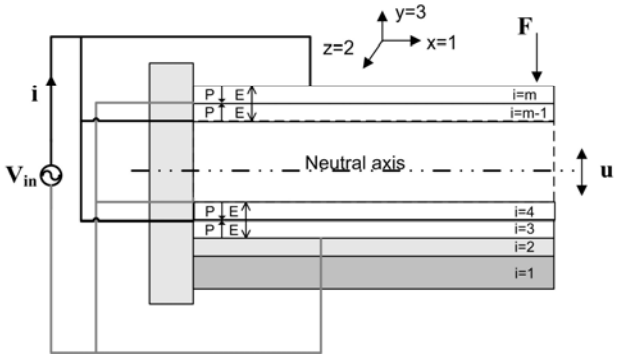

Figure 2-5: Schematic draw with the intensive variables "F" force, "V_{in}" voltage and the extensive, "u" deflection and "i" current.

considered zero. For the sign convention, associated to the different vectors, the axes in the Figure 2-5 are considered.

During many years the problem of the transversal vibrations on a cantilever has been treated by many authors. The more consolidated model is the Euler-Bernoulli model. In the 18th century, Euler proposed that the curvature of a beam is proportional to the torsion moment applied on that point. He presented the beam differential equations of motion. Another model is the Rayleigh model which introduces the influences of the rotations through its axial axis. Also there is the Timoshenko model which considers rotation and shear effects [Han1999]. In this work we focus on the Euler-Bernoulli model, therefore three assumptions are done. The first one is to consider a thin beam with no rotation. The second one is to consider the beam in its linear elastic region. The last one is to consider low curvatures.

The equations defining the dynamic response of the Euler-Bernoulli slender beam is based on the analysis of the transverse vibrations transmission in the beam. This is a classical approach in engineering mechanics. For the readers of this thesis not habituated to work with material resistance theory and modal analysis for transversal vibrations, the author of this thesis recommend them to read the Appendix A. In the appendix a detailed development of the dynamic equations that describe the actuator and sensor response for different piezoelectric based cantilever structures are presented. First of all a simple piezoelectric bimorph beam is studied, then the same mathematical development is used to study the dynamics of a generic multilayer beam structure. The generic solution is directly applicable to the structure from Figure 2-5. The mathematical development at the appendix starts by defining the forced partial differential equation PDE governing the motion of an infinitesimal element of the beam in terms of the spatial and temporal coordinates. To solve this PDE with two variables, spatial "x" and temporal "t", the separation of variables technique is used. It consists on the description of the vibration equation or beam deflection equation "u(x,t)" as the product of two functions u(x,t)=W(x)r(t), one dependent on the spatial coordinate "W(x)", and the other dependent on the temporal

coordinate "r(t)". The solution of the spatial equation is obtained from the unforced PDE. Using the separation of variables method it is possible to write the unforced PDE as two ordinary differential equations ODE, one for the spatial coordinate, and the other for the temporal. From the spatial unforced ODE and the mechanical boundary conditions it is found that the equation has infinite solution. These solutions are called the mode shapes of the beam "$W_n(x)$". Once the mode shapes equations are obtained, the appendix presents the solution of the forced equation under different excitation conditions. For this purpose the forced PDE is converted into a temporal ODE using the orthogonality properties of the mode shapes equations. This temporal ODE has a solution "$r_n(t)$" for each "$W_n(x)$" or vibration mode. The final vibration equation or beam deflection is then defined for each mode as $u_n(x,t)=W_n(x)r_n(t)$. In this section the analysis of the actuator response of the microrobot's leg starts with the definition of the ODE forced temporal equation developed in eqA.53.

$$K_n r_n(t) + c_n \dot{r}_n(t) + m_n \ddot{r}_n(t) = \Theta_n V_{in}(t) \qquad \textit{Eq 2-1}$$

This equation looks like a single-degree-of-freedom oscillator with a spring constant, a damping coefficient, a mass and an input force. However in this case "K_n" is the modal stiffness, "m_n" is the modal mass, "c_n" is the modal damping and "Θ_n" is the coupling coefficient. These parameters are different in terms of geometrical and material parameters for each vibration mode at eqA.43, eqA.44, eqA.45 and eqA.54 respectively.

Assuming an exponential input voltage $V_{in}(t)=Voe^{-j\gamma t}$, the solution for the temporal equation is written as

$$r_n(t) = \frac{\Theta_n}{m_n} \frac{V_{in}(t)}{\omega_n^2 - \gamma^2 + i\gamma \dfrac{c_n}{m_n}} \qquad \textit{Eq 2-2}$$

"ω_n" is the natural frequency of the system and is defined as $\omega_n^2=K_n/m_n$. "γ" is the frequency of input excitation. The modal analysis developed started considering the method of separation of variables, thus assuming the deflection of the beam "u(x,t)" as the product of a spatial solution, the mode shape "$W_n(x)$", and the temporal solution "$r_n(t)$", the final solution for the deflection of the leg is

$$u_n(x,t) = \frac{\Theta_n}{m_n} \frac{W_n(x)}{\omega_n^2 - \gamma^2 + i\gamma \dfrac{c_n}{m_n}} V_{in}(t) \qquad \textit{Eq 2-3}$$

This equation is rewritten in the Laplace domain

$$u_n(x,s) = \frac{\Theta_n}{m_n}\frac{W_n(x)}{s^2 + s\frac{c_n}{m_n} + \omega_n^2}V(s) = \frac{\Theta_n}{m_n}\frac{W_n(x)}{s^2 + s\frac{\omega_n}{Q_n} + \omega_n^2}V(s) \qquad \textit{Eq 2-4}$$

where "Q_n" is the quality factor of the system defined as $Q_n = \omega_n m_n / c_n$. Eq 2-4 is the classical equation for a harmonic oscillator where maximum appears at the natural frequency of the system. It is normal to describe this kind of systems with its static deflection "$u_n(x,s=0)$" Eq 2-5 for a given input "V_{in}".

$$u_n(x, s \cong 0) = \frac{\Theta_n}{K_n}V_{in} \qquad \textit{Eq 2-5}$$

The deflection at the resonance frequency of the system is directly computed as the static deflection multiplied by the quality factor. Substitution of $s=j\omega_n$ in equation Eq 2-4 and considering Eq 2-5 leads the resonance deflection as.

$$u_n(x, s \cong j\omega_n) = Q_n u_n(x, s \cong 0) \qquad \textit{Eq 2-6}$$

When manufacturing the robot legs it is important to design them with the highest static deflection. This is done increasing the coupling coefficient "Θ_n". This coefficient is increased by decreasing the thickness of the active layers in order to increase the electric field inside them. As far as the quality factor concerns, its value depends on the material selected. To design the system with an specific Q it is important to take a compromise, a high quality factor is an advantage since high displacement is obtained, but also it is a disadvantage since all legs has to be tuned at a very narrow resonance frequency or else a few legs will work at the resonance frequency generated by the robot electronics.

Eq 2-3 relates the leg deflection with an input voltage applied. Now it is important to obtain the electrical equation that relates the absorbed current when an input voltage is applied. The equation of the absorbed charge is here rewritten from appendix A:

$$Q(t) = \Theta_n r_n(t) + C_p V_{in}(t) \qquad \textit{Eq 2-7}$$

where "C_p" is the capacitance value of the actuator. This electrical equation shows that the generated charge is the summation of two terms, one due to the pure capacitive behavior of the material and another term due to the piezoelectric effect of the P(VDF-TrFE) layers. Thus, while the electrical impedance of the actuator is mainly capacitive, it is affected by the mechanical motion of the system. This effect will be emphasized near each natural frequency.

The model obtained in this point was presented by the author of this thesis in the SPIE conference [Brufau2006]. In that paper the model was experimentally validated with cm size self-made PVDF multilayer actuators. In the following lines, the model is applied to real I-Swarm legs.

2.1.2.3. Experimental test

The I-Swarm robots are conceived to be constructed with a modular approach, thus each module is tested separately. In this section the experimental response of the legs are characterized and compared with model simulations. The three legs were first manufactured attached to a PCB for an easy test of its performances. Figure 2-6a) presents a picture of the PCB with three legs and the pins for applying the input signals. Figure 2-6b) is a zoom of the legs. Conductive glue is used to finally interconnect the PCB strips with the metal electrodes in the polymer to avoid soldering.

The test realized involved to apply a voltage signal to the legs and measure the displacement. For this purpose a fiber optic displacement sensor D6-H1 from Philtec has been used. The sensor gives an output signal proportional to the displacement. To realize a good measurement, the sensor has to be located at a certain distance from the target, this distance is very small (in the range of mm). Figure 2-7a) and b) show a picture of the experimental setup. The tip of the displacement sensor is mounted on a 3D manual micropositioner in order to position the sensor at the exact relative distance from the leg. A magnifying glass helps to avoid collision of the tip of the sensor with the leg. The exciting voltage signal is generated with a HP2200 signal generator. All the measurements are obtained with a data acquisition card PCI-MIO-16E-1 from National Instruments and the software LabVIEW

Figure 2-6 a) Picture of the PCB with the electrcical connector pins. b) Zoom of the legs with the conductive glue.

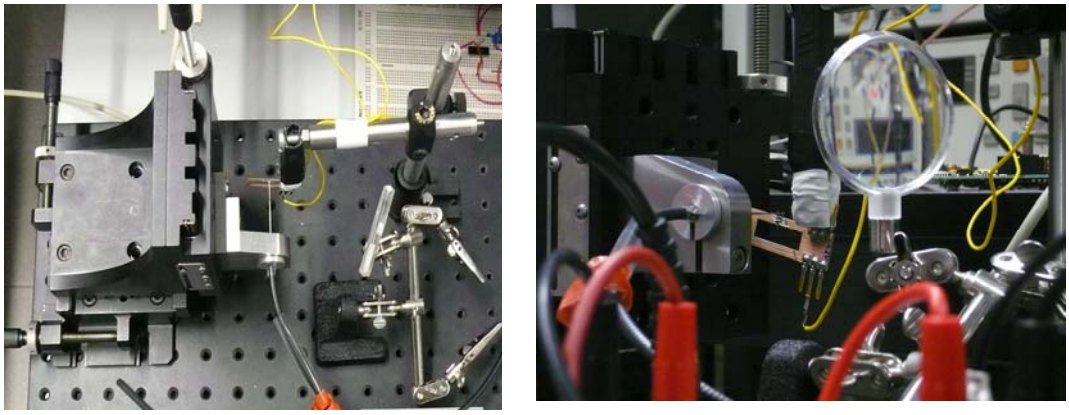

Figure 2-7 a) Top view of the experimental setup with the displacement sensor and the PCB. b) Later view of the experimental setup.

Number of active layers	10		
Height of the P(VDF-TrFE)	2e-6 m	Density P(VDF-TrFE)	1900 Kg/m^3
Height of the Cu layer	18e-6 m	Density Cu	9000 Kg/m^3
Height of the Pi layer	50e-6 m	Density Pi	1400 Kg/m^3
Height of the Al electrode layers	0.1e-6 m	Density Al	2700 Kg/m^3
Young modulus P(VDF-TrFE)	3.3e9 Pa	Quality factor	25
Young modulus Cu	128e9 Pa	Width	400e-6 m
Young modulus Pi	2e9 Pa	Length	2000e-6 m
Young modulus Al	69e9 Pa	Piezoelectric coefficient d31	18e-12 m/V
Height of the Al electrode layers	0.1e-6 m	Relative dielectric permittivity	14

Table 2-1 Material and geometrical parameters for the legs of the microrobots

The dimensions and physical parameters of the legs are reported at Table 2-1. Some of the reported values are measured and the others are from literature. Actually the quality factor "Q" and the dielectric permittivity have been measured by Upssala University. The piezoelectric coefficient is 18e-12 m/V, this is very small compared with piezoelectric ceramics. However the small height of the P(VDF-TrFE) layers and the multilayer structure permits driving with low voltage signals.

The first test realized is devoted to study the dynamic response of the leg. It consists on applying a sinusoidal sweep voltage signal and measure the displacement of the leg tip. To have enough frequency information in the input signal, the sweep was realized from 10 Hz up to 10 KHz during 3s with a sampling frequency of 100 KHz. To have a big displacement and avoid the effect of noise, the signal is 9Vpp instead of the maximum voltage of 3,3V we will use in the real ISWARM robot.

The experimental measurements are compared with evaluation of the model. Considering the material and geometrical parameters from Table 2-1, the model equation Eq 2-4 evaluated at the tip of the leg ($x=L_F$) remains

$$u_n(L_F, s) = \frac{8.28 \cdot 10^{-8}}{4.31 \cdot 10^{-10} s^2 + 8.29 \cdot 10^{-7} s + 1} V(s) \qquad \textit{Eq 2-8}$$

Figure 2-8 depicts the experimental and simulated results. Both curves show the resonant response of the leg. In the experimental curve it is observed the noise in the displacement measurement out from resonance. This noise is mainly attributed to the sensor resolution. Discrepancies arouses in the value of the simulated and experimental resonance frequency as well as in the amplitude at that frequency. The measured input output data is used together with Matlab® software to compute the bode function of the leg system. The results are presented at Figure 2-9. It is clearly observed the first resonant mode of the leg. Furthermore, the two curves have some discrepancies. The experimental curve has its resonance frequency in 7034Hz with a sensitivity 2.8µm/V and the simulated is at 7674Hz with 2µm/V. The mismatches between experimental and simulated data are attributable surely to deviations in the input specifications. The manufacturing process used for structuring the microrobots was proposed by Uppsala University [Snis2008]. This process has been briefly presented in section 2.1.2.1 it consists on a large quantity of steps. This steps involve, spin coating the piezoelectric layers and evaporation of the Aluminum layers, the plasma treatment for etching and the conducting glue for contacting. It is reasonable to think that the final prototype material parameters have some deviation compared from the expected ones. This deviation could produce the differences in the measurements and simulations.

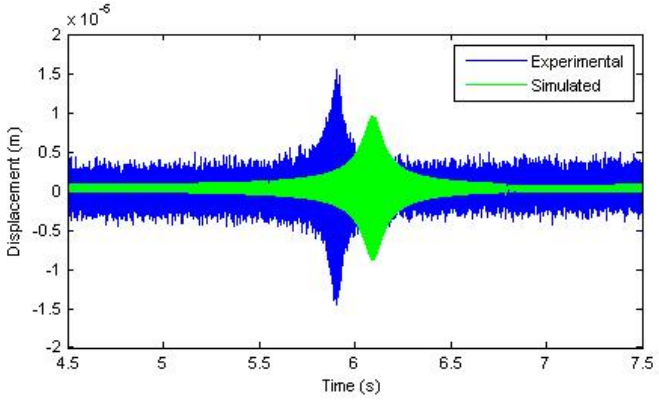

Figure 2-8 Experimental and simulated results for the microrobot leg response to a sinusoidal voltage sweep.

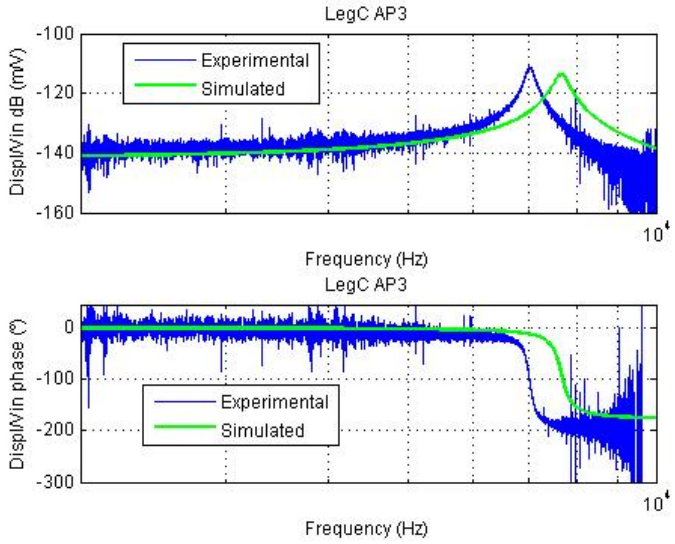

Figure 2-9 Experimental and simulated transfer function, at the top module, at the bottom phase.

I-Swarm microrobots are driven with low voltage square signal from the ASIC circuit. Figure 2-10 shows the experimental response of the leg when driven with a 3.3V signal at its resonance frequency. A 14μm peak to peak displacement is measured which is in the range of the project specifications. These results have demonstrated the validity of the microstructuring process. While P(VDF-TrFE) materials need large electric fields to be actuated, the proposed structuring process has permitted the actuation of these layers with a very low voltage 3.3V. In fact, the main problem when working with microrobotics is the power consumption more than the voltage. In this case, considering the input parameters of Table 2-1, the value of the capacitance for each layer is 49pF, thus for the ten layers working in parallel it becomes 490pF. A first estimation of the power consumption to drive one leg is realized assuming that the electrical impedance behaves as a pure capacitor, therefore the power is $P=\pi f V^2 C=117\mu W$ that is small enough for the project requirements. However, while the microstructuring technique is utile for developing low voltage actuated thin multilayer piezoelectric polymer structures, a problem arouses when trying to drive these legs with the ASIC designed for the microrobots. The low power and mass fabrication requirements of the project specification implied an open loop driving of the legs at one fixed frequency. Therefore those legs that have a resonance frequency shifted from the expected one due to the deviations in the manufacturing process will not be able to work with the ASIC. The solution pass through the integration of a displacement sensor in the leg and a closed loop driving start up. This functionality is implemented in the microrobot for controling the tool.

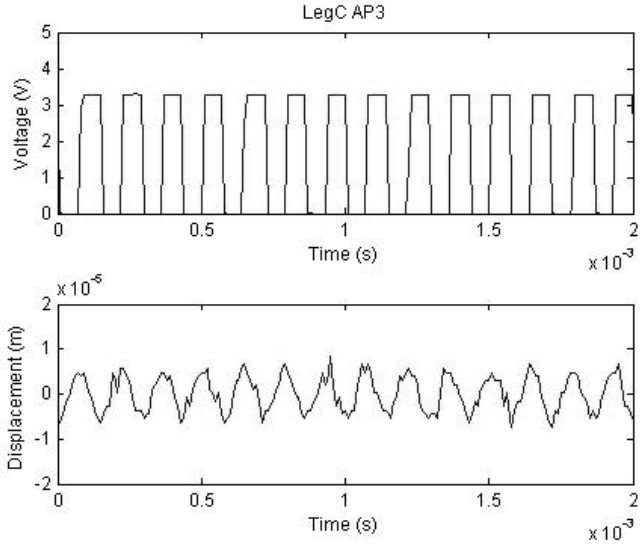

Figure 2-10 Experimental response of the microrobot leg drived at its resonance frequency 7034Hz with a square signal 3.3V.

The analysis and discussion presented in this point has been devoted to study the performances of the legs of the robot. A model has been theoretically developed and experimentally validated to describe the free motion of the legs. The model serves as a tool for designing the final leg structure since it is able to predict the free deflection dynamics in terms of material, geometrical and structural parameters for each vibration flexural mode. However, as far as these legs are the responsible of the robot motion, it is necessary to determine the maximum force they can achieve. The total mass of the final robot is hold by three legs, therefore these legs should be able to move this mass. Next, the model is used to obtain a prediction of the maximum force (blocked force) than the legs can produce.

In Eq 2-1 the ODE time equation for a voltage excitation was presented. Now this equation is extended considering also an external force applied at its tip $x=L_F$. Considering a linearly coupled electromechanical system, the equation is rewritten as:

$$K_n r_n(t) + c_n \dot{r}_n(t) + m_n \ddot{r}_n(t) = \Theta_n V_{in}(t) + W_n(L_F) F_{in}(t) \qquad \textit{Eq 2-9}$$

where "$F_{in}(t)$" is the external force applied at the tip. The maximum force that the leg can achieve is computed as the external force needed to counteract the deflection induced due to the application of an external voltage. Therefore the maximum force "F_{blk}" is computed with Eq 2-9 considering that the deflection is cero, in other words, "$r_n(t)=0$".

$$F_{blk}(t) = -\frac{\Theta_n V_{in}(t)}{W_n(L_F)} \propto nhwY / L \qquad \textit{Eq 2-10}$$

The blocked force is proportional to the coupling coefficient "Θ_n". This coefficient defined in EqA.54 is proportional to the number of piezoelectric layers, the height of the piezoelectric layers "h", the width of the layers "w", the young modulus "Y" and is inversely proportional to the length "L" of the beam. Considering the values of the microrobot legs from Table 2-1, and assuming a 3.3V drive voltage the maximum blocked force is 3.6mg (the force has been translated to grams). Therefore the maximum mass of the total microrobot can not exceed the 10mg that is the maximum weight the three legs can hold.

However, assuming a total mass of 10mg, the microrobot will not move. The locomotion principle of the microrobot is based on a type of resonant principle. This principle is described in detail in [Snis2008_2]. The principle consists mainly on one actuator tilt a certain angle with respect the base substrate or floor. Through the application of an alternative field at its resonance frequency the robot moves. During a certain time of the period the leg is in contact with the floor while bends and moves the mass, then during the rest of the period, the mass of the robot is hold by the other legs and the actuator is free to bends up and return to its initial position. The final motion of the robot depends on the angle of the actuators, the mass distribution of the robot, the frequency of the applied signals and the amplitude of the applied voltage.

It is quite difficult to define an exact value of the practical maximum allowable mass of the robot. Due to the large number of variables that play a significant role in the dynamic motion of the robot, it would be necessary to realize an experimental test to obtain a value of this mass. This test will be realized in the future, however the development of the analytical models presented in this point have deal with a maximum mass of 10mg for the final robot. The model developed point out different possibilities to increase this mass. A possible way to increase this force is microstructuring more piezoelectric layers, or increasing their width. An increase of the number of layers and the width will increase proportional the maximum mass but by the other side it will also increase the required electrical power need for driving. Decreasing the length of the legs will also increase the force each leg but it will also increase the resonance frequency increasing also the electrical power. Therefore, if more force is needed, it will be necessary to increase the electrical power.

2.1.3. Contact sensing tool

In this point, the performances of the contact sensing tool are analyzed. A brief description of the design is first presented and then a physical model is obtained. The physical model is used to determine the parameters that affect the output of the sensor and moreover to obtain an equivalent circuit model compatible with IC software design.

2.1.3.1. Design and manufacturing

The swarm microrobots are built with a tool for contact sensing. The tool consists on a multilayer structure as the microrobot legs, but in this case, two of the ten piezoelectric polymer layers are used as sensors while the other eight work as actuators. Piezo polymers, as smart materials, are materials able to actuate but at the same time they can be used as sensors. When a deformation is applied on them, they generate charge. This charge is proportional to the deformation applied. The working principle of the tool is simple, while the microcantilever is forced to resonate by applying a voltage signal to the eight layers; the generated voltage in the sensor layers is monitored by the IC. When the cantilever contacts some object, its resonance frequency changes thus the generated voltage too. This change is detected by the robot electronics thus the robot detects a collision. Figure 2-11 shows a picture of the backbone of the robot, the three legs are folded 55º while the tool is located planar.

2.1.3.2. Physical model

In this point a physical model devoted to describe the sensing and mechanical behaviour of the microrobot tool is developed. The structure is the same than the microrobot legs but it uses the two upper layers to sense. Moreover its length is 2.85mm and the width is 450μm.

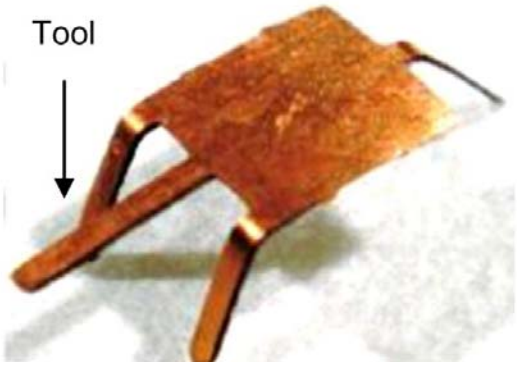

Figure 2-11 Picture of the locomotion and sensor platform of the ISWARM microrobot. Picture obtained from Snis_2008_2.

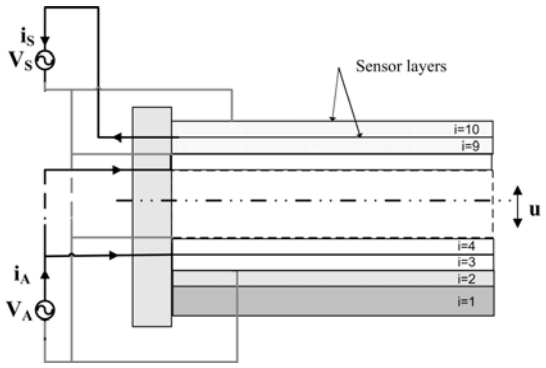

Figure 2-12 Schematic draw with the intensive variables "Va" actuation voltage and the extensive, "u" deflection and "Vs" sensor voltage.

Figure 2-12 depicts the schematic connection diagram of the tool. In order to obtain the model equations the same procedure used with the legs based on vibration transmission and modal analysis is performed. The ODE modal time forced equation from EqA.86 is rewritten here in Eq 2-11. In this equation the influence of the induced voltage appears in the temporal equation as a new term dependent of the output voltage

$$m_n \ddot{r}_n(t) + c_n \dot{r}_n(t) + K_n r_n(t) = -\Theta_{nA} V_A(t) - \Theta_{nS} V_S(t) \qquad \textit{Eq 2-11}$$

where "Θ_{nA}" is the coupling coefficient for the actuation layer and "Θ_{nS}" is the corresponding to the sensor layer. The electrical equation for the actuation is Eq 2-12 and the electrical equation in the sensor layer is Eq 2-13

$$Q_A(t) = \Theta_{nA} r_n(t) + C_A V_A(t) \qquad \textit{Eq 2-12}$$

$$Q_s(t) = \Theta_{ns} r_n(t) + C_S V_S(t) \qquad \textit{Eq 2-13}$$

"C_A" is the capacitance value of the parallel association of the actuator layers, and "C_S" is the capacitance value of the parallel association of the sensor layers.

It is important to remark the two possible configurations that exist to measure the displacement. The first one is to measure the induced charge with a charge amplifier imposing a short circuit condition in the sensor layer. The other possibility is to measure the induced voltage while imposing an open circuit condition in the sensor layer. In [Brufau2006_2] the authors presented a long discussion about the benefits of using on or the other method. While voltage measurement is easier to implement, the measure affects the mechanical response of the system. By the other hand, charge measurements do not affect the mechanical response but implementation of precise charge amplifiers is more complicated.

In the case of swarm robot, it is much easier to implement a voltage measurement so in the following lines, this case is discussed. For more information see Appendix A and [Brufau2006_2]. Considering an open circuit condition, the electrical equation in the sensor layer Eq 2-13 could be written as

$$V_S(t) = -\frac{1}{C_{pS}}\Theta_{nS} r_n(t) \qquad \textit{Eq 2-14}$$

To solve this equation, first the mechanical equation is solved. Substitution of this equation into Eq 2-11, leave to this new mechanical equation

$$m_n \ddot{r}_n(t) + c_n \dot{r}_n(t) + \left(K_n + \frac{\Theta_{nS}^2}{C_{pS}} \right) r_n(t) = -\Theta_{nA} V_A(t) \qquad \textit{Eq 2-15}$$

Therefore an open circuit condition in the sensor layer increases the spring constant. The sensor voltage generated acts against the actuation thus a virtual increase of the elasticity of the material arouses. This effect is translated in an increase of the resonance frequency of the system. This effect is more pronounced for those highly coupled materials with lower capacitance. Now the temporal equation is solved.

$$r_n(t) = \frac{\Theta_{nA}}{m_n} \frac{V_A(t)}{\left(\omega_n^2 + \frac{\Theta_{nS}^2}{C_{pS} m_n} \right) - \gamma^2 + i\gamma \frac{c_n}{m_n}} \qquad \textit{Eq 2-16}$$

So the deflection is written as

$$u(x,t) = \frac{\Theta_{nA}}{m_n} \frac{W_n(x)}{\left(\omega_n^2 + \frac{\Theta_{nS}^2}{C_{pS} m_n} \right) - \gamma^2 + i\gamma \frac{c_n}{m_n}} V_A(t) \qquad \textit{Eq 2-17}$$

Then the generated voltage is

$$V_S(t) = \frac{\Theta_{nA}\Theta_{nS}}{C_{pS} m_n} \frac{V_A(t)}{\left(\omega_n^2 + \frac{\Theta_{nS}^2}{C_{pS} m_n} \right) - \gamma^2 + i\gamma \frac{c_n}{m_n}} \qquad \textit{Eq 2-18}$$

The equation shows the relation between applied voltage and measured voltage in the sensing layer. It is observed how the generated voltage has a maximum at one frequency near the resonance frequency. The voltage is inversely proportional to the capacitance of the sensor layer and proportional to both coupling coefficients.

Once the equations defining the model are obtained, a Lumped Electromechanical Model LEM equivalent circuit is proposed. The equivalent circuit proposed is then used to design the integrated electronic circuitry of the robot for control the tool. Up to now, the analytical models developed are distributed models that define the deflection of the beam in spatial coordinate. However, the electrical measurements, voltage and currents are described as lumped variables. To define the system dynamics with lumped elements the deflection is considered at one point, this is the tip of the beam. Equivalent circuits and LEM models theory are based on the analogy between the differential equation governing a mechanical system and those equations governing an electrical circuit. This analogy is the result of similitude between the governing equations of these two systems. To find an equivalent circuit lets define the governing equation in terms of the deflection velocity of the tip of the cantilever "$v_n(t)$"

$$v_n(t) = W_n(L_F)\dot{r}_n(t) \qquad \textit{Eq 2-19}$$

Substitution on equation Eq 2-11 and dividing by the mode shape at both sides, the force equation in the Laplace domain is directly.

$$\frac{K_n v_n(s)}{sW_n^2(L_F)} + \frac{c_n v_n(s)}{W_n^2(L_F)} + \frac{sm_n v_n(s)}{W_n^2(L_F)} = -\frac{\Theta_{nA}}{W_n(L_F)}V_A(s) - \frac{\Theta_{nS}}{W_n(L_F)}V_S(s) \qquad \textit{Eq 2-20}$$

The electric equations in the Laplace domain for the actuation and the sensor are obtained from differentiating with respect time Eq 2-12 and Eq 2-13 and imposing open circuit conditions in the sensor $I_s(t)=0$.

$$I_A(s) = \frac{\Theta_{nA} v_n(s)}{W_n(L_F)} + sC_{pA}V_A(s) \qquad \textit{Eq 2-21}$$

$$V_S(s) = -\frac{\Theta_{nS} v_n(s)}{sC_{pS}W_n(L_F)} \qquad \textit{Eq 2-22}$$

Once the coupled equations are rewritten in terms of tip velocity and in the Laplace domain, the circuit of Figure 2-13 is proposed as the equivalent circuit.

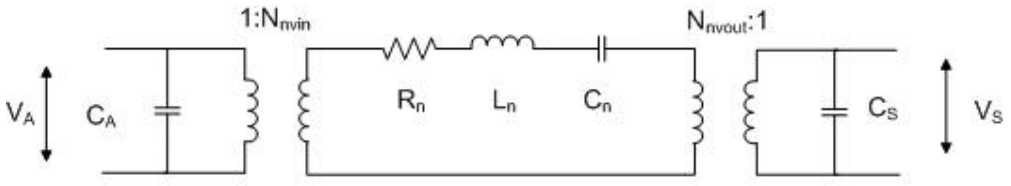

Figure 2-13 Equivalent circuit for the microrobot tool.

$$N_{nvin} = \frac{\Theta_{nA}}{W_n(L_F)} \quad \text{Eq 2-23} \qquad N_{nvout} = \frac{\Theta_{nS}}{W_n(L_F)} \quad \text{Eq 2-24}$$

$$R_n = \frac{c_n}{W_n^2(L_F)} \quad \text{Eq 2-25} \qquad C_n = \frac{W_n^2(L_F)}{K_n} \quad \text{Eq 2-26} \qquad L_n = \frac{m_n}{W_n^2(L_F)} \quad \text{Eq 2-27}$$

At the left side of the circuit, the electrical behaviour of the actuator is modelled with a capacitor "C_A". At the right side, the sensor electric behaviour with "C_S". The middle of the circuit represents the mechanical system with an inductor "L_n" that represents the normalized mass, a capacitor "C_n" that represents the mechanical compliance, and the resistor "R_n" that represents the mechanical damping or loss term. The current flowing in the mechanical part of the circuit represents the tip deflection velocity. The currents flowing in the electrical part represents the electrical current in the actuator and in the sensor. The two transformers are considered to be ideal and represent the electromechanical coupling between electrical and mechanical "N_{nvin}", and mechanical and electrical "N_{nvout}". The different elements of the circuit are directly related to mechanical and material parameters. Considering the constitutive equations of the equivalent circuit from Figure 2-13 and comparing with the three equations Eq 2-20, Eq 2-21 and Eq 2-22 of the physical model, the relations from Eq 2-23 to Eq 2-27 are obtained.

2.1.3.3. Experimental test

For the experimental test with the tool of the robots, another PCB has been used. In this case the PCB at Figure 2-14 has the tool located at the middle of the two legs. The test realized with the tool involves only voltage measurements. While in the case of the legs experimental tests there was the need of measuring the displacement, in this test we are interested to measure the voltage generated at the sensor layer. For the experimental tests the input voltage is generated by a HP2200 signal generation and the sensor voltage is measured directly by a TPS 2014 Tektronik oscilloscope.

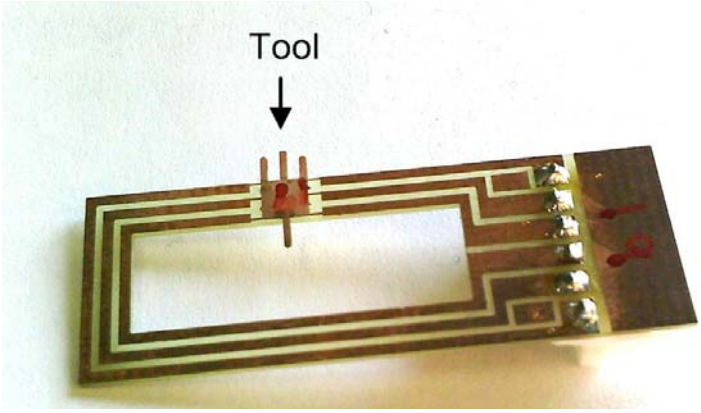

Figure 2-14 a) Picture of the PCB with the electrcical connector pins

The geometrical and material parameters for the tool are the same than in Table 2-1 but in this case the length is 2.85mm, w=450um and Q=40. Considering these parameters the values of the equivalent circuit are C_{pA}=630pF, C_{pS}=157pF, L=0.87nH, C=19mF, R=53.7μΩ, Nvin=7.28·10e-6, Nvout=1.86·10e-6.

To evaluate the ability of the model to reproduce the behavior of the microrobot sensing tool, an experimental test is realized. The tool is drive with a 10V sinusoidal frequency sweep signal. The sweep is applied linearly between 1kHz and 8kHz. The output signal is measured with a 10MΩ load resistance oscilloscope. Considering the obtained parameters of the equivalent circuit and oscilloscope load resistor the model transfer function in the Laplace domain is

$$V_S(s) = \frac{2.572 \cdot 10^{-6} s}{2.615 \cdot 10^{-12} s^3 + 3.264 \cdot 10^{-9} s^2 + 15.77 \cdot 10^{-4} s + 1} V_A(s) \qquad \textit{Eq 2-28}$$

A comparison between the experimental data and the simulation of the model using the same input data is depicted at Figure 2-15. The model simulations give a resonance frequency at 3.91kHz similar to the measured data 3.94kHz. The comparison shows how the model over predicts the magnitude of the generated voltage. The discrepancies between model and experimental results are assumed to be the consequence of deviations on the tool specifications. The differences in the voltage amplitude at resonance could be a consequence of deviations on the dielectric permittivity of the material. Other differences appear between experimental and simulated voltage at the beginning and at the end of the sweep. While the simulations predict a very small voltage generation out of the resonance due to the small motion of the beam, the experimental measurements show that some voltage is generated. This voltage generation is a consequence of electrical coupling between the input and output signals.

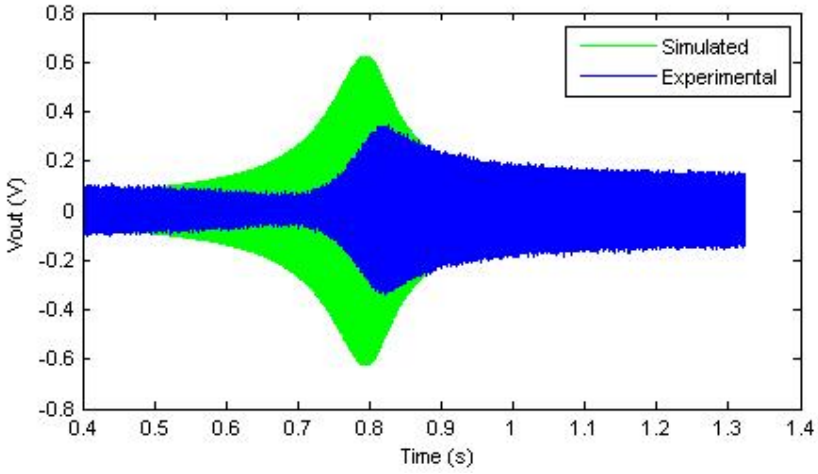

Figure 2-15 Experimental and simulated results for the tool output voltage for a given 10V sinusoidal sweep input voltage.

The model developed is useful to analyze the theoretical performances of the tool. This model serves as a tool for the optimization in the design of the vibrating contact sensor. Furthermore the description of the electromechanical performances of the tool with an equivalent electrical circuit has been used by researchers from the VLSI design group from the SIC research lab to design the electronic circuitry implemented in the robot necessary for detecting collisions.

In the following point, a brief explanation of the electronic circuit implemented in the microrobot for the control of the tool is presented together with the experimental results.

2.1.3.4. Control system

The vibrating contact tool is conceived to serve as a tool for detecting object collision of the robot. The working mode consists on actuate the tool to force a mechanical oscillation at its resonance frequency while measuring the sensor voltage. When an object is contacted, the mechanical vibration of the tool changes producing a change in the sensor voltage. This variation is detected with the robot electronics informing that a collision has been produced. Therefore to design the electronic circuitry it would be necessary to know the exact resonance frequency of the tool and the value of the generated voltage at the resonance. However in the experimental test realized it has been observed that the real values differ from the theoretical model values. As far as the same electronic circuitry will be used for different robots, and the dynamic behavior of each robot tool is expected to present small variations with respect each other, the electronic circuitry that is designed has to be flexible enough to adapt to each robot. This means that the electronics has to detect the resonance frequency and the value of the maximum voltage for each microrobot tool.

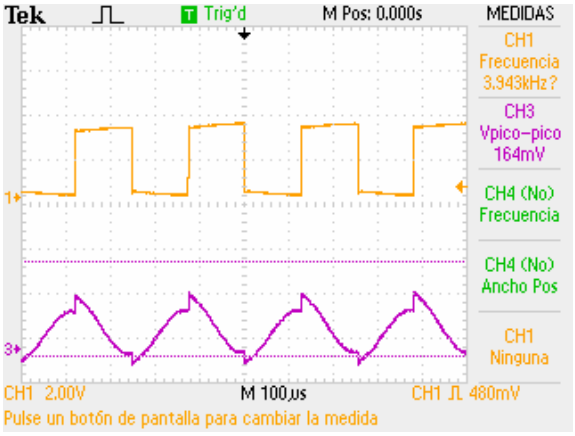

Figure 2-16 Oscilloscope capture for the IC test. Channel 1 is input voltage and Channel 3 is output voltage.

The first solution conceived to implement in the IC of the robot was based on an analog to digital converter followed by a lock in amplifier. However due to low power and small area restrictions of the project this solution was rejected. The solution adopted is based on an analog to digital converter and an algorithm implemented in a microprocessor of a custom designed ASIC to find the resonance frequency and lock the system in this frequency [Arbat2008].

The experimental test of the IC designed with a real robot tool was performed by the researchers from the VLSI group and the author of this thesis. Figure 2-16 shows the actuation signal (Channel 1) and the sensor signal (Channel 3) when the system is locked. It is observed how the IC actuation is locked at 3.943kHz that is the experimental resonance frequency measured before, therefore the system is effectively locked at the resonance frequency of the system. The measured voltage signal has amplitude of 164mVpp. A simulation of the equivalent circuit driven at 3,3V at its resonance frequency gave 190mVpp.

2.1.4. Conclusions

Piezoelectric polymers, as soft materials, have very interesting capabilities. The possibility to integrate these materials in sophisticated microstructures opens the door to a new field of applications for microrobotics, as it is in flexible insect-like microrobots. The good knowledge of the underlying physics in this kind of material together with the recent advances in the control of depositing thin layers for microstructuring have permitted the development of these advanced tools.

In this point the actuators and sensors forming the legs and antenna of a $1mm^3$ microrobotic insect-like have been theoretically modelled and experimentally tested. First of all the actuators forming the legs of the microrobot are studied. The legs consist on a monomorph multilayer structures with ten piezoelectric P(VDF-TrFE) of

2μm height connected in parallel and one flexible substrate made of Cupper and Polymide. The total dimensions of the legs are 2mm length, 0.4mm width and 0.09mm height. The small height of the piezoelectric layers together with a parallel configuration entails a low driving voltage. Through the development of analytical models the dynamic performances of the legs are analyzed. The models are based on the linearly coupled equations between electrical and mechanical domains in a piezoelectric material and in the modal analysis of mechanical vibrations transmission in a slender Euler-Bernoulli beam. The model predicts the first resonance frequency of the legs at 7.674kHz with a free displacement sensitivity of 2μm/V. Experimental measurements have been realized in a real microrobot and obtaining a resonance frequency of 7.034kHz and a free displacement sensitivity of 2.8μm/V. These mismatches are mainly attributed to deviations in the manufacturing parameters. The model is also used to predict the maximum weight of the microrobot and a 10mg is computed. Although these value is quite small it is in the range of the expected one at the beginning of the project, however as far as the robot is not already mounted it is not possible to test the whole system. The model developed shows that increasing the number of piezoelectric layers and the width of the beam or decreasing the length of the legs it is possible to increase the maximum force, by the other hand and increase in the maximum weight increases the electrical power needed to drive the leg.

The second part of this point analyzes the performances of the microrobot vibrating contact tool. It consists on the same structure than the legs but 2 layers are used as sensors. The working principle of the tool consists on actuate the structure at its resonance frequency while monitoring the voltage generated in the sensor layer. When the tool contacts an object, the oscillation changes and therefore the generated voltage too. This change in the voltage is detected with the electronics informing that a contact has occurred. The tool has the same form than the legs but it has a greater length 2.85mm and width 450μm. The change in the dimension is done to mechanically uncouple the tool and legs. As in the case of the leg an analytical model is developed using the same theory. The model predicts the generated voltage in the sensor layer for a given driving voltage in the actuation layers. The predictions are done in terms of material, geometrical and structuring parameters. The model predicts a resonance frequency of 3.91kHz and a generated voltage for a 3.3V square driving signal of 190mVpp. Experimental results on a real microrobot tool show a resonance frequency of 3.94kHz and a generated voltage of 164mV. The discrepancies are attributed again to mismatches in the material parameters. These discrepancies suggest to design a control system for detecting the resonance frequency of the tool and the maximum voltage generated. For this purpose a lumped equivalent electrical circuit compatible with electronic circuit design software is proposed. The model is used to design the electronic circuitry and programming algorithm of an IC that will be embedded in the microrobots for controlling the tool. The programmed IC is checked with a real microrobot tool. The test demonstrates the ability of the IC to find the resonance frequency of the tool and determine the generated voltage.

In this point the use of piezoelectric polymers as sensors and actuators for motion control of microrobotics has been studied. However, piezoelectric polymers are not the only active polymers that can be used in flexible microrobots, a new class of material has been early investigated to form part of such structures. These are the Ionic Polymers. In the next point these materials are analyzed to form part of a micropositioning part of a microrobot.

.

2.2. Ionic polymer based microrobot actuator

The work presented in this section is performed in the framework of the integrated action HG2007-8 named "*Development and control of a flexible microrobotic wing for underwater applications*". The action has been realized by the Instrumentation and Communication Systems SIC group from "Universitat de Barcelona (Spain)" and the Electronics Laboratory, Physics Department from "Aristotle University of Thessaloniki (Greece)". The project consists on the study and development of the motion control of a microrobotic actuator for underwater applications. The major part of the development presented here was published as a Journal paper by the author of this thesis together with the researchers from Thessaloniky. [Brufau2008_2]

Ionic Polymer Metal Composites seams a good choice to implement the flexible underwater actuator. Their transduction effect involves the motion of water inside their membrane thus they work properly in underwater conditions. In addition, IPMC are flexible materials and present large strokes under the application of relatively low voltage <3V. Furthermore, these materials are in an early stage of development and its use as actuators still have some drawbacks thus no commercial samples can be obtained. Just some spin-off companies supply samples for research. Unfortunately up to day there is not a clear vision on which effects are the responsible of the electro-chemo-mechanical transduction. During the last decade a great amount of different research studies with IPMCs are being realized. Many of these works focus on modeling, others on manufacturing, other on prototyping etc. However in most of these works the researchers remarks the inconsistency of the IPMC dynamics. The IPMC behavior is submitted to time variations due to different aspects such as water content, cations type and content, electrode oxidation or crack, etc. Therefore if a certain dynamic is required for an application with an IPMC a closed loop control system should be implemented.

In this section, the motion control for an IPMC working underwater is studied. The idea of the control is to assure always the same response even if the dynamic behavior of the beam changes with time. The control strategy adopted is based on the Model Reference Adaptive Control MRAC scheme. This is an adaptive control that modifies its control law to cope with the fact that the internal parameters of the system being controlled are slowly time-varying. The system adapts itself to follow a certain dynamic defined in a model reference. This control strategy seams a good solution for control ionic polymers. The dynamic of these materials is affected for several variables making difficult the obtaintion of a complete and reliable.

This part of the chapter is organized as follows. First of all the different elements of the underwater microrobot structures are briefly introduced. Next, the microrobot actuator is described and its dynamic behavior analyzed. Then a reduced empirical

model is identified. As far as the dynamics of these actuators drift with time a control system is proposed. The control system is devoted to reduce the influence of this drift in the final response of the system and assure always the same dynamics. For this purpose a model reference adaptive control system is designed. Before the experimental implementation of the control system a simulation of the control scheme proposed is realized in Matlab-Simulink environment. After the simulation the experimental implementation is presented.

Nevertheless, developing a control system is not the only objective of this part of the chapter. Another objective of this work regards the IPMC manufacturing. The idea is to propose a new process for electrode development compatible with standard microsystems technology (MST). Up to now most manufactured IPMC materials are based on chemical deposition, this technique has some drawbacks and is not compatible with microsystem technology. At the end of this chapter another technique MST compatible is proposed and its influence in the dynamic motion for the IPMC underwater is analyzed.

2.2.1. The underwater microrobot structure

The possibility to use low voltage flexible actuators for underwater motion opens the door to new applications and prospects for microrobotics. Ionic polymers are good candidates as materials for motion of underwater microrobots. However their response to an electrical stimulus is quite difficult to predict precisely. Their internal physics are complex to understand having many variables that could affect their response. Therefore their applicability in underwater microrobotics requires the use of external sensors to control their response.

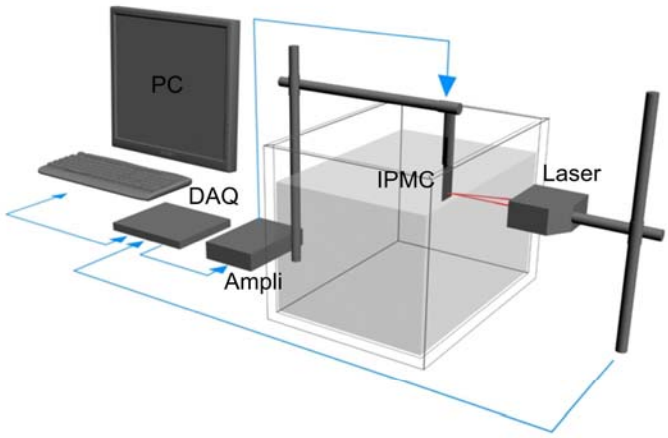

Figure 2-17 Schematic draw of the microrobot structure.

Figure 2-17 shows a schematic draw of the proposed microrobotic system structure. The structure is based on:

The motion actuator: consists on an IPMC strip clamped between two electrodes. Applying an alternate voltage signal to the strip, it bends with large strokes dragging water.

A displacement sensor is used for measuring the motion of the IPMC strip. In this point three different possibilities have been considered, these are a triangulation laser system, a camera approach and an embedded IPMC layer working as sensor. Researcher from the Thessaloniky University together with the author of this thesis presented a low-cost CCD camera system based on a webcam and a data process part and compared it with the laser system Figure 2-18. [Tsiakmakis2007], [Tsiakmakis2008].

The system is capable of measuring with satisfactory accuracy rather big displacements especially in low frequencies. CCD camera system displacement sensors are useful to characterize IPMC actuators. The main problem of these systems, compared to the laser sensor, is the computation time to process the images. Its advantages are, obviously the price, the global vision of the system, but mainly the possibility to measure displacements over a plane instead of the line vision of the laser sensor. This performance allows deflection measurements values greater than in the laser case. The other displacement measurement technique considered is based on an embedded structure with actuating and sensing IPMC layers as in the case of I-Swarm tool. Akle et al. [Akle2005] studied this possibility and reported many difficulties in the case of using IPMC layers. The work presented showed how there is an important feed through between the input signal and the output signal. In that work the IPMC sensor layer was electrically insulated using two ground contacts, and mechanically

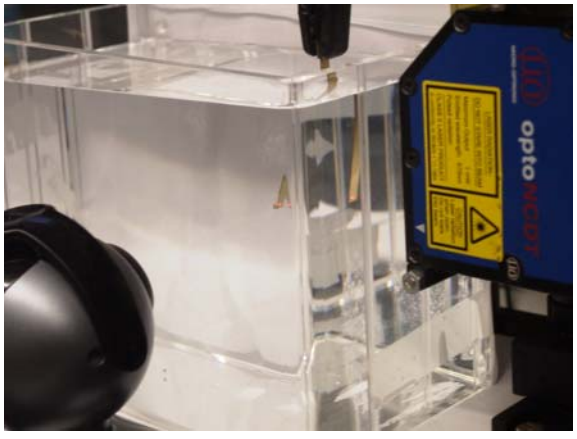

Figure 2-18 The two displacement sensors analyzed; the CCD camera and the Laser displacement sensor.

insulated evolving the sensing layer with a thin and elastic plastic. The authors declare that the feed-through has different sources, which can be classified in three main categories. The most important is the direct feed-through of the water, or water vapor existing between the sensor and the actuator stacks. The second is the feed-through of the insulation film between the sensor and actuator stacks. Those mentioned feed-through are both resistive in nature, while the third type is magnetic, which is due to the current flowing in the actuating polymer circuitry. Magnetic feed-through is insignificant; therefore they believe that water transport is the primary cause of feed-through. In this thesis for the development of the control and the characterization of the ionic polymer the laser based displacement sensor is adopted. Future work will focus on the use of the camera system.

The control electronics, are the responsible to generate, measure and the amplification of the signals involved on the structure. Furthermore it is the responsible for the implementation of the specific motion control algorithm. The project aims for the development of a microcontroller based electronics, however in this thesis the whole system is controlled with a PC. The microcontroller design is scheduled in future steps.

The power source and the communication elements are not specified in this project

All the measurements obtained in this part of the chapter are realized with the same experimental setup. The IPMC is clamped with a contact claw that serves as the contact electrodes. The laser system used for displacement measurements is the KEYENCE LC2400W. As a voltage driver, a TDA buffer is used which gives enough power to the sample. A data acquisition card is used to acquire and extract the signals from the system. Finally the LabVIEW software is used to realize all the control strategy needed.

.

2.2.2. Actuator motion

In this point the performances of an ionic polymer actuator strip working underwater are analyzed. First of all a brief explanation of the design and manufacturing of the ionic polymer is presented. Then the dynamic behavior of the an ionic polymer strip working underwater is analyzed. For this purpose an experimental test is realized. The test consists on applying a voltage step response to the polymer and measuring the displacement. From the experimental measured response an empirical model to describe the dynamics of the polymer actuation is obtained.

2.2.2.1. Design and manufacturing

The motion actuator consists on an IPMC strip clamped between two electrodes. Because there are not commercial companies to supply samples of the material, a spin-off company has been contacted. The company is Discover Technologies [DISCOVER] from Virginia Polytechnic Institute at USA and owned by Dr. Matt Bennett. This company supplied a 4x4 cm^2 IPMC membrane based on Nafion117 membrane as the ion-exchange membranes. Figure 2-19 shows a picture of the membrane. This membrane was cut to have an actuator with a 1cm length and 0.5cm width to form the actuator strip. All the measurements presented in this chapter are realized in this strip. The electrodes of the supplied sample were developed with a chemical deposition technique, nevertheless no more information was given by the company due to intellectual propriety rights. At point 2.2.4.- a new approach for developing electrodes is presented

Before starting the dynamic analysis of an ionic polymer actuator, it is important to remark that due to water content, IPMC actuation has a maximum voltage allowable value. In the case of piezoelectric ceramics and polymers, the maximum electric field applicable was determined by its polling history. There is a certain

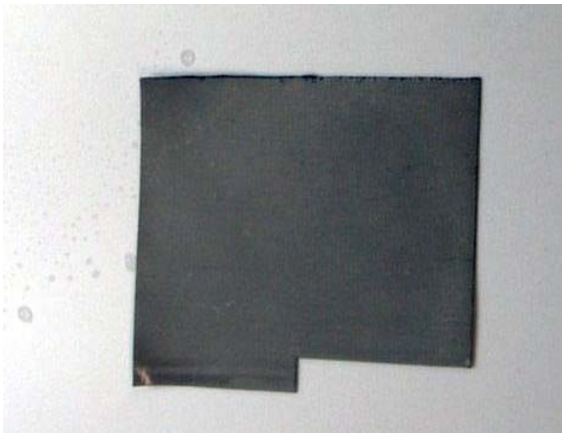

*Figure 2-19 Supplied 4*4cm^2 IPMC membrane from Discovery Technologies Inc.*

Figure 2-20 Bubles formed in water due to hydrolysis when driving IPMC with 5V. a) straight beam, b) bend beam.

electric field that depolarizes the materials and then the materials are not piezoelectric anymore. In the case of driving IPMC there is another critical value that is related to the water contents of the material. This value is determined by the water electrolysis. The electrolysis means that the molecule breaks and generates hydrogen causing degradation, heat and release of gasses.

$$2H_2O_{(l)} \rightarrow 2H_{2(g)} + O_{2(g)}$$

In typical IPMC membranes the electrolysis effect appears at voltages superior to 1.23V. Figure 2-20 shows two pictures of an experimental test realized at the laboratory where an IPMC strip is driven with a 5V square signal. While the induced mechanical deflection of the beam is considerable, the high value of the applied voltage produces hydrolysis effect and oxygen and hydrogen bubbles are formed. This effect can cause the degradation of the membrane.

Another effect related to the electrolysis of water is the appearance of non-linearity contribution in the absorbed current from the actuator. Some authors [Bonomo2007] have modeled this effect in the absorbed current, however its influence in the mechanical response in this thesis is neglected.

2.2.2.2. Empirical model

The study of the dynamics of an ionic polymer actuator has been of great interest since ionic polymers were first proposed to work as actuators in 1993 by Adolf et al. [Adolf1993]. Several studies have been presented to obtain a model to describe the IPMC electromechanical behavior. Some of these models are developed as physical models such as the ones presented by [Nemat-Nasser2000], [Tadakoro2000] or [de Gennes2000]. These models are based on the evaluation of the electrostatic and hydraulic forces acting inside the polymer membrane. Some others are considered as grey-box models [Kanno1996], [Newburry2003] or [Bonomo2007], where only few

physical laws are taken into account while the material parameters are experimentally identified. There are also the empirical models or black box models, where a curve fitting between experimental data and generic transfer functions is realized. Physical and grey box models are based on geometrical and material parameters. These models are very useful to understand the dynamic behavior of the system and can be used to design and optimize a system with a desired response. Furthermore these models are sometimes very difficult to find due to the complex physics of the system or due to difficulties to identify parameters. These problems increase when the system to model is working underwater. In this case more complicated functions as the hydrodynamic equations are needed [Brunetto2008] and moreover the experimental setups are more difficult to implement. Other models are the empirical models. These do not have information of the material neither the geometries, they only represent a dynamic input output relation of a system, but they are very easy to obtain, a fitting process is only needed. Empirical models are a fast tool to have a first insight in the internal dynamics responsible of the actuation. In this point an empirical model is obtained for an ionic polymer strip working underwater.

To start with the research on a specific empirical model for the IPMC, a first view in the experimental response of the polymer actuation is realized. The dynamic response of ionic polymer actuators was first studied by [Kanno1994], [Kanno1996] and [Mojarrad1997]. In that work they realize a set of tests applying voltage signals with different frequencies and amplitudes. They observe how the response of the beam behaves as a low pass filter. Since these works several authors have investigated the dynamic response of IPMC working under different conditions. A good test to have a first view of the dynamics of the system is to apply a step response to the actuator.

Figure 2-21 shows the response to a 1.2V voltage step of the 1cm length 0.5cm width ionic polymer strip. The figure shows a first fast rising time, attributed to the application of the electric field and to the fast motion of the mobile cations towards the cathode, and then a slow back relaxation appears due to the back motion of these cations. Finally a steady state appears in the opposite direction of the first motion. This kind of behavior is typical in most IPMC beams. The oscillations appearing in Figure 2-22 are attributed to the mechanical configuration of the beam that forces the system to resonate.

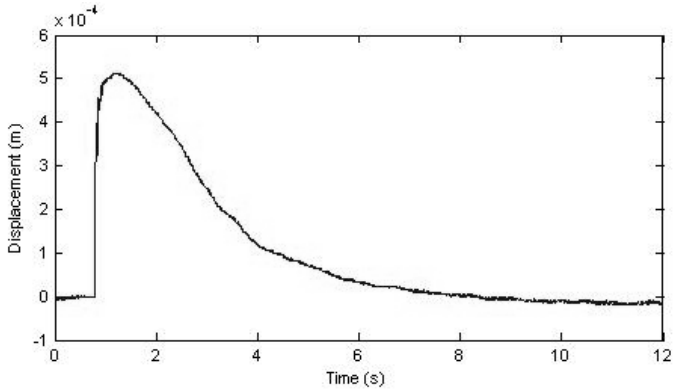

*Figure 2-21 Step response for1cm*0.5cm IPMC strip.*

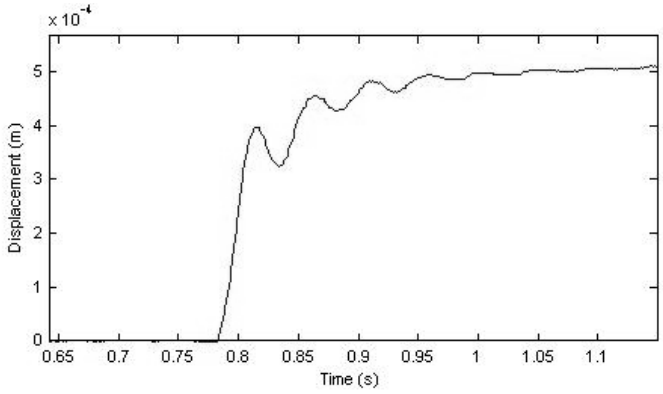

Figure 2-22 Zoom showing the oscilations due to the natural frequency.

The model adopted in this point is based on the one developed by [Kanno1994] and used for the beam underwater. Empirical models consist on fitting the evaluation of a certain transfer function with experimental data. Different authors have demonstrated the ability to use step response data for developing empirical models [Kanno1994], [Mallavarapu2001]. Therefore the experimental step response data from Figure 2-21 is used for the extraction of an empirical model. As far as the system responses with a first rising time followed with a slow back relaxation, the model to identify should have one zero and pole. As a first approximation it is possible to appreciate two time constants in the back relaxation, one faster than the other. The empirical model proposed is described as a transfer function G(s) relating the output displacement Y(s) and the input voltage U(s). It is defined with two poles and one cero as Eq 2-29.

$$G(s) = \frac{Y(s)}{U(s)} = G_o \frac{(s - z_1)}{(s - p_1)(s - p_2)} \qquad \textit{Eq 2-29}$$

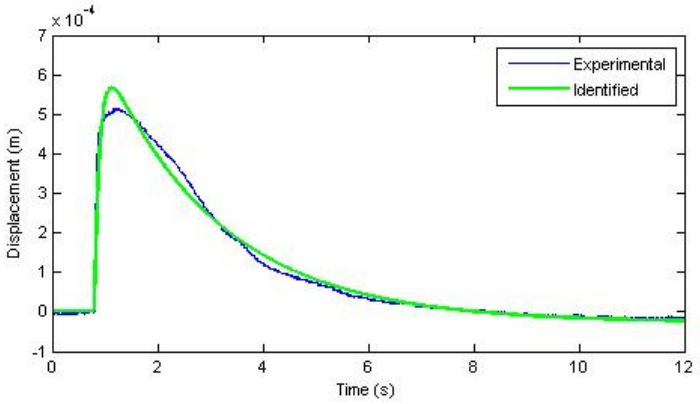

Figure 2-23 Fitted Step response: Blue line is experimental, Green line is fitted

The oscillation behavior at the initial rising time due to the mechanical resonance of the system is neglected. To obtain the model, an identification process is realized. This identification process is based on a minimization algorithm. The algorithm consists on the evaluation of a cost function based on least square method that compares the experimental data of a step response of Figure 2-21 to the second order transfer function of Eq 2-29.

The identified values are reported at Table 2-2. The fitted curve for the IPMC polymer and the experimental step response are shown at Figure 2-23. The identified model follows approximately the same dynamics than the real ionic polymer. For a better fit, more ceros and poles should be considered.

G_o	z_1	p_1	p_2
0.00534	0.0183	-9.694	-0.451

Table 2-2: Fitted values for the transfer fiunction model

Although the identified model seams to describe quite well the dynamic of the ionic polymer, drift variations in the internal parameters of the ionic polymers are expected. This drift could produce larger deviations between real and expected response. The unpredictable evolution of the dynamic behavior in ionic polymers reduces the number of applications where such actuators can be used. Therefore, there is the need to design control strategies to minimize these variations and assure always the same dynamic. In the next point a model reference adaptive control MRAC strategy is implemented to eliminate the influence of the drift in the final performances of the system. The identified model is used as a reference model of the MRAC, therefore, even if the parameters of the polymer drift, the polymer will respond always with same initial dynamics.

2.2.3. Motion control

Different authors have focused on the design of control strategies on IPMC materials with different objectives. Mallavaparu et al. [Mallavarapu2001] proposed the use of a control scheme to reduce the settling time and the overshoot on the dynamic response to an input step for two different lengths of IPMC materials working in air. They use an LQR (linear quadratic regulator) control scheme which reduces by a factor of 10 the settling time and the overshoot. By choosing a certain "R" weighting matrix, the influence of the drift in the resonance frequency due to dehydration appearing in the longer membranes is controlled. Newburry et al. [Newbury2002] develop a control system taking advantage of the transduction effect of this material. He used four IPMC strips located at different points of a rotary element, and a single IPMC as sensor. The final system was a controlled rotary motor device. Another interesting control system was developed by Richardson et al. [Richardson2003] where a control of displacement/force of an IPMC strip was presented by using a PID controller. Yamakita et al. [Yamakita2006] developed an integrated sensor/actuator strip where a control strategy is based on an 'H infinite' control. Kothera et al. [Kothera2005] demonstrated that the application of integral control can provide a precise tracking control to a reference step input. Moreover they developed a first attempt to a Model Reference Adaptive Control for an IPMC. The MRAC control is implemented to cope with the fact that the dynamic behavior of ionic polymers varies with time. This first attempt in developing MRAC control with IPMC failed. MRAC control is based on an adaptive control law that adjusts its internal parameters to fit the dynamics of the model reference, therefore, as we will see, the model reference must have the same order than the plant. In the control presented by Kothera the model reference was considered as order one and therefore there was only one parameter to adjust. However as far as IPMC behave at least as a second order system the whole control developed failed. In this point an efficient control system for an IPMC strip working in underwater conditions is proposed. The control strategy adopted is based on the model reference Adaptive Control MRAC scheme with a second order reference model.

There are different configurations and possibilities to design an MRAC control however most of them are based on four main parts. Figure 2-24 shows a schematic draw of the classical MRAC with the four parts. The first one is the plant or system we want to control. The plant is assumed to have a known structure although the parameters are unknown. For linear plants this mean the number of poles and zeros are assumed to be known. The second part is the reference model that is used to specify the ideal response of the adaptive control system. It provides the ideal plant response "y_m" which the adaptation mechanism should seek in adjusting the parameters. The choice of a model reference has to satisfy two requirements; on the one hand it has to satisfy the performance specifications of the control plant, and on the other hand this behavior has to be achievable by the adaptive control system [Slotine1991]. The third part is the controller parameterized by a number of adjustable parameters values "θ". The controller should have perfect tracking capacity allowing the tracking convergence between reference model output "y_m"

and plant output "y_p". The last one is the adaptation mechanism used to adjust the parameter values in the control law to ensure a zero tracking error "e", $e(t)=y_p(t)-y_m(t)$. It is clear that this last control part represents the main difference with classical controls where the control law is fixed. The adaptation mechanism is also the responsible to guarantee the stability of the control system.

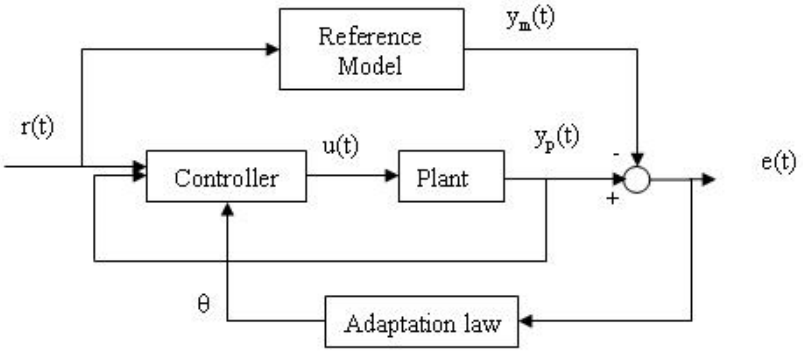

Figure 2-24 MRAC basic blog scheme.

In literature there are different control configurations to define MRAC systems. However, in order to choose a certain configuration, the order of the system and the relative degree of the system has to be taken into account. The relative degree of the system is defined as the difference between the number of poles and zeros of the system. In our case, the identified model is a second order model with a relative degree of one. A possible control strategy to use in this kind of systems is presented in Figure 2-25. This kind of configuration can be consulted in advanced control books [Slotine1991].

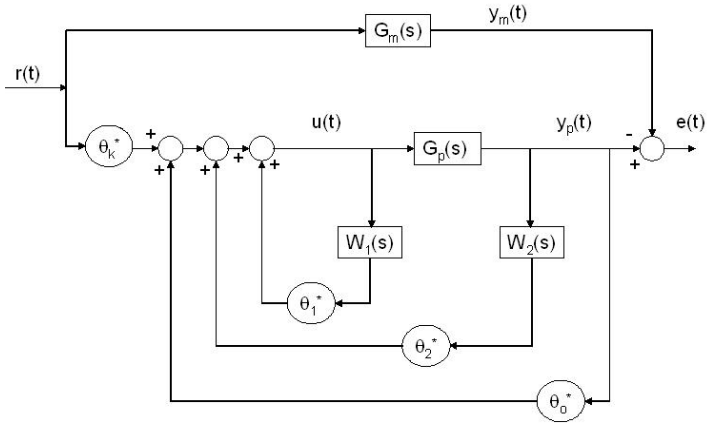

Figure 2-25 2nd order with relative degree of one MRAC control scheme.

This is a particular configuration that gives a very efficient error convergence. The block $G_p(s)$ is the plant to control where the parameters (k_p, P_{1p}, P_{2p}, Z_{p1}) are unknown but the structure is known

$$G_p(s) = \frac{k_p(s - Z_{1p})}{(s - P_{1p})(s - P_{2p})} \qquad \textit{Eq 2-30}$$

The reference model $G_m(s)$ is specified as the ideal response that we want for the system. The reference model has the same structure than the real plant. The parameters of the reference model (k_m, P_{1m}, P_{2m}, Z_{1m}) are known and are reported at Table 2-2.

$$G_m(s) = \frac{k_m(s - Z_{1m})}{(s - P_{1m})(s - P_{2m})} \qquad \textit{Eq 2-31}$$

Therefore the control law has been chosen with four adjustable parameters. One parameter adjusts the "gain", other for adjust the "cero" and two adjust the poles. The configuration adopted proposes to use two filtering blocks $W_1(s)$ and $W_2(s)$ for a perfect tracking. These blocks are introduced in the control scheme with one pole each. The location of these poles has to be equal to the location of the cero of the model reference.

$$W_1(s) = W_2(s) = \frac{1}{(s - Z_{1m})} \qquad \textit{Eq 2-32}$$

The control law from the configuration proposed is written as

$$u = \theta^T(t)\omega(t) \qquad \textit{Eq 2-33}$$

with

$$\theta = \begin{bmatrix} \theta_k(t) & \theta_1(t) & \theta_2(t) & \theta_0(t) \end{bmatrix} \qquad \textit{Eq 2-34}$$

$$\omega = \begin{bmatrix} r(t) & \omega_1(t) & \omega_2(t) & y(t) \end{bmatrix} \qquad \textit{Eq 2-35}$$

"θ" is the vector containing the adjustable controller parameters, and "ω" the vector containing the input signals of the controller. "$\omega_1(t)$" and "$\omega_2(t)$" are the output signals from the filters. Considering the scheme from Figure 2-25, the transfer function relating plant output "y_p" and reference input "r" is written as:

$$\frac{y_p(s)}{r(s)} = \frac{\theta_k G_p(s)}{1 - W_1(s)\theta_1 - (W_2(s)\theta_2 + \theta_0)G_p(s)} \qquad \textit{Eq 2-36}$$

The whole control scheme implemented is conceived to produce an output of the plant "y_p" equal to the output of the model reference "y_m", this is a cero error "e(t)". To do this, the system adapts the parameters "θ" to transform Eq 2-36 into Eq 2-31. Comparing both equations it is easily observed that the scalar gain "θ_k" is the responsible to adjust the ratio between plant and model reference gain. When the system is adjusted this parameter becomes "θ_k^*":

$$\theta_k^* = \frac{k_p}{k_m} \qquad \textit{Eq 2-37}$$

The "θ_1*" is responsible to cancel the zeros of the plant. The other two parameters are "θ_2*"and "θ_0*" are responsible to adjust the poles of the system. The adaptation law adopted for the parameters adjustment is

$$\dot{\theta} = sign(k_p) g e(t) \omega(t) \qquad \textit{Eq 2-38}$$

where dot denotes time differentiation. "k_p" is the gain of the open loop response of the plant that is supposed to be known. "e(t)" is the error signal, and "g" is the adaptation gain that is defined negative and tuned by the designer. It is possible to demonstrate that if the control scheme from Figure 2-25 is used with this adaptation law, the system is stable and the error converges to cero

$$e(t) = y_p(t) - y_m(t) = \left(\frac{\theta_k^* G_p(s)}{1 - W_1(s)\theta_1^* - \left(W_2(s)\theta_2^* + \theta_0^*\right) G_p(s)} - G_m(s) \right) r(t) = 0 \qquad \textit{Eq 2-39}$$

An important limitation when adjusting this second order system is the reference input signal "r(t)". As far as the system adapts itself, the input signal has to have enough frequency information to provide the control scheme with enough information for the parameters identification. In other words the input signal has to be "persistently exciting". In the case of adjusting a second order system, the input signal has to be persistently exciting with order 2 or higher. This means that the system will never be able to found the suitable parameters when the input is a step response that is persistently exciting with order 1. A sinusoidal input is of order two persistently exciting signal, then this signal can be used to find the suitable parameters [Astrom1994]. It is important to remark that this requirement limits the applicability of MRAC control schemes to work with higher order systems.

The adaptive control strategy based on a model reference has been chosen for control the ionic polymer motion because the dynamic behavior of these materials changes with time. The unpredictable drift in its internal dynamic rules out ionic polymers as actuators for applications where certain reliability is required. To avoid these dynamic variations, a MRAC strategy is adopted. In the next point simulations of the control system adopted are presented. The idea of the control is to assure always the same dynamics than Figure 2-23 even if the parameters drift. Therefore

the model reference adopted is the same than Eq 2-29 with the parameters of Table 2-2

2.2.3.1. Simulation results

The control scheme from Figure 2-25 with the parameters adaptation law from Eq 2-38 has been simulated in Matlab-Simulink® environment. As the reference model, the identified plant transfer function is used. A saturation block has been included in order to avoid greater voltages than 3V that could damage the samples. The whole control scheme is transformed to a discreet model with a sampling time 1kHz that is the expected sampling frequency of the final implementation.

The objective of the simulations is to better understand the operation of the control scheme. As far as the same model reference in the simulation is equal to the plant dynamics, the parameters should converge to $\theta^*=[1\ 0\ 0\ 0]$. The simulations also serve as a tool to define an adaptation gain "g". In the appendix B the whole block diagram programmed in Matlab-Simulink® environment is shown.

The Figure 2-26 and Figure 2-27 show the response of the system to a step input signal. It is observed how the tracking error between plant and model reference tends to zero while the control parameters do not converge. This un-convergence of the parameters will at the end force the system to saturate and the control to fail. This phenomenon is attributed to low frequency information of the input signal. A step response is a persistently exciting signal of order one while our system needs an input signal of order two.

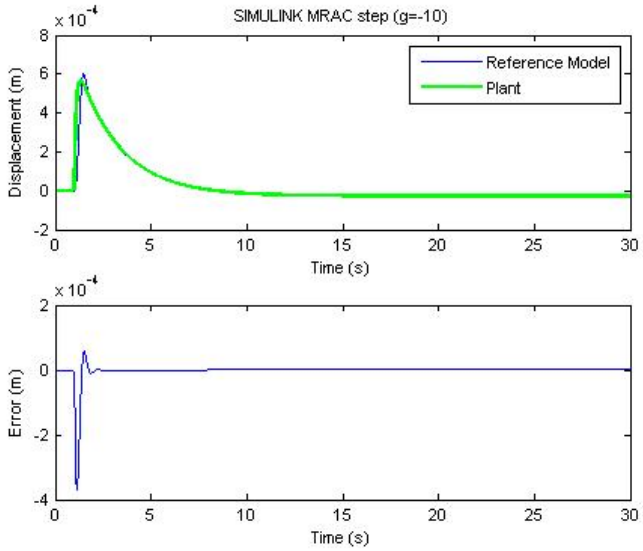

Figure 2-26 Simulated step response. Up: (Green) output plant, (Blue) reference model output. Down: Error

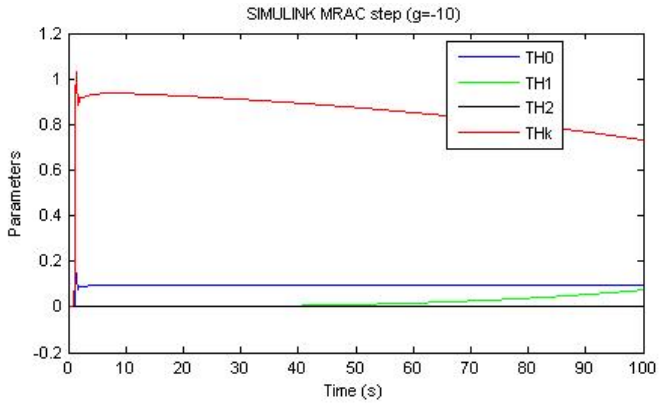

Figure 2-27 Step response parameters adaptation simulated. TH0=θ0, TH1= θ1, TH2= θ2, THk = θk

Figure 2-28 shows the simulated results of the control using a sinusoidal input that is a second order persistently exciting signal. It is observed how the output of the plant follows the output of the model reference, and the error tends to zero. Figure 2-29 shows the adaptation of the four parameters. It is observed how the "θ_k" parameter converges to one, while the other parameters seams to converge to zero. This was expected because the plant and the reference model are the same, so the ratio between dc gains is equal to 1 and no changes in the ceros and poles are needed. The system requires some time before the adaptation is completed. The value of the adaptation gain "γ" has been chosen -10 after some iteration. Decreasing this gain will produce a higher time to converge but the parameters variation will be smaller.

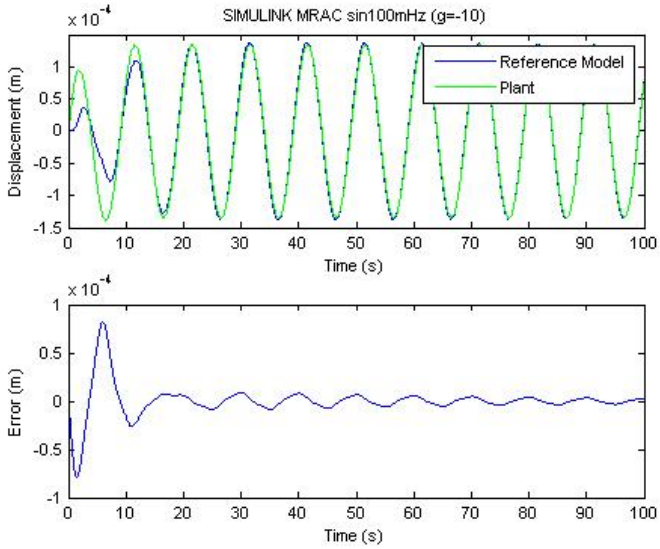

Figure 2-28 Simulated 100mHz sinusoidal: Up: (Green) output plant, (Blue) reference model output. Down: Error

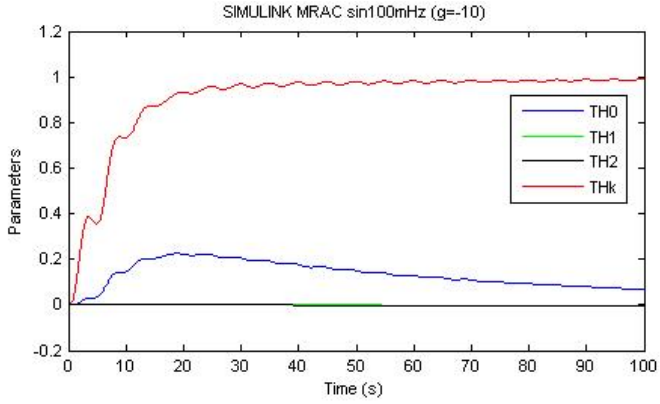

Figure 2-29 Parameters adaptation 100mHz simulated. TH0= θ0, TH1= θ1, TH2= θ2, THk = θk .

Increasing the gain will produce a fast convergence but the parameters will be submitted to higher fluctuations.

2.2.3.2. Experimental validation

The whole control strategy has been experimentally tested in a real workbench Figure 2-30. The control system is implemented within a LabVIEW framework in a PC. A Data Acquisition Card is used as the interface between the PC and the real system. The card uses an Analog converter to output the control signal "u(t)" and a Digital converter to input the measurements from the displacement sensor "$y_p(t)$". The software programmed in the LabVIEW framework generates the reference signal and compute all the mathematical operations need for the control. Computes

Figure 2-30 Experimental setup for the MRAC implementation.

the output of the model reference, generates the control signal and adapt the four parameters. The software records the four parameters evolution. The sampling frequency of the system is set to 1kHz. .

The first tests realized almost always failed. The system starts to oscillate until it saturates the output. This malfunctioning can be attributed to different aspects as external perturbations or un-modeled dynamics of the system. However it is possible to implement some techniques to reduce the influence of noise in MRAC systems. Datta et al. proposed a set of techniques to reduce noise in MRAC systems [Datta1998]. Here two of these techniques are implemented, these are the "dead zone" and the "parameter projection". The first one, the "dead zone", consists on changing the adaptation law to

$$\dot{\theta} = sign(k_p)g(e(t)+j)\omega(t) \qquad \textit{Eq 2-40}$$

where

$$j = \begin{cases} 0 \text{ if } |e(t)| \geq j_0 \\ -e(t) \text{ if } |e(t)| < j_0 \end{cases} \qquad \textit{Eq 2-41}$$

"j_0" has been chosen equal 0.002mm. This kind of technique is done to robustify the system against modeling error. When this error is small, it can be considered as something like white noise or in other words, a signal containing several frequencies. Due to the non-linearity of the control scheme these frequencies are amplified and transmitted to the IPMC beam. These signals could excite some un-modeled dynamics, such as the resonance observed at Figure 2-21, and make the system to diverge.

The other technique is the parameter projection. In this case the adaptation law has been constricted to

$$\dot{\theta} = \begin{cases} \text{sing(kp)}g\omega(t)e(t) & \text{if } |\theta| < M_0 \text{ or if } |\theta| = M_0 \text{ and } \theta e(t)\omega(t) \le 0 \\ 0 \text{ if } |\theta| = M_0 \text{ and } \theta e(t)\omega(t) > 0 \end{cases} \qquad \textit{Eq 2-42}$$

This technique is implemented in order to avoid parameter drift. The base of this technique is to suppose that the unknown parameters values are bounded to a set range. Then the parameters are ensured to belong to a bounded region.

Therfore the parameters adaptation law of the software implemented in the LabVIEW framework is changed to introduce these two techniques. The system is tested at different frequencies to determine the applicability of the control strategy.

Figure 2-31 shows the results from the implemented control with the IPMC for a 100mHz sinusoidal input signal. In this case the adaptation gain has been maintained to -1 in order to minimize the influence of perturbations into the system. Reducing this gain, the system becomes less sensitive to perturbations, but it increases the start-up time. Furthermore this time increase is not so critical because an initial start-up time can be accepted. Figure 2-32 shows the evolution of the sintonized parameters, it can be observed how these parameters tend to converge to stable values. The "θk" value tends to approximately 0.5 instead of the expected 1 because of the sensitivity of the laser system was set to 500um/V instead of the 1mm/V in the simulations. The other parameters seam to converge to a constant value. These values are near zero which means that the model reference is similar to the model plant.

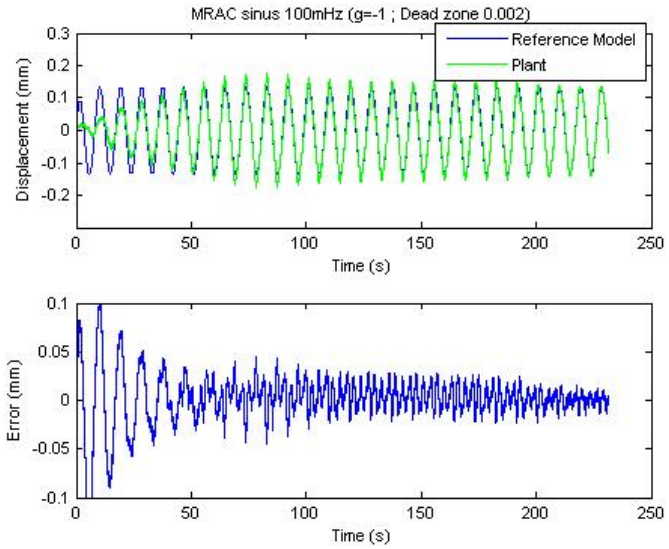

Figure 2-31 Experimental 100mHz Up :Green Output plant, Blue Ref model output. Down: Error

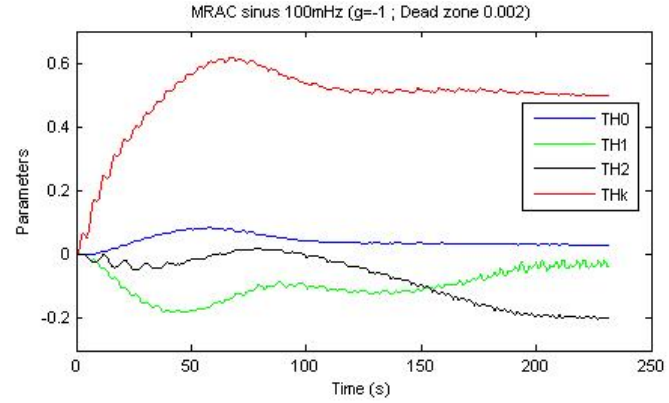

Figure 2-32 Parameters adaptation 100mHz experimental. TH0=θ0, TH1=θ1, TH2=θ2, THk =θk .

The system is then controlled for a 500mHz input signal. Figure 2-33 shows the result of the control. In this case, the same gain of -1 was used, thus the system needs more periods to converge than at 100mHz. The error shown at Figure 2-33 remains with an amplitude near 0.02mm. This error is due to the phase difference between plant output and model reference output. While both signals amplitude are very similar they are shifted, thus their difference produces the error signal shown. Figure 2-34 shows the parameters convergence.

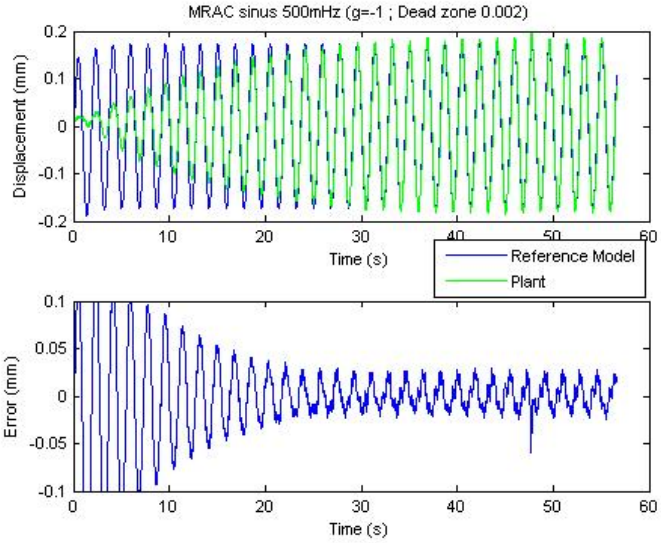

Figure 2-33 Experimental 500mHz Up: Green Output plant, Blue Ref model output. Down: Error

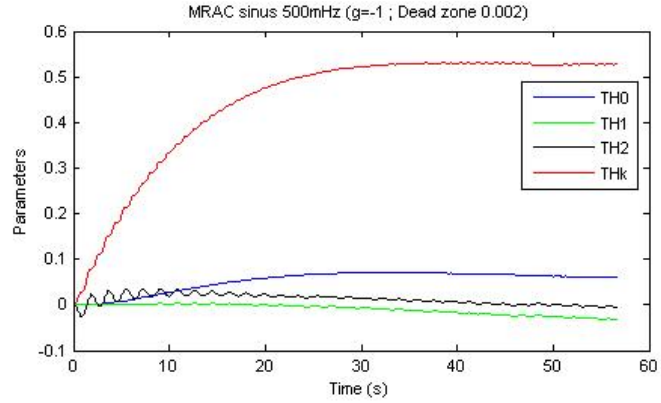

Figure 2-34 Parameters adaptation 500mHz experimental. TH0=θ0, TH1=θ1, TH2=θ2, THk=θk.

The system is controlled up to 1Hz and Figure 2-35 shows the outputs and the error. More periods than with 500mHz are needed to converge. Again both signals present a phase shift. Figure 2-36 shows the parameters adaptation. For higher frequency inputs, the output of the plant is not able to follow the output of the model reference.

Although ionic polymers present very interesting features its use as actuators and sensors for microrobotic systems is being limited by different aspects. In this point the problem of controlling the motion has been addressed, however there is still some other drawbacks that must be solved first. One of these challenges is the possibility to microstructure these polymers with MST technology. In the next point the

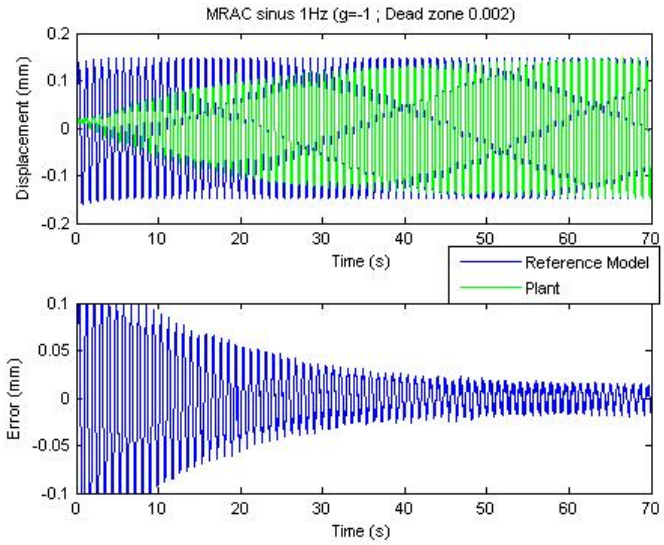

Figure 2-35 Experimental 1Hz Up: Green Output plant, Blue Ref model output. Down: Error .

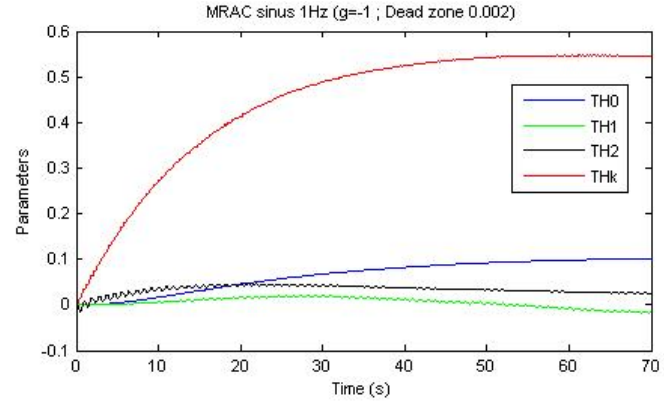

Figure 2-36 Parameters adaptation 1Hz experimental. TH0=θ0, TH1=θ1, TH2=θ2, THk=θk.

problem of patterning electrodes with compatible MST technology over a Nafion membrane is discussed.

2.2.4. Manufacturing ionic polymers IPMC

The manufacturing of IPMC starts with an ion exchange membrane called "ionomer". An ion exchange membrane is designed and synthesized to selectively pass ions of a single or multiple charges. Ion exchange membranes are typically manufactured from organic polymers that contain covalently fixed ionic groups. Most common exchange membranes used as the base of IPMCs are the perfluorinated alkenes with short side-chains terminated with ionic groups (these are registered as Nafion). Such fluorcarbone polymers have linear backbones with no cross-links and relative few fixed ionic groups attached. Short side-chains provide ionic groups that interact with water and the passage of appropriate ions. When swollen with water, Nafion TM undergoes phase separation ("clustering") on a supramolecular structure. When they are swollen it has been pictured that hydrophobic zones around the fluorcarbone backbones and hydrophilic zones around the fixed ionic groups coexist. Therefore the ionic groups attract water and can move water under an electric field though nanoscale pores and channels where ions along with water migrate within the polymer matrix.

This "ionomer" membrane is then treated to form two metal layers at each side of the membrane that act as the electrodes. While there are different companies that supply such membrane, there is still no commercial company that can supply the membrane with the formed electrodes. In this point a brief explanation of the most common technique to form the electrodes is presented, the technique consist in a chemical metal deposition and it is well studied and characterized. Furthermore, a novel technique based on a physical deposition is proposed and firsts results obtained presented.

2.2.4.1. Chemical deposition method.

Chemical deposition is the most common technique to form the electrodes onto the "ionomer" membrane. The current state of the art on chemical electrode deposition [Asaka1995], [Shahinpoor2000], [Shahinpoor2001], incorporates two distinct preparation process: initial composing process and surface electroding process.

The principle of the composing process is to metalize the inner surface of the material. It consists on soaking the membrane on a metal salt such as $Pt(NH_3)_4HCl$. This allows platinum containing cations to diffuse through via the ion-exchange process (Figure 2-37a) Later a proper reducing agent such as LiBH4 or NaBH4 is introduced to platinize the materials by molecular plating. Figure 2-37b) shows a SEM image of the electrode developed. A roughened surface can be seen. It has been reported that metals straight trough the membrane up to 1-20um [Shahinpoor2001].

The surface electroding process used later consists on plating more metal in addition to the initial composing metal layer Figure 2-37c). This is done by using multiple reducing agents to carry out reducing reactions predominantly on top of the

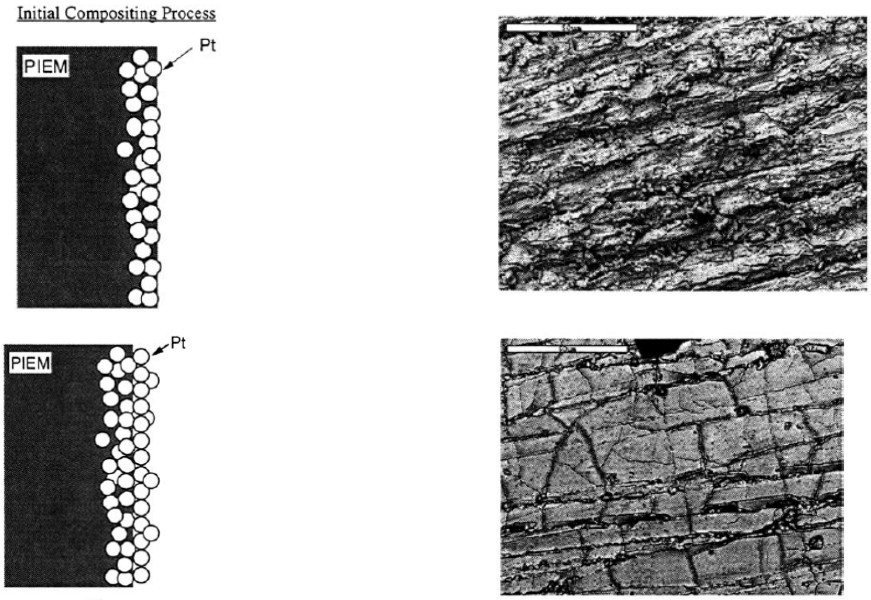

Figure 2-37 Two schematic diagrams showing different preparation processes: top left, a schematic diagram shows the initial compositing process; top right, its top view SEM micrograph; bottom left, a schematic diagram shows the surface electroding rocess, and bottom right, its top view SEM micrograph, where platinum has deposited predominately on top of the initial Pt layer. Note that PIEM stands for perfluorinated ion exchange membrane. Pictures obtained from Shahinpoor2001

initial platinum layer formed by the initial compositing process. Figure 2-37d) shows how the roughened of the surface has disappeared.

The performances of the electrodes depend heavily in the different parameters of the process. In this sense different effective "recipe" to manufacture IPMC material are described in [Oguro2001], [Onsihi2000] and others. The steps proposed by those authors start by roughen the surface of the polymer membrane by sandblasting, and then controlling the concentrations and times of the two previous commented processes. The sandblasting step is proposed to increase the effective contact surface of the metal and the polymer membrane.

As commented in the introduction there is still no a generally accepted model for the description of the electromechanical behaviour of IPMCs. Furthermore most of the researchers agree that the morphology of the electrodes plays a significant role in the response of the material. In [Onishi2000] an interesting analysis on the influence of the electrodes morphology in the actuating performances of the IPMC is presented. In the paper they prepared different samples which differ from each other that plating process was repeated several times.

Figure 2-38 shows four SEM images of four different samples where the plating process was repeated from one time up to four times. The pictures show how by repeating the process the electrodes straight through more into the membrane. In that paper the mechanical performances of different samples were compared. The study

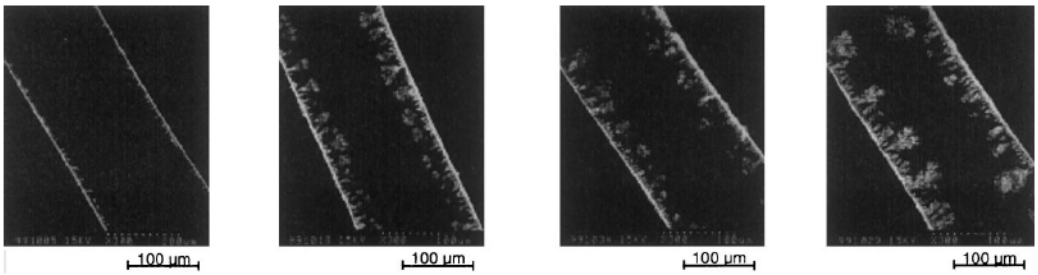

Figure 2-38 SEM micrograghs in cross-section of membrane electrode. 2, 4, 6 and 8 plating cycles respectively. Picture obtained from Onishi2000.

demonstrates the influence of different parameters in the performance. The first thing observed was that by repeating the process, more metal was deposited thus a reduction on the electrode resistance was observed, this reduction on the electrode resistance enabled a constant distribution of the applied voltage in the whole electrode surface. Then a grater penetration of the metal in the polymer increases the electrode surface thus an increase of the capacitance of the device was observed. This increase in the capacitance is traduced in an increase in the performed displacement [Paquette2003], [Shahinpoor2004], [Nemat-Nasser2003]. It is commonly accepted that the deformation of an IPMC depends with the absorbed current of the device. Thus a greater surface that means greater capacitance means better performances. Furthermore the paper shows that there is a compromise between displacement and metal deposition, this is because a major deposition of metal increases the elastic modulus of the beam, thus the material became stiffer.

While the chemical deposition is commonly used, it is a very expensive technique. From the whole metal contained in the salt solution there is only a small quantity that deposit in the membrane, thus big quantity of metal salt has to be used to deposit a small quantity in the polymer. Other inconvenient of this technique are the large time process necessary to develop the electrodes and the need of an accurate control of the different parameters. Another inconvenient that is important to remark and that provably is limiting the applicability of these materials is the difficulty to control the diffusion of the metal inside the membrane. Some authors are studying the possibilities to use IPMCs as microactuators. In those cases, it is important to define very small electrodes on the surface of the membrane thus the diffusion of the metal inside the membrane will limit the minimum distance between two electrodes. In the next point a novel approach is proposed to use for electrode deposition on the polymer membrane with the objective to overcome some of the previously described drawbacks and to define a process compatible with Microsystems Technologies.

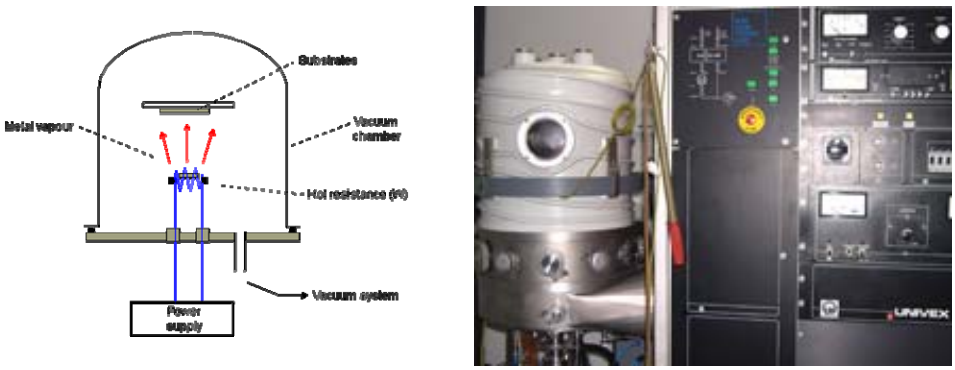

Figure 2-39 a) Schematic draw of the vaccum chamber of a Evaporator machine. b) Picture of the Univex 450 by Leybold.

2.2.4.2. Physical deposition by thermal evaporation

In the evaporation deposition technique, the membrane is placed in a vacuum chamber Figure 2-39. In the chamber a peace of metal in a solid state is heated until fusion by means of an electrical current passing through a filament or metal plate where the metal is deposited (Joule effect). The evaporated material is then condensed on the membrane.

By controlling the time and temperature, it is possible to control the quantity of metal deposited, then it is possible to control the thickness of the metal deposited. This technique allows a fast deposition technique and much less metal is needed. In the next point some experimental tests realized are presented.

2.2.4.2.1. Sample preparation procedure

A Nafion 117 membrane was acquired from Sigma Aldrich, this membrane has a thickness of 200um. The membrane was cut in peaces of 3cm*3cm and cleaned with ultrasounds in a deionised water bath.

Once the samples were cleaned, they were placed in the evaporation machine. The thermal metal evaporation machine used is the Univex 450 by Leybold from the “Parc Cientific de Barcelona”. Two different metals were evaporated, first of all a thin layer “15nm” of Titanium “Ti” was evaporated and then a thicker layer “400nm” of gold “Au”. The first Titanium layer was deposited to increase the adhesion of the metals to the polymer. It is commonly to use a first thin layer of Titanium when working with polymers, then, because of the poor conductivity of the Titanium, a Gold layer was deposited.

The evaporation process was realized in two steps. The first evaporation was devoted to deposit metal at one side of the membrane, and the other for the other side. A critical point is when the chamber is opened between both evaporations. When the first evaporation is done, the chamber is in vacuum, which means that the sample is completely dehydrated, and the metal is deposited at one side. When the

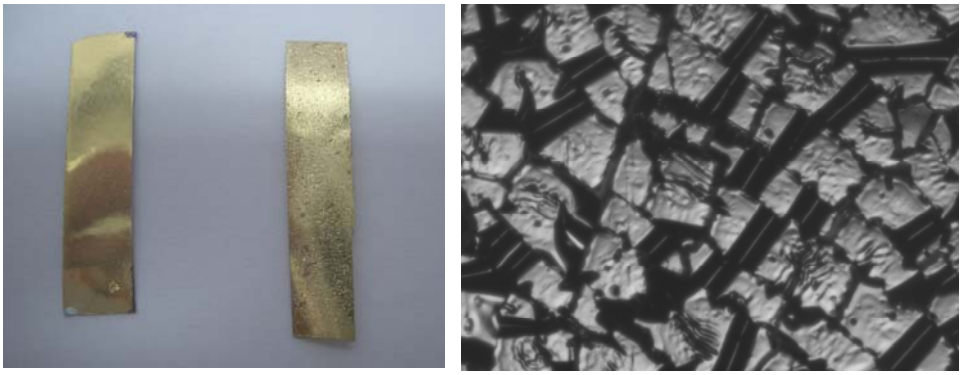

Figure 2-40 a) Picture of two strip of IPMC with 15nm Ti and 400nm Au. The left side strip has never been wet. The right side strip has been immersed in watter. b) A microscope picture of the immersed sample surface with the NAVITAR x10.

chamber is opened to revolve the sample, the hydration level increase thus a strain is forced in the polymer. The different strain coefficient between metal and polymer forces the sample to bends. This bend can produce the deposited metal to crack. Thus it is important to fix the sample to some plate. Once the metal has been deposited at both sides, a 2.5cm*0.5cm strip is cut.

Figure 2-40 shows the results of the evaporation experiment. At the left side, the samples just after the evaporation process and at the right side the sample after being immersed in deionised water. While the first sample presented a good conductivity, a very low resistance was measured 1.5 Ω. When the sample was submerged in water its whole volume expands breaking the electrodes and no conduction was measured. Figure 2-40 shows an image in an optic microscope NAVITAR where it can be clearly observed that the electrodes are broken. This break in the electrodes could be a consequence of the change in the surface strength when the material is hydrated. IPMC when hydrated change their volume so the strength in the surface changes.

In order to improve the adhesion of the metal layers in the Nafion membrane, the surface of the membrane was treated with a Reactive Ion Etching (RIE).

2.2.4.2.2. Adhesion improvement

The objective of treating the Nafion membrane with the Reactive Ion etching is to produce roughness on its surface. The main effect of the RIE is that it pulls up material from the surface. It is normally used to dry etching materials. The typical working principle of a RIE consists on forming plasma inside a chamber. Figure 2-41a) shows a illustrative draw of the plasma formed inside the chamber. The plasma is created by introducing a gas inside the chamber and applying a strong RF (radio frequency) electromagnetic field. The motion of free electrons and reactive ions striking the surface of the sample produces an etching in the material. Etch conditions in a RIE system depend strongly on the many process parameters, such as pressure, gas flows, and RF power

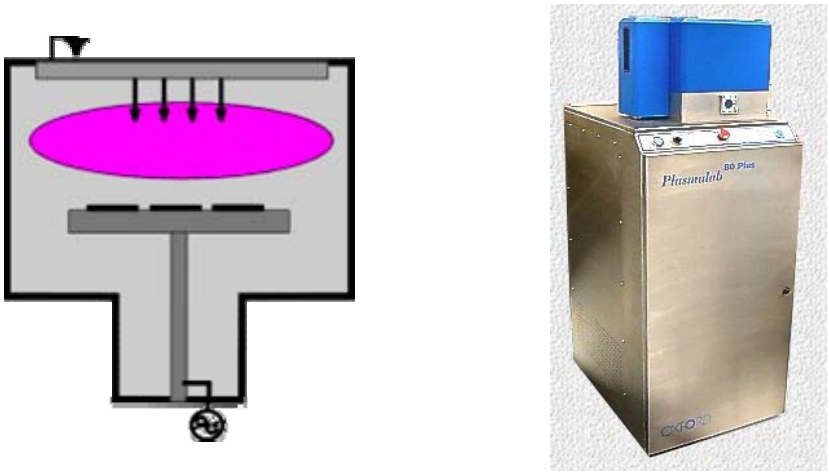

Figure 2-41 a) Draw of the RIE machnie. A gas is insered in the chamber and an RF field produces plasma (pink), the plasma attach the sample. b) Picture of the Plasmalab 80 from Oxford Instruments used at Parc Científic de Barcelona.

A rough surface will help the adhesion of the evaporated metals in the Nafion membrane. For the one hand roughening increases the area of contact between metal and polymer, and by the other hand, minimizes the effect of the changes in the surface strength due to hydration.

The machine used for the RIE was located at the "Nanotechnology Platform" at the "Parc Cientific de Barcelona", and it was the Plasmalab 80 from Oxford Instruments. A picture of the used machine is depicted at Figure 2-41b). The machine was configured to etch with the following parameters:

- Oxygen plasma "O_2".
- Pressure 50mTorr.
- Power 240W.
- 7 minutes.

The samples were then introduced into a SEM microscope to obtain pictures to characterize the change in the surface. Figure 2-42 a), b) show a SEM image of the RIE treated sample and a non-treated sample that serves as reference. While Figure 2-42a) shows a flat surface for the reference (unless a small dust), Figure 2-42b) shows the change in the morphology due to the RIE treatment. Plasma treatment forms needles-shaped microstructures in the Nafion surface. Image recognition software was used to make a fast estimation of the needle heights and the distance between them. The software gave a height of 2μm and a distance of 1 μm approximately.

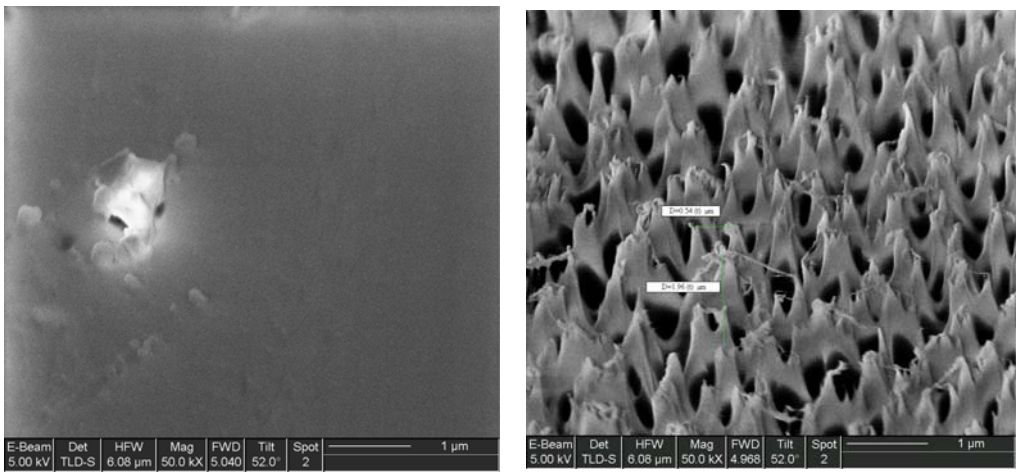

Figure 2-42 a) SEM image of a Nafion surface. A small piece of dust is observed. b) SEM image of a Nafion treated with the RIE.

After etching the Nafion, the electrode deposition process was repeated. Again 15 nm of Titanium and 400 nm of Gold were evaporated. Figure 2-43 shows three pieces of Nafion after the evaporation. Two of them have not the previously described plasma treatment and are reference (these located at the left side of the picture) and one is the plasma treated (located at the right side of the picture). It is observed that the reference samples are completely golden, thus reflect almost perfectly the light, while the plasma treated sample is almost brown and matt. This change in the relative colour is due to the change in the morphology of the surface sample. While in the reference sample the light reflects, in the treated sample the light bounds between sides of the needles.

Figure 2-43 Picture of the samples, the golden are not treated with RIE and the mate is treated with RIE.

2.2.4.2.3. Sodium counter-ion exchange

The performances response of IPMC is strongly dependent on the type of counter-ion it contains. There are different works that compare the performances of IPMCs depending upon the counter ion they have. In [Kim2003] nine different samples were studied which contain nine different cations. These were (Na^+, Li^+, K^+, H^+, Ca^{++}, Mg^{++}, Ba^{++}, $R_nNH_4{}^+{}_{4-n}$ (tetrabuthylammonium (TBA) and tetramethylammonium (TMA))). They observe that the Li^+ containing IPMC is superior to others producing higher forces. This means that hydration process with respect to mobile cations play a significant role in actuation behaviour. Following Li^+ was Na^+, many researchers use sodium because of it is easy to obtain and it is more biocompatible than Lithium.

The Nafion obtained from Sigma-Aldrich already contains the H^+ cations. It comes in its sulfonic acid $S0_3H$ form. In order to change the hydrogen cations for the sodium cations, the samples were immersed in a salt solution containing a 1.5N of NaCl during 3 days at a temperature of 50º (Figure 2-44)

Figure 2-44 Hot plate with the smaples in a solution with NaCl salt.

In the following lines, experimental measurements are realized over the samples prepared. In order to compare performances, the same tests are realized with samples obtained from "Discovery Technologies" from US where the electrodes technique deposition consists on a chemical deposition.

2.2.4.3. Experimental measurements:

In this point some experimental test are realized in order to estimate the goodness of the proposed electrode deposition method. To do this, the same measurements obtained with the new samples, are compared with measurements obtained with a sample from Discovery Technologies where the electrodes were deposited via the chemical deposition method. In Figure 2-45 the three samples studied are pictured. Sample A is the one obtained from Discovery Technologies,

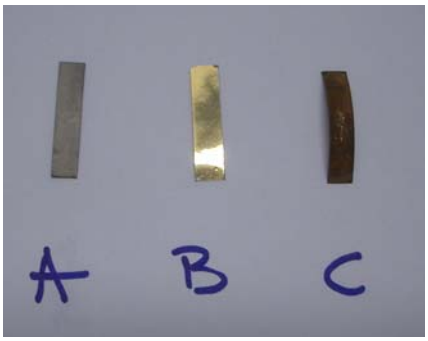

Figure 2-45 Three samples studied: "A" is chemical deposited from Discovery Technology, "B" is the no-treated sample, "C" is the RIE treated sample.

sample B is one manufactured with physical deposition without RIE treatment and before hydration and Sample C is with physical deposition technique and RIE treatment. The three samples are based on a Nafion 117 membrane. All samples are 2.5cm length by 0.5cm width.

Surface resistance: The surface resistance for the three samples have been measured when the sample is in dehydrated condition. The measurements are obtained with a digital multimeter HP34401. Five different measurements are obtained, one every 0.5cm. Table 2-3 presents the surface resistance per unit length with its standard deviation. The sample with a lower mean value for resistance is the sample B that is the sample with direct deposition of metals without RIE treatment. This value is small because the sample has a 15nm of Ti and 400nm of Au deposited on its flat surface. By the other hand the RIE sample has a larger mean resistance value. Although the same quantity of metals is deposited, its roughened surface produces larger resistances due to the increase in area. The standard deviations suggest that the RIE sample is more homogeneous than the others, however, the measuring technique with a two tips method could distort this conclusion.

	Chemical A	**Gold B**	**RIE C**
Surface Resistance (Ω/cm)	2.80+/- 0.80	0.96+/- 0.22	2.64+/-0.16

Table 2-3 Measured surface resistance for the three samples.

Resonance frequency: The resonance frequency for each sample in cantilever configuration is measured in dehydrated conditions. Measurements are obtained by applying a mechanical impulse at the free tip of the sample and measuring the oscillations with a displacement sensor laser LC2440 from Keyence Figure 2-46

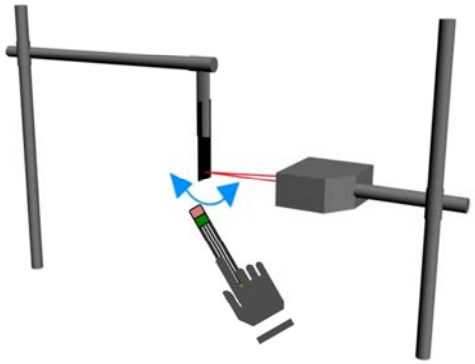

Figure 2-46 Schematic draw of the setup for resonance frequency measurement.

The frequency of the oscillations is directly the resonance frequency of the system. Table 2-4 shows the measurements of the resonance frequencies. It is clearly observed how the highest resonance frequency is for the chemical deposited sample. This is because in chemical deposition the electrodes thickness is thicker than in the other two cases. This is traduced in an increase in the stiffness of the samples thus an increase in the resonance frequency. The difference in resonance frequency between the RIE treated and non treated samples is non significant.

	Chemical A	**Gold B**	**RIE C**
Resonance (Hz)	100	34	32

Table 2-4 Measured values for the resonance frequency for the three samples.

Capacitance value: The value of the capacitance for each sample is computed applying a 2Vpp sinusoidal voltage signal and measuring the absorbed current at 1Hz where both signals are 90º phased. The measurements are realized in dehydrated conditions. Table 2-5 shows the value of the measured capacitance. It is clearly observed that the maximum value is for the chemical sample. This is because with the chemically deposited sample the metal penetrates inside the membrane and therefore the surface contact between polymer and metal is much larger. The difference between RIE treated and non treated samples is also a consequence of differences in the roughness of the surface.

	Chemical A	**Gold B**	**RIE C**
Capacitance (F)	120e-6	20e-9	100e-9

Table 2-5 Measured values for the Capacitance for the three samples

Actuation frequency response: The electromechanical responses of the samples have been measured with the setup of the Figure 2-30. The samples are immersed in a deionised water tank and mounted in a cantilever configuration with a contact claw that serves as the contact electrodes. A HP 2200 function generator is used for generate the driving signals. A TDA buffer voltage driver is used to give

enough power to the sample. The sensor laser is the triangulations laser LC2440. Experimental tests are realized on sample C (RIE treated) and sample A (chemically deposited). Sample B (non RIE treated) does not response due to its electrode's crack when hydrated. The two tests realized are devoted to analyze their frequency response. The first test consists on applying a 1V sinusoidal frequency sweep voltage, and the second test consist on applying 1V sinusoidal signals at different frequencies.

Figure 2-47 plots the time response for the physical deposition sample to a sinusoidal sweep from 100mHz up to 20Hz with a sweep time of 10s. And Figure 2-48 plots the time response for the chemical deposition sample to a sinusoidal sweep from 100mHz up to 40Hz with a sweep time of 5s. Both pictures depict the classical response to a sweep of an IPMC, the low pass filtering and a resonance response. Comparing both figures, it is observed that the displacement magnitude for the chemical deposited is one order of magnitude greater than the physical deposited sample.

Figure 2-49 show the frequency response acquired by applying a sinusoidal signal of 2Vpp at different frequencies and measuring the peak to peak displacement for both samples. This measurement confirms that while the amplitude between both samples is different, the dynamic response of the system is similar. Both samples present low pass filter behaviour due to the ionic nature of the transduction effect, and a resonance response due to the mechanical configuration of the system. It is important to remark that the resonance frequency measured underwater is slower than the one measured in air. This shift is due to the presents of water surrounding the sample which tends to slow down the resonance frequency.

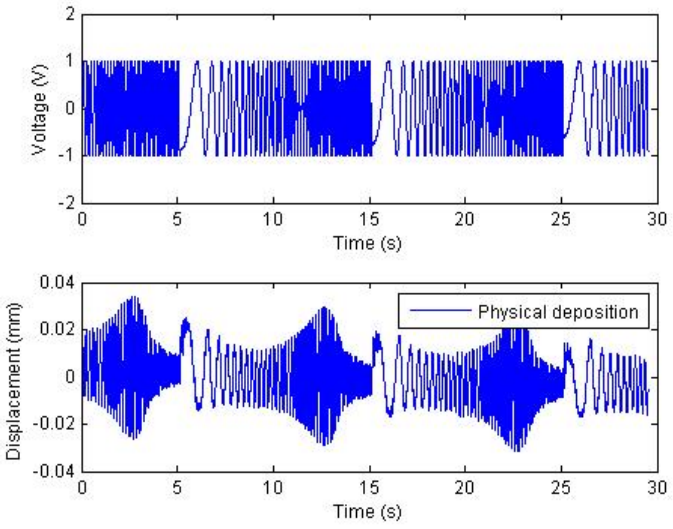

Figure 2-47 Sinusoidal sweep response of the sample with physical deposition.

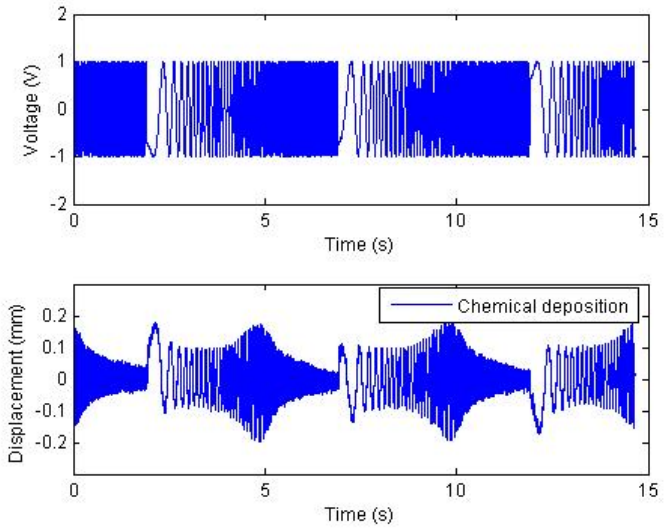

Figure 2-48 Sinusoidal sweep response of the sample with chemical deposition.

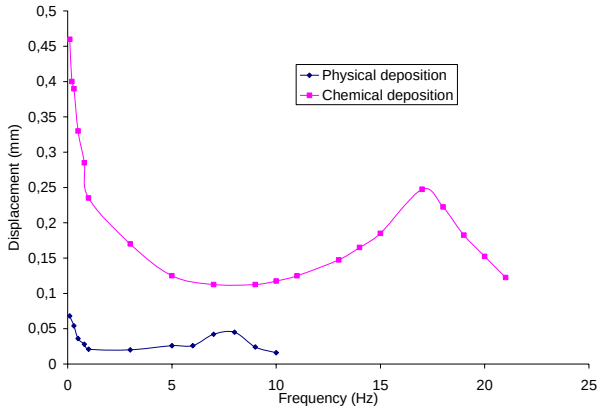

Figure 2-49 Frequency response of the Chemical and Physical desposited samples.

Physical vapour deposition with RIE surface treatment has been proven as an effective electrode deposition technique to form ionic polymer metal composites in a Nafion base substrate. This technique is compatible with common MEMS processes therefore it appears as a possible solution when developing high density patterned electrodes. However, although this is a technique to deposit the metals, other challenges must be solved first to effectively pattern with classical photolithography electrodes in the Nafion surface. In this sense the authors are working on defining a protocol to pattern electrodes via the classical photolithography process. The main steps of the process are first stack the Nafion membrane on a rigid surface, then spin coat a photosensible resin, apply a shadow mask in the mask aligner, develop the sample, physical vapour deposition and lift off the rest of the resin. It is very

important to have the membrane fixed on a substrate due to the constant hydration and dehydration that the membrane feels due to the wet etching through the different photolithpography steps. It has been also observed that most common used resin removers used in the lift off step contain acetone that damages the polymer therefore alternative solutions are being considered. The same problem arouses when trying to clean the membrane surface therefore alternative cleaning methods must be proposed.

2.2.5. Conclusions

Ionic polymers are very promising materials to work in microrobotic systems as actuators and sensors for motion control. Their biocompatibility and flexibility features, their low voltage activation propertied and the possibility to use them underwater opens the door to new motion control strategies for microrobotic and thus to new field of applications. However these materials are in an early state of development and there are still some drawbacks to solve first before bringing this materials to commercial or reliable microrobotic systems. In this chapter two of these drawbacks have been addressed, these are, by the one hand, the study of control system to assure a reliable motion dynamic underwater, and by the other hand, the proposal of a electrode deposition technique for patterning electrodes with compatible MST technologies.

The proposed control strategy presented in this point has been designed to avoid the effects of the inconsistent dynamic behavior of IPMC actuators. It is conceived to always follow a certain dynamic even if the internal parameters of the system changes with time. A measurement of the tip displacement is obtained with a laser system sensor to close the loop and adapt the control law to those internal changes. In piezoelectric polymers the internal physics responsible of the actuation are well known and their dynamic response is more stable than in IPMCs. This allows the possibility to obtain fine physical models and also to make more precise studies on sensitivities of the model parameters to other external variables. Therefore this material can be utilized in open loop, expecting a certain response, or also in closed loop using specific classical control laws for the application. By the other hand the unpredictable dynamic of the ionic polymers suggest to develop control laws that adapt itself to the variations of the dynamics. In this point a second order Model Reference Adaptive Control has been designed an experimentally implemented to work with a 1cm length IPMC polymer. The control system is able to follow the model reference dynamics with a small error at low frequency from 100mHz up to 1Hz. It has been demonstrated the ability of the dead zone and the parameter projection techniques to reduce perturbances of the system.

While the transduction effect in an IPMC is still not completely well understood by the researchers, many of them agree that it is directly related to its capacitance value. Manufacturing electrodes with the chemical deposition produces electrodes with a very large effective surface contact between polymer and metal and it produce a high adhesion between metal and polymer. This is traduced in very high

capacitance elements. In fact there are some applications where IPMCs are used as super capacitors. However, this is a consequence of the diffusion of metal particles inside the membrane of the IPMC. Therefore if small electrodes are need to pattern in a surface, this technique will limit its minimum distance. By the other hand the physical deposition technique with a RIE surface treatment proposed, produces small capacitance values thus the electromechanical effect is reduced, but it does not diffuse therefore it could be useful for patterning small electrodes.

2.3. References

[Adolf1993] D. Adolf, M. Shahinpoor, D. Segalman and W. Witkowski 1993 Electrically controlled polymeric gel actuators, (world's first patent on synthetic artificial muscles) US Patent Specification 5250167 (Issued 5 October)

[Akle2005] B.J. Akle. Characterization and Modeling of the Ionomer-conductor Interface in Ionic Polymer Transducers. Ph.D. Thesis, Virginia Tech . 2005

[Alonso2007] O. Alonso, R. Casanova, A. Sanuy, A. Dieguez, and J. Samuier, "A low power optical interface for inter-robot communication in a swarm of microrobots," *Proceedings of the 11th WSEAS International Conference on Circuits, Vol 1,* pp. 143-146, 2007.

[Arbat2008] A. Arbat, J. Canals, R. Casanova, A. Dieguez, J. Brufau, M. Puig, and J. Samitier, "Design and control of a micro-cantilever tool for micro-robot contact sensing," *2007 18th European Conference on Circuit Theory and Design (ECCTD '07),* pp. 100-3, 2008.

[Asaka1995] K. Asaka, K. Oguro, Y. Nishimura, M. Mizuhata and H. Takenaka. Polym. J. 27 (1995), p. 436 Bending of Polyelectrolyte Membrane-Platinum Composites by Electric (1995)

[Astrom1994] K. J. Astrom 1994 Adaptive Control 2nd edn (Englewood Cliffs, NJ: Prentice-Hall)

[Boletis2006] A. Boletis, W. Driesen, J. M. Breguet, and A. Brunete, "Solar cell powering with integrated global positioning system for mm(3) size robots," *2006 Ieee/Rsj International Conference on Intelligent Robots and Systems, Vols 1-12,* pp. 5528-5533, 2006.

[Bonomo2007] C. Bonomo, L. Fortuna, P. Giannone, S. Graziani, and S. Strazzeri, "A nonlinear model for ionic polymer metal composites as actuators," *Smart Materials & Structures,* vol. 16, pp. 1-12, 2007.

[Brufau2006] J. Brufau-Penella, J. Sanchez-Martin, and M. Puig-Vidal, "Pizeoelectric polymer model validation applied to mm size microrobot I-Swarm (Intelligent Swarm) - art. no. 61660Q," *Smart Structures and Materials 2006: Modeling, Signal Processing, and Control,* vol. 6166, pp. Q1660-Q1660, 2006.

[Brufau2006_2] J. Brufau-Penella, M. Puig-Vidal 2006_2 Piezoelectric smart actuator: model validation and charge vs voltage method for displacement sensing. ACTUATOR 2006, 10th international Conference on New Actuators, 14-16 June 2006, Bremen, Germany

[Brufau2008_2] J. Brufau-Penella, K. Tsiakmakis, T. Laopoulos, and M. Puig-Vidal, "Model reference adaptive control for an ionic polymer metal composite in underwater applications," Smart Materials and Structures, p. 045020 (9 pp.), 2008.

[Brunetto2008] P. Brunetto, L. Fortuna, S. Graziani, and S. Strazzeri, "A model of ionic polymer-metal composite actuators in underwater operations," *Smart Materials & Structures,* vol. 17, 2008.

[Casanova2007] R. Casanova, A. Dieguez, A. Sanuy, A. Arbat, O. Alonso, J. Canals, and J. Samitier, "An ultra low power IC for an autonomous mm(3)-sized microrobot," *2007 Ieee Asian Solid-State Circuits Conference, Proceedings of Technical Papers,* pp. 55-58, 2007.

[Datta1998] A. Datta 1998 Adaptive internal model control Advances in Industrial Control (Berlin: Springer)

[de Gennes2000] P. G. de Gennes, K. Okumura, M. Shahinpoor, and K. J. Kim, "Mechanoelectric effects in ionic gels," *Europhysics Letters,* vol. 50, pp. 513-518, 2000.

[DISCOVER] http://www.discover-technologies.com/

[Edqvist2008] E. Edqvist, N. Snis, and S. Johansson, "Gentle dry etching of P(VDF-TrFE) multilayer micro actuator structures by use of an inductive coupled plasma," *Journal of Micromechanics and Microengineering,* vol. 18, 2008.

[Han1999] S. M. Han, H. Benaroya, and T. Wei, "Dynamics of transversely vibrating beams

using four engineering theories," *Journal of Sound and Vibration,* vol. 225, pp. 935-988, 1999.

[Kanno1994] R. Kanno, A. Kurata, M. Hattori, S. Tadokoro and T. Takamori 1994 Characteristics and modelling of ICPF actuator Japan-USA Symp. on Flexible Automation 2 691–8

[Kanno1996] R. Kanno, S. Tadokoro, T. Takamori, and M. Hattori, "Linear approximate dynamic model of ICPF (ionic conducting polymer gel film) actuator," *1996 Ieee International Conference on Robotics and Automation, Proceedings, Vols 1-4,* pp. 219-225, 1996.

[Kanno1996_2] R. Kanno, S. Tadokoro, T. Takamori, and K. Oguro, "3-dimensional dynamic model of ionic conducting polymer gel film (ICPF) actuator," *1996 IEEE International Conference on Systems, Man and Cybernetics. Information Intelligence and Systems (Cat. No.96CH35929)|1996 IEEE International Conference on Systems, Man and Cybernetics. Information Intelligence and Systems (Cat. No.96CH35929),* pp. 2179-84 vol.3|4 vol. 3234, 1996.

[Kim2003] K. J. Kim and M. Shahinpoor, "Ionic polymer-metal composites: II. Manufacturing techniques," *Smart Materials & Structures,* vol. 12, pp. 65-79, 2003.

[Kothera2005] C. S. Kothera Characterization, modeling, and control of the nonlinear actuation response of ionic polymer transducers Thesis (Ph. D.)--Virginia Polytechnic Institute and State University, 2005.

[Mallavarapu2001] K. Mallavarapu and D. J. Leo, "Feedback control of the bending response of ionic polymer actuators," *Journal of Intelligent Material Systems and Structures,* vol. 12, pp. 143-155, 2001.

[Mojarrad1997] M. Mojarrad and M. Shahinpoor, "Ion-exchange-metal composite sensor films," *Smart Sensing, Processing, and Instrumentation - Smart Structures and Materials 1997,* vol. 3042, pp. 52-60, 1997.

[Nemat-Nasser2000] S. Nemat-Nasser and J. Y. Li, "Electromechanical response of ionic polymer metal composites," *Smart Structures and Materials 2000: Electroactive Polymer Actuators and Divices (Eapad),* vol. 3987, pp. 82-91, 2000.

[Nemat-Nasser2003] S. Nemat-Nasser and Y. X. Wu, "Comparative experimental study of ionic polymer-metal composites with different backbone ionomers and in various cation forms," *Journal of Applied Physics,* vol. 93, pp. 5255-5267, 2003.

[Newbury2002] M. Newbury, Characterization, modeling, and control of ionic polymer transducers, Ph.D. Thesis, URN etd-09182002-081047, Virginia Tech, 2002.

[Newbury2003] K. M. Newbury and D. J. Leo, "Linear electromechanical model of ionic polymer transducers - Part I: Model development," *Journal of Intelligent Material Systems and Structures,* vol. 14, pp. 333-342, 2003.

[Oguro2001] K. Oguro Prep. Proc. Ion-Exchange Polymer Metal Composites (IPMC) Membranes Web at http://ndeaa.jpl.nasa.gov/ nasande/lommas/eap/IPMC PrepProcedure.htm 2001

[Onishi2000] K. Onishi, S. Sewa, K. Asaka, N. Fujiwara, and K. Oguro, "Morphology of electrodes and bending response of the polymer electrolyte actuator," *Electrochimica Acta,* vol. 46, pp. 737-743, 2000.

[Paquette2003] J. W. Paquette, K. J. Kim, J. D. Nam, and Y. S. Tak, "An equivalent circuit model for ionic polymer-metal composites and their performance improvement by a clay-based polymer nano-composite technique," *Journal of Intelligent Material Systems and Structures,* vol. 14, pp. 633-642, 2003.

[Richardson2003] R. C. Richardson, M. C. Levesley, M. D. Brown, J. A. Hawkes, K. Watterson, and P. G. Walker, "Control of ionic polymer metal composites," *Ieee-Asme Transactions on Mechatronics,* vol. 8, pp. 245-253, 2003.

[Shahinpoor2000] M. Shahinpoor and K. J. Kim, "The effect of surface-electrode resistance on the performance of ionic polymer-metal composite (IPMIC) artificial muscles," *Smart Materials & Structures,* vol. 9, pp. 543-551, 2000.

[Shahinpoor2001] M. Shahinpoor and K. J. Kim, "Ionic polymer-metal composites: I. Fundamentals,"

Smart Materials & Structures, vol. 10, pp. 819-833, 2001.

[Shahinpoor2004] M. Shahinpoor and K. J. Kim, "Ionic polymer-metal composites: III. Modeling and simulation as biomimetic sensors, actuators, transducers, and artificial muscles," *Smart Materials & Structures,* vol. 13, pp. 1362-1388, 2004.

[Slotine1991] J.E. Slotine 1991 Applied Non-Linear Control (Englewood Cliffs, NJ: Prentice-Hall)

[Snis2008] N. Snis, E. Edqvist, U. Simu, and S. Johansson, "Monolithic fabrication of multilayer P(VDF-TrFE) cantilevers," *Sensors and Actuators a-Physical,* vol. 144, pp. 314-320, 2008.

[Snis2008_2] N. Snis (2008). Actuators for autonomous microrobots. Doctoral thesis Uppsala University

[Tadokoro2000] S. Tadokoro, S. Yamagami, T. Takamori, and K. Oguro, "Modeling of Nafion-Pt composite actuators (ICPF) by ionic motion," *Smart Structures and Materials 2000: Electroactive Polymer Actuators and Divices (Eapad),* vol. 3987, pp. 92-102, 2000.

[Tsiatmaikis 2007] K. Tsiakmakis, J. Brufau, M. Puig-Vidal and Th. Laopoulos Measuring Motion Parameters of Ionic Polymer-Metal Composites (IPMC) Actuators with a CCD camera [#7467]

[Tsiatmaikis 2008] K. Tsiatmaikis; J. Brufau-Penella; M. Puig-idal; Th. Laopoulos, ”A camera based method for the measurement of motion parameters of IPMC actuators.” IEEE Transactions on Instrumentation & Measurement 2008 Accepted, first revision

[Uchino1996] K. Uchino Piezoelectric Actuators and Ultrasonic Motors Springer; 1 edition (November 30, 1996)

[Yamakita2006] M. Yamakita, A. Sera, N. Kamamichi, K. Asaka, and L. Zhi-Wei, "Integrated design of IPMC actuator/sensor," *Proceedings. 2006 Conference on International Robotics and Automation (IEEE Cat. No. 06CH37729D)|Proceedings. 2006 Conference on International Robotics and Automation (IEEE Cat. No. 06CH37729D),* pp. 1834-9|CD-ROM, 2006.

3. POWER HARVESTING FROM VIBRATIONS

A step forward in the design of smart systems is the integration of autonomous power supply. Although up to day most common used power supplies in smart systems have been the batteries, the integration of these elements involve a set of problems. Batteries store a limited quantity of energy and require a recharge with a certain periodicity. Moreover batteries withstand a finite number of recharges and became useless after that. Furthermore, another big problem is that batteries are heavy pollutants. Considering the huge number of applications and devices that use batteries one can easily imagine the unsustainable of the situation.

The research in power harvesting is not new and different solutions and devices have been proposed. Each solution depends on the surrounding environmental energy sources and on the applications. There are different environmental energy sources i.e. the solar energy, thermal energy, energy from vibrations, etc. There are also different methods to transform this energy into electrical energy, i.e. photovoltaic cells, thermoelectric generators, electromagnetic converters etc. Solar energy has been extensively used in many applications as the main energy source, in fact in a sunny day the quantity of energy irradiated to one centimeter square is very big, about $15mW/cm^2$. However this power decreases tremendously when the day is cloudy or at night. Another energy source that surrounds us comes from mechanical vibrations as kinetic energy. It is quite common to find low level vibrations in many environments in our day life. The amount of energy possible to harvest depends on the frequency of the vibrations, its amplitude and the kind of transducer used. Nevertheless some authors give a number of about $200\mu W/cm^2$ assuming the typical vibrations that exist inside a building [Roundy2004_2]. This amount of power could be enough to supply a wireless sensor node [Rabaey2000], thus big efforts for developing systems to convert vibration energy into electrical energy are being done.

There are different methods to convert mechanical vibrations into electrical energy. The electromagnetic generators use a variable magnetic field to generate electrical current. Also the electrostatic generators use the variations of charge or voltage that are produced in a planar capacitor when one of its electrodes moves relatively to the other. There are also generators based on smart materials as piezoelectrics. Piezoelectric power generators are based on the electrical charge generation produced when the material is mechanically stressed. These generators have some advantages compared to electrostatic and electromagnetic. They have a greater energy density and they produce relatively acceptable levels of voltages. Furthermore they do not need any magnetic field neither external energy sources as is the case of the other options [Richards2004].

In this chapter the possibility to use smart materials to harvest energy from mechanical vibrations is studied. First of all, the energy source is analyzed. In this sense a general model to convert mechanical vibrations into electrical energy is discussed. The model describes the maximum power that can be removed from an oscillating mass. The model assumes a perfect adaptation between the mechanical domain and the electrical domain where the energy is transferred. The model serves as a tool to determine the maximum energy that can be harvested from vibrations. Once the general model is presented, the use of smart materials to convert this energy is analyzed. First of all the piezoelectric generator is considered. In this case the energy storing capability of piezoelectric materials is considered and a physical model is redefined. The model takes into account the influence of the electrical load where the electrical energy is generated and defines the optimum load conditions for a maximum energy generation. After this, a piezoelectric micropower generator MPG device is presented. The generator is based on a commercial piezoelectric ceramic transducer. This transducer consists on a piezoelectric ceramic embedded in a polymer matrix in a cantilever configuration. The composite nature of the transducer implies an experimental identification of the different model parameters. Once the MPG model is characterized and the optimum electrical load conditions are identified, an electronic circuitry for optimum energy storage is presented. The circuit converts the AC power obtained from a typical vibration source into electrical DC power. The circuit stores the energy optimally until there is enough power supply to drive an electrical load. Finally, an analysis of the capabilities to generate energy from mechanical vibrations using ionic polymers is presented.

3.1. General model for power harvesting from vibrations

In order to determine the quantity of energy that can be harvested from mechanical vibrations, a model is needed. When modeling a system it is important to take into account the level of precision required for the model. Generally for greater levels of precision the model became more complex. Nevertheless, the development of highly precise and complex models sometimes entails difficulties when trying to understand and comprehend the behavior of the system. Before starting with a more complex piezoelectric model a simpler general one is discussed.

In this point one of the first models developed in the literature to describe the energy that can be harvested from a vibration source is presented. The most interesting characteristic of the model falls on its simplicity. The model was presented by Williams and Yates in 1996 [Williams1996] and it has been largely commented in later bibliography [Stephen2006]. This model describes the conversion of a moving mass kinetic energy into electrical energy. It is based on linear systems theory and it does not consider the kind of transducer used for the conversion. The primary idea behind this model is that the conversion of energy from the oscillating mass to electricity (whatever the mechanism that takes place) looks like a linear damper. The model output quantifies the maximum energy possible to convert. The inputs considered from the source are the acceleration and the frequency of the vibration. The inputs considered from the transducer are the mass and the mechanical damping (or maximum displacement).

This model considers the mechanical system from Figure 3-1. It is a 1 degree of freedom (DOF) system where there is an inertial mass “m”, a spring constant “k”, and the damping coefficient “c”. The system is excited with a sinusoidal force “F” applied at the mass. The equilibrium of forces equation is described as Eq 3-1

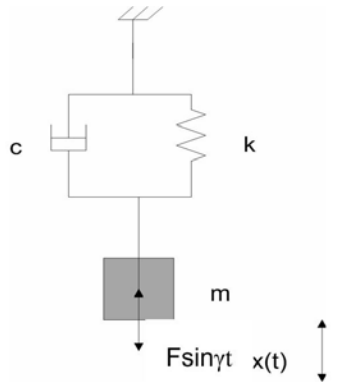

Figure 3-1 Spring mass damper with a sinusoidal force excitation applied at the mass.

$$m\ddot{x} + c\dot{x} + kx = F\sin\gamma t \qquad \textit{Eq 3-1}$$

Multiplying the equation Eq 3-1 by velocity and reorganizing, the power conservation equation is obtained.

$$\dot{x}F\sin\gamma t = c\dot{x}^2 + \frac{1}{2}\frac{d}{dt}\left(m\dot{x}^2 + kx^2\right) \qquad \textit{Eq 3-2}$$

This equation means that the instantaneous power that enters in the system is equal to the power dissipated in the damper plus the power time variations that represents the summation of the kinetic and elastic energy. Therefore, in a stationary state, after one period, all the energy that has entered in the system is the energy that has been dissipated in the damper. If the system is resonating, the temporal variation term becomes cero and the input power is directly the dissipated power.

Now, consider the real case where the generator is a mass that is located in a vibrating body, thus it is forced with an input acceleration from its base. The base vibration "$y_b(t)$" produce a motion of the generator mass "x(t)". The new configuration is depicted at Figure 3-2.

The equation of equilibrium of forces governing the system is

$$m\ddot{x} + c(\dot{x} - \dot{y}_b) + k(x - y_b) = 0 \qquad \textit{Eq 3-3}$$

Again multiplying by velocity and reorganizing, the new equation of power conservation is obtained.

$$k(y_b - x)\dot{y}_b + c(\dot{y}_b - \dot{x})\dot{y}_b = c(\dot{y}_b - \dot{x})^2 + \frac{1}{2}\frac{d}{dt}\left(m\dot{x}^2 + k(x - y_b)^2\right) \qquad \textit{Eq 3-4}$$

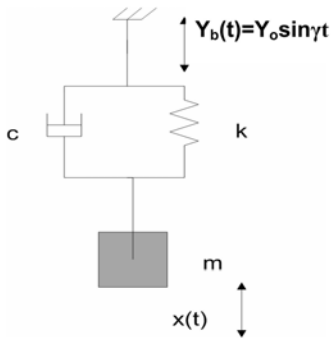

Figure 3-2 Spring mass damper with displacement base excitation.

As before, the instantaneous power introduced in the system by the vibrating source is equal to the power dissipated in the damper plus the time variation of the summation of the kinetic and elastic energy. These equations are rewritten in a simply way using the relative displacement $z=x-y_b$. Then the force equation becomes

$$m\ddot{z} + c\dot{z} + kz = m\ddot{y}_b \qquad \textit{Eq 3-5}$$

This equation has the same form than in the case of a force excitation Eq 3-1. Multiplying by the relative velocity the equation is rewritten as

$$m\ddot{y}_b\dot{z} = c\dot{z}^2 + \frac{1}{2}\frac{d}{dt}\left(m\dot{z}^2 + kz^2\right) \qquad \textit{Eq 3-6}$$

This equation is similar to the power conservation equation Eq 3-2 but its meaning is something different. It is important to note that in this case the first term inside the parenthesis is not directly the kinetic energy. However the quantity of energy that enters in the system after a whole period is equal to the wasted energy in the damper.

In the model presented by William and Yaltes, the damping coefficient "c" represents the conversion coefficient, the quantity of mechanical wasted energy and thus quantity of electrical energy generated. From now on this coefficient is named the electrical induced damping coefficient "c_{elec}". In order to consider losses due to internal frictions or due to air damping, another constant is introduced, this is the mechanical damping coefficient "c_{mec}". Therefore the force equation rewrites as:

$$m\ddot{z} + \left(c_{mec} + c_{elec}\right)\dot{z} + kz = m\ddot{y}_b \qquad \textit{Eq 3-7}$$

thus

$$m\ddot{y}\dot{z} = \left(c_{mec} + c_{elec}\right)\dot{z}^2 + \frac{1}{2}\frac{d}{dt}\left(m\dot{z}^2 + kz^2\right) \qquad \textit{Eq 3-8}$$

The quantity of energy converted into electrical energy in a whole cycle is computed as the wasted energy due to the electrical induced damping coefficient in a whole period:

$$E_{elec} = \int_0^{\tau=2\pi/\omega} c_{elec}\dot{z}(t)^2\,dt \qquad \textit{Eq 3-9}$$

In order to obtain a solution, first of all it is need to find a solution for the relative displacement "z(t)". This is obtained directly from the force equation Eq 3-7 and gives

$$z(t) = Z\sin(\gamma t - \phi) \qquad \textit{Eq 3-10}$$

$$Z = \frac{m\gamma^2 Y}{\sqrt{(k-\gamma^2 m)^2 + (c_{elec} + c_{mec})^2 \gamma^2}} \qquad \textit{Eq 3-11}$$

$$\phi = \tan^{-1}\left(\frac{(c_{elect} + c_{mec})\gamma}{k - \gamma^2 m}\right) \qquad \textit{Eq 3-12}$$

Therefore the quantity of energy generated has the form:

$$E_{elec} = c_{elec}\pi\gamma Z^2 \qquad \textit{Eq 3-13}$$

The average power is equal to:

$$P_{av} = \frac{E_{elec}}{\tau} = \frac{c_{elec}\gamma^2 Z^2}{2} \qquad \textit{Eq 3-14}$$

Substitution of equation Eq 3-11 into this equation gives:

$$P_{av} = \frac{1}{2}\frac{c_{elec} m^2 \gamma^6 Y^2}{(k-\gamma^2 m)^2 + (c_{elec} + c_{mec})^2 \gamma^2} \qquad \textit{Eq 3-15}$$

Equation already obtained by different authors [William1996], [El-Hami2001], [Roundy2004]. The generated power is the product of the square velocity multiplied by the electrical induced damping constant coefficient Eq 3-14. Writing the power equation Eq 3-15 in terms of its natural frequency "ω_n", Eq 3-16 and its damping ratio "ξ_n" Eq 3-17 leads Eq 3-18

$$\omega_n = \sqrt{\frac{k}{m}} \qquad \textit{Eq 3-16}$$

$$\xi_n = \frac{c_n}{2m\omega_n} \qquad \textit{Eq 3-17}$$

$$P_{av} = \frac{m\xi_{elec}\left(\frac{\gamma}{\omega_n}\right)^3 \gamma^3 Y^2}{\left(1-\left(\frac{\gamma}{\omega_n}\right)^2\right)^2 + \left(2(\xi_{elec} + \xi_{mec})\frac{\gamma}{\omega_n}\right)^2} \qquad \textit{Eq 3-18}$$

To maximize the power, the system has to be designed with a resonance frequency equal to the input vibration frequency. Thus the power equation is rewritten as:

$$P_{av} = \frac{m\xi_{elec}Y^2\omega_n^3}{4(\xi_{mec}+\xi_{elec})^2} = \frac{m\xi_{elec}A_{in}{}^2}{4(\xi_{mec}+\xi_{elec})^2\omega_n} \qquad \textit{Eq 3-19}$$

Therefore the maximum power depends on the "ξ_{mec}" and "ξ_{elec}". Normally "ξ_{mec}" depends on the environment and on the material while "ξ_{elec}" depends on the transduction system used for the generation of electrical energy, and as we will see, it depends on the electrical load.

Figure 3-3 shows a representation of a normalized power coefficient ($\xi_{elec}/(\xi_{elec}+\xi_{mec})^2$) versus the damping coefficients ratio ξ_{elec}/ξ_{mec}. It is observed how for a certain ratio the power is maximized, this is the case when $\xi_{elec}=\xi_{mec}$. Therefore to generate the maximum power the electrical circuit must be designed to fulfill the condition.

Figure 3-3 shows that for small "ξ_{elec}" the sacrifice of energy is more accentuated than in the case of having a large "ξ_{elec}". The equation that defines the maximum power is obtained when $\xi_{elec} = \xi_{mec}$ and then:

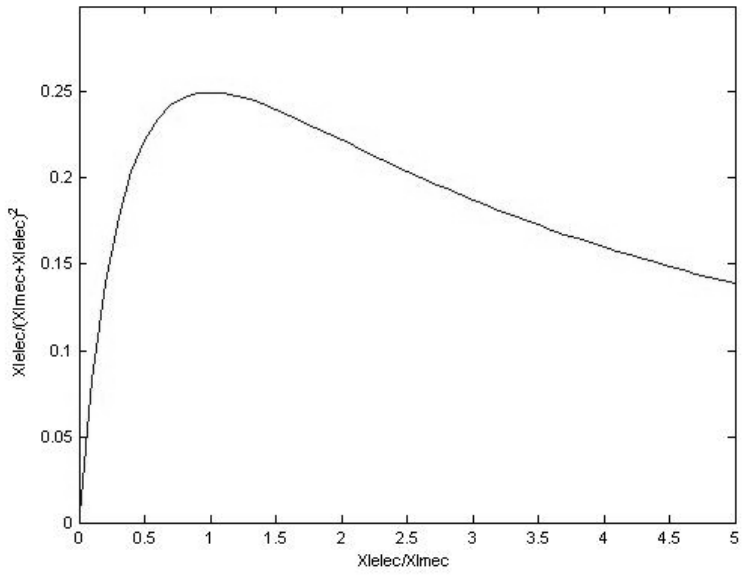

Figure 3-3 Representation of the power coefficient vs electrical and mechanical damping coefficient ratio. XI=ξ.

$$P_{av} = \frac{mA_{in}^{\ 2}}{16\xi_{mec}\omega_n} \qquad \textit{Eq 3-20}$$

Now a first estimation of the power that can be harvested from a vibrating mass is performed. Assume a vibrating source with a frequency of 24Hz and an acceleration of $1m/s^2$ (this type of vibration is easily found inside a building). Then consider that the converter used for the generation has a 13g mass and a 0.027 mechanical damping ratio (these values fulfils the specifications of the piezoelectric commercial converter used at section 3.2.). Therefore, using the model equation Eq 3-20, the model outputs a maximum power generation of about 190μW that could be enough power to drive a sensor node.

Some interesting conclusions are extracted from this analysis:

- The power is proportional to the square of the vibration acceleration.
- For a given vibration acceleration, and a given device damping ratio, the generated power is higher at low frequency.
- Power is optimized when the electrical induced damping ratio equals the mechanical damping ratio $\xi_{elec}=\xi_{mec}$. This is accomplished by adapting the electrical circuit to the mechanical part.
- The generated power is proportional to the oscillating mass and this power is bigger for smaller "ξ_{mec}". It is important to remark that a small "ξ_{mec}" means large displacements "Z", thus the system will have to suffer large strains which can damage it.
- The natural frequency of the system must match the vibration frequency of the input vibrations. This point is critical to optimize the power, however it is not always easily to achieve. Many vibrations sources have a constant and fixed vibrating frequency. Other sources have a bigger bandwidth with a variable vibrating frequency. While for the first case, the fit is accomplished by controlling the mechanical parameters, the mass and the spring constant, for the second case it is necessary to actively tune the resonant frequency of the device. This thesis focuses on the study of system with a fixed input vibration frequency.

The model presented is useful to determine the maximum power that can be extracted from a vibrating body, nevertheless this power depends on the generator parameters as the mass and the damping coefficient. However the damping coefficient is not an input constrain of the application. It is more common to have restrictions in the total volume of the converter. These constrictions impose a

maximum displacement of the oscillating mass, therefore it is interesting to write the power equation in terms of this maximum displacement instead of damping. Consider the displacement equation Eq 3-11 in terms of damping ratios.

$$Z = \frac{m\gamma^2 Y}{\sqrt{\left(\omega_n^2 - \gamma^2\right)^2 + 4\omega_n^2\left(\xi_{elec} + \xi_{mec}\right)^2\gamma^2}} \qquad \textit{Eq 3-21}$$

The displacement for the maximum power generation is achieved when the input frequency is equal to the natural frequency $\gamma=\omega_n$, and the condition for the maximum energy generation $\xi_{elec}=\xi_{mec}$ is accomplished. Therefore substitution of these conditions in Eq 3-21 leaves to a damping ratio written in terms of the displacement as

$$\xi_{mec} = \frac{A_{in}}{4Z_{\max}\omega_n^2} \qquad \textit{Eq 3-22}$$

Substitution of this equation into the power equation Eq 3-20 gives

$$P_{av} = \frac{\omega_n m A_{in} Z_{\max}}{4} \qquad \textit{Eq 3-23}$$

This function is useful for obtaining a first estimation of the maximum harvested power for a given application constrains. However this is only an approximation since it does not consider the way this energy is generated.

The model presented in this point starts with the assumption that the conversion of energy looks like a linear damper. This assumption is not always correct, while for some specific converters such as electro-magnetic converters the model is fairly accurate [Williams1996], if the converter is piezoelectric or electrostatic, the energy conversion differs from a linear damper thus the model has to be changed somewhat. Nevertheless the obtained conclusions can be extrapolated.

In the following point, the vibration energy harvesting using piezoelectric materials is analyzed in detail. The general model is modified considering the piezoelectric transduction, and then, the electrical load specifications for an optimization of the generated power are determined. Next an electrical circuit considering these specifications is implemented to manage the power generated.

3.2. Piezoelectric power harvesting

An efficient and interesting solution to harvest energy from mechanical vibrations is to use piezoelectric materials. These materials, when mechanically stressed, produce an electric charge. The idea is to anchor a piece of this material in a vibrating source in such a way that the mechanical vibrations of its base are transmitted to the material. These vibrations produce a mechanical stress in the material. This stress produces an electrical charge variation in the material. If a simple resistive load is attached to the piezoelectric material, an electrical current will flow into it. Therefore electrical power is generated from mechanical vibrations.

Piezoelectric materials are not the only possible choice to harvest energy from vibrations. Other possible converters are the electrostatic and the electromagnetic based ones. However, this point focuses on the use of piezoelectric materials because they have some interesting characteristics and advantages compared to others. The first one is that piezoelectric materials have the greatest energy density from the three [Richards2004]. Furthermore, piezoelectric converters do not need any external power source neither any mechanical stop to avoid electrodes collapse, as in the case of electrostatic based devices. Moreover they do not need magnetic fields neither coils, as in the case of electromagnetic based devices. The voltage and current output levels of piezoelectric based harvesting devices really depend on the physical implementation and the particular electrical load circuit used. In reality, it is quite easy to design a piezoelectric converter that produces voltages and currents in a useful range.

One disadvantage when designing piezoelectric converters is the higher complexity for implementation on the micro-scale and integration with microelectronics. PZT film is not a normal material for general silicon processing, often requiring many more mask steps. Therefore, the potential for integration with microelectronics is less than that for electrostatic converters [Roundy2003]. The difficulties in microstructuring the piezoelectric materials have limited the design of more complex mechanical structures that could increase the harvesting power.

When working with piezoelectric material for energy harvesting, there are two main possible configurations for the device. The first one is converting the vibrations in the <33> direction. In this case the generated voltage and the induced strain are in the same direction. Piezoelectric devices using the <33> direction are normally build up as stack of many layers polled in series to produces axial motion. Normally this configuration is used in systems where piezoelectric acts as force actuators. In the case of energy harvesting this configuration is not very useful for different reasons. Piezoelectric stacks have very high resonance frequencies thus they only serve to convert energy from very high vibrating frequencies. Moreover the stress transmitted in such linear actuator is very small thus low power will be generated [Ramsay2001], [Sodano2004]. The other possible configuration is using the <31> direction where the voltage acts in the <3> direction and the mechanical stress acts in the <1>

direction. A configuration in <31> means that the system is conceived to bend. Most common type of <31> elements are bimorphs, in which two separate sheets are bonded together. Although the electrical/mechanical coupling for <31> mode is lower than for <33> mode, there is a key advantage to operating in <31> mode. The system is much more compliant, therefore larger strains can be produced with smaller input forces. Also, the resonant frequency is much lower. [Roundy2003]. More recently, some researchers have proposed to use the <33> mode in a bending element using interdigitated electrodes in piezoelectric MEMS cantilever [Jeon2003]. That system take advantage of the greatest value of the coupling but in a bending configuration to maximize the strain produced. However this configuration requires the definition of the interdigitated electrodes in a photolithography process.

Most part of the developed work about recovering energy from an oscillating vibration source using piezoelectric materials are based on bending elements formed by or embedded with piezoelectric material. Bending elements have been mounted in many configurations to generate power. Umeda et al. [Umeda1996] mounted a clamped bronze disk with a piezoelectric layer attached. When a steel ball impacted the disk, the system bends generating energy. White et al. [White2001] developed a prototype designed to recover the energy coming from a vibration source produced by vibrating machinery at a fixed frequency. The generator consisted on a 2cm long triangular shape stainless steel camped-free cantilever with a screen piezoelectric thick film layer. Roundy et al. [Roundy2004] developed a $1cm^3$ prototype based on a commercial piezoelectric ceramic triple layer rectangular cantilever. A mass is attached at the tip of the cantilever to fit the natural frequency with the input frequency. Kim et al. [Kim2005] presented a study to analyze the suitability to harvest energy of a piezoelectric based clamped circular plate that bends under pressure application. Moreover the use of bending piezoelectric generators in cantilever configuration with a tip mass has been also used in Microelectromechanical systems (MEMs) [Fang2006]. In 2005 a patent of a piezoelectric MEMs generator appeared. The system consists on large arrays of piezoelectric MEMS bimorph bend cantilevers with different weights to recover energy in a broadband of frequencies [Nishida2005].

Apart from the mechanical configuration an important choice when designing a piezoelectric energy harvesting device is the material selection. There are different materials available in the market, each of them with different performances. When comparing them there are some properties that have to be considered. The piezoelectric coefficient "d_{ij}" is one of the important parameters to consider. The coupling coefficient "k_{ij}" from Eq 3-24, give information about the material ability to convert mechanical energy into electrical energy. Clearly to obtain maximum harvested energy it is preferable to have high piezoelectric and coupling coefficients.

$$k_{ij} = d_{ij}\sqrt{\frac{Y_{jj}}{\varepsilon_{ii}}} \qquad \textit{Eq 3-24}$$

Other important parameter is the Young modulus "Y_{jj}" that gives information about the stiffness of the system. The dielectric permittivity "ε_{ii}" is also important because it defines the equivalent capacitance of the material and will define the matching impedance of the electrical circuit, therefore the levels of voltage and current. Another important property of piezoelectric material is the maximum strength it can withstand, in other words, its yield strength.

At the beginning of the research on piezoelectric energy harvesting the most used materials were the PZTs. One of the first researchers working with piezoelectric energy harvesting was Umeda [Umeda1996] who used a PZT material in his device to convert impact energy from a steel ball. A very interesting work was presented by Kymissis [Kymissis1998] where both PZT and PVDF materials were used to harvest energy from human walking. A shoe was modified with two distinct methods to harvest the energy. The first method consist on introducing 8 PVDF layers forming a bimorph with a stave shape on the shoe plant. The shape was chosen to conform the footprint and bending distribution of the shoe. When the shoe bends, the PVDF bimorph generates power. The other method consists on a PZT device designed to exploit the high pressure exerted in a hell strike. It consists on a PZT layer bonded to a curved piece of spring steel forming an unimorph actuator. When the foot comes down it forces the PZT to flat against a rigid plate. When the foot pressure is realized, the unimorph springs back. This motion generates power through the PZT layer. The work takes advantage of the high coupling coefficient of PZT by the one hand, and by the other hand it takes advantage of the flexibility and yield strength of PVDF material. As PVDF has a low dielectric permittivity they generate relatively large voltage signals thus the prototype connects the 8 layers in parallel to increase the capacitance thus slow down the voltage. Another interesting work was performed by Elvin et al. [Elvin 2001] where a thin PVDF layer was bonded to a bending structure to develop a wireless strain sensor. The sensor consists on a PVDF layer that converts the mechanical energy into electrical energy. The charge is stored and used to power a telemetry system that indicates the averaged mechanical energy applied to the sensor.

Recently more complex structures are being developed to overcome some of the limitations of the monolithic materials as PZTs and PVDFs. These new materials are named piezofiber composites (PFC) and give more flexibility and increase the coupling coefficient. The first is done by the use of piezoceramic fibers embedded in an epoxy matrix which provide the PFC with significant flexibility. The second is done using of interdigitated electrodes which capitalize on the higher d_{33} piezoelectric coupling coefficient. Due to these improvements, the PFC is also far more robust to damage than monolithic piezoceramic, which cracks very easily, making it a more reliable power harvesting device [Sodano2006].

Once the material and the mechanical configuration are selected for an application, the next step in the design of a piezoelectric energy harvesting device is the development of the electronic circuitry to manage the generated energy.

Although piezoelectric materials are able to convert mechanical energy into electrical energy and, compared to other methods, they present a higher energy density, the amount of energy generated is still not sufficient for directly powering most of electronic devices. Therefore the key point for a successful power harvesting system lies on an efficient generation and storage procedure for powering [Sodano2005]. Many works have been done about circuitry for piezoelectric energy harvesting. Some of the most interesting are here reported. In 1997 Umeda et al. [Umeda1997] continued their work on harvesting the impact energy from a steel ball with a piezoelectric element by designing an electronic circuitry to store that energy. The circuit consists on a full bridge diode rectifier followed by a capacitor where the energy was stored. They found that the efficiency of the system was 35%. Following this work, Kymissis et al. [Kymissis1998] proposed a completely autonomous circuit able to harvest the energy from human walking to supply an RF transmitter. The circuit consists on a full bridge diode rectifier followed with a capacitor that charges while walking. When the voltage in the capacitor raises a certain value, a voltage regulator is turned on through a specific electronic circuitry that discharges the capacitor. The voltage regulator activates an encoder and an RF transmitter. The transmission is on until the voltage in the capacitor falls below a minimum value then the regulator turns off and the capacitor starts charging again. The same circuit was used by Elvin et al. [Elvin2001] but in that case the diode rectifier was a half bridge configuration.

The circuits commented above are designed to manage the energy harvested from a variable energy source. When the source of vibration has a fixed frequency it is possible to design systems with an impedance adaptation between the piezoelectric generator and the electrical circuit. One of the most referenced works was developed by Ottman et al [Ottman2002]. The work started assuming a piezoelectric transducer vibrating at a fixed frequency and amplitude. They propose to use a full-bridge rectifier to convert the input ac power to a dc power. Then a dc/dc converter is used to charge an output battery. The idea of their system was to constantly measure the current supplied to the battery while changing the duty cycle of the converter to always to ensure the maximum output current. They used a processor to implement an algorithm that search the optimal duty cycle that maximize that current. The harvested energy was found to be four times higher than by direct charging, this is using the circuit proposed by Umeda et al. However, the circuit had a drawback, this was that the processing required to much power, thus an external power sources was needed to power the processor. One year later, the same group proposed a new approach [Ottman2003], this one used a fixed duty cycle. The circuit consisted on a bridge rectifier and a step-down converter working on discontinuous mode. Using a simple piezoelectric model they found an expression of the converter duty-cycle for the maximum power transfer. The equation was found assuming that the power is maximized when the voltage on the bridge rectifier is one half of the generator's open circuit voltage. In this case, the electrical circuit input impedance is matched with the equivalent impedance modulus of the piezoelectric generator.

Many other interesting works have been presented, however it is possible to classify them in three groups. First group, the electrical output circuits manage the energy without modeling the dynamics of the piezoelectric generator neither using any feedback [Umeda1997], [Kymissis1998], [Roundy2003], [Sodano2005], etc. Second group, the electrical output circuits feedback some variable to assure a maximum power generation normally by indirectly adapting impedances or by some other modern techniques [Ottman2002], [Guyomar2005], [Badel2006]. In the last third group, a model of the piezoelectric generator is considered and a specific configuration that assures an impedance match is obtained [Ottman2003], [Kasyap2002], [Lefeuvre2007]. Among the research on this last group, the authors focus on adapting the electrical circuit impedance to the piezoelectric generator electrical specifications. The adaptation they use is almost always based on a simplification of the model. The assumption they do is that the electrical impedance of these generators is mainly capacitive. In these cases, the maximum power transfer is achieved adapting the electrical input resistance of the electrical interface circuit to the modulus of the piezoelectric equivalent impedance. This assumption is not always correct, although the electrical equivalent impedance of the piezoelectric generators is mainly reactive (capacitive), near the resonance frequencies, a significant real (resistive) part appears. In this case it is worth to propose a complex conjugate impedance matching. Thus the electrical system impedance has to be equal to the complex conjugated impedance of the piezoelectric generator. In other words, the optimal electrical impedance load value has a real part and a reactive part.

In this point a detailed analysis of a piezoelectric energy harvesting device is presented. First of all a specific general model for vibration harvesting using a piezoelectric element is defined and compared with the general one. The mechanical configuration adopted consists on a bending piezoelectric beam anchored at one end to a vibration source. The source is assumed to be not affected by the generator, it is considered to have a fixed amplitude and frequency. The model is developed in order to have a method to estimate the energy generated by the beam and to determine the equations defining the optimal complex electrical load conditions for maximum energy generation for different vibration modes. After this theoretical analysis, an experimental characterization of a real micro power generator piezoelectric device is realized. The piezoelectric cantilever beam used is the commercial Quick Pack 40w from Midé Corporation. It is a composite beam based on PZT wafers embedded in an epoxy matrix for increasing its maximum yield strength, therefore its maximum energy generation. The device is characterized for the first three resonance modes by means of an experimental identification. Then the model equations defining the power generation and the optimum electrical loads are validated. Once the micro power generator (MPG) device is characterized, a complete design of an energy harvesting system is realized. The system is conceived to harvest the energy from typical vibrations inside a building, and use this energy to supply a certain electronic device. For this purpose a discreet electronic implementation is realized to manage the energy efficiently from the MPG. The analytical model developed at the

following point and the experimental identification at the next point are published in journal paper by the author of this thesis. [Brufau2008_3]

3.2.1. Model for piezoelectric power harvesting from vibrations

In this point a physical model for the piezoelectric energy harvesting system of the Figure 3-4 is developed. The mechanical configuration studied consists on a piezoelectric based cantilever forced to vibrate from its base. To study the vibrations transmission and to develop the theoretical analysis, the same methodology than in chapter 2 is adopted. This is, considering the beam as an Euler-Bernoulli beam with a distributed mass and adopting the modal expansion theory. A detailed description of the model development is reported at the Appendix A. In the following a brief description of the model is presented. To start with the analysis, the force equation governing the motion of the beam when forced to vibrate from its base with a displacement "$y_b(t)$" is presented in Eq 3-25 and Eq 3-26.

$$m_n \ddot{r}_n(t) + c_n \dot{r}_n(t) + \Theta_n V(t) + K_n r_n(t) = F_{on}(t) \qquad \textit{Eq 3-25}$$

$$F_{on}(t) = \ddot{y}_b(t) \int_0^L \rho A W_n(x) dx \qquad \textit{Eq 3-26}$$

At the left side of Eq 3-25, there is the inertia force due to the distributed mass "m_n", the elastic force due to the elasticity of the beam "K_n", and the dissipative force due to mechanical viscous damping "c_n". Moreover an induced force appears due to the generation of voltage "V(t)" and the coupling between mechanical and electrical domains "Θ_n". At the right side of the equation there is the input distributed

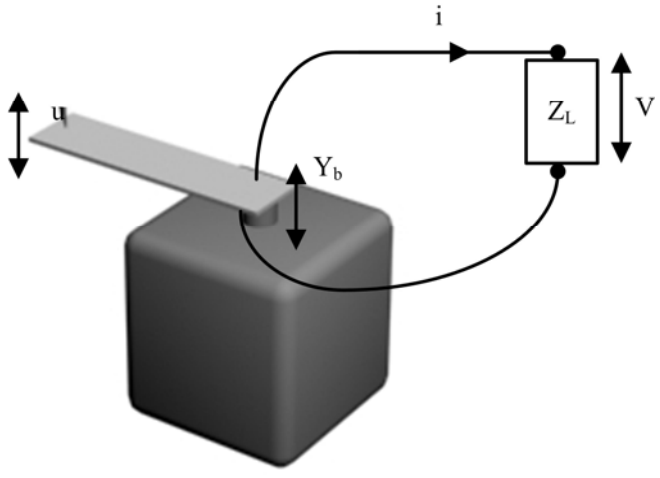

Figure 3-4 Shcematic draw of a cantilever piezoelectric based for vibration energy harvesting.

force that appears due to the imposed base acceleration and the distributed mass of the system.

Once the equation governing the mechanical domain is obtained, we proceed to obtain the equation governing the electrical domain. Considering the piezoelectric system, the electrical equation defining the generated charge is given by:

$$Q(t) = \Theta_n r_n(t) + C_P V(t) \qquad \textit{Eq 3-27}$$

The generated charge "Q(t)" has two contributions, the first one due to the piezoelectric effect and the second one due to the dielectric nature of the material. Application of a time differentiation to the electric equation gives

$$i(t) = \Theta_n \dot{r}_n(t) + C_P \dot{V}(t) \qquad \textit{Eq 3-28}$$

This equation defines the generated current by the piezoelectric material. This current depends on the electrical boundary conditions of the system. Considering that the current is generated in a pure resistive load "R", the equation is rewritten as

$$\frac{V(t)}{R} = \Theta_{nS} \dot{r}_n(t) + C_P \dot{V}(t). \qquad \textit{Eq 3-29}$$

Assuming an exponential base excitation $y_b(t)=Y_b e^{j\gamma t}$ with frequency "γ", and after some mathematical treatment the equation defining the voltage generated is written as:

$$V(t) = \frac{\Theta_n R}{1+\gamma^2 R^2 C_p^2} \dot{r}_n(t) + \frac{\gamma^2 \Theta_n R^2 C_p}{1+\gamma^2 R^2 C_p^2} r_n(t) \qquad \textit{Eq 3-30}$$

Substitution of this equation into the force equation leaves

$$m_n \ddot{r}_n(t) + c_n \dot{r}_n(t) + \frac{\Theta_n^2 R}{1+\gamma^2 R^2 C_p^2} \dot{r}_n(t) + K_n r_n(t) + \frac{\gamma^2 \Theta_n^2 R^2 C_p}{1+\gamma^2 R^2 C_p^2} r_n(t) = F_{on}(t) \qquad \textit{Eq 3-31}$$

This is the force equation governing the mechanical motion of the beam. The solution of this equation depends on the electrical circuit loaded to the beam, in this case a resistive load. If the equation is rewritten as the power conservation equation, it is obtained

$$\frac{d}{dt}\left(m_n \dot{r}_n^2(t) + \frac{\gamma^2 \Theta_n^2 R^2 C_p}{1+\gamma^2 R^2 C_p^2} r_n^2(t) + K_n r_n^2(t) \right) + c_n \dot{r}_n^2(t) + \frac{\Theta_n^2 R}{1+\gamma^2 R^2 C_p^2} \dot{r}_n^2(t) = F_{on}(t)\dot{r}_n(t)$$

Eq 3-32

The equation shows that there is another conservative term added to the inertial and elastic terms. This term is a consequence of the capacitive nature of the piezoelectric layer that stores energy.

Now it is interesting to analyze the special case where the capacitive of the piezoelectric layer is very small, Cp=0. In this case the power equation remains:

$$\frac{d}{dt}\left(m_n \dot{r}_n^2(t) + K_n r_n^2(t)\right) + c_n \dot{r}_n^2(t) + \Theta_n^2 R \dot{r}_n^2(t) = F_{on}(t)\dot{r}_n(t)$$

Eq 3-33

This equation is analogous to the William-Yates equation Eq 3-6 where the transduction effect is only modeled as a loss term in the mechanical equation. Therefore if the capacitive nature of the piezoelectric beam is very small (this would be the case of some PVDF MPGs) the same conclusions obtained with the general model can be adopted. Thus the same design considerations for the maximum power generation must be adopted. These means:

- The system must be designed with a "ω_n" equal to the input base frequency vibration "γ"

$$\omega_n = \sqrt{\frac{K_n}{m_n}} = \gamma$$

Eq 3-34

- The optimum electrical load must impose that the electrical damping becomes equal to the mechanical damping $c_{elec}=c_{mec}$.

$$R = \frac{c_n}{\Theta_n^2}$$

Eq 3-35

If this happens, all the instantaneous power introduced in the system by the vibrating source is directly dissipated as mechanical friction losses and as electrical power; then the energy balance is cero at each time instant. Therefore the generated power is maximized.

By the other hand, if $C_p \neq 0$, thus the power conservation equation is Eq 3-32, it will not be always possible to find an electrical load resistor "R" and an input frequency "γ" that assures a $c_{elec}=c_{mec}$ and at the same time implies a energy balance

of the conservative terms equal cero for each time instant. Therefore it will be necessary to use a complex electrical load to compensate the energy balance and the dissipative terms.

In order to determine the characteristics of the complex electrical load that maximize the generated electrical power, an equivalent electrical circuit is used. To obtain the circuit it is necessary to redefine the governing equations in terms of the new variables of the circuit. Considering, as the mechanical variables, the tip velocity "v" and the base vibration velocity "B_{in}"; and as the electrical variables, the electrical current "i", and the electrical voltage "V", the governing equations are rewritten in the Laplace domain as:

$$\frac{K_n v_n(s)}{sW_n^2(L)} + \frac{c_n v_n(s)}{W_n^2(L)} + \frac{\Theta_n V(s)}{W_n(L)} + \frac{sm_n v_n(s)}{W_n^2(L)} = \frac{sB_{in}(s)\rho A\int_0^L W_n(x)dx}{W_n(L)} \qquad \textit{Eq 3-36}$$

$$i(s) = \frac{\Theta_n v_n(s)}{W_n(L)} + sC_p V(s) \qquad \textit{Eq 3-37}$$

A possible representation of the system dynamics is drawn in Figure 3-5a) as an equivalent circuit. On the left side the circuit represents the mechanical system where the vibration base velocity is introduced as a current source "$B_{in}(s)$". The current flowing through the transformer is the tip velocity "v(s)". At the right side, the electrical system is modeled with a capacitor and the variables are the voltage in the electrodes "V(s)" and the electrical current "i(s)". Comparing the constitutive equations of the equivalent circuit with the governing equations of the system, the functions defining each circuit element are obtained. The equations describing the circuit elements "C_n", "R_n", "N_n", "$L1_n$", "$L2_n$" are defined in equations from Eq 3-38 since Eq 3-43 :

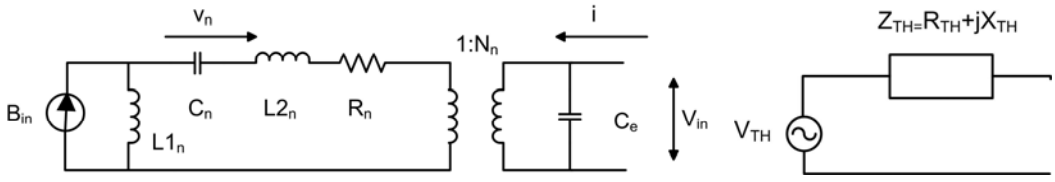

Figure 3-5 a)Lumped Equivalent Circuit for a piezoelectric cantilever composite beam. b) Equivalent Thevenin circuit.

$$N_n = \frac{\Theta_n}{W_n(L_F)}$$

Eq 3-38

$$L1_n = \frac{\rho A \int_0^L W_n(x)dx}{W_n(L)}$$

Eq 3-39

$$L2_n = L_n - L1_n$$

Eq 3-40

$$R_n = \frac{c_n}{W_n^2(L_F)}$$

Eq 3-41

$$C_n = \frac{W_n^2(L_F)}{K_n}$$

Eq 3-42

$$L_n = \frac{m_n}{W_n^2(L_F)}$$

Eq 3-43

In order to analyze the power generated to a load "Z_L", the piezogenerator is considered as a voltage source "V_{TH}" with internal impedance "Z_{TH}" according to the equivalent Thevenin circuit from Figure 3-5b). From the maximum power transfer theorem, it is known that the maximum power transmission is achieved when the load impedance value is the complex conjugated of the equivalent Thevenin impedance value. In the following derivation, the equations defining the equivalent Thevenin impedance are obtained. Regarding the mechanical domain, the natural frequency of the mechanical system "ω_n" Eq 3-44, the resonance frequency of the system when the beam is in open circuit conditions "ω_t" Eq 3-45 and the damping contribution of an oscillating system "ξ_n" Eq 3-46 are defined.

$$\omega_n = \frac{1}{\sqrt{C_n L_n}}$$

Eq 3-44

$$\omega_t = \omega_n \sqrt{\frac{C_n N_n^2 + C_p}{C_p}}$$

Eq 3-45

$$\xi_n = \omega_n \frac{R_n C_n}{2}$$

Eq 3-46

Considering these definitions and applying Kirchoff laws and circuit theory analysis, the equivalent Thevenin impedance can be written as the sum of a real part Eq 3-47 and a reactive part Eq 3-48.

$$R_{TH}(\omega) = \frac{1}{C_p} \frac{2\xi_n \omega_n \left(\omega_t^2 - \omega_n^2\right)}{\left(\omega_t^2 - \gamma^2\right)^2 + \left(2\xi_n \omega_n \gamma\right)^2}$$

Eq 3-47

$$X_{TH}(\omega) = -\frac{1}{C_p \gamma} \frac{\left(\gamma^2 - \omega_n^2\right)\left(\gamma^2 - \omega_t^2\right) + \left(2\xi_n \omega_n \gamma\right)^2}{\left(\omega_t^2 - \gamma^2\right)^2 + \left(2\xi_n \omega_n \gamma\right)^2}$$

Eq 3-48

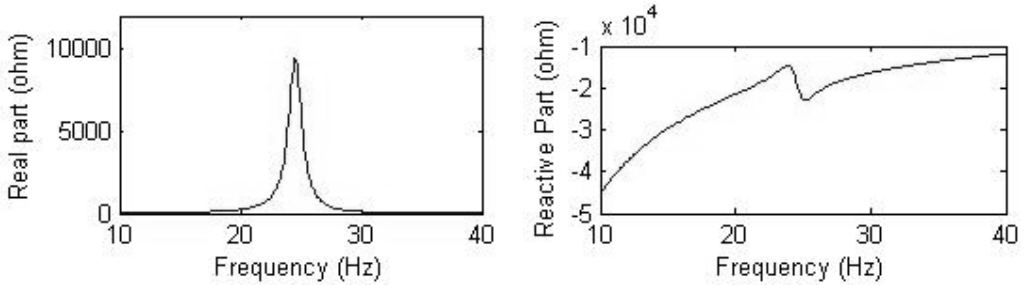

Figure 3-6 Thevenin equivalent impedance Real and Reactive part for the piezoelectric based trasnducer Qp40w.

An evaluation of these functions is presented in Figure 3-6. The evaluation is done using the values identified for the piezoelectric used at the following section as an example. It can be observed how the impedance is mainly reactive unless in the vicinity of the resonance of the system where a real part appears. This fact forces the electrical load to compensate the phase between the generated voltage and current for a maximum power transfer, or in other words, to maximize the work developed by the mechanical source. However, the ratio between the real and the mechanical part depends on the type of converter, for those system that have a poor coupling, this is $\omega_t = \omega_n$, the impedance will be mainly reactive.

The next step is to obtain the equation defining the equivalent Thevenin voltage. In this case the voltage of the circuit at Figure 3-5 is the open circuit voltage and it is defined with the following equation.

$$V_{TH}(\omega) = \frac{N_n G_n}{C_p} \frac{j\gamma B_{in}}{\omega_t^2 - \gamma^2 + j2\xi_n \omega_n \gamma} \qquad \textit{Eq 3-49}$$

with

$$G_n = \frac{L1_n}{L_n} \qquad \textit{Eq 3-50}$$

where "G_n" is a dimensionless gain factor dependent of the mode shape analyzed. The equation shows how this voltage is greater for small capacitance, this is the case of PVDF materials. Once the system is modeled with its equivalent Thevenin model, the power generation is analyzed and the conditions for a maximum power generation are defined. To do this, two distinct cases are considered, these are the system adapted with a resistive load, and a system adapted with a complex load with a real and a reactive part. In both cases the power to maximize is the instantaneous averaged power dissipated in the load, this is:

$$P = \frac{|V_L||I_L|}{2}\cos(\theta) = \frac{|V_L||I_L|}{2}\frac{R_L}{|Z_L|} = \frac{|I_L|^2 R_L}{2} = \left|\frac{V_{TH}}{Z_{TH}+Z_L}\right|^2 \frac{R_L}{2}$$

Eq 3-51

where "θ" is the phase angle between output voltage and current.

3.2.1.1. Power generation with resistive load

In this point it is considered the case that the electrical circuitry behaves as a pure resistive load R_L. Thus considering the load impedance $Z_L=R_L$, the power equation Eq 3-51 after substitution of the Thevenin voltage and impedance equation remains

$$P = \frac{(N_n G_n A_{in})^2 \left[\left(\omega_t^2 - \gamma^2\right)^2 + \left(2\xi_n \omega_n \gamma\right)^2\right]^2 \gamma^2 \frac{R_L}{2}}{\gamma^2\left[2\xi_n\omega_n\left(\omega_t^2-\omega_n^2\right)+C_e R_L\left(\omega_t^2-\omega_n^2\right)^2+\left(2\xi_n\omega_n\gamma\right)^2\right]^2+\left[\left(\gamma-\omega_n^2\right)\left(\gamma-\omega_t^2\right)+\left(2\xi_n\omega_n\gamma\right)^2\right]^2}$$

Eq 3-52

This equation represents the amount of power dissipated in a load resistor in terms of frequency and resistive load (R_L). To maximize this equation the theorem of maximum power transfer is adopted. This theorem says that when the electrical load is pure resistive, the maximum power is obtained when the output resistor load value is equal to the modulus of the equivalent input impedance. Thus the resistive load must accomplish the equation Eq 3-53 and thus the power generated "P_{mod}" has the form of Eq 3-54

$$R_L(\omega) = |R_{TH} + X_{TH}| = \frac{1}{C_p\gamma}\sqrt{\frac{\left(\gamma^2-\omega_n^2\right)+\left(2\xi_n\omega_n\gamma\right)^2}{\left(\gamma^2-\omega_t^2\right)+\left(2\xi_n\omega_n\gamma\right)^2}}$$

Eq 3-53

$$P_{\text{mod}} = \frac{\frac{\omega_n}{4C_p}(N_n G_n A_{in})^2}{\sqrt{\left(\gamma^2-\omega_n^2\right)+\left(2\xi_n\omega_n\gamma\right)^2}\sqrt{\left(\gamma^2-\omega_t^2\right)+\left(2\xi_n\omega_n\gamma\right)^2}+\left(2\xi_n\omega_n\left(\omega_t^2-\omega_n^2\right)\gamma\right)}$$

Eq 3-54

It is interesting to remark that for those systems with a poor coupling, these are system with the equivalent impedance only reactive and equal to $Z_{TH}= -j1/C_p\gamma$, the frequency for the maximum power generation will be "ω_n" and the value of the optimum resistive load equal to $R_L=1/C_p\omega_n$. For the systems with a higher coupling

coefficient, the frequency for the maximum generation will be different than "ω_n" and the value of the optimum resistive load must accomplish the equation Eq 3-53.

3.2.1.2. Power generation with a complex load:

When the electrical load has a real and complex part, the maximum energy power generation is produced when this impedance load value is the complex conjugated of the equivalent input Thevenin impedance value. This is $Z_L = R_{TH} - jX_{TH}$. Thus the power equation is computed as

$$P_{comp} = \left| \frac{V_{TH}}{Z_{TH} + Z_L} \right|^2 \frac{R_L}{2} = \frac{|V_{TH}|^2}{8R_{TH}} \qquad \textit{Eq 3-55}$$

This equation could originate some wrong conclusions. For example, an infinite power when the real part of the system R_{TH} is cero. Obviously it is not possible. In the case of having R_{TH} equal cero, a complex adaptation would means to use a reactive load without any resistive part, this means that no real power would be dissipated in the load. In this case the adaptation must be with the impedance modulus value.

The substitution of the voltage and load equations Eq 3-49 and Eq 3-47 in the power equation, gives this new equation for power

$$P_{comp} = \frac{(N_n G_n A_{in})^2}{16 C_p \xi_n \omega_n (\omega_t^2 - \omega_n^2)} \qquad \textit{Eq 3-56}$$

This equation depends directly on the base acceleration square. However, assuming a constant acceleration, the equation does not depend on the frequency "γ"; this means that the maximum energy generation can be achieved at any frequency while the adaptation is completed. In fact, forcing the impedance adaptation at one frequency means that the system is resonating at that frequency. However, if the system is adapted far from its natural frequency, the real part contribution will be small thus the system will have a very high quality factor. This means that the dynamics of the power function will have a maximum value at one frequency but a small variation of this frequency will produce a drastically reduction of this power, thus it will be very difficult to fix the input vibration frequency at a frequency for the maximum power generation.

Substitution of the equations defining the equivalent circuit elements in the power equation Eq 3-56 and after some mathematical treatment, it is possible to obtain a final equation with the same form than the Eq 3-20 from William and Yates model but with some dimensionless corrections due to the mode shape of operation. In the general model, it was considered that the converter did not store energy, it was

only modeled as a viscous contribution that loss energy. Therefore at the resonance frequency, all the instantaneous introduced power by the vibrating source was directly dissipated in the electrical and mechanical circuit. For a maximum energy generation, both losses terms should be equal. By the other hand, when using a piezoelectric material, the energy storing capability of the material affects the energy balance, thus it is needed to use a complex electrical circuit to put the system in resonance and, at the same time, to ensure that the dissipated power in the electrical domain is equal to the dissipated power in the mechanical domain

3.2.1.3. Effectiveness function:

In this point, a function called "effectiveness" or "power ratio" is defined as the ratio between the maximum power obtained with a modulus match and the maximum power obtained with a complex match.

$$\eta = \frac{P_{\mathrm{mod}}}{P_{comp}} = 2\frac{R_{TH}}{\sqrt{R_{TH}^2 + X_{TH}^2} + R_{TH}^2} \qquad \textit{Eq 3-57}$$

This equation serves as a tool to decide when a complex adaptation is needed by measuring the equivalent impedance of the system. An example of the evaluation of this function is shown at Figure 3-7. The graph has been computed using the impedances from Figure 3-6a) and Figure 3-6b).

The effectiveness function shows that using a modulus match it is only possible to obtain a 60% of the total available power, in other words, of the power that could be generated with a complex match. Therefore if the same example used in section 3.1 where a 13g mass converter was used at 24Hz to generate 190μW is considered, but now the converter is piezoelectric with an effectiveness function of 60%, the maximum power generated with a modulus match will be 114μW.

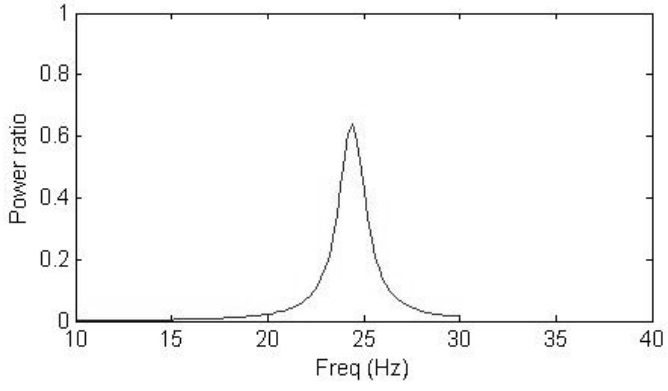

Figure 3-7 Power ratio function for the piezoelectric based trasnducer QP40w at the first mode.

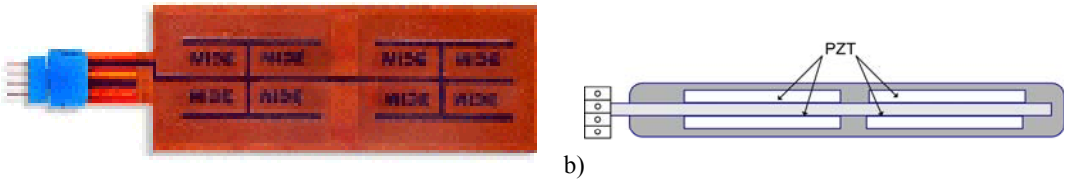

Figure 3-8 a) Picture of the piezoelectric based QP40w from Mide Technology Corp. b) Schematic drawn of theQP40w cross section.

Specifications	
Device size (in)	4.00*1.50*0.03
Device weigth (oz)	0.51
Active elements	2 stacks of 2 piezos
Piezo wafer size (in)	1.81*1.31*0.01
Device capacitance	(μF) 0.40
Full scale voltage range (V)	+/- 200

Table 3-1 Quick pack QP40w piezoelectric transducer specifications

Although the effectiveness function strongly recommends the use of a complex adaptation, this is not always possible. As piezoelectric materials have quite high values of reactance, it is not always possible to design a matching network using commercially available elements. At low frequency vibrations, the match requires the use of unrealizable high values of inductances or too long matching networks. However as far as the vibration frequency increases, it is possible to work at higher resonance modes thus the reactance decreeses and the complex match becames realizable.

In the following point the power analysis developed is applied to a commercial MPG device. The system response is investigated for different resonance modes in order to permit the comparison between modulus and complex match.

3.2.2. Micro power generation (MPG) device

The micro power generator device used is the commercial Quick Pack QP40w model (Mide Technology Corporation). It consists on a piezoelectric transducer formed by four PZT layers embedded in a Kapton epoxy matrix. Figure 3-8a) depicts a picture of the trasnducer. The system works as a bimorph with two PZT layers in the upper side and two layers in the lower side. The system uses the d31 mode with the traditional electrodes distribution. Four contacts release at the left of the beam, two for each side. The system can be configured to work in serial or in parallel.

This kind of structures has been designed specially for use as energy generators and can be easily obtained in the market. The piezoelectric layers are formed of PZT to give a high piezoelectric coefficient. Moreover the whole transducer is covered with the epoxy to increase the yield strength of the whole system

The specifications given by the manufacturer are reported at Table 3-1. One complication when modeling this structure is due to the composite structure of the beam. As it is depicted at Figure 3-8b), the piezoelectric layers do not span in the entire length of the beam and no information about relative distance between layers is given. While the theoretical model presented in the last point is flexible enough to be computed for any multilayer structure, the misinformation of the relative distance together with the fact that the structure of the system is relatively complex, suggests us to proceed with an experimental model identification process.

3.2.2.1. Model identification:

The identification process realized in this point deals with an experimental recognition of the elements of the equivalent circuit from Figure 3-5. To start with the process, it is needed to define the theoretical functions that are involved. To do this, the device model at Figure 3-5 is described as the two-port system from Figure 3-9:

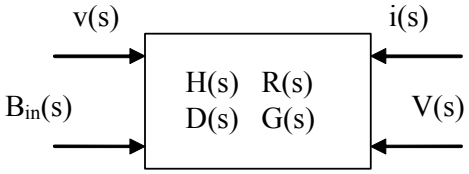

Figure 3-9 Two-port representation.

This two-port is defined by four transfer functions. Considering the equivalent electrical circuit from Figure 3-5, the transfer functions are defined as

$$H(s)=\left.\frac{v_n(s)}{B_{in}(s)}\right|_V=\frac{L1_n}{L_n}\frac{s^2}{s^2+s\frac{R_n}{L_n}+\frac{1}{L_nC_n}} \qquad \textit{Eq 3-58}$$

$$R(s)=\left.\frac{v_n(s)}{V(s)}\right|_{B_{in}}=\frac{N_n}{L_n}\frac{s^2}{s^2+s\frac{R_n}{L_n}+\frac{1}{L_nC_n}} \qquad \textit{Eq 3-59}$$

$$D(s)=\left.\frac{i(s)}{B_{in}(s)}\right|_V=\frac{N_nL1_n}{L_n}\frac{s^2}{s^2+s\frac{R_n}{L_n}+\frac{1}{L_nC_n}} \qquad \textit{Eq 3-60}$$

$$G(s) = \left.\frac{i(s)}{V(s)}\right|_{B_{in}} = C_p s \frac{s^2 + s\frac{R_n}{L_n} + \frac{C_n N_n^2 + C_p}{C_p L_n C_n}}{s^2 + s\frac{R_n}{L_n} + \frac{1}{L_n C_n}} \qquad \textit{Eq 3-61}$$

Once the system is described mathematically, the identification process is done. To start with the process, some experimental tests are realized. These experimental tests are performed to obtain three experimental transfer function of the model (H(s), R(s) and G(s)). The identification process is done comparing the output obtained by simulation (using these transfer functions) with the output obtained experimentally. A minimization error algorithm identifies the different elements of the model.

In the following lines, the three experimental tests are presented. The methods and electronic hardware, used to perform and measure the electrical and mechanical input-output variable values, are described. For the three experiments the collected data is processed in the frequency domain; therefore the plots presented below are implicitly defined as a ratio of functions in the frequency domain. Data was acquired with an Acquisition Card supported with Labview. The sampling frequency was set to 50kHz. The transfer functions are estimated using the averaged Welch periodogram with 8 segments and 50% of overlap. All inputs are generated by a linear frequency sinusoidal sweep from 10Hz up to 2kHz with a window time of 5 seconds.

3.2.2.1.1. Mechanical measurements H(s)

The first experimental test aims to evaluate the transfer function H(s). This function relates the tip velocity for an input base velocity. This test involved to mechanically drive the transducer base. To do this the transducer was mounted and clamped over an electromagnetic vibration shaker ET-132 Labworks Inc. The shaker was driven with a specific amplifier Pa-119 Labworks Inc. with the command signals coming from a function generator. Figure 3-10 shows a picture of the setup. For the displacement measurements, a triangulation laser LC2440 from Keyence was used.

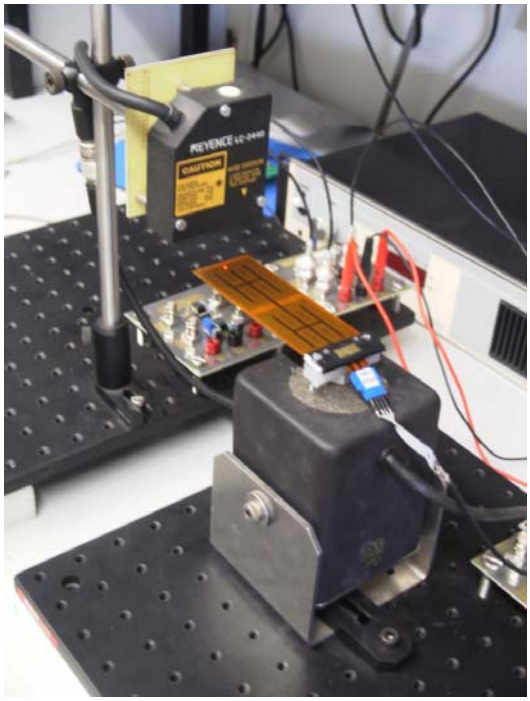

Figure 3-10 Picture of the experimental setup.

The measurements on the base displacement have a quite poor signal to noise ratio (SNR) at the high frequency region. At those frequencies the shaker produces a small displacement and the laser sensor measurements introduce a lot of noise. Figure 3-11 depicts the experimental results. The obtained transfer function shows an important noise when frequency increases. However five maximum peaks are observed, corresponding to the first five resonance modes of the beam.

3.2.2.1.2. Electrical measurements G(s)

The second experimental test consist on evaluate the G(s) transfer function or admittance function. In this case the setup consists to clamp the QP40w transducer in a fixed anchor. Input voltage sweeps are applied to the transducer. These voltage sweeps are generated using a HP2200 function generator and a piezoelectric power amplifier from Thorlabs MDT693A. The absorbed current is measured by means of a 1ohm shunt resistor and electronic circuitry based on instrumentation amplifier INA111.

The computed transfer function obtained is depicted at Figure 3-12 where four peaks appear. While piezoelectric generators are capacitive in nature, its transduction effect modifies its electrical impedance. The picture shows how at the third mechanical resonant mode there is no change in the absorbed current, this could mean that in this mode no electromechanical effect aroused. This is an unexpected

behavior that could be a consequence of the composite nature of the beam and/or a consequence of the relative position of the piezoelectric layers inside the beam.

3.2.2.1.3. Free deflection measurements R(s)/s:

The third experimental test consists to measure the displacement of the beam tip under the same conditions than in the second test. In this case, the computed transfer function is R(s)/s, tip displacement for a given voltage. Figure 3-13 shows the transfer function where three clear peaks appear. These are located at the first, second and fourth resonant mode of the beam. A very small peak appears at the third resonant mode confirming that in that frequency, the coupling effect is almost negligible. A noise region appears due to the small displacement generated.

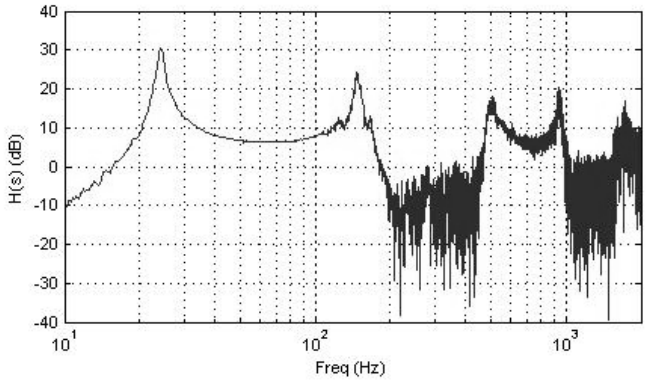

Figure 3-11 H(s) experimental transfer function

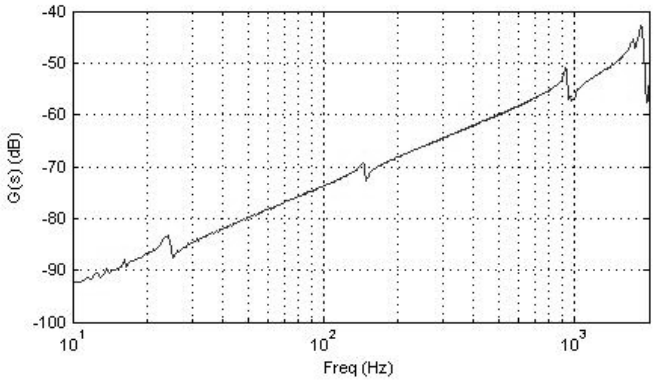

Figure 3-12 G(s) experimental transfer function

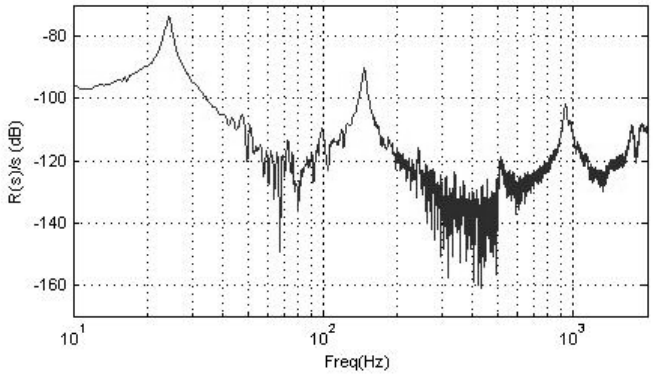

Figure 3-13 R(s)/s experimental transfer function

3.2.2.1.4. Parameter identification

Once the resonance modes are recognized, the identification step is presented. The parameters are identified separately for each mode. The studied modes are the first, second and fourth mode. Only the data constrained in the vicinity of each mode is considered. The identification process is based on the minimum lead square method. The routine evaluates the cost function that compares experimental and simulated data, and then proceeds to the minimization of this cost function. In order to give the same weight to each of the three experiments, the three functions are normalized. The normalization constants are λ_H, λ_R, λ_G.

$$Cost^2 = \sum_{m=1}^{npo\,\mathrm{int}\,s} \left(|H_e(j\omega_m)|\lambda_H - |H_S(j\omega_m)|\lambda_H\right)^2 + \sum_{m=1}^{npo\,\mathrm{int}\,s} \left(|R_e(j\omega_m)|\lambda_R - |R_S(j\omega_m)|\lambda_R\right)^2 + \sum_{m=1}^{npo\,\mathrm{int}\,s} \left(|G_e(j\omega_m)|\lambda_G - |G_S(j\omega_m)|\lambda_G\right)^2$$

Eq 3-62

The results of the identification process are plotted at Figure 3-14. It is possible to say that a good match is obtained for the three modes. The identified values for the model parameters are reported at Table3.2. As expected the identified values for the "R_n" increase for higher modes while the identified capacitor "C_n" decreases. The transformer gain "N_n" also increases as the mode shape increases. Nevertheless the identified values for the "L_n" should be constant. The value of the inductor is directly related to the mass of the beam multiplied by four for all modes. The identified values for the first and fourth mode suggest a total mass of about 13g while the second mode suggests a total mass of 16.5g. The input specifications of the Qp40w specifies a total mass of 15g, however this measure considers the connectors and the total length of the beam. In the experimental test realized the beam is clamped thus a small piece of the total beam is anchored, therefore the identified values for the first and fourth mode agree with the expected. The differences in the identified value for

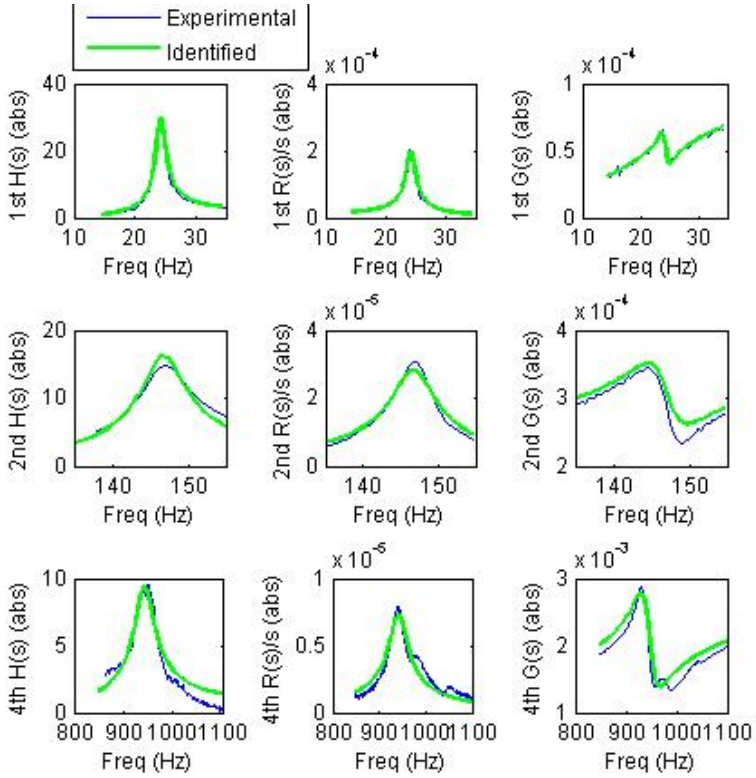

Figure 3-14 Experimental (black) and identified (grey) transfer functions

	R_n (Ω)	C_n (F)	$L1_n$ (H)	L_n (H)	N_n
n=1	2.7418e-002	1.31e-002	5.49e-003	3.27e-003	8.46e-004
n=2	1.4799e-001	2.86e-004	-2.69e-003	4.11e-003	3.84e-003
n= 4	7.6904e-001	8.85e-006	-1.21e-003	3.22e-003	3.35e-002

Table 3-2 Qp40w identified model parameters for the 1st 2nd and 4th vibration modes.

the second mode are attributed to deviations from the real response of the beam with the linear vibration transmission theory developed probably due to the composite nature of the beam. It is important to notice the sign in the L1 parameter. This parameter changes the sign in the even modes with respect the odd modes. This is a consequence of the nature or shape of each mode. Once the model has been identified, a validation of this model is presented.

3.2.2.2. Model validation

The model validation lies on analyzing the ability of the model to reproduce the system behavior. The aim of the model is to reproduce the power generated over electrical loads and to identify the optimum load conditions for a maximum power generation. In this point, the validation is done by qualitatively comparison of the power generated over a resistive load and a complex load.

All the data is presented and compared with transfer functions, these relate the generated power and the input given base acceleration. The implemented test consists to apply a frequency sweep vibration at the base of the beam and measure the voltage generated over an electrical load. The voltage obtained and the measurement of base displacement is used to compute the transfer function that relates the generated voltage for a given acceleration, then this function is used to compute the transfer function that relates the dissipated power for the square of the acceleration.

3.2.2.2.1. Power generation with Resistive load

In this point the generated power is analyzed over a set of different resistors for three vibration modes. The experimental results are compared with the simulations under the same conditions.

Figure 3-15, Figure 3-16 and Figure 3-17 show the measured voltage and computed power for experimental and simulated conditions. The generated voltage has a maximum value at a given frequency. This frequency value is shifted from the natural frequency of the system when the load resistor increases. This means that the voltage generated at the output resistance modifies the mechanical response of the system. The frequency value where the maximum voltage exists is constrained between "ω_n" (natural frequency when the system is in short-circuit) and "ω_t" (natural frequency when the system is in open circuit). By the other hand the voltage is always increasing as the load resistor increases. As far as the power curves concerns, it is observed as expected, that for each mode there is a maximum power generation at a given frequency and resistance. The values of these powers, resistances and frequencies are reported at Table 3-3 for the three modes and for the experimental and simulated transfer functions.

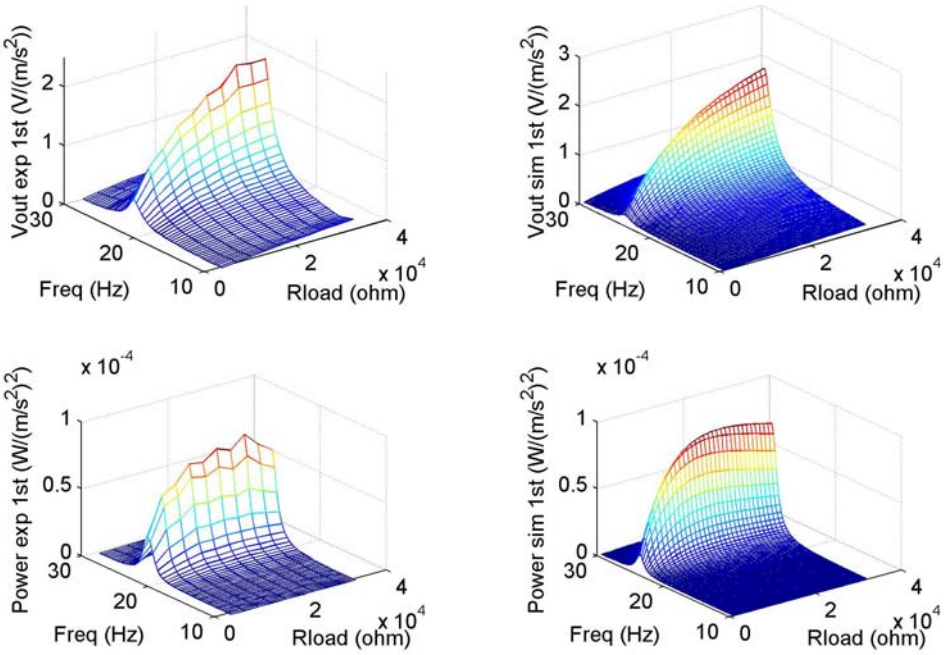

Figure 3-15 1st mode transfer functions. a) Experimental Voltage, b) Simulated Voltage, c) Experimental Power, d) Simulated Power.

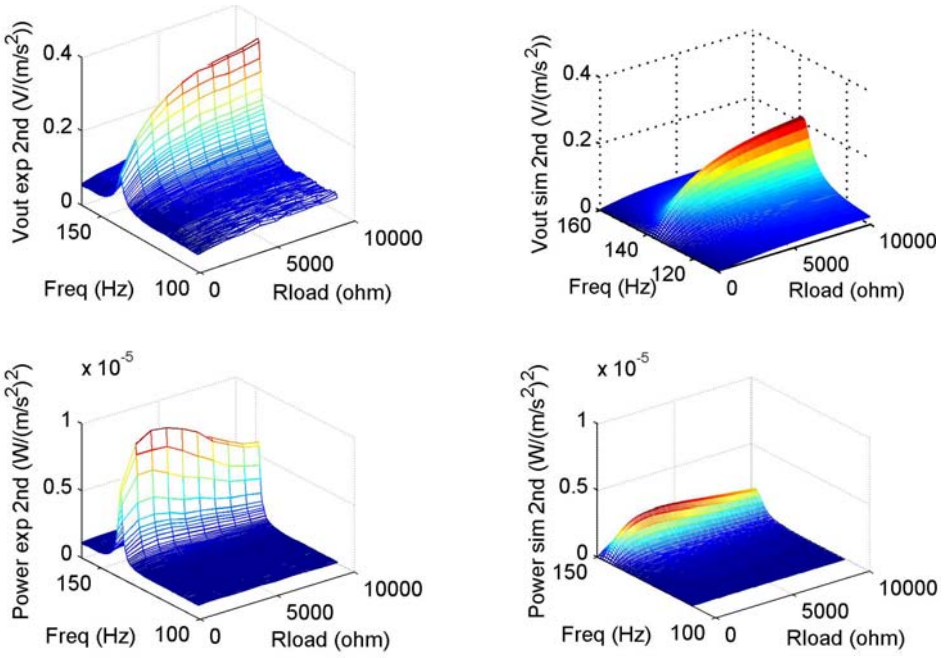

Figure 3-16 2nd mode transfer functions. a) Experimental Voltage, b) Simulated Voltage, c)Experimental Power, d) Simulated Power

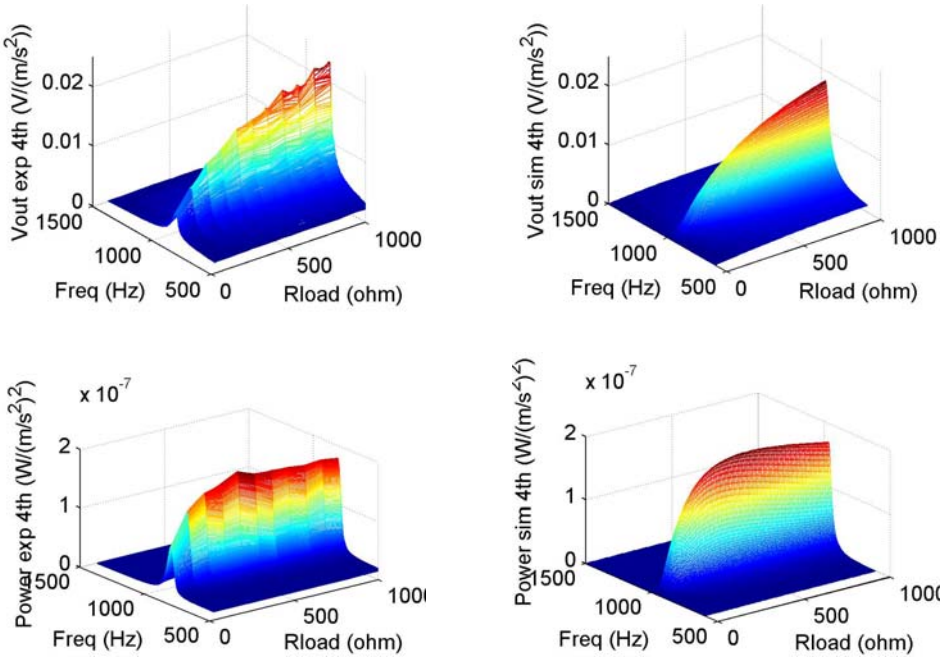

Figure 3-17 4th mode transfer functions. a) Experimental Voltage, b) Simulated Voltage, c) Experimental Power, d) Simulated Power.

	Experimental			**Simulated**		
	Power $(W/m/s^2)^2$)	**Freq (Hz)**	**Rload (Ω)**	**Power $(W/m/s^2)^2$)**	**Freq (Hz)**	**Rload (Ω)**
1st mode	8.61e-5	22	25600	1.14e-4	24	23000
2nd mode	9.34e-6	138	3000	3.52e-6	139	3300
4th mode	1.78e-7	935	500	1.89e-7	950	500

Table 3-3 Maxmimum power generation and optimal load for a impedance modulus adaptation for the three modes. Experimental vs Simulated values

Figure 3-15 shows a good match between experimental and simulated results for the first vibration mode. Both curves present a maximum power generation of about 100µW for a given acceleration of $1m/s^2$ when the match is done with a resistor of about 24KΩ at around 24Hz. This results agree with the computed at point 3.2.1.3. Figure 3-16 shows the comparison at the second resonance mode. While the frequency and resistance where the maximum power is generated matches quite well, these are about 138Hz and 3KΩ, the magnitude of the generated power differs noticeably. A 9.3µW for $1m/s^2$ acceleration is measured in front of the 3.5µW simulated. In the identification steps it was observed some discrepancies between the theory and the identified elements. Those discrepancies are traduced in a lower estimation on the generated power. The fourth mode comparison is shown at Figure 3-17. In this figure the curves matches quite well showing that a maximum power generation of about 180nW is obtained at about 940Hz with a load resistance of 500Ω.

The simulations and experimental results presented in this point have permitted the validation of the identification model parameters and the characterization of the energy harvesting capabilities of the commercial piezoelectric Qp40w transducer over a load resistance. The ability to generate energy has been tested for the first, second and fourth vibration mode. For a given input acceleration, this energy is higher at lower vibration modes. The first mode shows a power generation of about 100μW, enough to drive a sensor node, for an input acceleration of $1m/s^2$ at 24Hz. It is possible to identify a vibration source with this characteristics in the table presented in this thesis introduction where some vibration sources occurring inside a building were reported. Measurements realized at the second vibration mode showed a power generation of about 9μW for $1m/s^2$ base acceleration at 138Hz. This amount of power is small to drive a sensor node, however it is possible to find vibration sources with this frequency and accelerations up to $10m/s^2$ in some environments as for example in a milling machines or even inside a car tire. Therefore as the power is proportional to the acceleration square the studied piezoelectric transducer could be used to drive a sensor node in that environment. The measurements realized at the fourth mode showed a poor generation of 180nW at 950Hz for $1m/s^2$. However, it is possible to find some rotating machinery, as turbines or motor engines that present harmonic vibration at frequencies around kHz [Sakamoto1999], [Verma1998]. These vibrations will sometimes produce accelerations high enough to use the piezoelectric transducer as the energy generator for a sensor node.

The measurements and simulations presented in this point have been devoted to validate the ability of the model to reproduce the power generated over a set of load resistors. The maximum power and optimal load resistors conditions are validated. In the next point the concept of complete impedance matching is validated and the increase of generated power is measured

3.2.2.2.2. Power generation with complex load.

The "complete" match is done when the generator output impedance matches with the load complex impedance value. The impedance value has to be the complex conjugated of the generator equivalent impedance value. When this happens the mechanical work is maximized so the electrical power is also maximized.

Due to the capacitive behavior of the piezogenerator the match has to be done with a resistor and an inductor. Figure 3-18 shows a simulation of the optimal matching inductors values and the computation of the expected power ratio. The expected effectiveness or power ratio function is computed as the ratio of the power extracted by optimizing the impedance with only one resistor load or with a complex conjugate load value. In other words, is the ratio between Eq 3-54 and Eq 3-56. The simulations are realized using the identified model for the three resonant modes. The simulation results show that the matching is only feasible with commercial inductors values when we work at the fourth resonant mode. As the frequency increases, the reactive part of the optimal load decreases, making feasible the complex conjugate matching process.

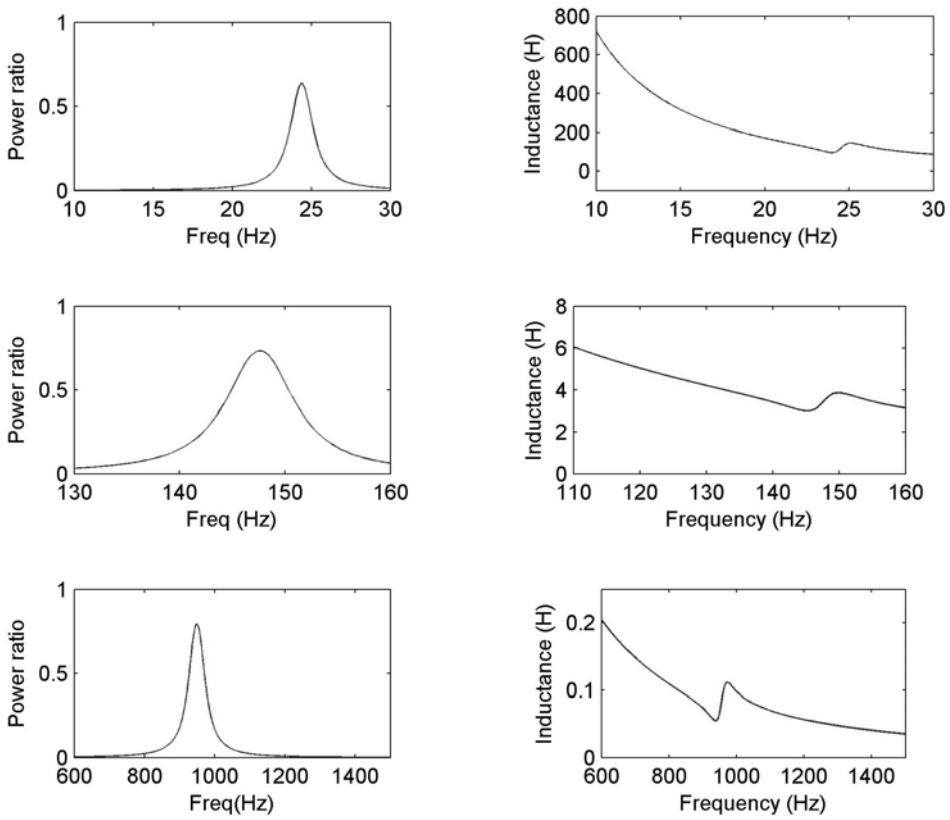

Figure 3-18 a), c), e) are the power ratio funcion, and b), d), f) are the optimal inductanceload for a complete match for the first second and fourth mode respectively

The computation of the simulated power ratio function gives a quantitative measure of the power missed due to a "non-complete" match. In other words, when the match is done with the generator output impedance modulus, less mechanical work enters into the electromechanical converter. The power mist is about a 40%, 35% and 20% for the first, second and fourth modes respectively.

Figure 3-19 shows experimental results of the generated power at the fourth resonant mode when the piezogenerator is loaded with a fixed 50mH inductor value and a variable resistor values. The power is measured for a frequency sweep and for a set of different load resistor values. The maximum power sensitivity is now 0.24 $\mu W/(m/s^2)^2$, at a frequency of 925Hz with a load resistor of 200Ω. The experimental results agree with the simulated ones using the transducer model. Compared with the previous results obtained with a non-complete matching process shown in Figure 3-17, an increase of 20% of the generated power is achieved with a complex conjugate matching process of the impedance at the fourth vibration mode of the piezogenerator.

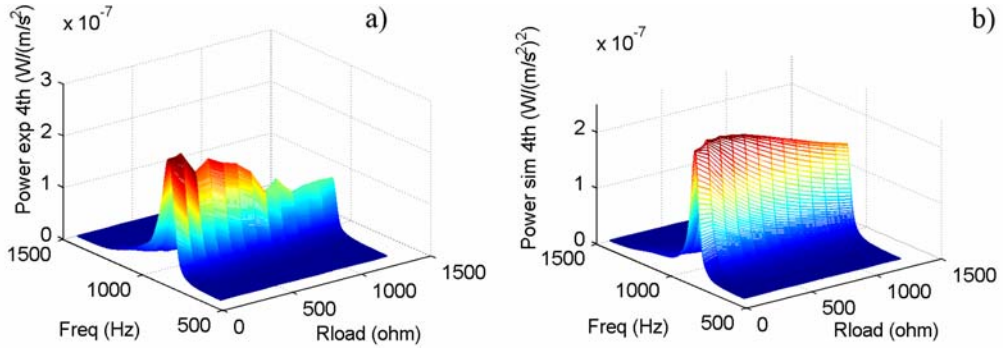

Figure 3-19 4th mode power transfer fucnions with a 50mH load inductance. a) experimental, b) simulation.

The increase of power using a "complete" impedance match has been experimentally validated, however the practical implementation of this technique has some drawbacks. The high reactive behavior of the piezogenerator forces to use very high values of inductors to make a "complete" match at low frequencies. Piezoelectric materials with higher dielectric coefficients and with higher coupling coefficients will allow using lower inductance values for the matching process. A higher dielectric coefficient reduces their capacitance thus it reduces their reactive value. A higher coupling coefficient increases the influence of the mechanical part varying the phase shift between voltage and current.

However in most piezoelectric energy harvesting systems, the power generated by the piezoelectric device is not high enough to directly supply a sensor load. Thus intelligent energy management systems are implemented. Many of these systems consist on a first stage to rectify the power coming from the MPG. Thus they use a

voltage rectifier and a capacitor to filter the signal. The second stage is normally different form each designer but it basically adapts the power to the load requirements. In the next point a specific circuitry is designed and the influence of this circuitry in the energy generation is analyzed. Up to now, the power analysis has been conducted thinking that the electrical load behaves as a pure resistor or as a complex load, in the next point the influence of the rectification and the power management circuit in the maximum power generation is considered.

3.2.3. Electronic circuitry for optimum energy management

In any energy harvesting system, the key point for an efficient energy generation is always the way this energy is stored and managed. In the last section it has been discussed the influence of the electrical load in the final power generation and it has been demonstrated that there is an optimal value for the maximum generation. However other constrains have to be considered when harvesting energy. As the system generates power from an oscillating vibrating source, this power is alternating, thus there is the need to convert this AC power to DC one. Therefore the way this power is rectified will affect the maximum energy generation. Another important constrain is the way this energy is managed. In many applications the quantity of power generated by a piezoelectric MPG is not high enough or has to be managed some what to directly supply any node. These nodes sometimes need specific regulated voltages, thus DC/DC converters or voltage regulators.

In this point a complete energy harvesting system is implemented. The system is designed to work as energy harvester from the vibrations around 150Hz and $10m/s^2$. This type of vibrations surrounds us in our daily life, for example in a microwave oven or a milling machine [Roundy2003]. The system is based on the one proposed by [Kasyap2002], it consists on a full wave diode bridge rectifier followed by a buck-boost converter that drives a resistor load. First of all the influence of the AC/DC rectifier in the optimum load conditions for the maximum energy generation is analyzed. The MPG from the point above is used working in its second resonance mode and the DC power generated over a set of different load resistors is measured. After a buck-boost converter is designed to carry out with the matching impedance needed for the maximum generation. The converter is designed to work in the Discontinuous Condition Mode (DCM) where it is possible to fix its input impedance to a certain value whatever the electrical load is. Therefore it is possible to have the system matched, this is generating the maximum energy, and use it for different loads.

3.2.3.1. AC/DC rectifier

In order to rectify the alternative signal coming from the MPG, it is needed to implement a rectifier. The rectifier implemented in this point consists on a full bridge diode rectifier as the one in the Figure 3-20b. The bridge is implemented with shockty diodes BAT48 in order to minimize the voltage drop and a 100μF capacitor to filter the signals.

The experimental test consists on apply a base acceleration to the QP40W piezoelectric transducer at 148Hz with an acceleration of about 10m/s^2. The measurements of the DC power for a set of different load resistors using circuit from Figure 3-20b are compared with the measurements of the averaged AC power dissipated in the same set of electrical loads without rectifier using circuit of Figure 3-20a.

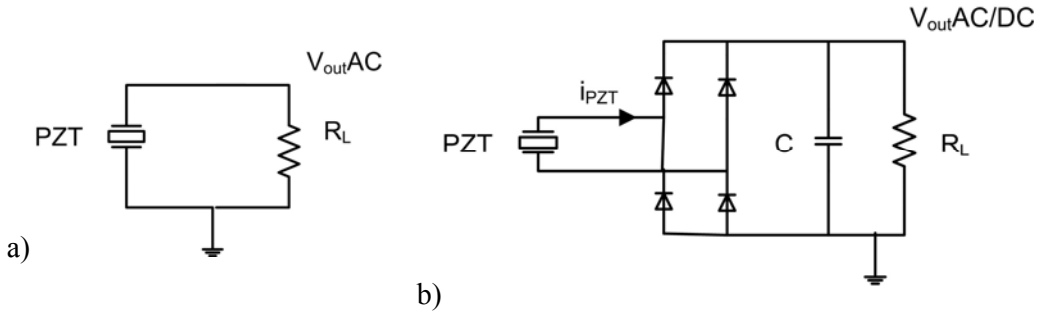

Figure 3-20 a) Schematic of the standar AC connection. b) Schematic of the full bridge AC/DC rectifier

Figure 3-21 shows the measurements using the circuit from Figure 3-20b with a 1200ohms load resistor. The figure depicts the voltage from the piezoelectric transducer "V_{PZT}", the voltage at the electrical load "V_{out}AC/DC" and the current generated by the piezoelectric transducer "I_{PZT}". The current has been measured with a 1ohm shunt resistor and an instrumentation amplifier INA111. It is observed that the maximum generated voltage value from the MPG (V_{PZTmax}=1.3V) is approximately the output voltage (V_{out}DC/DC=0.8V) plus the threshold voltage of the Schottky diodes (Vd=0.5V), when this diodes becomes ON all the current generated by the MPG flows to the load.

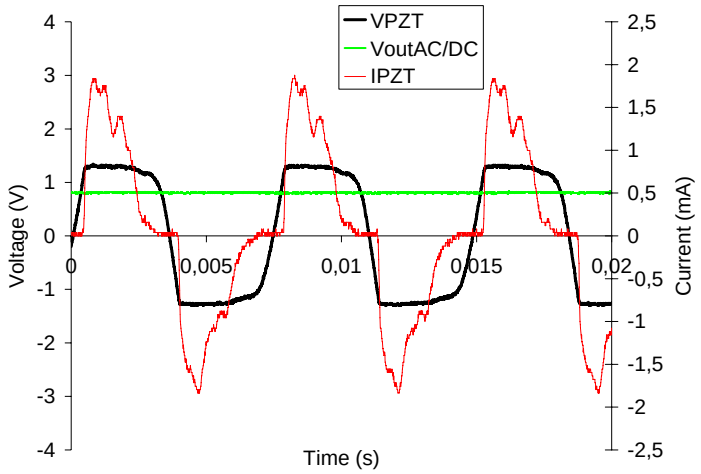

Figure 3-21 Waveforms measurements of the full bridge rectifier circuit with a load resistor 1.2kΩ.

Figure 3-22 and Figure 3-23 show a comparison of the performances when the MPG is directly loaded to a resistor using the circuit from Figure 3-20a), thus an AC power is generated, and the performances when the rectifier is used and the same resistors are loaded to it using circuit from Figure 3-20b). At Figure 3-22 the voltages in the load are compared, these are "V_{out}AC" and "V_{out}AC/DC" respectively and at Figure 3-23 the power delivered to this load "P_{out}AC" and "P_{out}AC/DC" respectively. In the case of the AC power, the power is computed as the averaged power dissipated in the load. Figure 3-23 depicts the reduction of power delivered to the load using the rectifier compared with a direct load. This is a consequence of the bridge rectifier that introduces power losses in the system. The other phenomenon observed is the change in the optimal load. While in the AC the optimal load was 3000 ohm with a generated power of 1.5mW, in the case with the rectifier, the AC/DC power is maximized at 5600 ohm and its value is 0.9mW. This change in the value is a consequence of the discontinuous behavior of the rectifier. When a bridge rectifier is used, the system is ON during a certain time. During that time the source is giving current to the load. This discontinuous behavior produces a variation on the resistor value seen from the source. Thus, assuming a perfect bridge, for a load resistor R, the resistance seen from the source becomes $R\pi/2$.

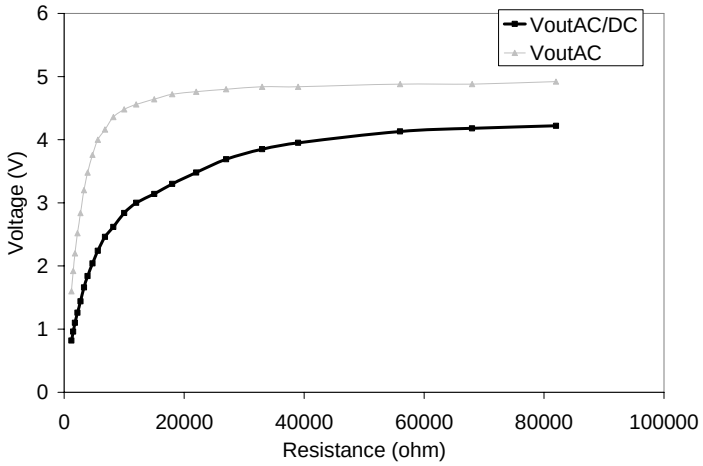

Figure 3-22 Generated voltage vs resistors loads. $V_{out}AC$ is the amplitued with the AC circuit, and $V_{out}AC/DC$ is the voltage using the AC/DC circuit.

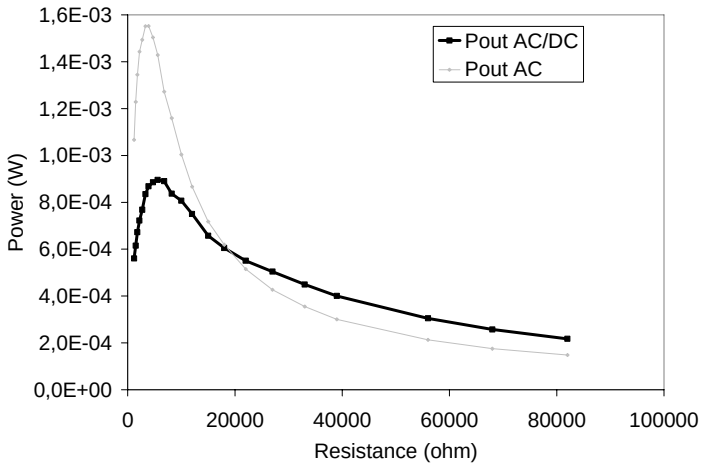

Figure 3-23 Power vs load resistor with the AC circuit and with the AC/DC circuit.

Another interesting point to remark is the value of the output voltage when the system is optimized. In the case without the rectifier the voltage "$V_{out}AC$" for 3000 ohm is 3.48V while the open circuit voltage is 5V. This relation confirms that the MPG has complex equivalent impedance and thus the adaptation is not perfect. In the case of a complete match, the voltage should be a half of the open circuit voltage. For the system with the rectification, the output voltage when the power is maximized is 2.24V.

3.2.3.2. DC/DC buck boost converter:

In energy harvesting system, the energy generated by the MPG is used to drive a wireless sensor node. These nodes behave as electrical loads each of them with different electrical behaviors. Thus, in order to ensure a maximum energy generation, a DC/DC is designed to match the impedance from the generator to the final node load.

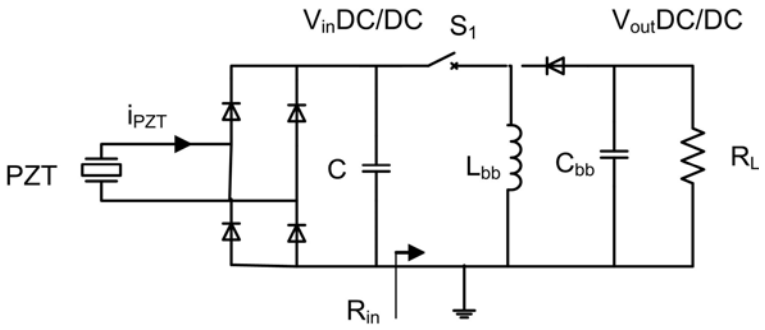

Figure 3-24 Schematic draw of the buck-boost DC/DC converter.

The converter used is the buck-boost converter from the Figure 3-24. In Discontinuous Conduction Mode (DCM), the input resistance of the converter is equal to

$$R_{in} = \frac{2L_{bb}}{TD^2} \qquad \textit{Eq 3-63}$$

where "L_{bb}" is the inductor value, "T" is the period of the MOS switching time and "D" is the duty cycle. Thus, designing the system to work in a DCM permits to define a input resistance of the DC/DC independent of its output. This allows fixing this resistance equal to the optimum value thus maximum power is delivered to the electrical load.

However, it is required to ensure that the system is working in a DCM. To assure this, the duty cycle has to fulfill the equation.

$$D \le \frac{1}{1 + \frac{V_{inDC/DC}}{V_{outDC/DC}}} \qquad \textit{Eq 3-64}$$

Assuming no losses in the converter, this specification are rewritten in terms of input and output resistance as

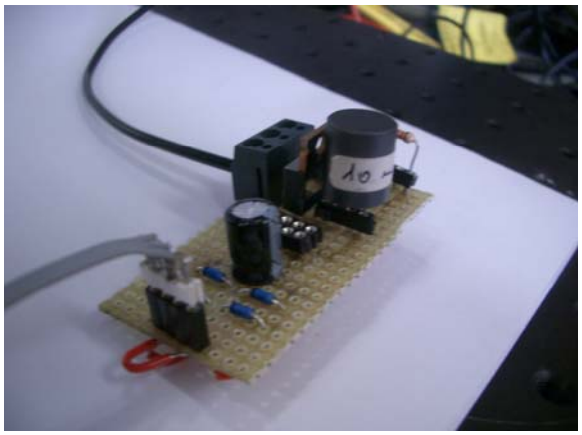

Figure 3-25 Picture of the buck-boost electrical circuit used for the measurements.

$$R_L \geq \frac{R_{in}}{\left(\frac{1}{D}-1\right)^2} \qquad \textit{Eq 3-65}$$

In order to be able to assure a DCM state for the maximum number of output load, the duty cycle must be designed as low as possible.

Figure 3-25 shows a picture of a discreet implementation of the whole system. The converter is configured to give an input resistance "R_{in}" equal to 5600ohms. This is the value for the maximum energy generation of the MPG obtained from Figure 3-23. The implemented values are: 10mH inductor, a switching frequency 25,2kHz, a duty cycle D=30% and a 10µF capacitor. With these conditions the minimum output resistor that ensures the DC mode is approximately 1kohms. The system is experimentally tested by loading different resistors to the DC/DC output and measuring the power generated.

Figure 3-26 shows the signals for an output load of 12kohms using the circuit from Figure 3-24. It is observed how the input current has more noise than in Figure 3-21, this is because of the switching nature of the converter. The output voltage is negative and gives -2.9V. The buck-boost converters have negative outputs. However the most remarkable thing of the figure is the input voltage to the converter, this voltage is about 2.4V, this means that the load seen from the rectifier, thus the input of the converter is fairly the expected 5600ohms thus the maximum power is delivered.

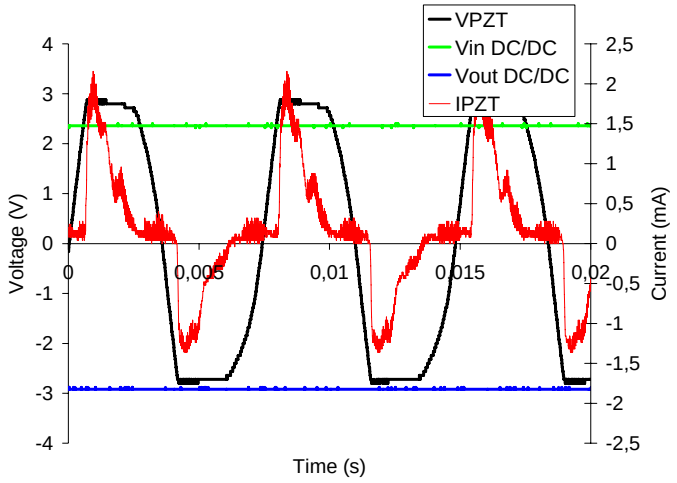

Figure 3-26 Exp. measurements of the waveform signals of the buck-boost circuit with a 12kΩ load resistor.

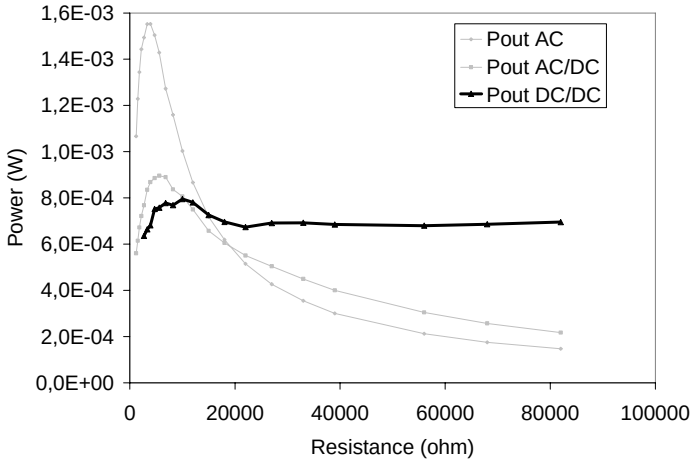

Figure 3-27 Output power for load resistor using the buck-boost converter.

Figure 3-27 shows the output power "P_{out}DC/DC" delivered to different loads maintaining the same values of duty, frequency and inductance, thus the same input resistor and the maximum energy generation condition. The graph is pictured together with the signal from Figure 3-23 for comparison. It is observed how the output power delivered to the load "P_{out}DC/DC" is almost flat for all resistors. Some fluctuations are attributed to classical non-idealities of the elements of the converter. However about 0.7mW is given for all resistors. This power is a little bit smaller than the maximum value obtained with the rectifier "P_{out}AC/DC" of 0.9mW. These differences are attributed to some losses due to the switching.

Figure 3-28 shows the voltage measured in the input and output of the converter. It is seen how the input voltage is almost flat, and remains in the 2.4V

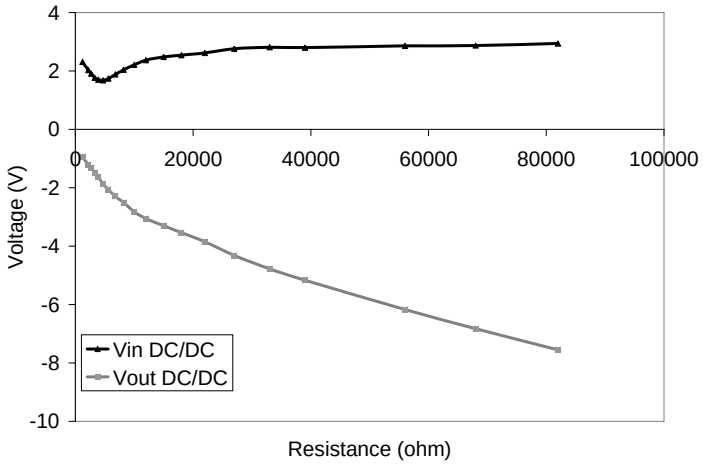

Figure 3-28 Buck-boost iInput and output voltage vs load resistors.

expected value. This confirms the idea that the resistance seen from the MPG is constant. The output voltage increases in magnitude as the resistor increases.

Next test is devoted to confirm the ability to change the input resistance of the DC/DC converter using Eq 3-63. The system is configured with the input DC/DC resistance equal to 2133 ohm first and then with 12000 ohm. This is achieved using 9.6kHz first and then 54 kHz as the switching frequency. Figure 3-29 shows the measured power in the output load compared with the values from Figure 3-27. Figure 3-30 shows the input and output voltage of the DC/DC. Both curves confirm the ability of the converter to tune its input resistance to a desirable value defined by the equation Eq 3-63. Figure 3-29 shows how the maximum power is delivered when "R_{in}" is equal 5600. Figure 3-30 shows how the input voltage is almost flat for the three curves and that this voltage increases as the "R_{in}" increase while the output voltage is greater for the 5600 ohms that is the optimal load.

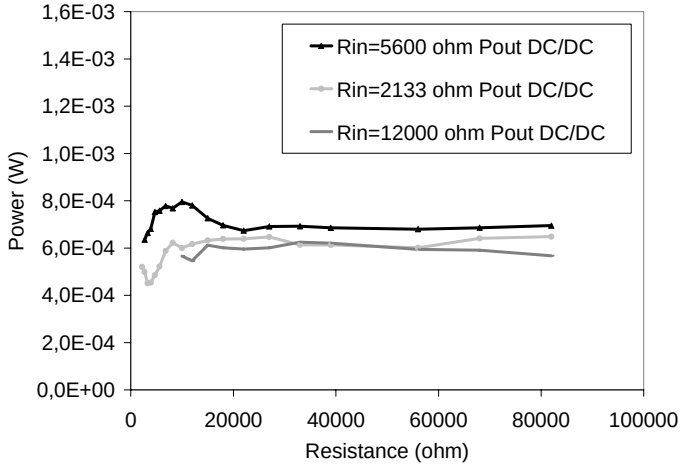

Figure 3-29 Output power for load resistor using the buck-boost configured with fs=9.6kHz, 25,2kHz and 54kHz to lead its input resistance as 2133Ω, 5.6kΩ and 12kΩ respectively.

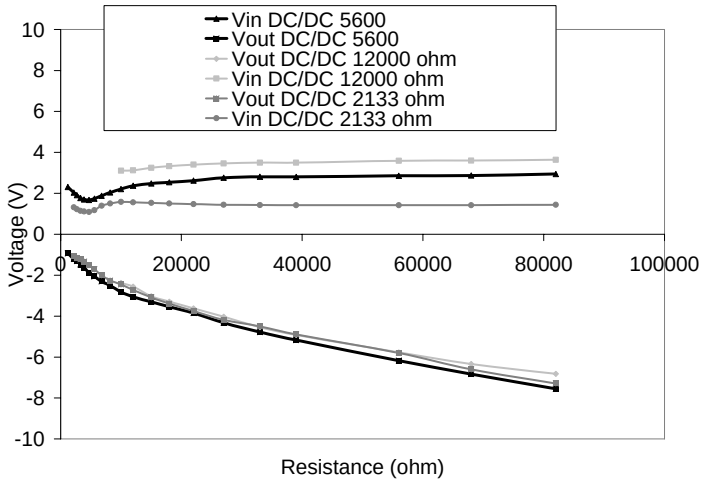

Figure 3-30 Buck-boost converter input and output voltage vs load with fs=9.6kHz, 25,2kHz and 54kHz to lead its input resistance as 2133Ω, 5600 Ω and 12kΩ respectively

.

3.2.3.3. Power management

The test involved in the last section have demonstrated the ability of designing an electronic circuitry able to assure an impedance match whatever the output load value is. This permits to have always the maximum energy generation. However, the energy generated by the MPG is still small to power any node. The idea of the energy harvesting system is to burst the generated power. During a certain time, the power is stored in a supercapacitor, this is the "Charging time", then the power is discharged to the node for another certain time, this is the "Discharge time". The discharge time is normally defined by the application, in other words, it is what the node demands, for example a certain time to measure a parameter, or a certain time to send some information etc. By the other hand the "Charging time" is defined by the maximum energy that can be supplied by the MPG (P_{max}).

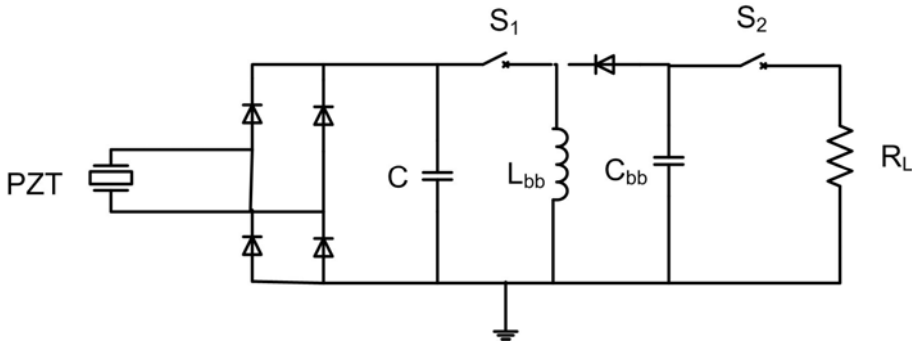

Figure 3-31 Power bursting shcematic drawn

Figure 3-31 shows a schematic draw of the final circuit. The circuit is the same than in Figure 3-24 but now a new switch is used to burst the power to the load. Thus assuming a node that demands a certain power "P_{load}" during a certain time "T_{disc}", the duty cycle of the burst time D_2 must be equal

$$D_2 = \frac{P_{\max}}{P_{load}} \qquad \textit{Eq 3-66}$$

where "P_{max}" is the maximum power generated by the MPG. Then the node will works each period equal to "T_2"

$$T_2 = \frac{T_{DISCH}}{D_2} \qquad \textit{Eq 3-67}$$

As an example, a specific case is considered. Assume that the whole system is devoted to drive a low power transceiver. Otis and Rabaey [Otis2003] designed a custom low power transceiver transmitting at 1.9GHz. The power consumption of the

transceiver is expected to be 10mA at 1.2V. The transmitting time depends on the frame that is needed to send. However in this example a 100ms frame time is assumed. Therefore considering this requirements the power consumption of the transceiver is 12mW for 100ms, if the Qp40w is located in a base milling machine vibrating at 148 Hz with a acceleration of 10m/s^2 (these are the conditions from the section above giving 0.7mW), the D_2 duty cycle must be 5.8%, thus the information will be send with a period of 1,7s.

3.2.4. Conclusions

The fast evolution of autonomous smart systems and structures is being limited by the powering systems technologies. For a long time, battery technology has been the only way to supply energy to those systems and to provide them with some autonomous capabilities. However the use of batteries entails a set of limitations and disadvantages. Their limited life time together with the fact that batteries are heavy pollutants have caused an increase in the demand of the research in new power sources. In this sense researchers are focusing in the development of energy harvesting systems able to convert dust energy from the ambient into useable electrical energy to drive low power systems. The researcher's proposed solutions depend on the applications, however most of the works focus on solar energy, thermal variations or mechanical vibrations.

This chapter have analyzed the possibility to use micro power generators (MPGs) to generate electrical energy from environmental mechanical vibrations. A general model to estimate the amount of energy that can be harvested from a vibration source is presented and discussed. The model is useful to make a first estimation of the maximum power that can be generated from a vibration source without considering the method used for the conversion. The model considers a micro power generation device anchored to a vibrating source. The model concludes that there is an optimum electrical resistive load that maximizes the power generated from the vibration source. The maximum power is obtained when the mechanical system is configured with its natural frequency equal to the input base vibration frequency. The final model equation shows that for a given base acceleration the maximum generated power is higher for low frequencies. Moreover this power is proportional to the mass of the converter. The model developed permits to make a first evaluation of the maximum power that can be generated from a vibrating source with a typical MPG in a typical application. Considering a typical vibration inside a building with a frequency of 24Hz and an acceleration of 1m/s^2, and considering a converter with a mass of 13g and a damping ratio 0.027, the model outputs a maximum power generation of about 190μW. If properly managed, this amount of power can be enough to drive a sensor node in a wireless network. Nevertheless, the general model discussed is something ideal and some modifications are required. The model development starts with an assumption that is not always correct. The model considers that the conversion of energy looks like a linear damper. While for some specific converters such as electro-magnetic converters the model is fairly accurate,

if the converter is piezoelectric or electrostatic the model has to be changed somewhat.

Following the general model, a specific model considering the piezoelectric transduction has been done. The model shows that the optimal electrical load value for the maximum power generation has to be complex. While in the general model the optimal load was resistive, in the case of piezoelectric this load has to be complex. This is a consequence of the energy storing capabilities of piezoelectric due to its dielectric nature and to the high coupling between electrical and mechanical domains. Therefore when a piezoelectric micro power generator is used to harvest power and supply a resistive load, an impedance adaptation network has to be developed. However, the high value of the reactive part of the optimal impedance make difficult to implement the adaptation network especially at low frequency. Therefore in those cases where the vibrations excitation frequency is low, it is not possible to harvest the maximum power from a vibrating source using a MPG piezoelectric device. Therefore an effectiveness function is defined as the ratio of the maximum power extractable with a piezoelectric MPG with a resistive load and the maximum power extractable from the source (this is with a complex impedance load value). Depending on the type of converter and material, this effectiveness function will be closer to one or not. Piezoelectric polymers posses a lower capacitance value and lower coupling coefficient than piezoelectric ceramics, therefore the effectiveness function will be much closer to one. However the optimal resistor will be very high therefore the voltage generated too. This is sometimes an inconvenient when low power circuits are designed. By the other hand piezoelectric ceramics have a lower effectiveness function but the voltage and current levels are more acceptable. The ability to convert energy with a piezoelectric transducer from a vibration source has been tested with the commercial transducer Qp40w from Midé corporation. This transducer is formed with four piezoelectric ceramic layers embedded in an epoxy matrix to increase its yield strength. The mechanical configuration is based on a cantilever anchored from its base to the source. The experimental tests realized have proven the ability to generate electrical power over a resistive load at three resonance modes of the beam. Assuming a constant acceleration of $1m/s^2$, the maximum power measured was 86μW (at 22Hz, with 25.6kΩ resistive load), 9.34μW (at 148Hz with 3kΩ resistive load) and 0.178μW (at 935Hz with 500Ω resistive load) corresponding to the first, second and fourth resonance mode. This power represents the 60%, 65% and 80% of the maximum power available from the source. Unfortunately the complete match is not possible for the first two modes, nevertheless it has been possible to make a complete match at the fourth mode with a load inductor of 50mH and a load resistor of 200Ω given the maximum power of 0.24μW. This value represents an increase approximately of 20% with respect the amount of power harvested with the modulus match.

Although the general model and the specific model for piezoelectric describe the amount of power generated to an electrical load, the final system is far to harvest this energy. In fact the models compute the averaged delivered power to a resistive

load in AC. However these signals have to be filtered to became a DC power and then, this power has to be managed somewhat to finally drive a certain node. Therefore a power lost in the management is expected. In order to handle and optimize the power harvested, it is possible to implement an electronic circuitry that manage the power and at the same time, impose the impedance matches. For this purpose a discreet circuit has been implemented following the requirements of impedance match for the commercial piezoelectric MPG that has been experimentally identified. The circuit consist on a full bridge rectifier followed by a buck-boost converter working on DCM. The converter is configured to harvest the energy from a vibration source at 148Hz and an input acceleration of $10m/s^2$, using this piezoelectric transducer working at its second resonance mode (148Hz). The input resistance of the buck-boost converter is fixed to the optimal value by choosing a proper duty cycle, switching frequency and inductor. Due to the nonlinear nature of the full bridge rectifier the optimal resistance value is modified by a factor of approximately $\pi/2$. The final system is able to deliver 700μW of DC power to a sensor node even if the load resistance of this node changes.

Although the total circuit presents some power losses, and even if some control signals are generated externally, the circuit demonstrates the ability to impose the maximum power restrictions without the need of any feedback. Future efforts on the design of advanced integrated circuits to reduce losses and generate the control signals by self-powering will be done. Actually some works have been already published in a collaboration with integrated design researcher from SIC [Colomer2007] and [Colomer2007_2].

.

3.3. IPMC power harvesting

Ionic Polymer Metal Composite materials are soft materials that can be used as actuators in a wide variety of applications. In fact, in this thesis this material has already been used to perform a micropositioner underwater actuator. In section 2.2, the performances of the material to work as an actuator together with the design of an adaptive control based on a model reference were presented. However, IPMCs are not exclusively used as actuators. Although the main attractive properties of these materials are their low voltage activation and their lightness and flexibleness nature, they are also interesting for their sensing capabilities. IPMCs when forced to mechanically bend, a change in the distribution of internal charges appears and a voltage is measured between electrodes. In fact along the contracted side of the beam, there is an excess of negative charges while at the elongated side of the beam, the contrary occurs. It is thought that this change produces a motion of the mobile cations towards the region characterized by a lower charge density. The use of IPMC sensors is in a more embryonic state, however a significant amount of research works have been presented in the last years [Bonomo2006], [Newburry2003_3], [Bonomo2008_2].

In the previous point of this thesis, the piezoelectric effect was used to generate electrical energy. Actually it was the ability to convert applied mechanically stress into internal electrical charge variation. Although the internal physics responsible of the transduction in the ionic polymers is different, the same phenomenon occurs as in the piezoelectric transducers, the appearance of an internal charge variation due to the application of a mechanical stress. Therefore it is reasonable to analyze the possibility to use ionic polymers to harvest energy from mechanical vibrations. Moreover, ionic polymers have some interesting features as light weight, flexibility, and biocompatibility that could open the door to harvest energy in other environments than piezoelectric ones. All these aspects have encouraged the authors to investigate the capabilities of ionic polymers to harvest energy from vibrations.

Among the worldwide research in ionic polymers, the author was not able to find any journal contribution devoted to the research of ionic polymers. However there is a very interesting research work in a thesis dissertation from the Virginia Polytech. Institute submitted in 2005 [Martin2005]. This thesis presents an experimental characterization of the power generated by an IPMC based specific bending device designed to harvest energy from the low level frequency vibrations in ship propulsion (0.2Hz-4.2Hz). The experimental results show the low power generation capabilities of the design but attributes it to the input constrains of the application as the low frequency. The author remarks that the limiting factor in the energy generation is the extremely low current generated at the low frequency, however, he concludes that with other designs the generated power from an IPMC device could be enough to be used as a renewable energy source.

In this point the possibilities to use IPMCs to harvest energy is studied in more detail. While the study at the Virginia Polytech. [Martin2005] is pure experimental, in this point a model to predict the energy harvested from vibrations with an IPMC strip is proposed. The model is described in terms of the material and geometrical parameters and outputs the power generated by an IPMC when vibrates from its base. Thus it is possible to recognize the parameters that optimize the power. As far as the internal physics responsible of the transduction in such materials are unknown, the proposed model is obtained with the gray-box approach. A gray box approach is a kind of modeling where a few physical laws are taken into account while some of the material parameters are experimentally identified. The model proposed in this section is based on the model obtained in the last section for piezoelectric transducers. Piezoelectric materials respond to output stimuli as ionic polymers, this is, present a mechanically induced strain under the application of an external electrical field, and induces an electrical charge when mechanically stressed. However, as far as the identification process takes part, some modifications are introduced in the model to better represent the dynamic behavior of the IPMC strip. It is not the first time that a piezoelectric model is used to describe the IPMC dynamic behavior. Newburry et al. [Newburry2003_3] developed a gray-box model based on the piezoelectric equations. The model they presented consists on a bidirectional model that describes the actuator and the sensor dynamic response of a full hydrated IPMC strip. With that model, Newbury was one of the first to demonstrate the bidirectionality in the ionic polymer transduction.

The study presented is realized in a "dehydrated" IPMC strip (from now on a dehydrated sample means a sample in equilibrium with the environment). It is known that the sensor response of these materials works better when the membrane is dehydrated. Bonomo et al. [Bonomo2006] showed that the need for a wet environment is not a key point for IPMC sensor. They remark that the sensing behavior of IPMCs is better when the membrane is in equilibrium with the environment and the excess water is lost. Therefore the study presented analyzes the energy harvesting with a dehydrated sample. The study starts with the description of the MPG device. Next an experimental identification of the model parameters is presented. Then the power generation capabilities of the IPMC are discussed. The whole work presented in this point is published as a journal paper by the author of this thesis together with the researchers from the Catania Univeristy. [Brufau2008]

3.3.1. Model for ionic polymer power harvesting from vibrations

Ionic polymers are bending transducers, therefore the best configuration to harvest energy from mechanical vibrations is the cantilever design. The mechanical configuration studied in this point is the same than Figure 3-4 where a cantilever beam was anchored from its base to a vibrating source.

The physics involved in the transduction of ionic polymers are quite complex. Up to day, there is still no consensus in which are the responsible phenomena of the transduction. In this point the modeling approach is realized as a gray-box approach. Through some initial physical relations, the different parameters of the equations are experimentally identified.

As far as the mechanical configuration is a bending beam excited from its base, the same mechanical analysis than in the case of an Euler-Bernoulli beam is considered as a starting point. For the electrical analysis, ionic polymers are considered as dielectric forming planar capacitors. The coupling between mechanical and electrical domain is modeled as in the case of piezoelectric where a linearly coupled pair of equations defines the relations between strain and electric displacement with stress and electric field. Therefore the initial model adopted for the description of the system dynamics is the same than with the piezoelectric configuration of section 3.2. Here the two coupled equations are rewritten:

$$m_n \ddot{r}_n(t) + c_n \dot{r}_n(t) + \Theta_n V(t) + K_n r_n(t) = F_{on}(t) \qquad \textit{Eq 3-68}$$

$$i(t) = \Theta_n \dot{r}_n(t) + C_P \dot{V}(t) \qquad \textit{Eq 3-69}$$

The first equation is the mechanical equation and the second equation is the electrical equation. These equations are taken as starting point, however through observations of experimental responses and some knowledge from bibliography, these equations are modified to better represent the dynamic of the system.

In the piezoelectric analysis, the identification process was devoted to obtain the elements of the equivalent circuit for the specific composite transducer. In the following points the identification is devoted to better comprehend the dynamics of the ionic polymers in general.

3.3.2. Micro power generation (MPG) device

The micro power generation configuration studied is the same than with the piezoelectric system from Figure 3-10. It consists on a cantilever beam anchored to a vibrating body. In this case the beam is an IPMC strip. The samples studied are different than the ones used in chapter 2 with the MRAC control scheme. In this case the samples were developed at the “Dipartimento di Ingegneria Elettrica, Elettronica e dei Sistemi, Università degli Studi di Catania” with we have stablished a cooperation framework. The samples consist in a Nafion® Na+117 membrane manufactured by Dupont. The electrodes are deposited following the Oguro procedure [Oguro2001] and the counter ions introduced are Na+, see Figure 3-32.

The geometrical dimensions of the sample studied are L=22 mm length, w=4 mm width and h=200μm height. These values are in the same range as is used in

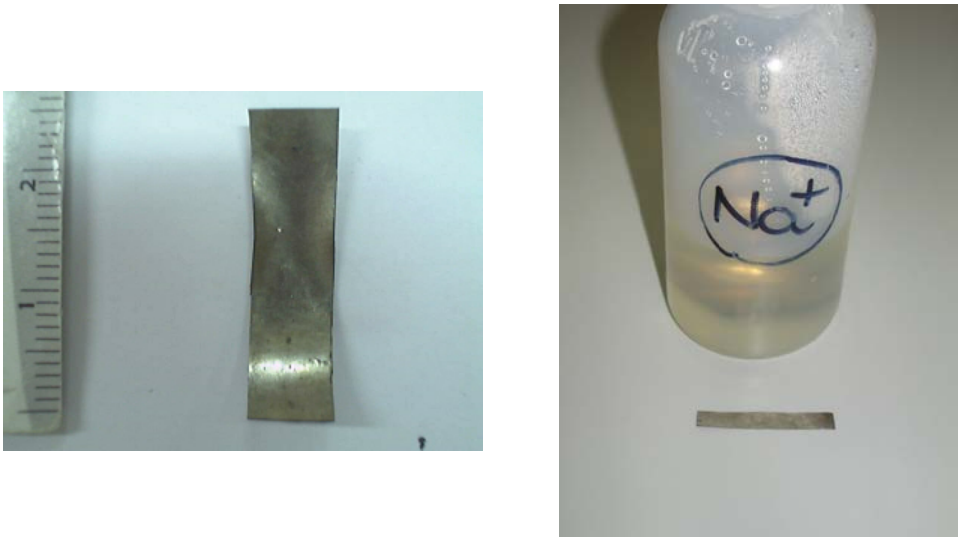

Figure 3-32 Ionic polymer sample with Na+ as counter ion.

most IPMC studies in the literature. The beam is clamped at one end with a conductive clamp leading L_F=18mm as free length. To assure a dehydrated condition, the membrane was always maintained outside water. In the following steps, these samples are submitted to different experimental tests in order to obtain measurement of the material parameters. The parameters are obtained through an identification process.

In the next point a model identification step is realized. Although the ionic polymer generator is treated as a piezoelectric generator with the same model equations, the final response of the system will differ. Therefore there is a need to introduce changes in the model equations to describe these differences. These changes are identified qualitatively and quantitatively through the submission of the ionic polymer to a set of different experimental tests,

3.3.3. Model identification

The identification of the material parameters of ionic polymers defining the equations of the model requires a set of different experimental tests. The measured experimental data is used to identify the model parameters through an identification process based on a minimization algorithm. The algorithm consists of evaluation of a cost function that compares the experimental data with evaluation of the theoretical model equations Eq 3-68 and Eq 3-69 in the time domain. Three experimental tests are realized, the first one involves the measurements of the electrical impedance. The second test involves the measurements of the mechanical impedance. The last test involves measurements of the electromechanical coupling by analyzing the actuator response of the polymer.

The relatively inconsistent behavior of this kind of material is well known. For this reason the minimization process considers the response of the membrane over several cycles; in this way the solution found is considered as an average value. The power spectrum of the input signals is also important in order to perform a wide frequency analysis. For a more detailed explanation of this algorithm the reader is referred to [Bonomo2006].

For the following experimental tests data was acquired using an Acquisition Card PCI160520 (National Instruments) supported by LabVIEW. The frequency region of interest is from 0.1Hz up to 100Hz. For those experimental tests that need a displacement measurement a triangulation laser OADM 12U6460/S35A from Baumer was used. The force measurements were performed using a load cell (GS0-10, Transducer Techniques). The absorbed current was measured using a differential amplifier and a shunt resistor with a defined value of 0.1 Ω. The actuating voltage signals were generated by a voltage source controlled by LabVIEW software. To impose a mechanical deformation on the sample, an electromagnetic shaker was used [Bonomo_2006_2]. For the sensor current measurements a short circuit current amplifier was used.

The first experimental test implies the electrical measurement of the dynamic response of the ionic polymer. Following the electrical measurements, a mechanical experimental test is realized devoted to identify the mechanical behavior of the polymer. Once the electrical and the mechanical response are identified separately, it is possible to identify the way these domains couple in the polymer. Therefore the electromechanical response of the polymer is analyzed.

3.3.3.1. Electrical impedance

This point is devoted to find the pure electrical impedance of the ionic polymer MPG. This is the relation between input voltage and absorbed current. In order to avoid effects of the mechanical response in the electrical measurements, the material is fixed and no motion is permitted. Therefore, considering the electrical equation Eq 3-69 and imposing the condition of motionless $r_n(t)=0$, the electrical equation is rewritten in the Laplace domain as:

$$i(s) = sC_P V(s) \qquad \textit{Eq 3-70}$$

This is the case of a motionless piezoelectric transducer, where the electrical impedance is well defined as a unique capacitor “Cp”. Nevertheless in ionic polymers this impedance is different.

A great amount of work has been done in order to find a model to describe the electrical impedance of an Ionic polymer membrane. One of the first things to consider is the electrode resistance due to the porous nature of the electrodes. Different techniques are being under research to decrease the electrode resistance of

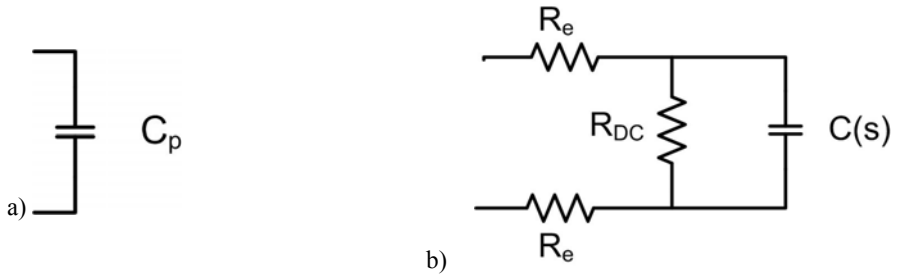

Figure 3-33 a) Piezoelectric ideal electrical impedance, b) ionic polymer electrical impedance.

ionic polymers. However, reducing the porous nature of the beam is transduced into a minor water uptake of the solvent when hydrated. The electrode resistance affects the distribution of the electric field through the length of the strip and has to be taken into account. Some papers present a distributed lumped equivalent circuit over the whole membrane to take into account the influence of the electrode resistance [Shahinpoor2000]. These kinds of models are not very convenient when working with simulation software due to the large number of elements. Other works consider a non-linear contribution due to the hydrolysis effect when the applied voltage is greater than 1.2V [Bonomo2006]. In this part of the section, the model considered for the impedance identification is the same but, due to the low level hydration of the sample, the non-linear branch is not considered. This model considers two electrode resistances "Re", a leakage resistance of the membrane "Rdc" and a capacitor "C(s)" with a dielectric permittivity frequency dependent "μ(s)"

The equation defining the electrical impedance is Eq 3-71. Each of the elements defining the electrical impedance are identified realizing three distinct measurements

$$Z(s) = 2R_e + \frac{1}{C(s)\left(s + \frac{1}{R_{dc}C(s)}\right)} \qquad \textit{Eq 3-71}$$

The electrode resistance "Re" is measured with a multimeter and gives 22Ω for the whole length. Therefore the resistance distribution is Re=1 Ω/mm.

The leakage resistance "R_{dc}" is calculated with the conductivity of Nafion given by the manufacturer ρ=1205 Ω/mm. Therefore the resistance is computed with the equation Eq 3-72 and gives R_{dc}= 2.55kΩ

$$R_{dc} = \frac{\rho h}{wL} \qquad \textit{Eq 3-72}$$

The next element to identify is the capacitance C(s) of the circuit from Figure 3-33. This capacitance is related to the ionic nature of the polymer and the double

layer electrode surface. Nevertheless ionic polymers are not perfect capacitors. Other effects as internal serial resistance due to the high penetration of electrodes inside the membrane must be considered. However these effects are modeled as a frequency dependent capacitance. A way to model this behavior is to consider this impedance as a capacitor Eq 3-73 with a dielectric permittivity frequency dependent with the form of the equation Eq 3-74 [Newbury2003].

$$C(s) = \mu(s)\frac{wL}{h} \qquad \textit{Eq 3-73}$$

$$\mu(s) = \sum_{i=1}^{m} \frac{\varepsilon_i}{1 + s\varepsilon_i \rho_i} \qquad \textit{Eq 3-74}$$

Therefore the parameters to identify are ε_i and ρ_i for i=1:m. Function μ(s) is named the permittivity, however this is a way to represent the dynamics of the electrical impedance similar to piezoelectric one with a capacitance. The physical meaning of this function is not necessarily a permittivity. Actually it represents parallel association of capacitor resistor serial branches [Newbury2003]. It is also important to remark that the surface area of contact between electrode and polymer is not flat at all. The metal particles penetrate inside the material forming a highly craggy surface, therefore the area computed as "wL" must be much more higher.

The experimental test realized for the parameters identification consist on applying a signal voltage and measure the absorbed current when the material is fixed. The voltage signal consists on a train of a 2Vpp sinusoidal sweeps from 0.1 Hz to 100 Hz followed by a train of six 100mHz square signal and finished with a train of triangular signal sweeps from 0.1Hz to 100Hz at 2Vpp

Figure 3-34 shows the final stage of the time domain fitting between the measured current and the calculated current by considering the circuit from Figure 3-33b) with m=2. It is observed the high value of the absorbed current. This means that ionic polymers have a low impedance. Figure 3-35 shows the transfer function estimated after the identification process. At low frequencies a capacitive effect is observed while at higher frequencies resistive behavior is exhibited. The values identified are reported at Table 3-4. A plot of the function defining the "μ(s)" with the identified values is shown at Figure 3-36.

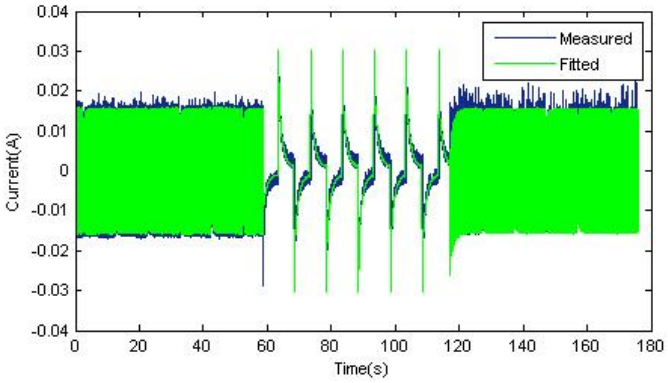

Figure 3-34 Fitting curves for the absorbed current. Green is fitted and blue is measured.

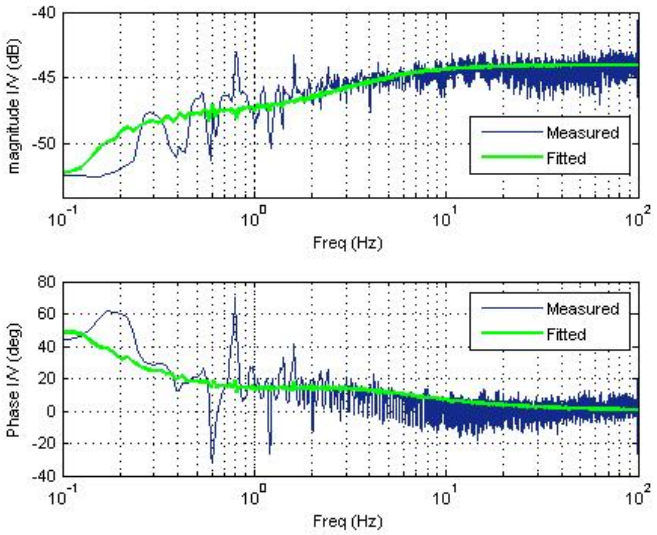

Figure 3-35 Electrical admittance Bode plot. Green is fitted and blue is measured.

ρ_1	94.31614280
ε_1	0.009980012
ρ_2	121.298861
ε_2	3.184524e-4

Table 3-4 Identified parameters of the equivalent permittivity.

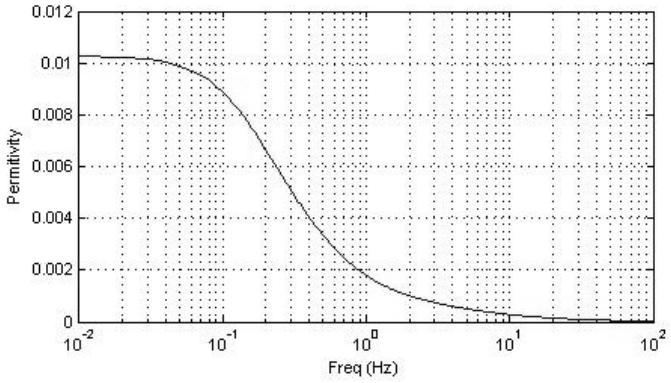

Figure 3-36 Equivalent permitivitty μ(s) frequency response.

At very low frequency, the values of the function μ(s) are very big compared with classical dielectric permittivity of piezoelectric, this means that ionic polymers behave as very big capacitors at low frequency. In fact in some works ionic polymers have been proposed to be used as supercapacitors [Martin2005].

The experimental test was repeated with the ionic polymer in cantilever configuration free to move obtaining exactly the same results. This effect has been already pointed out by other authors in literature and will be discussed later [Franklin2003].

3.3.3.2. Mechanical impedance

Ionic polymers are generally considered as viscoelastic materials. This behaviour is commonly modelled by the Golla-Hughes-McTavish GHM model [Trindade2004], [Newburry2003]. This model describes the Young's Modulus as a transfer function similar to a mass damper oscillator. Eq 3-75 illustrates this behaviour; it has a resonance frequency "ω_y", a gain "k_y", a damping ratio "ξ_y" and a static Young's Modulus "Yc". However in dehydrated conditions, the resonance frequency "ω_y" is shifted up to frequencies higher than 100 Hz [Bonomo2006]. Assuming dehydrated conditions with the resonance frequency "ω_y" much higher than 100 Hz, Eq 3-75 is reduced to Eq 3-76, which is the classical equation for a linear elastic material as a piezoelectric with an internal damping contribution modelled with the constant "B".

$$Y = Y_C(1 + k_Y \frac{s^2 + 2\xi_Y \omega_Y s}{s^2 + 2\xi_Y \omega_Y s + \omega_Y{}^2}) \qquad \textit{Eq 3-75}$$

$$Y = Y_C + sB \qquad \textit{Eq 3-76}$$

Therefore the pure mechanical equation of the piezoelectric model is accepted for modelling the ionic polymer mechanical response in dehydrated conditions

$$m_n \ddot{r}_n(t) + c_n \dot{r}_n(t) + K_n r_n(t) = F_{on}(t) \qquad \textit{Eq 3-77}$$

This equation is then written substituting the elements of the equation in terms of the material and geometrical parameters Eq A43, Eq A44, Eq A45.

$$\rho A L_F \ddot{r}_n(t) + \lambda_n^4 B I L_F \dot{r}_n(t) + \lambda_n^4 Y_c I L_F r_n(t) = F_{on}(t) \qquad \textit{Eq 3-78}$$

Where "ρ" is the density of the material, "λ_n" is the normalized natural frequency and "I" is the moment of inertia. From this equation the parameters to identify are the "Yc" and "B". The density of the material was directly computed measuring the weight of the sample and gave 2.32 kg/m^3. In order to identify these parameters two different experimental tests are realized.

The first experimental test is devoted to identify the damping constant "B". To identify this coefficient, the modal damping coefficient "c_n" is first identified. The experimental test realized is easily implemented. The ionic polymer is clamped in cantilever configuration. A mechanical perturbation is applied at the free end of the beam, and the oscillating motion of the tip is measured with the laser. The electrodes of the polymer are short circuited to avoid any influence of the electrical domain in the mechanical response

Figure 3-37 shows the response of the tip to the perturbation. An oscillating motion with an exponential decay is measured. Figure 3-38 shows its power spectral density. As can be observed, the main contribution of the signal is due to the first resonance mode located at fr=64 Hz. Measuring the beam deflection exponential decay, a value of ς1=0.025 was estimated. This value is calculated with the equation Eq 3-79 where "x1" and "x2" are the values of tip displacement separated "n" periods. The damping constant "c_n" is computed with equation Eq 3-80. Therefore the constant "B" is computed Eq 3-81 and gives B=74e^{3}Pa·s/rad

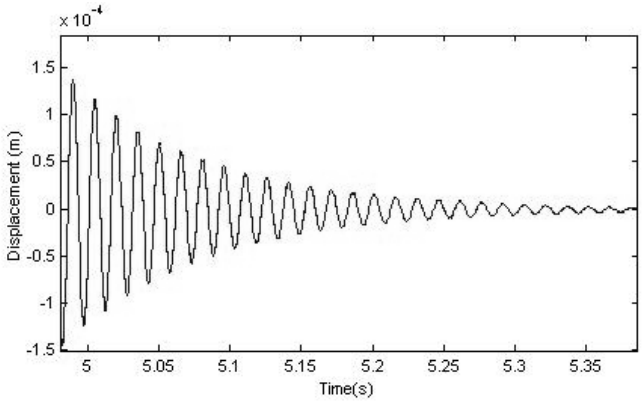

Figure 3-37 Tip displacement response to an input impulse.

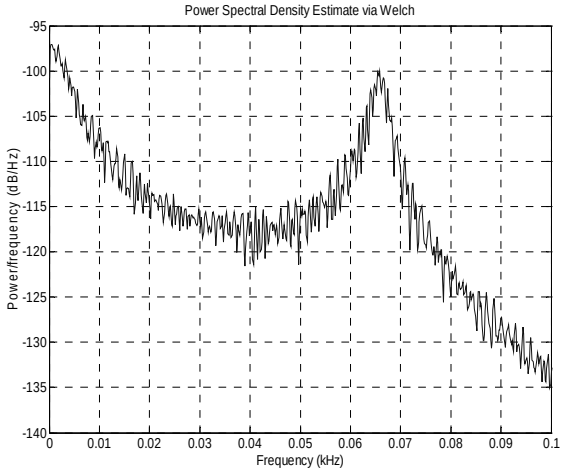

Figure 3-38 Power spectral density of the tip displacement.

$$\zeta = \frac{1}{2\pi m}\ln\left(\frac{x1}{x2}\right) \qquad \textit{Eq 3-79}$$

$$c_n = 2m\zeta\omega_n \qquad \textit{Eq 3-80}$$

$$B = \frac{c_n}{\lambda_n^4 I L_F} \qquad \textit{Eq 3-81}$$

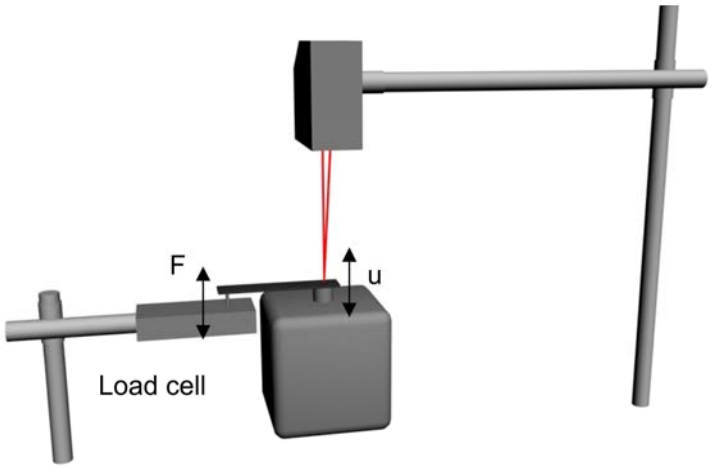

Figure 3-39 Mechanical configuration for Young modulus measure .

The second experimental setup is implemented to determine the Young's Modulus "Yc". The natural way to measure this would be to apply a force at the free tip of the IPMC and measure its deflection, but this procedure has a number of disadvantages. Some authors have proposed replacing this procedure with an easier one: applying a deformation at one end of the IPMC and measuring the force at the other end. This is the procedure adopted here. Figure 3-39 shows a schematic draw of the mechanical configuration.

With this configuration the mechanical equation that relates the deflection the beam deflection at x=0 with the force applied at the other tip x=Lf in the Laplace domain is written as [Franklin2003]:

$$u(0,s) = \frac{4L_F{}^3}{Y_c w h^3} F(L_F, s) \qquad \textit{Eq 3-82}$$

This equation is only valid up to the second resonance mode of the sliding pin configuration. For the identification of the young modulus, a displacement signal is applied with the shaker at one end, and at the other end the force is measured.

Figure 3-40 shows the fit between the measured and simulated force after the identification process. A good agreement is observed between the signals. The value obtained is Yc=0.6GPa. This value is comparable to values obtained by other authors [Nemat-Nasser2002].

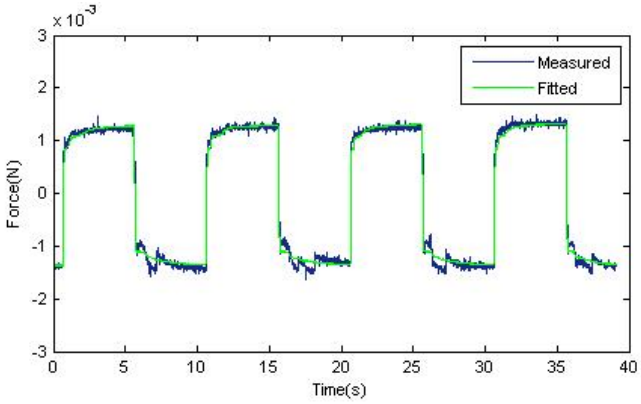

Figure 3-40 Simulated and measured tip force for an input base displacement.

The experimental tests realized have been devoted to identify the mechanical parameters of the ionic polymer. In order to have a perfect decoupling between mechanical and electrical domains, the electrodes were short circuited during the execution of the tests. The next test consisted on repeating the two experimental tests but imposing an open circuit conditions in the electrodes of the beam. In this case assuming the two model equations Eq 3-68 and Eq 3-69, the mechanical equation is rewritten as.

$$m_n \ddot{r}_n(t) + c_n \dot{r}_n(t) + \frac{\Theta_n^2}{C(s)} r_n(t) + K_n r_n(t) = F_{on}(t) \qquad \textit{Eq 3-83}$$

The measurements with open circuit conditions Eq 3-83 and short circuit Eq 3-77 were compared and no differences were appreciated between both. Therefore it is possible to conclude that in the case of this ionic polymer the term $\Theta_n^2/C(s)$ is negligible.

The next experimental tests are devoted to identify the electromechanical coupling between mechanical and electrical domains. As smart materials, ionic polymer work as sensors or as actuators. In the next point the electromechanical response is measured when the polymer work as a motion actuator.

3.3.3.3. Free deflection

The equations defining the dynamics of the ionic polymers are Eq 3-68 and Eq 3-69. Therefore the free deflection is modeled with the mechanical equation Eq 3-68 considering the base motion equal cero, this is "F_{on}" equal cero.

$$s^2 m_n r_n(t) + s c_n r_n(s) + K_n r_n(s) = -\Theta_n V(s) \qquad \textit{Eq 3-84}$$

At the right side of the equation there is the induced force due to the application of an external voltage. This force depends on the coupling factor "Θ_n" and on a certain voltage. In the case of piezoelectric actuation this voltage is directly the applied voltage however in ionic polymers, the electrical impedance of the system depicted at Figure 3-33 has two electrodes and one leakage resistances that has to be taken into account. The voltage assumed to be the responsible of the actuation is the voltage applied to the capacitor C(s). Therefore, considering the impedance equation, this voltage is

$$V(s) = \frac{R_{DC}}{sC(s)R_{DC}+1}\frac{V_{in}(s)}{Z(s)} \qquad \textit{Eq 3-85}$$

Apart from electrical differences, the transduction is also different. The coupling factor from the governing equation is defined as (see Appendix A):

$$\Theta_n = M_V W'_n(L_F) \qquad \textit{Eq 3-86}$$

Where $W'_n(L_F)$ is the spatial derivative of the mode shape evaluated at the free tip of the beam, and "M_V" is the induced moment. While in piezoelectric and in ionic materials the application of an electric field produces an induced strain that forces a bending moment "Mv", it is reported in the literature that the induced strain in ionic polymers appears in the region next to the electrodes. In the case of piezoelectric the strain is induced in the whole volume of the active material. Therefore the induced bending moment for the ionic polymer must be calculated as:

$$M(t) = -2w\int_0^{+h/2}\frac{h}{2}T(t)_x\,dy = 2w\int_0^{+h/2}\frac{h}{2}d\frac{E_3(t)}{s_{11}^E}dy = wdY_C\frac{h}{2}V(t) = M_V V(t) \qquad \textit{Eq 3-87}$$

Another difference from piezoelectric transducers is in the constant "d". While in piezoelectric transducer the coupling is not dependent on the frequency, the ionic nature of the transduction in the ionic polymers impose a low pass dynamics therefore d(s) depends on the frequency.

Therefore considering the voltage defined in Eq 3-85, the induced moment obtained in Eq 3-87 and the frequency dependence of d(s), the governing Eq 3-84 is rewritten as:

$$s^2 m_n r_n(s) + sc_n r_n(s) + K_n r_n(s) = -\frac{wd(s)Y_C h}{2}\frac{R_{DC}}{R_{DC}C(s)s+1}\frac{V_{in}(s)}{2R_e + \frac{R_{DC}}{R_{DC}C(s)s+1}}$$

Eq 3-88

Therefore the deflection of the free tip of the polymer when drive with voltage is written as

$$u_n(L_F,s) = -\frac{wd(s)Y_C h}{2m_n\left(s^2+\frac{c_n}{m_n}s+\frac{K_n}{m_n}\right)}\frac{R_{DC}}{R_{DC}C(s)s+1}\frac{V_{in}(s)}{2R_e+\frac{R_{DC}}{R_{DC}C(s)s+1}} \qquad \textit{Eq 3-89}$$

Once the electrical and the mechanical elements defining the ionic polymer response (R_e, R_{DC}, μ(s), B and Yc) have been identified, the last parameter to identify is the coupling parameter "d(s)". For this purpose an experimental test is realized. This test consists on applying a sinusoidal sweep voltage with 2.0Vpp and frequencies in the range [0.1 Hz-100 Hz].

Figure 3-41 shows the experimental and fitted time domain response of the IPMC membrane to a sinusoidal sweep input voltage. A maximum deflection of 50 μm is observed at its resonance frequency. Working in dehydrated conditions reduces the number of hydrated ions while the stiffness of the membrane increases. This phenomenon is translated into a small deflection of the membrane. Figure 3-42 shows the Bode plot of the transfer function for the experimental and fitted data corresponding to the deflection/voltage transfer function defined with Eq 3-89. It is possible to recognize the good fit between the signals. Various equations were considered for the estimated coupling coefficient d(s). Equation Eq 3-90 is the function that gives the best results

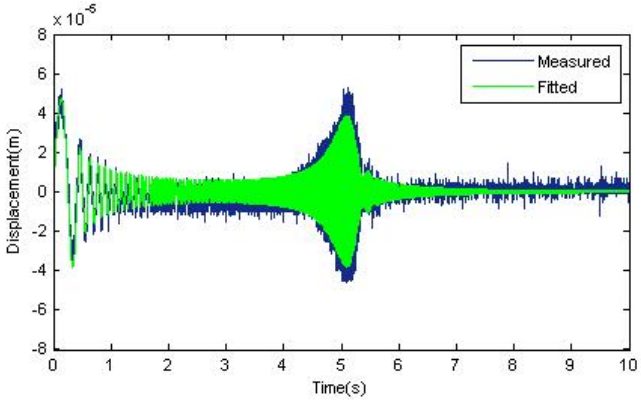

Figure 3-41 Experimental and fitted tip deflection for a sinusoidal sweep applied voltage.

.

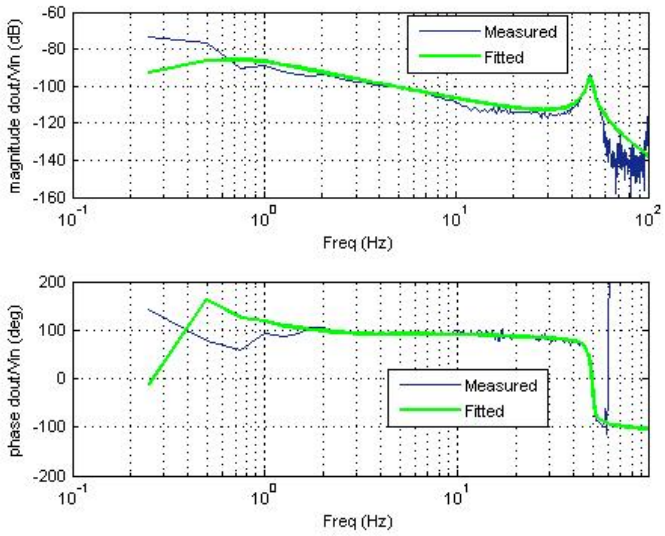

Figure 3-42 Experimental and simulated Bode plot for the transferfunction deflection/voltage.

$$d(s) = \frac{K_d}{(s + P1_d)(s + P2_d)} \qquad \textit{Eq 3-90}$$

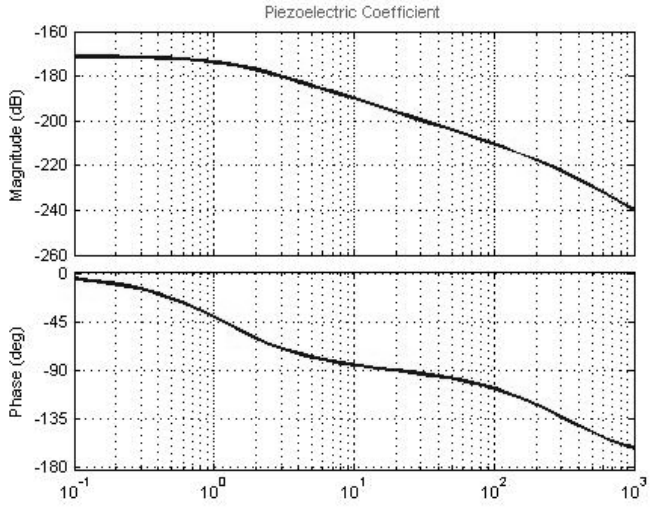

Figure 3-43 Frequency response of the identified coupling coefficient.

K_d	4.0150171e-005
$P1_d$	7.2701289e+000
$P2_d$	2.0312182e+003

Table 3-5 Identified parameters of the coupling coefficient function.

Figure 3-43 shows the transfer function for the coupling coefficient. This coefficient is frequency-dependent and behaves as a low-pass filter with a pole at a very low frequency. This behaviour could be due to the ionic material performances, which make this kind of material good candidate to work as an actuator motion at low-frequency regions.

3.3.3.4. Model performances discussion

Once the model parameters have been identified, the two equations Eq 3-68 and Eq 3-69 defining the dynamic behavior of the ionic polymer are completed. Before starting the analysis on the power generation capabilities of ionic polymers, a brief resume of the more noteworthy features of the model are presented in this point.

In order to model the dynamic behavior of ionic polymers, a piezoelectric linear electromechanical model has been considered. However the parameters of the material have been experimentally identified to better represent the real response of the ionic polymers. The first modification in the model regards the electrical impedance. The first difference is in their electrodes, while piezoelectric transducers have almost perfectly conductive electrodes, in ionic polymers, the electrodes have a certain resistance. The other modification regards the ability to store charge; while piezoelectric behaves as pure capacitors, ionic polymers present more complex dynamic behavior. Actually they behave as capacitors at very low frequency and become like resistors as the frequency increases. The electrical impedance of the ionic polymers has been modeled as a capacitor but with a frequency dependent dielectric permittivity $\mu(s)$. It is worth to say that the physical meaning of these parameters is not as a permittivity. Since the internal physics in ionic polymers transduction are quite complex, it is difficult to identify this response with some physical effect. However as far as the mechanical transduction is mainly considered, as a consequence of the motion of charged particles (hydrated cations), the frequency dependence of the permittivity can be attributed to their dynamics. Furthermore it is important to remark the low value of the electrical impedance of the ionic polymers. While one of the most interesting features of these materials is their low actuation voltage, due to their low electrical impedance a big amount of electrical power is needed for actuation. The other main modification introduced in the ionic polymer model with respect piezoelectric model is in the piezoelectric coefficient d(s). While in piezoelectric models this coefficient is considered as a constant, in the case of ionic polymers, it is modeled with frequency dependence. Again, due to the complex physics in polymers it is quite difficult to extract a reliable conclusion on the reason

of this dynamics. Furthermore in piezoelectric model the coupling coefficient is reversible, this means that the same mechanism is responsible for the energy conversion between mechanical and electrical domains, regardless of the direction of the conversion. In the case of ionic polymers, Newbury demonstrate this reciprocity, however there is still no consensus in this point. In the identification presented in this point, the coupling coefficient was obtained from measurements of actuation as free deflection, thus, a way to validate the reciprocity is to realize a sensor measurement. In this sense an experimental test is performed involving the measurements of the short circuit current generated by the ionic polymer when a tip displacement is imposed. The equation defining this sensor dynamics is the electrical equation Eq 3-69 here rewritten in the Laplace domain

$$i(s) = s\Theta_n r_n(s) + sC_P V(s) \qquad \textit{Eq 3-91}$$

Writing this equation in terms of the tip deflection $u_n(L_F,s)=W_n(L_F)r_n(s)$ and imposing a short circuit condition V(s)=0, the short circuit current equation is written as

$$i_{SC}(s) = \frac{s\Theta_n(s)}{W_n(L_F)} u_n(L_F, s) \qquad \textit{Eq 3-92}$$

The experimental test for the validation consists on applying a displacement at the tip of the free end of the ionic cantilever and measure the short circuit current generated by the polymer. The tip motion is applied with the LabWorks shaker and the displacement measured with the KEYENCE triangulation sensor. The applied displacement consists on a sinusoidal sweep from 0.1Hz-100Hz.

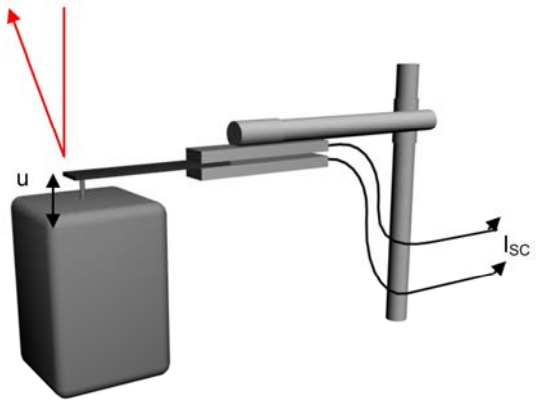

Figure 3-44 Configuration for sening characterization.

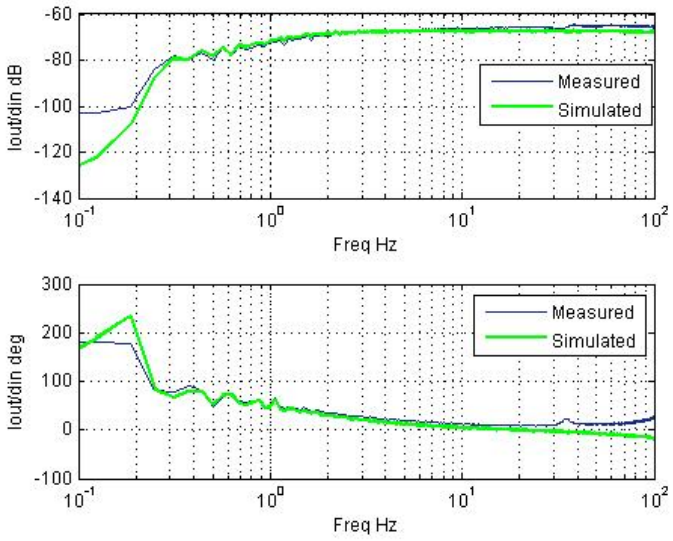

Figure 3-45 Experimental and simulated bode plot for the sensor transfer function short circuit current for an applied tip displacement.

Figure 3-45 shows the frequency response of the experimental results compared with simulations of the model. Both curves present a good match. Therefore as far as "$\Theta_n(s)$" is proportional to the piezoelectric coefficient, this experimental test has validated the bidirectional of the coupling term.

3.3.4. IPMC power generation performances

Once a model for the description of the dynamics of an ionic polymer has been proposed and the different parameters have been identified, the capabilities for the power generation of the ionic polymers are studied. The coupled equations, defining the mechanical and electrical equations of an ionic polymer cantilever beam forced to vibrate from its base, are here rewritten in the Laplace domain considering the influence of the electrical impedance and the frequency dependence in the material parameters.

$$s^2 m_n r_n(s) + s c_n r_n(s) + \frac{\Theta_n(s) R_{DC}}{R_{DC} C(s) s + 1} \frac{V_{in}(s)}{Z(s)} + K_n r_n(s) = F_{on}(s) \qquad \textit{Eq 3-93}$$

$$i(s) = s\Theta_n(s) r_n(s) + \frac{V_{in}(s)}{Z(s)} \qquad \textit{Eq 3-94}$$

In order to estimate the amount of power generated by the IPMC device submitted in a vibrating environment, it is useful to represent the system with its equivalent Thevenin circuit. This circuit consists on a voltage source in series with

the equivalent electrical impedance of the powering IPMC device. In the case of the ionic polymer, its equivalent electrical impedance is directly their electrical impedance. During the identification of the electrical impedance parameters it was observed that the electrical response of the ionic polymer was not affected by its mechanical boundary conditions. The small value of the pure electrical impedance of the polymer makes the current to be high enough to hide any change due to the mechanical motion. Therefore the equivalent Thevenin impedance is directly the electrical impedance Z(s)

$$Z_{TH}(s) = Z(s) = 2R_e + \frac{R_{DC}}{R_{DC}C(s)s + 1} \qquad \textit{Eq 3-95}$$

As in the case of the electrical measurements, during the identification of the mechanical impedance of the ionic polymer, it was observed that the electrical boundary condition did not affect the mechanical response. This is again a consequence of the small electrical impedance value of the polymers. Therefore the strain induced through the vibrations transmission due to base excitation is always the same whatever the electrical load conditions are. Thus, as far as ionic polymers are charge generators, the open circuit voltage is computed with the equation Eq 3-96 where “Isc” is the short circuit current.

$$V_{TH}(s) = I_{SC}(s)Z_{TH}(s) \qquad \textit{Eq 3-96}$$

where the equation defining the short circuit current for a base vibration is obtained from the model equations Eq 3-68 and Eq 3-69 considering Vin=0.

$$I_{SC}(s) = \frac{s\Theta_n(s)}{s^2 m_n + sc_n + K_n} F_{on}(s) \qquad \textit{Eq 3-97}$$

The power equation defining the generated power over an electrical load by a Thevenin circuit was presented in section 3.2.1. and it is here rewritten:

$$P_{av} = \frac{|V_L||I_L|}{2}\cos(\theta) = \left|\frac{V_{TH}}{Z_{TH} + Z_L}\right|^2 \frac{R_L}{2} \qquad \textit{Eq 3-98}$$

The power is maximized when the load impedance matches the equivalent Thevenin impedances. As far as the Thevenin equivalent impedance is a complex function with a real and a reactive part, the electrical load must be equal to its complex conjugated to assure the perfect match between impedances. However, at low frequencies the equivalent impedance behaves as a pure capacitor and at higher frequencies as a pure resistor, thus it has no sense to make a complete impedance match with a complex load. Assuming that a modulus match is done, the averaged power delivered to the resistive load is computed directly as

$$P_{av} = \frac{\left|V_{TH}(s) I_{SC}(s)\right|}{8} \qquad \textit{Eq 3-99}$$

This is an easy and direct way to compute the generated power from a polymer and permits the recognition of the parameters optimizing this power. Therefore through the evaluation of the short circuit generated current and the open circuit generated voltage, it is possible to determine the maximum power generation.

Two experimental tests are realized to determine the ability of the ionic polymer to generate power. The first one involves the measurement of the short circuit current, and the second one the measurement of the open circuit voltage. For the two experimental tests, the ionic polymer is clamped, with a conductive clamp, at the electromagnetic shaker that generates the base vibration. The shaker is forced to vibrate at a frequency ranging from 0.1 to 100 Hz. The measurements are obtained using a short circuit current driver for the first set of tests, and a high impedance voltage amplifier for the second set of tests. The experimental results are compared with simulations results, using the previously obtained model, for model validation.

In order to increase the voltage and current generation, a larger sample is used. The new sample has a length L=32mm, a width w=5mm and its free length is L_F=25mm.

Figure 3-46 shows the experimental and simulated transfer functions for the short circuit output current for a given base displacement. The system behaves as a high pass filter with a resonance frequency at a 24Hz. At the first resonance frequency of the mechanical structure, the transfer function presents a maximum of about -40dB that is equal to 0.01 A/m or 0.439μA/(m/s^2). The two curves match quite well in the range between 5 Hz and the first resonance at (24Hz). At a low frequency the mismatch is surely due to the small current measured. Far beyond the first resonance, the mismatch is considered as a consequence of the influence of the second resonance mode, which is not considered in the models

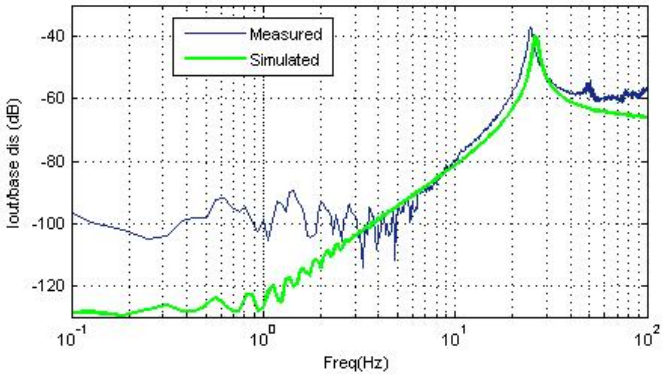

Figure 3-46 Experimental and simulated the short circuit curre vs base displacement transfer function (A/m).

Figure 3-47 shows the experimental and simulated obtained transfer functions for the Open Circuit output voltage. The dynamic behaviour for both curves matches quite well, while the magnitude of the simulated one is overestimated. At the first resonance frequency (24Hz), the experimental voltage found is about -12dB equal to 0.25V/m or 10.99μV/(m/s^2). The discrepancies between both curves can be attributed to different error sources. The generated voltage is computed as the product of the short circuit current and the electrical impedance, therefore the mismatch can be attributed to an error of the electrical impedance computation. The different parameters identified have been considered as dimensionless parameters. However this is only an assumption that comes from the modelling of the ionic polymer as a piezoelectric transducer where those parameters are dimensionless. A more complete study with samples with different dimensions must be realized in order to demonstrate the dimensionless of the identified parameters. Another possible source of error is on the concept of the model. Because of the small voltage generated by the membrane, the input base acceleration imposed when measuring the open circuit voltage (22m/s^2) was five times higher than when measuring the short circuit current (4.5m/s^2). Due to the softness of ionic polymers, this relatively small acceleration produces great deflections in the membrane. As can be noticed, the Euler-Bernoulli beam theory assumes low curvatures, so the great deflection is probably traduced into an overestimation of the generated voltage. Therefore the initial model must be changed somewhat to deal with the effect of high curvatures.

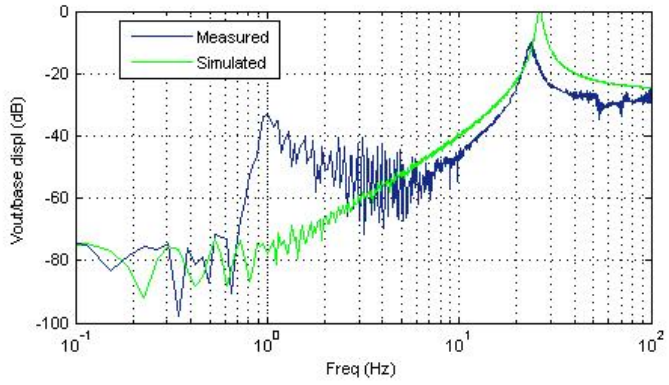

Figure 3-47 Experimental and simulated open circuit voltage vs base displacement transfer function (V/m).

However, from the two experimental tests, a measure of the maximum generated power can be extrapolated. Assuming an electrical load matched with the equivalent electrical impedance of the ionic polymer sample and the input frequency equal to the resonance frequency of 24Hz, the maximum power that can be generated from the membrane is computed with equation Eq 3-99 and taking into account the measured values of Isc=0.439μA/(m/s^2) and Voc=10.99μV/(m/s^2) gives a power generation about 0.61pW/(m/s^2)^2 at 24Hz. This amount of power is very small, although the computation is for 1m/s^2 and the beam can sustain higher accelerations for example 22m/s^2, therefore the amount of power would be 0.29nW, it is still insufficient to drive any sensor node.

In order to have a better comprehend of the responsible parameters in the generation, the power equation is written in terms of material and geometrical parameters. Substitution of equation Eq 3-97 and Eq 3-96 into Eq 3-99 leads the power equation:

$$P_{\text{mod}} = \frac{|Z(s)|}{8} \frac{|\Theta_n(s)|^2}{\left(\omega_n^2 - \gamma^2\right)^2 + \left(2\xi_n \omega_n \gamma\right)^2} \frac{\gamma^2}{m_n^2} |F_{on}(s)|^2 \qquad \textit{Eq 3-100}$$

The equation has certain dynamics due to the mechanical motion of the beam together with some dynamics due to the frequency dependence nature of the material parameters. Actually the part of the equation related to mechanics has a maximum at the resonance frequency of the system. As a harmonic oscillator, the beam presents a maximum deflection, thus, a maximum induced strain, at its resonance frequency. However when this frequency is high, the low pass filtering of the coupling term "$\Theta_n(s)$" due to the ionic nature of the transduction, drastically reduces the power generation. By the other hand the electrical impedance equation behaves as a high pass filter, therefore as the frequency rises an increase of power is expected.

However the square dependence of the power with the coupling term will therefore hide this effect. The induced force "$F_{on}(s)$" due to the base vibration of the system is proportional to base acceleration and mass. Therefore considering as input the base acceleration, and assuming an input frequency equal to the natural frequency of the beam, the power is maximized at low frequency. Considering the system working at resonance $\gamma=\omega_n$, and substituting the equation defining the induced force Eq 3-26, the power equation Eq 3-100 is rewritten as:

$$P_{\mathrm{mod}} = \frac{|Z(s)|}{8} \frac{|\Theta_n(s)|^2}{4\xi_n^2 \omega_n^2} G_n^2 A_{in}^2 \qquad \textit{Eq 3-101}$$

That is the equation defining the power generated for a given input acceleration "A_{in}". The equation shows that the power is maximized for low frequency vibrations, however it is needed to increase the impedance and the coupling term to increase the generated power.

Now it is worth to make a comparison with the different models proposed along this chapter first with the piezoelectric and then with the general model. The ionic polymer power generation equation Eq 3-100 has the same form to the equation from the piezoelectric case when the impedance match is maximized with the modulus Eq 3-54. In that equation, the natural frequency "ω_n" was different than "ω_t", however in the case of ionic polymers the electrical equation do not affect the mechanical one, thus $\omega_n=\omega_t$. Taking into account this equality, considering the ionic electrical impedance as a pure capacitor and the coupling coefficient as a constant, both power equations are the same.

At the beginning of this chapter, a general model to describe the maximum power that can be extracted from a vibrating power source was presented. From a mechanical point of view, a main conclusion was extracted. The conclusion point out that the power generated is maximized when the mechanical damping equals the electrical induced damping. Nevertheless the measurements realized in the ionic polymer have shown that the electrical boundary conditions do not affect the mechanical response, therefore this damping equality never happens. Therefore the equation for the power generation with the general model considering the ionic polymer as a transducer, must be changed somewhat. We consider the equation of the general model where the power dissipated in the electrical domain is computed as a power loss in an electrical induced damping constant "ξ_{elec}" Eq 3-19. Then, due to the small value of the electrical impedance $\xi_{elec}<<\xi_{mec}$ the denominator of the equation is rewritten as

$$P_{av} = \frac{m\xi_{elec} A_{in}{}^2}{4(\xi_{mec}+\xi_{elec})^2 \omega_n} = \frac{m\xi_{elec} A_{in}{}^2}{4\xi_{mec}^2 \omega_n} \qquad \textit{Eq 3-102}$$

This equation has the same form than the equation for ionic polymers (Eq 3-101) assuming the electrical load resistor matched with the equivalent Thevenin electrical impedance of the polymer and writing the electrical induced damping ratio in terms of the polymer material.

$$\xi_{elec} = \frac{\Theta_n^2(s)Z(s)}{8m\omega_n} \qquad \textit{Eq 3-103}$$

Although ionic polymers present high coupling terms at low frequencies, their low electrical impedance value reduces drastically the ability to generate electrical power. The high permittivity values of ionic polymers reduce the internal generated electric field, thus the electrical power generated. A possible way to decrease the dielectric permittivity, thus to increase the impedance, is by means of a change in the internal counter-ions. The experimental tests realized in this section have been done with a Nafion membrane with Na^+ as the counter-ions. In [Farinholt2004] a study of the influence of different counter-ions in the performances of an ionic polymer is presented. Experimental results show that the sensor sensitivity using Li+ as counter-ions is higher than with Na+. The use of different counter ions could increase the impedance and at the same time the coupling, thus it could be a possible solution to increase the total power generated.

3.3.5. Conclusions

The analysis presented in this point has been devoted to study the capabilities to convert mechanical vibrations into electrical energy using ionic polymers. The intrinsic nature of these polymers to work as sensors, thus to convert internal strain in electrical current, together with the fact that these polymers are soft and biocompatible, thus could be used in applications where the piezoelectric material can not, give rise to this study.

The complex internal physics responsible of the ionic polymers transduction have entailed the development of a gray box model to predict the amount of harvested power. The model adopted is based in the piezoelectric model however the material parameters are experimentally identified with an IPMC strip. The sample used is a Nafion based strip with dimensions of 2cm length and 0.5cm width and the Na+ as counter ions. Experimental tests have been performed on this sample under hydration conditions in equilibrium with the ambient. The measurements have shown the sample poor capability to convert mechanical vibrations into electrical energy. The sample has been tested under conditions of typical vibrations inside a building. Acceleration of $1m/s^2$ at the resonance frequency of the sample 24Hz leave an electrical power generation with the IPMC strip assuming a perfect impedance match of $0.61pW/(m/s^2)^2$. This amount of power is not enough to drive any sensor node even if an energy storing electrical circuit could be designed. Compared to the piezoelectric transducer based used at section 3.2.- with the same vibration conditions that leave a generation of $86\mu W/(m/s^2)^2$ ionic polymer generated several orders of magnitude smaller powers. However the gray box model developed has permitted to identify the electrical impedance of the ionic polymer as the main factor limiting the energy generation. Therefore methods to increase this impedance while maintaining the ability to generate electrical charge from mechanical strain are the key point in the development of energy harvesting system with ionic polymers. In this sense, efforts can be done in two directions. According to the application restrictions, some specific mechanical structures could be designed to maximize the induced strain in the material, however in order to decrees the electrical impedance, multilayer structures in serial configuration must be designed. While the same current is generated, the serial configuration increases the electrical impedance thus the generated power will be proportional to the number of layers. The other research effort direction focuses on the optimization of physical reactions and material parameters as changing or mixing different counter-ions, improvements in the membrane polymerization, etc.

Although the model developed and the experimental results conclude that the power generated is very small the work developed in this last point have permitted a better comprehend in the internal dynamics of these polymers. The gray box model developed together with the experimental tests and methods developed for the identification are also valid for future design where ionic polymers could work as sensors or as actuators.

3.4. References:

[Badel2006] A. Badel, D. Guyomar, E. Lefeuvre, and C. Richard, "Piezoelectric energy harvesting using a synchronized switch technique," *Journal of Intelligent Material Systems and Structures,* vol. 17, pp. 831-839, 2006.

[Bonomo2006] C. Bonomo, L. Fortuna, P. Giannone, S. Graziani, and S. Strazzeri, "A model for ionic polymer metal composites as sensors," *Smart Materials & Structures,* vol. 15, pp. 749-758, 2006.

[Bonomo2006_2] C. Bonomo, L. Fortuna, P. Giannone, S. Graziani, and S. Strazzeri, "Improved frequency investigation of IPMC based sensors," *2006 Ieee Instrumentation and Measurement Technology Conference Proceedings, Vols 1-5,* pp. 2338-2341, 2006.

[Bonomo2008_2] C. Bonomo, L. Fortuna, P. Giannone, S. Graziani, and S. Strazzeri, "A resonant force sensor based on ionic polymer metal composites," *Smart Materials & Structures,* vol. 17, 2008.

[Brufau2008] J. Brufau-Penella, M. Puig-Vidal, P. Giannone, S. Graziani, and S. Strazzeri, "Characterization of the harvesting capabilities of an ionic polymer metal composite device," Smart Materials & Structures, vol. 17, 2008

[Brufau2008_3] J. Brufau-Penella. M. Puig-Vidal. "Piezoelectric Energy harvesting improvement with complex conjugate impedance matching". Journal of Intelligent Material Systems and Structures OnlineFirst, published on September 29, 2008

[Colomer2007] J. Colomer, J. Brufau, P. Miribel, A. Saiz-Vela, M. Puig, and J. Samitier, "Novel autonomous low power VLSI system powered by ambient mechanical vibrations and solar cells for portable applications in a 0.13 mu technology," *2007 Ieee Power Electronics Specialists Conference, Vols 1-6,* pp. 2786-2791, 2007.

[Colomer2007_2] J. Colomer, J. Brufau, P. Miribel-Catala, A. Saiz-Vela, M. Puig-Vidal, and J. Samitier, "Power conditioning circuitry for a self-powered mobile system based on an array of micro PZT generators in a 0.13 mu m technology," *2007 Ieee International Symposium on Industrial Electronics, Proceedings, Vols 1-8,* pp. 2353-2357, 2007.

[El-hami2001] M. El-hami, R. Glynne-Jones, N. M. White, M. Hill, S. Beeby, E. James, A. D. Brown, and J. N. Ross, "Design and fabrication of a new vibration-based electromechanical power generator," *Sensors and Actuators a-Physical,* vol. 92, pp. 335-342, 2001.

[Elvin2001] N. G. Elvin, A. A. Elvin, and M. Spector, "A self-powered mechanical strain energy sensor," *Smart Materials & Structures,* vol. 10, pp. 293-299, 2001.

[Fang2006] H. B. Fang, J. Q. Liu, Z. Y. Xu, L. Dong, L. Wang, D. Chen, B. C. Cai, and Y. Liu, "Fabrication and performance of MEMS-based piezoelectric power generator for vibration energy harvesting," *Microelectronics Journal,* vol. 37, pp. 1280-1284, 2006.

[Farinholt2004] K. Farinholt and D. J. Leo, "Modeling of electromechanical charge sensing in ionic polymer transducers," Mechanics of Materials, vol. 36, pp. 421-433, 2004.

[Franklin2003] J. W. Franklin 2003 Electromechanical modelling of encapsulated ionic polymer transducers Thesis Faculty of the Virginia Polytech Institute

[Guyomar2005] D. Guyomar, A. Badel, E. Lefeuvre, and C. Richard, "Toward energy harvesting using active materials and conversion improvement by nonlinear processing," *Ieee Transactions on Ultrasonics Ferroelectrics and Frequency Control,* vol. 52, pp. 584-595, 2005.

[Jeon2003] Y. Jeon, R. Sood, L. Steyn, and S. G. Kim Energy Harvesting MEMS Devices Based on d33 Mode Piezoelectric Pb(Zr,Ti)O3 Thin Film Cantilever CIRP Seminar on Micro and Nano Technology Copenhagen, Denmark, November 13-14, 2003

[Kasyap2002] A. Kasyap, J. Lim, D. Johnson, S. Horowitz, T. Nishida, K. Ngo, M. Sheplak and L. Cattafesta 2002 Energy reclamation from a vibrating piezoceramic composite beam *Proc. 9th Int. Congr. on Sound and Vibration (Orlando, FL)* Paper No. 271

[Kymissis1998] J. Kymissis, C. Kendall, J. Paradiso, and N. Gershenfeld, "Parasitic power harvesting in shoes," *Digest of Papers. Second International Symposium on Wearable Computers (Cat. No.98EX215)|Digest of Papers. Second International Symposium on Wearable Computers (Cat. No.98EX215),* pp. 132-9|xiv+174, 1998.

[Lefeuvre2007] E. Lefeuvre, D. Audigier, C. Richard, and D. Guyomar, "Buck-boost converter for sensorless power optimization of piezoelectric energy harvester," *Ieee Transactions on Power Electronics,* vol. 22, pp. 2018-2025, 2007.

[Martin2005] B. R. Martin 2005 Energy harvesting applications of ionic polymers Thesis The Faculty of the Virginia Polytech Institute (submitted)

[Nemat-Nasser2002] S. Nemat-Nasser, "Micromechanics of actuation of ionic polymer-metal composites," *Journal of Applied Physics,* vol. 92, pp. 2899-2915, 2002.

[Newbury2003] K. M. Newbury and D. J. Leo, "Linear electromechanical model of ionic polymer transducers - Part I: Model development," *Journal of Intelligent Material Systems and Structures,* vol. 14, pp. 333-342, 2003.

[Nishida2005] T. Nishida, L. N. Cattafesta, M. Sheplak , K. Ngo Resonant energy MEMS array and system including dynamically modifiable power processor 2005 United States Patent 6954025

[Otis2003] B. P. Otis and J. M. Rabaey, "A 300-mu W 1.9-GHz CMOS oscillator utilizing micromachined resonators," *Ieee Journal of Solid-State Circuits,* vol. 38, pp. 1271-1274, 2003.

[Ottman2002] G. K. Ottman, H. F. Hofmann, A. C. Bhatt, and G. A. Lesieutre, "Adaptive piezoelectric energy harvesting circuit for wireless remote power supply," *Ieee Transactions on Power Electronics,* vol. 17, pp. 669-676, 2002.

[Ottman2003] G. K. Ottman, H. F. Hofmann, and G. A. Lesieutre, "Optimized piezoelectric energy harvesting circuit using step-down converter in discontinuous conduction mode," *Ieee Transactions on Power Electronics,* vol. 18, pp. 696-703, 2003.

[Rabaey2000] J. M. Rabaey, M. J. Ammer, J. L. da Silva, D. Patel, and S. Roundy, "PicoRadio supports ad hoc ultra-low power wireless networking," *Computer,* vol. 33, pp. 42-+, 2000.

[Ramsay2001] M. J. Ramsay and W. W. Clark, "Piezoelectric energy harvesting for bio MEMS applications," *Smart Structures and Materials 2001: Industrial and Commercial Applications of Smart Structures Technologies,* vol. 4332, pp. 429-438, 2001.

[Richards] C. D. Richards, M. J. Anderson, D. F. Bahr, and R. F. Richards, "Efficiency of energy conversion for devices containing a piezoelectric component," *Journal of Micromechanics and Microengineering,* vol. 14, pp. 717-721, 2004.

[Ronudy2003] S. Roundy Energy scavenging for wireless sensor nodes with a focus on vibration to electricity conversion Berkeley, CA, 2003.

[Roundy2003_2] S. Roundy, P. K. Wright, and J. Rabaey, "A study of low level vibrations as a power source for wireless sensor nodes," *Computer Communications,* vol. 26, pp. 1131-1144, 2003.

[Roundy2004] S. Roundy and P. K. Wright, "A piezoelectric vibration based generator for wireless electronics," *Smart Materials & Structures,* vol. 13, pp. 1131-1142, 2004.

[Roundy2004_2] S. Roundy, D. Steingart, L. Frechette, P. Wright, and J. Rabaey, "Power sources for wireless sensor networks," *Wireless Sensor Networks. First European Workshop, EWSN 2004. Proceedings. (Lecture Notes in Comput. Sci. Vol.2920)|Wireless Sensor Networks. First European Workshop, EWSN 2004. Proceedings. (Lecture Notes in Comput. Sci. Vol.2920),* pp. 1-17|xiv+363, 2004.

[Sakamoto1999] S. Sakamoto, T. Hirata, T. Kobayashi, and K. Kajiwara, "Vibration analysis considering higher *harmonics* of electromagnetic forces for rotating electric machines," *Ieee Transactions on Magnetics,* vol. 35, pp. 1662-1665, 1999.

[Shahinpoor2000] M. Shahinpoor and K. J. Kim, "The effect of surface-electrode resistance on the

performance of ionic polymer-metal composite (IPMIC) artificial muscles," *Smart Materials & Structures,* vol. 9, pp. 543-551, 2000.

[Sodano2004] H. A. Sodano, G. Park, and D. J. Inman, "Estimation of electric charge output for piezoelectric energy harvesting," *Strain,* vol. 40, pp. 49-58, 2004.

[Sodano2005] H. A. Sodano, D. J. Inman, and G. Park, "Generation and storage of electricity from power harvesting devices," *Journal of Intelligent Material Systems and Structures,* vol. 16, pp. 67-75, 2005.

[Sodano2006] H. A. Sodano, J. Lloyd, and D. J. Inman, "An experimental comparison between several active composite actuators for power generation," *Smart Materials & Structures,* vol. 15, pp. 1211-1216, 2006.

[Stephen2006] N. G. Stephen, "On energy harvesting from ambient vibration," *Journal of Sound and Vibration,* vol. 293, pp. 409-425, 2006.

[Trindade2004] M. A. Trindade, A. Benjeddou, and R. Ohayon, "Modeling of frequency-dependent viscoelastic materials for active-passive vibration damping," *Transactions of the ASME. Journal of Vibration and Acoustics|Transactions of the ASME. Journal of Vibration and Acoustics,* vol. 122, pp. 169-74, 2000.

[Umeda1996] M. Umeda, K. Nakamura, and S. Ueha, "Analysis of the transformation of mechanical impact energy to electric energy using piezoelectric vibrator," *Japanese Journal of Applied Physics Part 1-Regular Papers Short Notes & Review Papers,* vol. 35, pp. 3267-3273, 1996.

[Umeda1997] M. Umeda, K. Nakamura, and S. Ueha, "Energy storage characteristics of a piezo-generator using impact induced vibration," *Japanese Journal of Applied Physics Part 1-Regular Papers Short Notes & Review Papers,* vol. 36, pp. 3146-3151, 1997.

[Verma1998] S. P. Verma and A. Balan, "Experimental investigations on the stators of electrical machines in relation to vibration and noise problems," *Iee Proceedings-Electric Power Applications,* vol. 145, pp. 455-461, 1998.

[Williams1996] C. B. Williams and R. B. Yates, "Analysis of a micro-electric generator for microsystems," *Sensors and Actuators a-Physical,* vol. 52, pp. 8-11, 1996.

4. FINAL CONCLUSIONS

This thesis investigated the use of “smart materials” in microrobotics systems. The thesis focused on three electroactive induced strain materials: the piezoelectric ceramics, piezoelectric polymers and ionic polymers. The similitude in their way to react to external stimuli demands a study to discern the performances and capabilities for each one. In particular the work was centered on the study of piezoelectric polymers and ionic polymers to form part in a microrobotic motion control system. Moreover the thesis studied the ability of piezoelectric ceramics and ionic polymers to harvest vibration energy from the ambient.

The capabilities to use piezoelectric polymers as a low voltage actuated microstructures for mm^3 microrobot motion control were studied. The first microstructure studied consists on 10 layers of P(VDF-TrFE) polymers with a 2μm thickness stacked in parallel and microstructured on a flexible base substrate to form a monomorph structure. This structure served as the leg of the microrobot and is 2mm length and 0.4mm width. The good knowledge of the underlying physics acting in the transduction of a piezoelectric polymer permitted the development of a theoretical model to study the performances of the actuator. The model developed was based on the analysis of the transversal vibrations on an Euler-Bernoulli cantilever beam. It described the dynamic motion for the different vibration modes of the beam and the maximum achievable force of the actuator in terms of the material, geometrical and structural parameters. A real microrobot leg was experimentally tested. The tests demonstrated the possibility to drive the structure with low voltage signals. The leg was driven at its resonance frequency of 7034Hz with a 3.3V square voltage signal and a 14μm peak to peak deflection motion was measured. Comparisons between theoretical model predictions and experimental results showed some mismatches attributed to deviations in the material parameters. The need for developing multilayer structures since thin P(VDF-TrFE) layers generate low forces, probably entailed deviations between design specification and final prototype. The second microstructure studied was a vibrating contact sensor tool for the microrobot to avoid object collision. The microstructure had the same form than the microrobot leg but in this case 2 of the 10 P(VDF-TrFE) active layers were used as sensors while the other 8 layers were low voltage actuated. The theoretical model developed for the leg of the microrobot was extended to predict the generated voltage in the sensor layers while the tool was actuated. The analytical model was presented along with a lumped equivalent electrical circuit that describe the response of the tool. The circuit was useful to design the electronic circuits needed for controlling the tool. Experimental test realized on a real microrobot tool showed the ability to use embedded layers as displacement sensors for the tool. When the tool was driven at its resonance frequency of 3943Hz with 3.3V a 164mVpp were measured in the senor layers.

The use of ionic polymers as motion actuators working underwater was studied. The dynamic response of these materials is subjected to time variations and is sometime unpredictable therefore there is the need to implement control strategies to assure a certain dynamic of motion. In this thesis an adaptive control strategy was been implemented. The control adopted was the Model Reference Adaptive Control (MRAC) where the final dynamic of the system was defined by the reference model. The control was designed for a 1cm length ionic polymer strip. The dynamic response of the beam was modeled and then used as the reference model. In this case the model adopted was a second order empirical model with one cero and two poles to model the fast bending and the slow back relaxation. A setup was build for experimentally tested the control system. In order to avoid fluctuations in the parameters estimation due to unmodelled dynamics or noise perturbation, the control law was implemented along with two robustifying techniques: the parameter projection and the dead zone. The final control was able to follow the model reference dynamic with an error less than 10% from 100mHz up to 1Hz using an adaptation gain of 1. Increasing the adaptation gain would increase the bandwidth however the system would be more sensible to perturbations.

One aspect that is limiting the use of ionic polymers in microrobotic system is the difficulty in developing patterned electrodes and its compatibility with MEMS process. In this thesis a method compatible with MEMS technology for developing electrodes was presented. The method consisted on using a physical vapour deposition which is compatible with photolithography processed instead of the chemical deposition technique that is incompatible. In order to improve the adhesion of the metal in the polymer surface and also to increase the area of contact, the polymer surface was first treated with a reactive ion etching. The electrode deposition technique was applied to a Nafion117 membrane. The sample was first etched with the RIE using oxygen plasma at 50mTorr with an RF power of 240W during 7 minutes. The etching produced a needle shaped surface with 2μm high needles separated a 1μm distance approximately. Then the metals were deposited with an Evaporator. A 15nm Titanium layer was first deposited to improve the adhesion with the polymer, then a 400nm Gold layer was deposited to form the final electrode. Once the electrodes were built, a counter ion exchange process was performed to increase the transduction effect of the ionic polymer. The sample was immersed in a 1.5N NaCl solution during three says at 50º to exchange the internal H+ cations by the Na+. The dynamic motion response of a 2.5cm length and 0.5cm width developed sample was tested underwater along with a chemical deposited sample with the same dimensions. The experimental test showed the same dynamic response although the magnitude of the obtained motion is reduced one order of magnitude with this new technique. This performances reduction was attributed to the lower effective area of contact between metal and polymer.

This thesis also investigated the use of piezoelectric ceramics to generate electrical energy from mechanical vibrations. The mechanical configuration studied was based on a piezoelectric beam that exploited the 31 mode of operation anchored

to a mechanical vibrating source. An analytical theoretical model based on the analysis of the transversal vibrations on an Euler-Bernoulli cantilever beam was performed. The model obtained an equation defining the power delivered to an electrical load and was used to define the optimum load conditions to maximize the power generated for the different vibration modes. Two conditions for the maximum generation were obtained, one considering complete impedance match using a complex electrical load and the other considering a modulus match using a resistive electrical load. An effectiveness function was defined as the ratio between the powers obtained with the two conditions. The power generation capability of a commercial piezoelectric based QP40w transducer was experimentally tested at different vibration modes. First the power generated using a modulus match was tested. The power measured was 86μW/(m/s^2) (at 22Hz, with 25.6kΩ resistive load), 9.34μW/(m/s^2) (at 148Hz with 3kΩ resistive load) and 0.178μW/(m/s^2) (at 935Hz with 500Ω resistive load) corresponding to the first, second and fourth resonance mode. This power represented the 60%, 65% and 80% of the maximum power that could be extracted with a complete match for the first, second and fourth modes. Unfortunately the complete match was not possible for the first and two modes, nevertheless it was possible to make a complete match at the fourth mode with a load inductor of 50mH and a load resistor of 200Ω given the maximum power of 0.24μW. This value represents an increase approximately of 20% with respect the amount of power harvested with the modulus match.

In any energy harvesting system, the generated electrical power must be treated some way to finally drive a sensor node or recharge a battery. In this thesis an electronic circuit was implemented to store the energy optimally from the QP40w when forced to vibrate at its second vibration mode at 148Hz with 10m/s^2 which could be the case of a milling machine. The circuit implemented consisted on a full bridge rectifier with a capacitor for filtering and a buck-boost converter working in its DCM. The input converter was configured with an input resistance fixed at the optimal load resistance for the maximum power generation. Due to the non-linear effect of the rectifier the optimal value was modified with a factor approximately π/2 thus it was configured with a Rin=5600Ω. The final system was able to deliver 700μW of DC power to a sensor node even if the load resistance of this node changes. If the node to supply requires more power, this must be burst.

In the last section of this thesis the capabilities to harvest power using ionic polymers were studied. The work was performed on air with a 2cm length and 0.5cm width Nafion based sample with Na+ counter ions. The sample was in hydration equilibrium with the medium. The analysis was realized developing a gray-box model to describe the behaviour of the transducer. The model started using the piezoelectric theoretical model developed. The model was then modified through the observation of different experimental results and the identification of material parameters. The first change with respect the piezoelectric models was the electrical impedance. Ionic polymers have an electrode resistance, moreover these polymers behave as big capacitors at low frequency and as a resistor when the frequency

increases. This electrical response was modelled and identified as a capacitor with a frequency dependent permittivity term. The other change was observed in the coupling constant. Ionic polymers involve motion of hydrated cations thus the transduction effect is modelled with a coupling constant low pass filter. The mechanical impedance was modelled with a young modulus and a damping constant experimentally identified. The bidirectionality of the model transduction was experimentally validated. Once the gray-box modelled was obtained, the ability to generate power of the ionic polymer sample was tested. The sample was tested under conditions of typical vibrations inside a building. Acceleration of $1m/s^2$ at the resonance frequency of the sample 24Hz leaved an electrical power generation with the IPMC strip assuming a perfect impedance match of $0.61pW/(m/s^2)^2$. The amount of power generated by the ionic polymer strip was very small, however the development of the gray-box model permitted the identification of the electrical impedance as the main responsible of the poor harvesting capabilities. Thus methods to increase this impedance must be addressed.

A. APPENDIX A

The appendix here reported is devoted to develop the mathematical equations describing the electromechanical dynamic behavior of a cantilever beam composed with smart materials forming different kind structures.

Smart materials for microrobotics are commonly used in cantilever clamped-free configuration when they work as actuators, sensor or as energy harvesters. It is possible to form cantilever configurations in different ways depending on the relative distribution of the active element of the beam. It is sometimes preferable to use a bimorph structure with two active layers, or to use a monomorph structure with a base substrate and one active layer, or to use multilayer structures with several active layers. In this appendix the constitutive equations of these structures under different excitation conditions are developed and presented.

The first part of this analysis is a repetition of classical material resistance theory and engineering vibrations theory. This theory is here repeated for the completeness of the thesis, and to provide it with the mathematical tools needed for the development of the analysis realized.

Once the bases of the mathematical analysis are presented, the first active structure analyzed is a bimorph structure. The analysis is devoted to find the constitutive equations describing the dynamic response of the bimorph beam for the different vibration modes as a 2x2 matrix which combines the extensive parameters force applied at the tip "F" and applied electrical voltage "V_{in}" with the intensive parameters defection "u" and electrical charge "Q".

After the dynamic response of the bimorph is analyzed in detail, a generic multilayer structure is studied. First of all the position of the neutral axis inside the beam is calculated. Then the same procedure realized with the bimorph structure to obtain its constitutive equations is adopted formulating the equations relatively to this axis.

The next point studies a special application of a multilayer structure where one of the active layers is used to sense the tip deflection while the other layers are used actuators to produce this deflection. This structure is named sensor/actuator structure. Following the same type of derivation, the actuating response and the sensitivity of the sensor are analyzed. The analysis is performed for two cases, these are: assuming a voltage measurement and assuming a charge measurement in the sensor layer.

The last part of the appendix presents the derivation of the force equation of a multilayer beam considering as a new extensive mechanical variable a displacement vibration at the clamped end of the beam.

A.1. Euler-Bernoulli cantilever beam

During many years the problem of vibration transmission in a beam has been treated by different authors. The more consolidated model was proposed by Euler-Bernoulli in the 18th century. The model proposed that the curvature of a beam should be proportional to the bending moment applied in that point. Next they presented the differential equations of motion of the beam. Another model was proposed by Rayleigh who considered the influence of the rotation through the axial axes of the beam. Then Thimosheko proposed another model and considered rotations and shear effects. The study presented here is based in the Euler-Bernoulli model, no rotation and shear effects are considered. In the next lines a detailed study of the governing equations of the motion of a beam with the Euler-Bernoulli model is presented. Although the main development can be consulted in many mechanics vibrations books it has been considered of interest to have all this theory here rewritten. Then when the piezoelectric elements are introduced inside the beam, the theoretical development is better comprehended.

In the following lines the longitudinal vibration transmission in the beam from Figure A-1 are studied. Let's consider that the deflection of the beam in the "y" direction and defined with the function "u(x,t)". The beam has a transversal section equal to "A" and a rigidity term defined as "YI" where "Y" is the young modulus and "I" is the moment of inertia of a section area through in the plane "xy". From the theory on materials resistance it is possible to demonstrate that there is a bending moment "M(x,t)" that is related with the deflection as

$$M(x,t) = YI\frac{\partial^2 u(x,t)}{\partial x^2} \qquad \textit{EqA.1}$$

In order to obtain a solution for the deflection of the beam, the force equation governing the motion of an infinitesimal element of the beam is considered. Assuming that the deflection is small enough to avoid a deformation in the lateral walls of the element "dx", the equilibrium of forces equation is written as:

$$\left(V_{SH}(x,t) + \frac{\partial V_{SH}(x,t)}{\partial x}dx\right) - V_{SH}(x,t) + f(x,t)dx = \rho A dx \frac{\partial^2 u(x,t)}{\partial t^2} \qquad \textit{EqA.2}$$

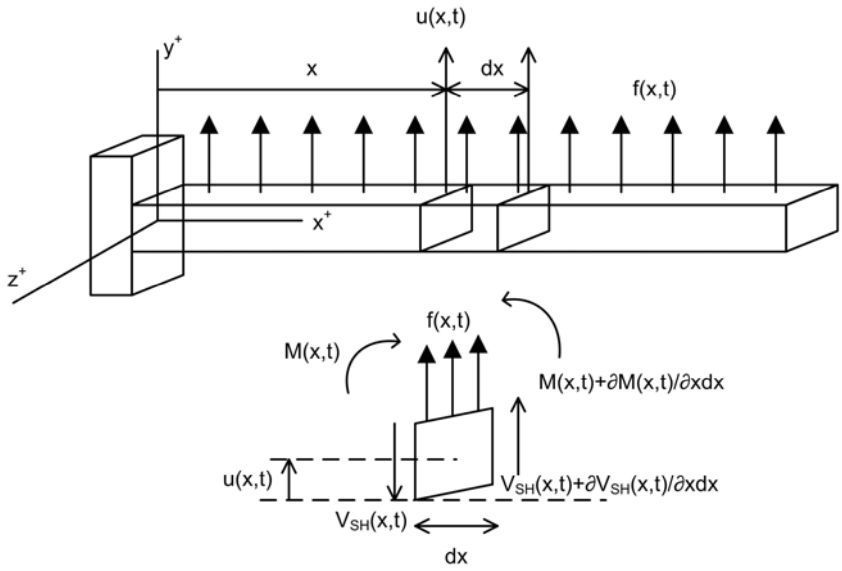

Figure A-1: Simple beam in transverse vibration and a free body diagram of a small element of the beam as it is deformed by a distributed force per unit length, denoted by f(x,t).

where "$V_{SH}(x,t)$" is known from material resistance theory as shear force, "f(x,t)" is the external force applied for unit length and the term at the right of the equation is the inertial term. Once the force equation is presented the analysis of the internal moments acting in the infinitesimal element are considered. Assuming no rotation the summation of the moments acting around the "z" axis is equal to cero.

$$\left(M(x,t)+\frac{\partial M(x,t)}{\partial x}dx\right)-M(x,t)+\left(V(x,t)+\frac{\partial V(x,t)}{\partial x}dx\right)dx+\left(f(x,t)dx\right)\frac{dx}{2}=0$$

EqA.3

Simplifying the equation

$$\left(\frac{\partial M(x,t)}{\partial x}+V(x,t)\right)dx+\left(\frac{\partial V(x,t)}{\partial x}+\frac{f(x,t)}{2}\right)(dx)^2=0$$

EqA.4

Assuming that "dx" is very small, it is possible to consider $dx^2=0$, therefore the equation that relates the shear force with the spatial variation of the bending moment is obtained.

$$V(x,t)=-\frac{\partial M(x,t)}{\partial x}$$

EqA.5

Substituting this equation into the force equation EqA.2 gives

$$-\frac{\partial^2 M(x,t)}{\partial^2 x}dx + f(x,t)dx = \rho A dx \frac{\partial^2 u(x,t)}{\partial t^2} \qquad \textit{EqA.6}$$

Substitute the equation relating moment and deflection EqA.1 into EqA.6 and divide by "dx"

$$\rho A \frac{\partial^2 u(x,t)}{\partial t^2} + \frac{\partial^2}{\partial x^2}\left(YI \frac{\partial^2 u(x,t)}{\partial x^2} \right) = f(x,t) \qquad \textit{EqA.7}$$

This equation is known as the undamped Euler-Bernoulli beam equation. The equation does not have any dissipative force to model the losses in the system. Therefore it is necessary to introduce a loss term. There are different dissipative sources that actuate in this kind of systems. The more common are the internal friction between material planes and the external friction with the air. Both forces are proportional to the velocity of the beam. Therefore they are introduced in the force equation as:

$$\rho A \frac{\partial^2 u(x,t)}{\partial t^2} + YI \frac{\partial^4 u(x,t)}{\partial x^4} + BI \frac{\partial^5 u(x,t)}{\partial x^4 \partial t} + \beta \frac{\partial u(x,t)}{\partial t} = f(x,t) \qquad \textit{EqA.8}$$

The internal friction is modeled with the constant "B" and the external friction with the constant "β". From now on, the unique friction term considered is the internal friction. Therefore the force equation remains.

$$\rho A \frac{\partial^2 u(x,t)}{\partial t^2} + YI \frac{\partial^4 u(x,t)}{\partial x^4} + BI \frac{\partial^5 u(x,t)}{\partial x^4 \partial t} = f(x,t) \qquad \textit{EqA.9}$$

This equation is a partial differential equation PDE. This type of equations is treated first as the unforced equation solution and then the forced equation is obtained. Let's consider the unforced equation

$$\rho A \frac{\partial^2 u(x,t)}{\partial t^2} + YI \frac{\partial^4 u(x,t)}{\partial x^4} + BI \frac{\partial^5 u(x,t)}{\partial x^4 \partial t} = 0 \qquad \textit{EqA.10}$$

This equation has temporal and spatial differential terms. In order to obtain a solution of this equation the method of separation of variables is adopted. For this purpose the deflection equation is described as "u(x,t)=W(x)r(t)" the product of a temporal "r(t)" equation and a spatial equation "W(x)". Substituting this equation in the unforced equation gives

$$\rho A W(x)\ddot{r}(t) + YIW''''(x)r(t) + BIW''''(x)\dot{r}(t) = 0 \qquad \textit{EqA.11}$$

wre dots denote temporal differentiation and comas denote spatial differentiation. It is possible to rewrite this equation as.

$$-\frac{EI}{\rho A}\frac{W(x)''''}{W(x)}=\frac{\ddot{r}(t)}{r(t)+\frac{B}{E}\dot{r}(t)}=\omega^2 \qquad \textit{EqA.12}$$

At the left side of the equation there are the spatial functions and at the right side of the equation there are the temporal functions. This equality must be always a constant. In this case for convenience the constant is defined as "ω^2". This constant will define the natural frequencies of the beam.

Once the equation is equaled to a constant it is possible to find the solution for the spatial function, the solution will define the natural frequencies and mode shapes of the beam. Now the spatial equation is written as

$$W(x)''''-\omega^2\frac{\rho A}{YI}W(x)=0 \qquad \textit{EqA.13}$$

A mathematic operator is defined as $\nabla^2=d^4/dx^4$, this operator is introduced in the equation

$$\left(\nabla^2-\lambda^4\right)W(x)=0 \qquad \textit{EqA.14}$$

where a new parameter named normalized frequency or spatial frequency is introduced as "λ".

$$\lambda^4=\omega^2\frac{\rho A}{EI} \qquad \textit{EqA.15}$$

The equation EqA.14 defines the eigenvalues and eigenvectors of the operator. Therefore there are an infinite number of eigenvalues "λ" associated each one to a eigenvectors "W(x)" that are solution of the equation. A possible solution to the differential equation EqA.14 is

$$W(x)=C_1\sin\lambda x+C_2\cos\lambda x+C_3\sinh\lambda x+C_4\cosh\lambda x \qquad \textit{EqA.16}$$

In the differential temporal equation there are four order derivative terms, therefore there will be four integration constants "C_x" that must be obtained from the boundary conditions. Up to now the theory developed is useful for any bending slender beam even if it has different mechanical configuration. Now the boundary conditions are imposed to obtain a solution for the spatial equation or mode shape of the system. In this case the clamped-free boundary conditions are:

W(0)=0, the deflection in the clamped end is always cero

W'(0)=0, The curvature angle in the clamped end is cero

W''(L_F)=0, The bending moment in the free end is cero.

W'''(L_F)=0, The shear force in the free end is cero.

From the first and third condition it is obtained that C_1=-C_3 and C_2=-C_4. The other two conditions are represented in its matrix form

$$\begin{pmatrix} W'(0) \\ W'''(L_F) \end{pmatrix} = \begin{pmatrix} -\sin\lambda L_F - \sinh\lambda L_F & -\cos\lambda L_F - \cosh\lambda L_F \\ -\cos\lambda L_F - \cosh\lambda L_F & \sin\lambda L_F - \sinh\lambda L_F \end{pmatrix} \begin{pmatrix} C_1 \\ C_2 \end{pmatrix} = \begin{pmatrix} 0 \\ 0 \end{pmatrix} \qquad \textit{EqA.17}$$

To avoid a trivial solution as W(x)=0, the matrix must be a singular matrix, therefore its determinant must be equal cero.

$$1 + \cos\lambda L_F \cosh\lambda L_F = 0 \qquad \textit{EqA.18}$$

This equation is the characteristic equation of the system and defines the eigenvlaues "λ_n" of the equation. There are an infinite number of values that are solution of the equation some of them are $\lambda_n L_F$ =1.8751040, 4.6940911, 7.8547574, etc. Each of these eigenvalues has associated an eigenfunction that is solution of the spatial differential equation EqA.14

$$W_n(x) = C_n\left(\left(\cos\lambda_n x - \cosh\lambda_n x\right) - \frac{\cos\lambda_n L_F + \cosh\lambda_n L_F}{\sin\lambda_n L_F + \sinh\lambda_n L_F}\left(\sin\lambda_n x - \sinh\lambda_n x\right)\right) \qquad \textit{EqA.19}$$

These functions are named as the mode shapes of the beam and are solution of the spatial equation. Moreover any linear combination of these functions is also a solution of the equation. Therefore it is possible to write the solution in its linear expansion form

$$W(x) = \sum_{n=1}^{\infty} C_n\left(\left(\cos\lambda_n x - \cosh\lambda_n x\right) - \frac{\cos\lambda_n L_F + \cosh\lambda_n L_F}{\sin\lambda_n L_F + \sinh\lambda_n L_F}\left(\sin\lambda_n x - \sinh\lambda_n x\right)\right)$$

EqA.20

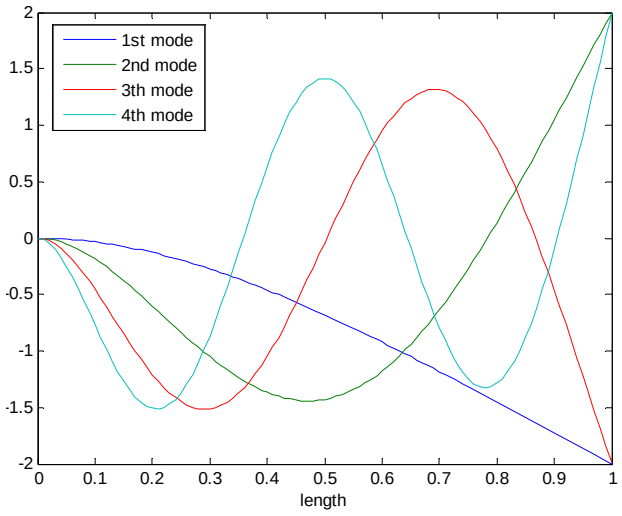

Figure A-2 Representation of the four first mode shapes for a clamped-free beam.

Figure A-2 depicts the shape for the first four mode shapes. The first mode have one point with no deflection located at x=0. The second, third and fourth modes have two, three and four point with no deflection respectively. These modes have some interesting properties as its orthogonality properties. This means that

$$\int_o^{L_f} W_m(x)W_n(x) = 0 \qquad \text{if } n \neq m \qquad \textit{EqA.21}$$

$$\int_o^{L_f} W_m(x)W_n(x) = L_F \qquad \text{if } n = m \qquad \textit{EqA.22}$$

Therefore from the analysis developed until now it is possible to conclude that there is an infinite discreet number of natural frequencies that can be transmitted through the beam. These frequencies are higher for stiffer and lighter materials, see EqA.15. The deflection of the beam in a certain point is defined by the summation of the infinite modes that can be transmitted through it

$$u(x,t) = \sum_{n=1}^{\infty} W_n(x) r_n(t) \qquad \textit{EqA.23}$$

Once the unforced equation of an Euler-Bernoulli beam has been introduced, the forced equation is analyzed. However the force equation is analyzed considering a beam with piezoelectric elements. In the following analysis different piezoelectric based structures are considered. First of all the classical piezoelectric bimorph is analyzed, then the analysis is extended to any multilayer structure. In both analyses

the actuating and sensing behavior of the structures are analyzed and its constitutive equations are developed.

A.2. Piezoelectric bimorph cantilever smart beam

In this point the equations that define the electromechanical behavior of a system formed with smart materials as piezoelectric are developed. The mechanical configuration consists on a cantilever beam. The use of this kind of structures has been extended a lot during the last decades. Piezoelectric bimorph cantilevers is a good configuration to work as an actuator to produce large displacement, by the other side it is also extensively used as force sensors due its high sensitivity. The description of the equations that govern the electrical and mechanical behavior is crucial when designing the electronic instrumentation to interface with these structures.

The bimorph structure studied in this point is drawn at Figure A-3. This structure consists on two active layers submitted to opposite elongations in order to produce an effect, as the bimetal effect, that induces a deflection at the tip of the beam. This effect is produced in two ways according to the relative disposition of the two layers, this is applying an electric field in one direction "serial" Figure A-3a) or applying the electric field in opposite direction "parallel" Figure A-3b). The same structure is used as a sensor when a force is applied at its tip. The induced bending produces an internal strain that generates an induced electrical charge.

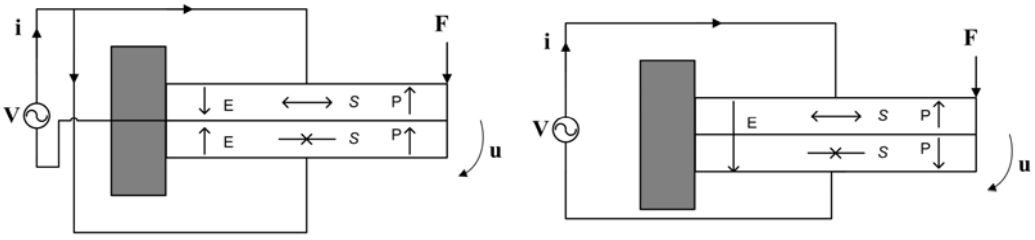

Figure A-3: a) Bimorph parallel configuration. b) Bimorph serial configuration.

In the following lines, the constitutive equations that describe the linear coupled behavior of these structures are obtained. These constitutive equations are

$$u = a_{11}F + a_{12}V \qquad \textit{EqA.24}$$

$$Q = a_{21}F + a_{22}V \qquad \textit{EqA. 25}$$

where “u” and “Q” are the extensive variables of the system named deflection and electrical charge respectively. By the other hand “F” and “V” are the intensive variables that represent the applied force and the applied voltage respectively

In the point above the vibration transmission problem has been treated in a pure mechanical structure, now the coupled equations between electrical and mechanical domain are introduced. This coupling is considered linear with the classical piezoelectric coupled equations:

$$S_1 = s_{11}^E T_1 + d_{31} E_3 \qquad \textit{EqA.26}$$

$$D_3 = d_{31} T_1 + \varepsilon_{33}^T E_3 \qquad \textit{EqA. 27}$$

In this case the extensive variables are “S_1” y “D_3”, these are the strain in the “x” axes and the electric displacement vector in the “y” axis. The intensive variables are the “T_1” and “E_3” that represent the mechanical stress in the “x” axis and the electrical field in the “y” axis. The coefficient relating these variables are the “s_{11}^E” that is the elastic compliance at constant electric field, the “d_{31}” is the piezoelectric coefficient and the “ε_{33}^T” is the dielectric permittivity at constant stress. The first equation describes the mechanical part, the strain is related to the mechanical stress and the electric applied. The second equation describes the displacement vector that is related to the applied electric field and the mechanical stress.

Once the piezoelectric equations are introduced, the force equation governing the vibrations of the beam is redefined. Actually the application of an electric field is modeled as a new contribution to the flexural moment. Consider the equation of flexural moment

$$M = -w\int_{-h}^{h} y T_x dy \qquad \textit{EqA.28}$$

Assuming the piezoelectric equations, it is possible to define the mechanical stress in terms of strain and electrical field

$$T_x = \frac{S_x}{s_{11}^E} - \frac{d_{31}}{s_{11}^E} E_z \qquad \textit{EqA.29}$$

Now considering that the strain in a certain point “x” inside a bending beam and at a certain distance “y” from its neutral axis is proportional to the radius of curvature of the beam “r” as:

$$S_x = y\frac{1}{r} \qquad \textit{EqA.30}$$

Substitution of this equation and equation EqA.29 into equation EqA.28 leads to the new equation for the bending moment

$$M = -2w\int_{-h}^{h} y\left(\frac{1}{r}\frac{y}{s_{11}^E} - \frac{d_{31}}{s_{11}^E}E_z\right)dy \qquad \textit{EqA.31}$$

As far as the radius of curvature is related to the deflection of the beam with the equation

$$\frac{1}{r} = -\frac{\partial^2 u(x,t)}{\partial x^2} \qquad \textit{EqA.32}$$

and considering that the compliance coefficient "s_{11}^E" in the piezoelectric equations is the reverse of the young modulus "Y_{11}", it is possible to rewrite the equation of the bending beam as

$$M = YI\frac{\partial^2 u(x,t)}{\partial x^2} + wEh^2 d_{31}E_z \qquad \textit{EqA.33}$$

In this equation the first term is the same that was presented at the beginning of this appendix however a new term is added dependent of the electric field. Now it is possible to write this equation as

$$M = YI\frac{\partial^2 u(x,t)}{\partial x^2} + M_V V(x,t) \qquad \textit{EqA.34}$$

were the electric field is assumed to be produced by the application of an electrical voltage "V(x,t)". Assuming a serial configuration "E_z=V/2h", the term "Mv" is written as

$$M_V = \frac{wYhd_{31}}{2} \qquad \textit{EqA.35}$$

Once the flexor moment equation is redefined it is possible to write the new force equation as

$$-M_V\frac{\partial^2 V(x,t)}{\partial^2 x}dx - YI\frac{\partial^4 u(x,t)}{\partial^4 x}dx + f(x,t)dx = \rho A dx\frac{\partial^2 u(x,t)}{\partial t^2} \qquad \textit{EqA.36}$$

The internal friction term is introduced in the equation

$$YI\frac{\partial^4 u(x,t)}{\partial^4 x}+BI\frac{\partial^5 u(x,t)}{\partial^4 x\partial t}+\rho A\frac{\partial^2 u(x,t)}{\partial t^2}=f(x,t)-M_V\frac{\partial^2 V(x,t)}{\partial^2 x} \qquad EqA.37$$

Once the force equation is redefined with the new force terms, the constitutive equations are obtained.

A.2.1. Coefficient a11

This coefficient was introduced in EqA.24, it defines the deflection of the beam for an input force . This coefficient is obtained by the solution of the force equation considering that the applied voltage is equal cero V(x,t)=0.

$$YI\frac{\partial^4 u(x,t)}{\partial^4 x}+BI\frac{\partial^5 u(x,t)}{\partial^4 x\partial t}+\rho A\frac{\partial^2 u(x,t)}{\partial t^2}=F(t)\delta(x-L_F) \qquad EqA.38$$

To solve this partial differential equation the separation of variables technique is used, therefore substitution of EqA.23 into the EqA.38 gives

$$\sum_{n=1}^{\infty}\left(YIW_n''''(x)r_n(t)+BIW_n''''(x)\dot{r}_n(t)+\rho AW_n(x)\ddot{r}_n(t)\right)=F(t)\delta(x-L_F) \qquad EqA.39$$

It s possible to eliminate from the equation the spatial differentiation Substitution of EqA.12 into the force equation leaves

$$\sum_{n=1}^{\infty}\left(\lambda_n^4 YIW_n(x)r_n(t)+\lambda_n^4 BIW_n(x)\dot{r}_n(t)+\rho AW_n(x)\ddot{r}_n(t)\right)=F(t)\delta(x-L_F) \qquad EqA.40$$

To eliminate the spatial coordinate, the orthogonality properties of the mode shapes are considered. For this purpose multiply at both sides of the equation by the mode shape function "$W_m(x)$", then, after integration over the whole length of the beam from 0 to L_F and considering the equations EqA.21 and EqA.22 it is possible to obtain

$$\lambda_n^4 YIL_F r_n(t)+\lambda_n^4 BIL_F\dot{r}_n(t)+\rho AL_F\ddot{r}_n(t)=F(t)W_n(L_F) \qquad EqA.41$$

This temporal equation is similar to the classic harmonic oscillator equation, therefore it is possible to write it in a more common form as

$$K_n r_n(t)+c_n\dot{r}_n(t)+m_n\ddot{r}_n(t)=F(t)W_n(L_F) \qquad EqA.42$$

with

$$K_n = \lambda_n^4 YIL_F \qquad \textit{EqA.43}$$

$$c_n = \lambda_n^4 BIL_F \qquad \textit{EqA.44}$$

$$m_n = \rho AL_F \qquad \textit{EqA.45}$$

where "K_n" is the modal spring constant, "c_n" is the modal damping coefficient and "m_n" is the modal mass. The modal spring constant and the modal damping coefficient are proportional to the normalized frequency "λ_n", they depend on the vibration mode therefore they are higher for higher modes.

In order to solve this ordinary differential equation it is assumed that the input force has the form $F(t)= F_o\, e^{i\gamma t}$, therefore the solution is directly written as

$$r_n(t) = \frac{F_o e^{i\gamma t} W_n(L_F)}{K_n - \gamma^2 m_n + i\gamma c_n} = \frac{F_o e^{i\gamma t}}{m_n} \frac{W_n(L_F)}{\omega_n^2 - \gamma^2 + i\gamma \frac{c_n}{m_n}} \qquad \textit{EqA.46}$$

Therefore the coefficient a11 is written as:

$$a_{11} = \sum_{n=1}^{\infty} \frac{1}{m_n} \frac{W_n^2(L_F)}{\omega_n^2 - \gamma^2 + i\gamma \frac{c_n}{m_n}} \qquad \textit{EqA.47}$$

where "ω_n" is the constant defined at EqA.12 and describe the natural frequencies of the system for each vibration mode

A.2.2. Coefficient a12

This coefficient defines the coupling between the electrical and the mechanical domains. It describes the beam deflection for an applied input voltage while there is no applied force. In order to find the equation describing the coefficient, the force equation EqA.37 assuming no applied force is rewritten as

$$YI \frac{\partial^4 u(x,t)}{\partial^4 x} + BI \frac{\partial^5 u(x,t)}{\partial^4 x \partial t} + \rho A \frac{\partial^2 u(x,t)}{\partial t^2} = -M_V \frac{\partial^2 V(x,t)}{\partial^2 x} \qquad \textit{EqA.48}$$

Assuming that in the bimorph structure the electrodes cover the whole surface of the beam, it is possible to describe the applied voltage with the following equation

$$V(x,t) = V_{in}(H(x) - H(x - L_F))e^{j\gamma t} \qquad \textit{EqA.49}$$

where "H(x)" is the Heavyside function. The partial derivatives from the voltage equation are given as

$$\frac{\partial}{\partial x}V(x,t) = V_{in}(\delta(x) - \delta(x - L_F))e^{j\gamma t} \qquad \textit{EqA.50}$$

$$\frac{\partial^2}{\partial x^2}V(x,t) = V_{in}(\delta'(x) - \delta'(x - L_F))e^{j\gamma t} \qquad \textit{EqA.51}$$

Therefore the force equation is rewritten as

$$YI\frac{\partial^4 u(x,t)}{\partial^4 x} + BI\frac{\partial^5 u(x,t)}{\partial^4 x \partial t} + \rho A\frac{\partial^2 u(x,t)}{\partial t^2} = -M_V V_{in}\left(\delta'(x) - \delta'(x - L_F)\right)e^{j\gamma t} \qquad \textit{EqA.52}$$

To solve this equation the same procedure is realized. The method of separation of variables and the orthogonality properties of the modes shapes are used. Thus the force equation is rewritten as

$$K_n r_n(t) + c_n \dot{r}_n(t) + m_n \ddot{r}_n(t) = \Theta_n V_{in} e^{j\gamma t} \qquad \textit{EqA.53}$$

Where "Θ_n" is named the electromechanical coupling term and defined with.

$$\Theta_n = \int_{x=0}^{L_F} M_V W_n(x)\left(\delta'(x) - \delta'(x - L_F)\right)dx = M_V W_n'(x)\Big]_{x=L_F} \qquad \textit{EqA.54}$$

This term is proportional to "Mv", defined at EqA.35, and to the mode shape slope evaluated at the tip of the beam $x=L_F$. Figure A-4 depicts a representation of the slope for the first four mode shapes transmitted in the beam. This figure graphs the spatial differentiation of the modes from Figure A-2. It is observed that the slope at the tip of the mode is higher for higher modes, therefore the coupling term is higher for higher vibration modes.

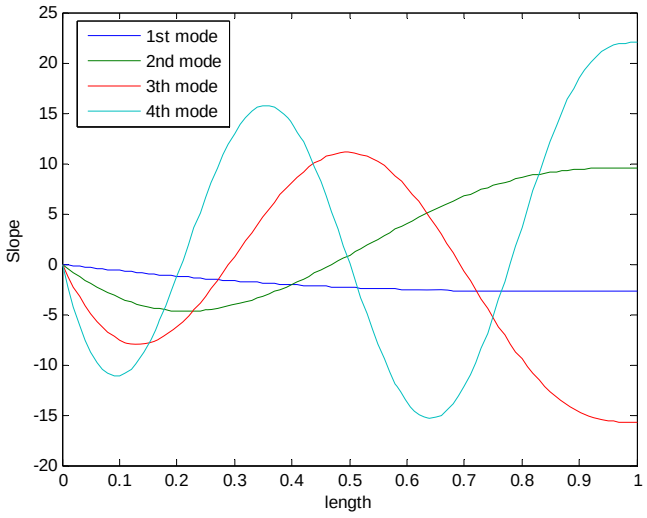

Figure A-4: Representation of the slope or spatial differentiation of the four first mode shapes in a clmape-free configiration.

It is possible to write a solution for the temporal function "$r_n(t)$" from force equation EqA.53 as

$$r_n(t) = \frac{1}{m_n} \frac{\Theta_n V_{in} e^{i\gamma t}}{\omega_n^2 - \gamma^2 + i\gamma \frac{c_n}{m_n}} \qquad \textit{EqA.55}$$

Therefore the a12 coefficient has the form

$$a_{12} = \sum_{n=1}^{\infty} \frac{\Theta_n V_{in} e^{i\gamma t}}{m_n} \frac{W_n(L_F)}{\omega_n^2 - \gamma^2 + i\gamma \frac{c_n}{m_n}} \qquad \textit{EqA.56}$$

A.2.3. Coefficient a21

This coefficient describes the charge generated in the bimorph when a force is applied at the tip of the beam. Due to the reciprocity in the equations defining the coupling in a piezoelectric material EqA.26 and EqA. 27, this coefficient is directly equal to the coefficient a12.

A.2.4. Coefficient a22

This coefficient defines the amount of charge accumulated in the electrodes when an input voltage is applied and the external force is cero. In this case the charge

is obtained integrating the electric displacement vector in the whole volume of the dielectric material. To find this coefficient, the electric equation from EqA. 27 is considered. The equation is modified in terms of electrical field and mechanical strain.

$$D_3 = \frac{d_{31}}{s_{11}^E} S_1 - d_{31}^2 \frac{E_3}{s_{11}^E} + \varepsilon_{33}^T E_3 \qquad \textit{EqA.57}$$

This equation is written in terms of the deflection as

$$D_3 = y \frac{d_{31}}{s_{11}^E} \frac{\partial^2 u(x,t)}{\partial x^2} - d_{31}^2 \frac{E_3}{s_{11}^E} + \varepsilon_{33}^T E_3 \qquad \textit{EqA. 58}$$

Thus the displacement vector has two contributions, one due to the beam deflection and the other due to the applied voltage. The part affected by the deflection is directly related to the curvature of the beam. Figure A-5 shows the evaluation of curvature of the mode shapes from Figure A-2. It is possible to observe that the maximum curvature is located at the initial point while at the free end, this curvature is cero. Moreover the figure shows that for modes higher than the first one, the curvature change the sign, thus in some parts of the beam the induced electrical displacement vector charge is positive and in the other negative.

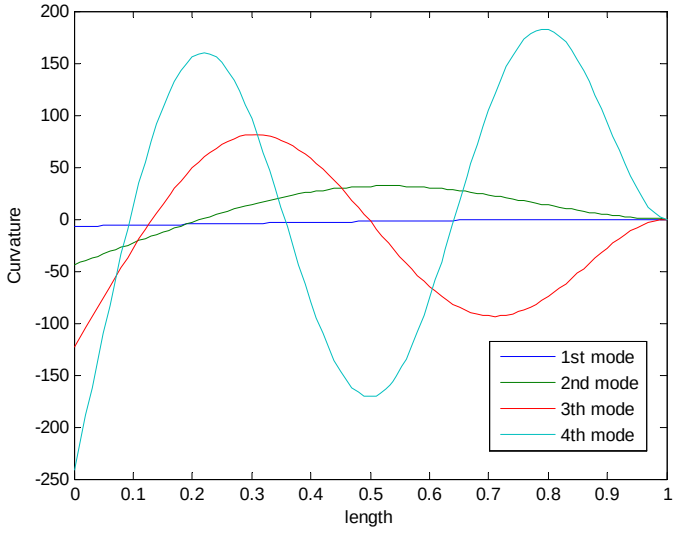

Figure A-5 Representation of the curvature of the beam or second spatial differentiation for the firts four mode shape in a clamped-free configuration.

To obtain an equation of the induced charge, the electrical displacement vector is integrated over the whole length of the beam. Substitution of EqA.31 and EqA.35 and after integration over the whole volume of the dielectric material, the equation gives

$$Q = M_V \frac{\partial u(x,t)}{\partial x}\Bigg]_0^{L_F} + \left(- d_{31}^2 \frac{wL_F}{2hs_{11}^E} + \varepsilon_{33}^T \frac{wL_F}{2h} \right) V_{in} e^{j\gamma t} \qquad \textit{EqA.59}$$

Thus the charge induced due to the beam deflection is proportional to the slope of the beam measured at its tip. Although the curvature of the beam has positive and negative parts along the beam for higher modes, the final integration over the whole length is grater for higher modes. Now the deflection equation for a given voltage is introduced in the equation and spatially differentiated. Thus the a22 coefficient gives

$$a_{22} = \sum_{n=1}^{\infty} \frac{M_V^2}{m_n} \frac{\left(\frac{\partial W_n(L_F)}{\partial x} \right)^2}{\omega_n^2 - \gamma^2 + i\gamma \frac{c_n}{m_n}} + \left(- d_{31}^2 \frac{wL_F}{2hs_{11}^E} + \varepsilon_{33}^T \frac{wL_F}{2h} \right) \qquad \textit{EqA.60}$$

The term at the right side of the equation is directly the equation of a planar capacitor while the rest of the equation defines the charge variations due to the mechanical motion of the beam.

With the definitions of these four coefficients the behavior of the piezoelectric bimorph beam to work as sensor or actuator is fully described.

A.3. Piezoelectric multilayer cantilever smart beam.

In the point above the mechanical structure studied was formed with only two layers. However it is possible to define more complex structures with several active and non-active layers. In this point a generic multilayer cantilever structure is studied.

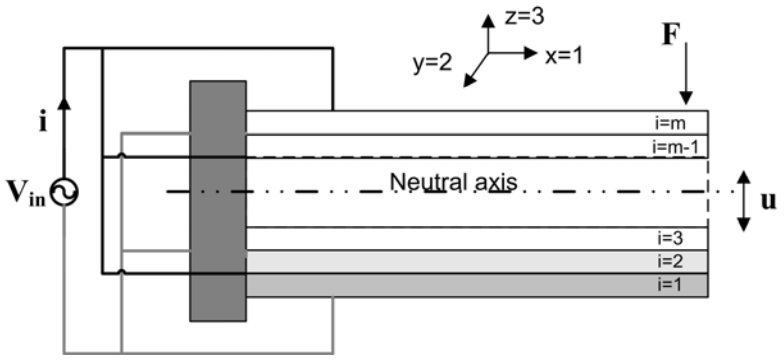

Figure A-6: Generic multilayer piezoelectric based cantilever.

This structure has the same form than the bimorph but it contains more layers, therefore the major part of the mathematical development from the last point is here adopted. However some changes have to be considered. The first thing to define is the neutral axis needed to relate the radius of curvature with the strain EqA.30. The neutral axis of a beam is defined as the axial axis that presents no strain when the beam is bent. To obtain the position of the neutral axis in the beam the condition of static equilibrium is imposed, the net axial force in a lateral section of the beam is cero.

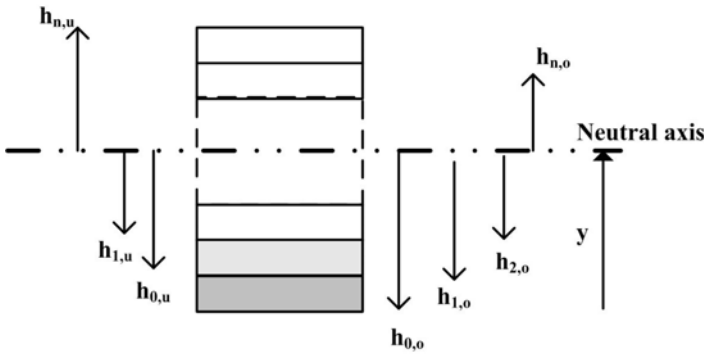

Figure A-7 Integration limits from the neutral axis .

$$\sum F_x^i = \sum \int T_x^i dA_i = \sum \int \frac{S_x^i}{s_{11}} dA_i = 0 \qquad \textit{EqA.61}$$

The integration limits are defined with respect to the position of the neutral axis "$\bar{y}$ ". "$h_{i,o}$" denotes the lower distance and "$h_{i,u}$", the upper distance of the layer "i" from the main inertia axis.

$$h_{i,u} = -\bar{y} + \sum_{j=0}^{i} h_j \qquad \textit{EqA.62}$$

$$h_{i,o} = -\bar{y} + \sum_{j=0}^{i-1} h_j \qquad \textit{EqA.63}$$

Now the equation is rewritten considering the integration limits

$$\sum F_x^i = \sum \int T_x^i dA_i = \sum \int \frac{S_x^i}{s_{11}} dA_i = \sum \int_{hio}^{hiu} k \frac{y_i w_i}{s_{11}^i} dy = 0 \qquad \textit{EqA.64}$$

Assuming the equations defining the integration limits, the solution of the equation leaves an equation defining the neutral axis from the lower edge of the bending actuator.

$$\bar{y} = \frac{\sum_{i=1}^{n} \frac{w_i}{s_{11}^i} h_i^2 - 2\sum_{i=1}^{n} \frac{w_i}{s_{11}^i} h_i \sum_{j=1}^{i} h_j}{2\sum_{i=1}^{n} \frac{w_i}{s_{11}^i} h_i} \qquad \textit{EqA.65}$$

Once the neutral axis is defined, the new bending moment is computed. In EqA.34 there are two contributions. These two contributions must be computed assuming the new integration terms

$$YI = w\left(\sum_{i=1}^{n} \int_{hio}^{hiu} \frac{y^2}{s_{11}^i} dy \right) \qquad \textit{EqA.66}$$

$$M_V = w\left(\sum_{i=1}^{n} - \int_{hio}^{hiu} \frac{y d_{31}^i}{h_i s_{11}^i} dy \right) \qquad \textit{EqA.67}$$

Therefore the constitutive equations of the multilayer structures have the same form than in the bimorph case but considering the new equations defining the rigidity term “YI” and the induced moment “M_v”. Moreover the term “a22” must be modified considering the number of piezoelectric layers “p”.

$$a_{22} = \sum_{n=1}^{\infty} \frac{M_V^2}{m_n} \frac{\left(\frac{\partial W_n(L_F)}{\partial x} \right)^2}{\omega_n^2 - \gamma^2 + i\gamma \frac{c_n}{m_n}} + p\left(-d_{31}^2 \frac{wL_F}{2hs_{11}^E} + \varepsilon_{33}^T \frac{wL_F}{2h} \right) \qquad \textit{EqA.68}$$

A.4. Piezoelectric multilayer cantilever smart beam sensor/actuator:

Up to now, the studied structures have been considered to work as actuator or as sensor, however a multilayer structure can work at the same time as actuator and sensor. While some layers are used to actuate some other layers are used to sense. In this point the same multilayer structure is studied but using two active layers as sensor. The analysis is developed for two measurement conditions. The first considers a measurement of the generated voltage in the sensor layer with open circuit conditions and the second considers a measurement of the generated current with short circuit conditions.

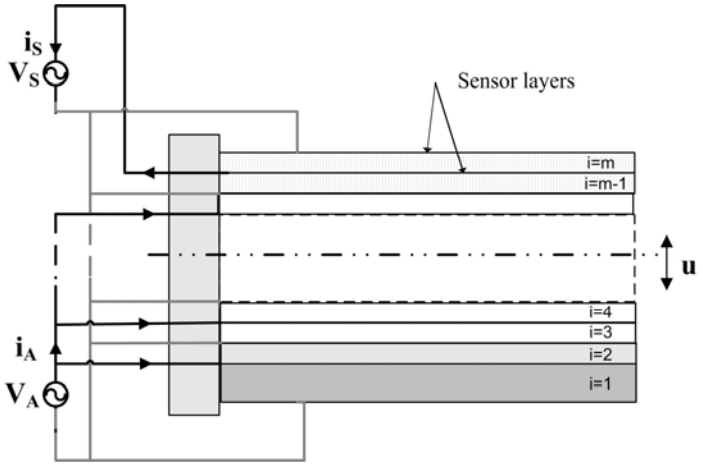

Figure A-8: Generic multilayer actuator/sensor piezoelectric based cantilever.

To start the new model, the bending moment equation is modified to consider the influence of the sensor layer.

$$M = YI\frac{\partial}{\partial^2 x}u(x,t) + M_{VA} + M_{VS} \qquad \textit{EqA.69}$$

"M_{VA}" is the induced moment due to the voltage drive of the "n" actuating layers. "M_{VS}" is the bending moment due to the voltage in the sensor "m" and "m-1" layers.

$$M_{VA} = w\left(\sum_{i=1}^{n} -\int_{hio}^{hiu} \frac{yd_{31}^{i}}{h_i s_{11}^{i}} dy\right) \qquad \textit{EqA.70}$$

$$M_{VS} = -w\int_{hm-1o}^{hm-.1u} \frac{yd_{31}^{m-.1}}{h_{m-1}s_{11}^{m-1}} + -w\int_{hmo}^{hmu} \frac{yd_{31}^{m}}{h_m s_{11}^{m}} \qquad \textit{EqA.71}$$

Once the bending moment equation is redefined, it is introduced into the force equation leading

$$YI\frac{\partial^4 u(x,t)}{\partial^4 x} + BI\frac{\partial^5 u(x,t)}{\partial^4 x \partial t} + \rho A\frac{\partial^2 u(x,t)}{\partial t^2} = -M_{VA}V_A(x,t) - M_{VS}V_S(x,t) \qquad \textit{EqA.72}$$

Once more the solution is obtained using the separation of variables method and the orthogonality properties of the mode shape functions. Proceeding as in the cases above, the force equation is rewritten in a more common way as

$$m_n\ddot{r}_n(t) + c_n\dot{r}_n(t) + K_n r_n(t) = -\Theta_{nA}V_A(t) - \Theta_{nS}V_S(t) \qquad \textit{EqA.73}$$

where "Θ_{nA}" and "Θ_{nS}" are defined as:

$$\Theta_{nA} = \int_o^{L_F} M_{VA}W_n(x)\left(\delta'(x) - \delta'(x - L_F)\right)dx = M_{VA}W'_n(L_F) \qquad \textit{EqA.74}$$

$$\Theta_{nS} = M_{VS}W'_n(L_F) \qquad \textit{EqA.75}$$

Once the force equation is redefined, the electrical equations in the sensor and the actuating layers are rewritten

$$Q_A(t) = M_{VA}\frac{\partial u(x,t)}{\partial x}\Big]_0^{L_F} + C_A V_A(t) \qquad \textit{EqA.76}$$

where

$$C_A = \sum_{i=1}^{n} \frac{wL_F}{h_i}\left(\varepsilon_{33}^{Ti} - \frac{d_{31}^{i2}}{s_{11}^{iE}}\right) \qquad \textit{EqA.77}$$

and

$$Q_s(t) = M_{VS}\frac{\partial u(x,t)}{\partial x}\Big]_0^{L_F} + C_S V_S(t) \qquad \textit{EqA.78}$$

where

$$C_S = \frac{wL_F}{h_{m-1}}\left(\varepsilon_{33}^{Tm-1} - \frac{d_{31}^{m-12}}{s_{11}^{m-1E}}\right) + \frac{wL_F}{h_m}\left(\varepsilon_{33}^{Tm} - \frac{d_{31}^{m2}}{s_{11}^{mE}}\right) \qquad \textit{EqA.79}$$

Now the governing equations for the two boundary conditions are solved.

A.4.1. Short circuit conditions or charge sensing

Most charge amplifier imposes a short circuit in the sensor layer through a virtual ground in its input. Therefore the governing equations are rewritten as

$$m_n\ddot{r}_n(t) + c_n\dot{r}_n(t) + K_n r_n(t) = -\Theta_{nA}V_A(t) \qquad \textit{EqA.80}$$

$$Q_s(t) = M_{VS}\frac{\partial u(x,t)}{\partial x}\Big]_0^{L_F} = \sum_{n=1}^{\infty}\Theta_{nS}r_n(t) \qquad \textit{EqA.81}$$

The solution for the temporal equation is

$$r_n(t) = \frac{\Theta_{nA}}{m_n}\frac{V_A(t)}{\omega_n^2 - \gamma^2 + i\gamma\dfrac{c_n}{m_n}} \qquad \textit{EqA.82}$$

Therefore the deflection is

$$u(x,t) = \sum_{n=1}^{\infty}\frac{\Theta_{nA}}{m_n}\frac{W_n(x)V_A(t)}{\omega_n^2 - \gamma^2 + i\gamma\dfrac{c_n}{m_n}} \qquad \textit{EqA.83}$$

The induced charge is obtained substituting EqA.82 into EqA.81

$$Q_s(t) = \sum_{n=1}^{\infty}\frac{\Theta_{nA}\Theta_{nS}}{m_n}\frac{V_A(t)}{\omega_n^2 - \gamma^2 + i\gamma\dfrac{c_n}{m_n}} \qquad \textit{EqA.84}$$

To obtain the equation relating the tip deflection with the induced electrical charge, the EqA.84 is divided by EqA.83 for each mode.

$$H_n = \frac{Q_s(t)}{u(L_F,t)} = \frac{\Theta_{ns}}{W_n(L_F)} = \frac{M_{VS}W'_n(L_F)}{W_n(L_F)} \qquad \textit{EqA.85}$$

A.4.2. Open circuit conditions o Voltage sensing

For measuring voltage, it is normally used a high input impedance amplifier, therefore it is possible to consider an open circuit conditions in the sensing layer. Assuming this condition the force equation is rewritten as

$$m_n \ddot{r}_n(t) + c_n \dot{r}_n(t) + K_n r_n(t) = -\Theta_{nS} V_S(t) - \Theta_{nA} V_A(t) \qquad \textit{EqA.86}$$

The electric equation is obtained considering EqA.78 with "$Q_s(t)$"=0.

$$V_S(t) = -\frac{1}{C_S}\sum_{n=1}^{\infty} \Theta_{nS} r_n(t) \qquad \textit{EqA.87}$$

To solve these equations it is needed to solve first the force equation that is rewritten as

$$m_n \ddot{r}_n(t) + c_n \dot{r}_n(t) + \left(K_n + \frac{\Theta_{nS}^2}{C_S} \right) r_n(t) = -\Theta_{nA} V_A(t) \qquad \textit{EqA.88}$$

It is observed that the measure of voltage modifies the mechanical response of the system. The solution of the temporal coordinate is obtained as

$$r_n(t) = \frac{\Theta_{nA}}{m_n} \frac{V_A(t)}{\left(\omega_n^2 + \frac{\Theta_{nS}^2}{C_S m_n} \right) - \gamma^2 + i\gamma \frac{c_n}{m_n}} \qquad \textit{EqA.89}$$

Therefore the deflection equation remains

$$u(x,t) = \sum_{n=1}^{\infty} \frac{\Theta_{nA}}{m_n} \frac{W_n(x) V_A(t)}{\left(\omega_n^2 + \frac{\Theta_{nS}^2}{C_S m_n} \right) - \gamma^2 + i\gamma \frac{c_n}{m_n}} \qquad \textit{EqA.90}$$

The generated voltage equation is obtained substituting EqA.89 into EqA.87

$$V_S(t) = \sum_{n=1}^{\infty} \frac{\Theta_{nA}\Theta_{nS}}{C_S m_n} \frac{V_A(t)}{\left(\omega_n^2 + \frac{\Theta_{nS}^2}{C_S m_n} \right) - \gamma^2 + i\gamma \frac{c_n}{m_n}} \qquad \textit{EqA.91}$$

To obtain the transfer function that relates voltage with deflection the equation EqA.91 into EqA.90 for each vibration mode

$$H_n = \frac{V_S(t)}{u(L_F,t)} = \frac{\Theta_{nS}}{C_S W_n(L_F)} = \frac{M_{VS} W'_n(L_F)}{C_S W_n(L_F)} \qquad \textit{EqA.92}$$

A.5. Piezoelectric multilayer cantilever smart beam with base excitation.

In this point the governing equations are rewritten considering a new configuration. In this case the structure analyzed consists on a cantilever anchored to a vibrating body. The beam is clamped from its base to a vibrating structure that oscillates with a displacement "$y_b(t)$"

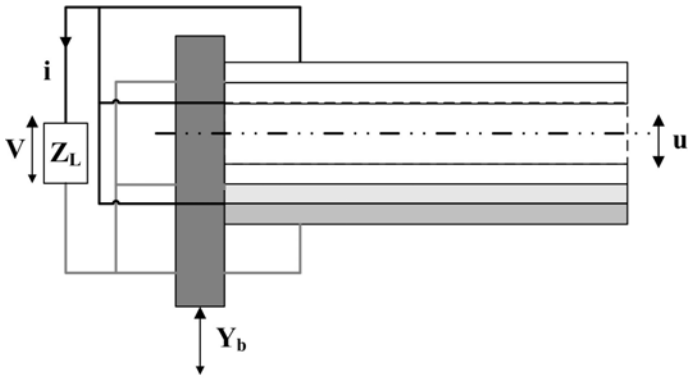

Figure A-9 Generic mulitlayer piezoelectric cantilever with base vibration for power harvesting.

With this new configuration the force equation is redefined. Assuming a smart beam with active materials the new force equation in a small piece of the beam is rewritten as

$$YI\frac{\partial^4 u(x,t)}{\partial^4 x} + BI\frac{\partial^5 u(x,t)}{\partial^4 x \partial t} + \rho A\frac{\partial^2 u(x,t)}{\partial t^2} = -M_V\frac{\partial^2 V(x,t)}{\partial^2 x} + \rho A\frac{\partial^2 y_b}{\partial t^2} \qquad \textit{EqA.93}$$

At the left side there are the elastic, viscous and inertia forces due to the deflection motion of the beam. At the right side there is the induced force due to the voltage in the active layers and a new inertia term due to the motion of mass produced by the base vibration.

To solve this equation, the separation of variables method and the modal analysis is performed again. Therefore the partial differential force equation is rewritten as an ordinary temporal equation as

$$m_n \ddot{r}_n(t) + c_n \dot{r}_n(t) + K_n r_n(t) = -\Theta_n V(t) + F_{on}(t) \qquad \textit{EqA.94}$$

$$F_{on}(t) = \ddot{y}_b(t) \int_0^L \rho A W_n(x) dx \qquad \textit{EqA.95}$$

were there is an induced force EqA.95 proportional to the base acceleration and multiplied by the distributed mass along the shape of the beam. With the force equation redefined the solutions of the constitutive equations are obtained directly as in the other. Therefore it is considered not to repeat them here.

B. APPENDIX B

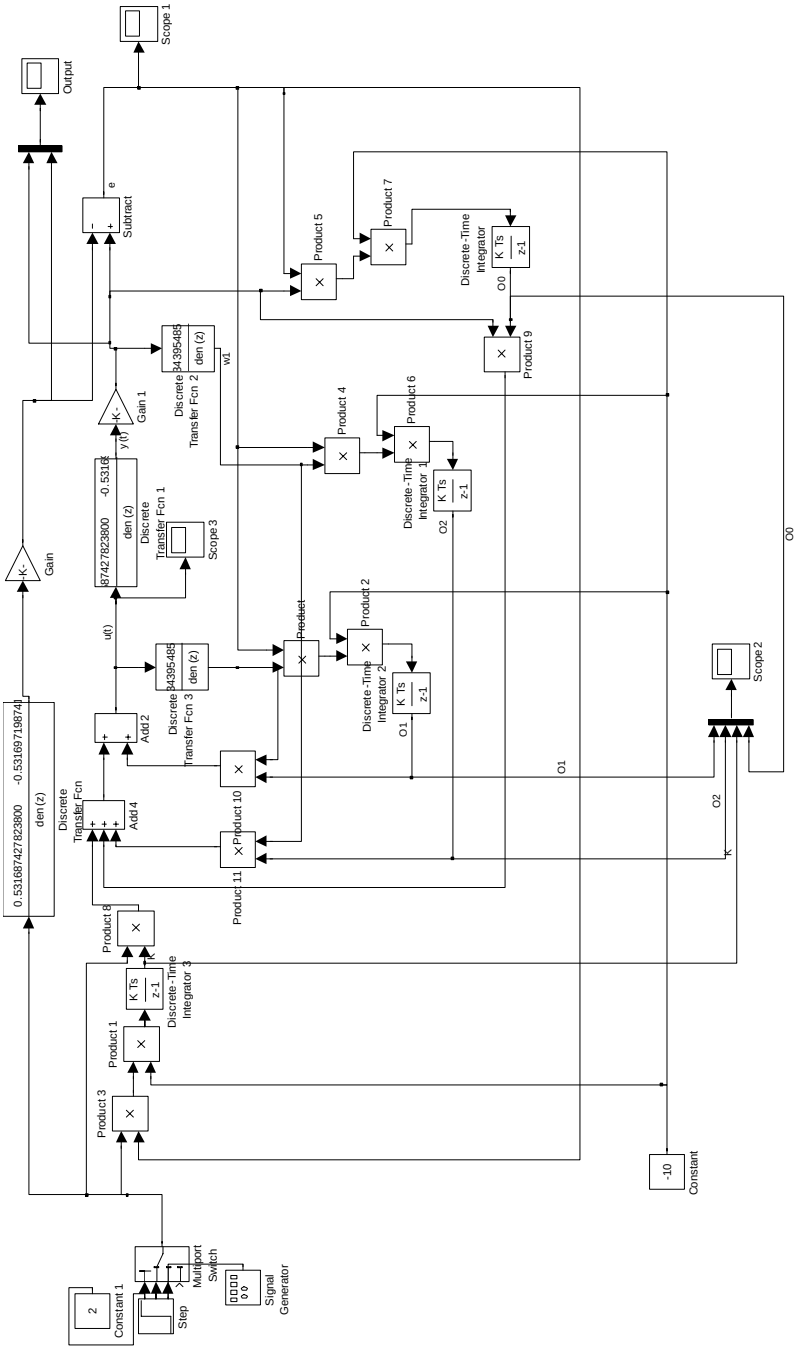

Figure B-1: Matlab-Simulink block diagram for the MRAC simulations.

List of publications:

Journal Papers:

Brufau-Penella, J.; Puig-Vidal, M.; Giannone, P.; Graziani, S.; Strazzeri, S.
Characterization of the harvesting capabilities of an ionic polymer metal composite device
Smart Materials & Structures
Volume: 17, Pages, Initial: 1 final: 15 Year: 2008

Brufau-Penella, J.; Tsiakmakis, K.; Laopoulos, T.; Puig-Vidal, M
Model reference adaptive control for an ionic polymer metal composite in underwater applications
Smart Materials & Structures
Volume: 17 Number: 4 Pages, Initial: 045020 final: 045020 (9 pp.) Year: 2008

Brufau-Penella, J; Puig-Vidal, M.
Piezoelectric Energy harvesting improvement with complex conjugate impedance matching
Journal of Intelligent Material Systems and Structures. *Online first published on September 29.*
Year: 2008

Tsiatmaikis, K.; Brufau-Penella, J.; Puig-idal, M.; Laopoulos, Th.
A camera based method for the measurement of motion parameters of IPMC actuators
IEEE Transactions on Instrumentation and Measurement. *Accepted in its current form. Waiting for publishing.*

Brufau-Penella, J.; Otero, J.; Puig-Vidal, M.
Microrobotic technologies for biological micro-nanohandling
Emerging technologies robotics and control systems International society for advanced research
ISBN 978-88-901928-2-1 Volume: 2 Pages, Initial: 9 final: 16 Year: 2007

A. Arbat, R. Casanova, J. Canals, J. Brufau, J. Samitier, A. Diéguez, E. Edqvist, S. Johansson
A complet microcantilever tool for microrobot contact sensing
Sensors and Actuators. *Paper sent. Waiting for first review*.

Relevant Proceedings:

Brufau-Penella, J.; Sánchez, J.; Puig-Vidal, M.
Piezoelectric Polymer model validation applied to mm size microrobot I-SWARM (Intelligent Swarm)
Proceedings of the Society of Photo-Optical Instrumentation Engineers Structures and Materials 2006: Modeling, Signal Processing, and Control
Volume: 6166 Pages, Initial: Q1660 final: Q1660 Year: 2006

Brufau J, Puig-Vidal A, Lopez-Sanchez J, Samitier J, Driesen W, Breguet JM, Snis N, Simu U, Johansson S, Velten T, Gao J, Seyfried J, Estana R, Woern H
MICRON: Small autonomous robot for cell manipulation applications
Proceedings of the IEEE International Conference on Robotics and Automation
Volume: 1-4 Pages, Initial: 844 final: 849 Year: 2005

Brufau-Penella, J. Puig-Vidal, M.
Piezoelectric Smart actuator: Model validation and Charge vs Voltage method for displacement sensing
Proceeding of the Actuator Conference.
Volume:1, Pages, Initial: 507 final: 514 Year:2006

Tsiakmakis K , Brufau J, Puig-Vidal M, Laopoulos T.
Measuring motion parameters of Ionic Polymer-Metal Composites (IPMC) actuators with a CCD camera
Proceedings IEEE Instrumentation and Measurement Technology Conference IMTC
Volume: 1-5 Pages, Initial: 1562 final: 1567 Year: 2007

Colomer J, Brufau J, Miribel-Catala P, Saiz-Vela A, Puig-Vidal M, Samitier J
Power conditioning circuitry for a self-powered mobile system based on an array of micro PZT generators in a 0.13 um technology
Proceedings IEEE International Symposium on Industrial Electronics
Volume: 1-8 Pages, Initial: 2353 final: 2357 Year: 2007

Colomer J, Brufau J, Miribel-Catala P, Saiz-Vela A, Puig-Vidal M, Samitier J
Novel autonomous low power VLSI system powered by ambient mechanical vibrations and solar cells for portable applications in a 0.13 mu technology
Proceedings IEEE Electronic Specialists Conference
Volume: 1-6 Pages, Initial: 2786 final: 2791 Year: 2007

Lacort, J.; Casanova, R.; Brufau, J.; Arbat, A.; Dieguez, A.; Nierlich, M.; Steinmetz, O.; Puig-Vidal, M.; Samitier, J.
An integrated controller for a flexible and wireless Atomic Force Microscopy.
Proceedings of the SPIE Microtechnologies for the new millenium 2005.
Volume: 5837 Pages, Initial: 321 final: 328 Year: 2006

Other Conferences:

Brufau-Penella, J.; Puig-Vidal, M.
Electromechanical model of a multi-layer piezoelectric cantilever
IEEE Eurosime 2006
Como (Italy) (ITALY) Year: 2006

Brufau-Penella, J.; López-Sánchez, J.; Puig-Vidal, M.; Samitier, Tagliareni, F.; Nielrich, M.; Steinmetz, O.; Velten, T.
Manipulating biological cells with a micro-robot cluster
IEEE International conference on intellignet robots and systems IROS05
Montreal (CANADA) Year**:** 2005

Brufau-Penella, J.; Saiz-Vela, A.; Otero, J.; López-Sánchez, J.; Miribel-Català, P.; Puig-Vidal, M.; Samitier, J.
Autonomous Atomic Force Microscopy System based on self-sensing AFM probes.
Proceedings of the XX Conference on Design of Circuits and Integrated Systems, DCIS 2005
Lisboa (PORTUGAL) Year**:** 2005

Brufau-Penella, J.; Ruiz-Montero, R.; Otero,J.; López-Sánchez, J.; Puig-Vidal, M.; Samitier, J.
Diseño de un cabezal AFM como herramienta de un microrobot de reducidas dimensiones.
Annual seminari on automatic control, industrial electronics and instrumentation SAEEI05
Santander (SPAIN) Year: 2005

Brufau-Penella, J.; Sánchez-Martín, J.; Puig-Vidal, M.; Samitier, J.
Diseño e impementación de un microgenerador de energía piezoeléctrico para redes de sensores wireless.
Annual seminari on automatic control, industrial electronics and instrumentation SAEEI05
Santander (SPAIN) Year: 2005

Brufau-Penella, J.; López-Sánchez, J.; Puig-Vidal, M.; Samitier, J.
Implementacion de un sistema electrónico para un microrobot autónomo en aplicaciones biomédicas.
Annual seminari on automatic control, industrial electronics and instrumentation SAEEI04
Place of celebration: Toulousse (FRANCE) Year: 2004

Brufau-Penella, J.; Garcia-Vázquez, I.; López-Sánchez, J.; Puig-Vidal, M.; Samitier, J.
Sistemes d'actuació i control per a un capçal AFM d'un microrobot amb sensor de força integrat.
IV Jornades de recerca en enginyeria biomèdica, JEBC04
Barcelona (SPAIN) Year: 2004

Tsiatmaikis, K.; Brufau-Penella, J.; Puig-idal, M.; Laopoulos, Th.
Modeling IPMC actuators for model reference motion control
IEEE IMTC-2008
Victoria (CANADA) Year: 2008

Colomer,J.; Miribel,P.; Saiz-Vela,A.; Brufau,J.;Maña,J.; Puig-Vidal,M.;Samitier,J.
SiP Power Management Unit with Embedded Temperature Sensor Powered by Piezoelectric Vibration Energy Harvesting
IEEE- MWSCAS 2007 (IEEE- International Midwest Symposium on Circuits and Systems)
Montréal (CANADA) Year: 2007

Otero, J.; Saiz, A.; Brufau, J.; Colomer, J.; Ruiz, R.; Lopez, J.; Miribel, P.; Puig, M.; Samitier, J.;
Reduced Dimensions Autonomous AFM System for working in Microbiorobotics
Biomedical Robotics and Biomechatronics, 2006. BioRob 2006. The First IEEE/RAS-EMBS International Conference on
Pisa (ITALY) Year: 2006

Casanova, R.; Saiz, A.; Lacort, J.; Brufau, J.: Arbat, A.; Dieguez, A.; Miribel, P.; Puig-Vidal, M.; Samitier, J.
Towards Co-operative Autonomous and Intelligent 1cm3 Robots for Micro and NanoManipulation Applications: MICRON.
IEEE/RSJ International Conference on Intelligent Robots and Systems, IROS 2005
Edmonton (CANADA) Year**:** 2005

Saiz-Vela, A.; Miribel-Català, P.; Brufau, J.; Casanova, R.; Puig-Vidal, M.; Samitier, J.
Specific Drivers and Integrated 20V Regulated Charge Pump for an Autonomous MicroRobot: MiCRoN
XIX Conference on Design of Circuits and Integrated Systems, DCIS 2004
Bordeaux (FRANCE) Year: 2004

Lacort, J.; Casanova, R.; Arbat, A.; Dieguez, A.; Brufau, J.; Lopez, J.; Samitier, J.
An integrated controller for a AFM tool mounted in a wireless microrobot.
Conference on Design of Circuits and Integrated Systems, DCIS 2005
Lisboa (PORTUGAL) Year: 2005

Arbat, A.; Canals, J; Casanova, R.; Diéguez, A.; Brufau, J.; Puig, M.;Samitier, J.
Design and control of a micro-cantilever tool for micro-robot contact sensing
2007 European Conference on Circuit Theory and Design, ECCTD'07
Sevilla (SPAIN) Year: 2007